studies in surface science and catalysis

42

LABORATORY STUDIES OF HETEROGENEOUS CATALYTIC PROCESSES

Erhard G. Christoffel

Revised and edited by
Zoltán Paál

elsevier

LABORATORY STUDIES OF HETEROGENEOUS CATALYTIC PROCESSES

This Page Intentionally Left Blank

LABORATORY STUDIES OF HETEROGENEOUS CATALYTIC PROCESSES

Erhard G. Christoffel
FH Ostfriesland and University Witten/Herdecke, F.R.G.

Revised and edited by
Zoltán Paál
Institute of Isotopes, Hungarian Academy of Sciences, P.O. Box 77, H-1525 Budapest, Hungary

CONTENTS

ERHARD G. CHRISTOFFEL
(1941 - 1985)

Erhard G. Christoffel graduated as a chemical engineer in 1972 from
Darmstadt University (F.R.G.). He started his professional career
at the Ruhr University, Bochum, where he obtained his habilitation
degree in 1980. It was during his years in Darmstadt that his
interest in catalytic hydrocarbon transformation started. This
developed into a committment to the chemical engineering aspects of
this topic in Bochum, as reflected by his numerous and valuable
publications full of original ideas that date from this period.
He developed further interests when he was appointed a full
Professor at the Fachhochschule Ostfriesland in Emden, where he had
the opportunity to build a new laboratory for teaching and research
in catalysis. During this period he was busy cultivating contacts
abroad and fruitful collaborations started with institutions in
Hungary and China. He was invited to China twice as a guest
lecturer and visited Hungary several times. Joint publications
indicated that he took these cooperations very seriously. Another
challenge followed soon: an invitation to be Professor of Chemical
Engineering at Germany's first private university, which had
recently been founded at Witten/Herdecke; this provided another
opportunity to create a new school. However, he could not take part
in its realization. When he returned from China in September, 1985,
full of plans, the headache he felt after this trip was not due to
jet lag but proved to be the first sign of his fatal illness which

soon brutally terminated a productive life. He is survived by a
loving mother and two teenage daughters who were his pride and joy
and to whom he dedicated this book.

Erhard G. Christoffel led an almost Spartan outward life: he
preferred the values of Nature to those offered by the consumer
society. His mentality was close to the ideal of the Renaissance
"uomo universale": in addition to his profession, he was deeply
involved in natural and moral philosophy, too. A guitar was an
almost inseparable companion and he sang often and with pleasure -
frequently his own compositions.

We, the friends of the late Erhard G. Christoffel, mourn not
only the irreparable loss of a friend but also the fact that he
took to the grave many ideas and plans. One small blessing is that
his first book - which turned out to be also his last - was
complete apart for some minor editing work. Let this book be a
final tribute to Erhard G. Christoffel; it is worthy of both the
scientist and man.

Zoltán PAÁL

To Andrea and Ursula

This Page Intentionally Left Blank

PREFACE

One of the major activities of man is the conversion of
naturally occurring materials with the aim of utilizing their
stored energy or producing new materials. This activity is
strongly coupled with economics, which, together with replacing
the traditional values of society, such as truth, beauty and
goodness, by feasibility, allurement and conformity, results in a
situation where products create markets and things are believed to
be true by virtue of the fact that they can be done or to be good
by virtue of the fact that they fit with conformity. Nevertheless,
in order to handle many of the problems with which we are faced
today, we are compelled to re-establish a relationship with these
traditional values and develop a more basic understanding of the
global space-time structure and the principles of evolution of the
surroundings in which we live.

This book is concerned with one of the fundamental principles
through which reactants are transformed into products in both
living and man-made systems: catalysis. Catalysts are substances
that initiate and accelerate chemical reactions and affect the
direction of chemical transformations. In order to preserve the
catalysts without additional separation procedures, the majority
of large-scale processes in the chemical industry are based on
heterogeneous catalytic reactions, where fluid-phase reactants are
passed over solid catalytic material. The improvement of existing
or the introduction of new processes is mostly a result of
developing new catalysts or modifying existing ones.

Laboratory studies in this context cover catalyst preparation,
catalyst screening, scale-up from the laboratory scale to pilot
and industrial plants and process simulation and optimization. The
last three tasks are related to the basic aim of scientific
investigations in chemical engineering, the forecasting of the
performance of industrial chemical reactors on the basis of
experimental data from laboratory reactors. For this to take
place, a kinetic analysis of the reaction system is required,
where the rates of the individual processes - surface reactions,
adsorption, mass and heat transfer within and outside the catalyst
pellets - are analysed, preferably under reaction conditions that

are compatible with industrial reactors. The accomplishment of
this analysis demands a qualitative understanding of the structure
and reactivity of the chemical species that make up the reaction
network, a quantitative description of the dynamics of open
reactive systems and the application of suitable parameter
estimation procedures. All these subjects cannot be presented
comprehensively within the scope of a single book.

In this work we shall begin by considering the basic phenomena
of heterogeneous catalytic reaction systems and then, in more
detail, the experimental methods and procedures for investigating
the dynamics of these systems will be discussed. Accordingly, the
text is structured in the following way: after the intoductory
Chapter 1, which illustrates the whole procedure with an actual
example, in Chapter 2 the basic phenomena of catalytic systems and
the concepts used in studying these systems are presented; Chapter
3 covers the description of methods for investigating reaction
mechanisms and the dynamics of heterogeneous catalytic reaction
systems; in Chapter 4 the design and operation modes of laboratory
reactors, frequently used for the investigation of heterogeneous
catalytic reactions, are discussed.

Many colleagues and friends have contributed directly and
indirectly to the contents of this book, and I wish to express my
sincere appreciation to them. Furthermore, I thank Karin Steinberg
for her excellent typing of the manuscript and Brigitte Blunck and
Jürgen Lappe for preparing the drawings.

<div align="right">Erhard G. CHRISTOFFEL</div>

Owing to the unexpected and untimely death of Erhard G.
Christoffel, I was asked, as his friend and colleague, to add the
last finishing touches to the almost complete manuscript. Chapter
1 and the historical part of Chapter 2 have undergone a major
revision, as have Sections 3.1.1 and 3.4. I added Sections 3.1.2
and 4.5 to the manuscript. Other revisions consisted mainly of
updating the text by incorporating new references to recent work.
These changes were intended to be made in a manner true to the
thoughts, intentions and spirit of the author and, I hope, not
without success.

This Page Intentionally Left Blank

Chapter 1

INTRODUCTION

In operating an industrial plant, where reactants are converted into products *via* heterogeneous catalytic reactions, a typical task might be to replace the catalyst in the reactor and to choose from among the different available catalysts one, to be used in the reactor. Similar tasks arise if new catalysts have been developed and new chemical processes are designed or feedstocks in operating processes are changed and space velocities of reactants have to be adjusted to achieve desired conversions. Laboratory studies in this context include catalyst preparation and screening, scale-up as well as process simulation and optimization (ref. 1).

For example, of the C_8-aromatics, o- and mainly p-xylene are valuable products; it is therefore desirable to convert m-xylene and ethylbenzene in C_8-aromatic fractions to the first two isomers. This can be realized by heterogeneous catalytic processes, the catalyst to be selected depending on the feed composition. When only xylenes are present, acidic catalysts can be used. Established ones are of the platinum-silica-alumina or platinum-alumina type of controlled acidity while the newer catalysts are zeolites (refs. 2,3). If the feed also contains ethylbenzene, the strategy must be different. Ethylbenzene is dealkylated and/or disproportionated over pure acidic catalysts. A hydrogenation—dehydrogenation function has to be included in the catalyst for the isomerization of this compound (see in detail, Section 3.1.3). Such catalysts can be obtained by adding 1-2% platinum to an acidic - zeolite - catalyst with suppressed acidity (refs. 2,4,5).

In practical xylene isomerization, where the aim is to isolate o- and p-xylene, the C_8-aromatic cut of platforming benzene is used frequently as feed and this contains 42-47% m-xylene, 20-22% p-xylene, 18-20% o-xylene and 12-19% ethylbenzene. Using the C_8-aromatic cut of pyrolysis benzene, the portion of ethylbenzene in the feed will be 50% or more. Isomerization reactions among the xylenes on bifunctional Pt/zeolite catalysts involve 1,2-methyl shifts of arenium ions or, in case of a bifunctional mechanism, of carbenium ions which are fast compared with interconversions of ethylbenzene with the xylenes which require ring contraction and expansion reactions of naphthenes (refs. 6,7). Hence, in replacing the C_8-aroma-

tic cut of <u>platforming benzene,</u> as feed for the xylene isomeriza-
tion process, by a corresponding <u>pyrolysis benzene</u> cut, longer
reaction times in the reactor are needed.

In practice there are three different scales of experiment
needed to solve the problems considered so far: the laboratory, the
pilot plant and the industrial plant scale, and one of the basic
aims of investigations in chemical engineering is to predict the
performance of industrial reactors on the basis of experimental da-
ta obtained from the laboratory. These laboratory studies involve
a kinetic analysis of open reactive systems which, due to the
coupling of mass and heat transfer rates with rates of adsorption
and surface reactions, should be formulated in the following way:
first the underlying reaction mechanism is investigated from which
a simplified reaction scheme can be derived; this is then used to
set up the kinetic model equations which act as entries into the
dynamic reactor model equations. In the final step the model para-
meters have to be estimated by fitting a set of suitable experi-
mental data.

One possible strategy of model development is shown in Figure
1.1 where such chemical engineering parameters like diffusivities
are also considered (ref. 8). It is rare that the same research
group carries out systematic studies simultaneously with as many
reactor types as shown in the figure; the results reported in
(ref. 8) gave a surprisingly close approximation of the actual
experimental data using only five parameters (k-values for the
meta $\rightarrow$ para and meta $\rightarrow$ ortho transformations and for coking; and
the respective energies of activation, the E values for the two
xylene isomerization reactions having been considered as equal).

Applying a similar procedure to a consideration of the effects
of different reactant materials fed into a xylene isomerization
reactor, the underlying reaction mechanism has been investigated by
comparing product distributions of various model compound conver-
sions on different catalysts with theoretically expected product
distributions (ref. 6). To reduce the complex reaction network to
a simplified scheme, C_8-aromatic and hydrogen partial pressure de-
pendencies of ethylbenzene and o-xylene conversions have been
determined and, assuming a constant C_8-aromatic partial pressure
in the reactor, a scheme was derived in which the xylene isomers
and ethylbenzene were linked together by reversible pseudo-monomole-
cular reactions and cracking products and naphthenes were formed
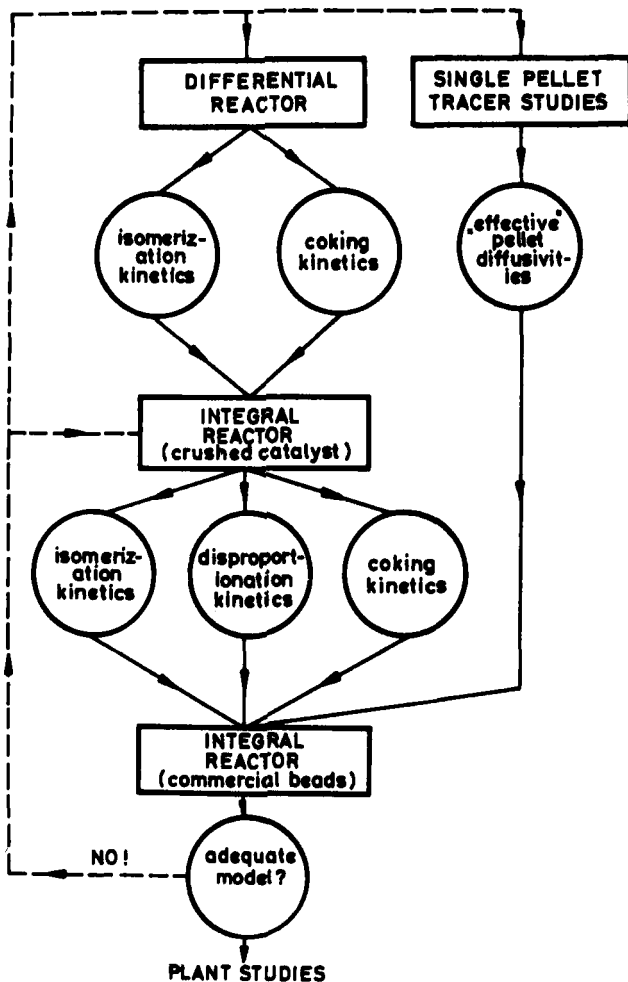
Fig. 1.1. The overall strategy of model development (used in the example of xylene isomerization). Reproduced with permission from (ref. 8). Copyright 1983 by American Chemical Society.

from each of the C_8-aromatics by irreversible pseudo-monomolecular reactions. The rate coefficients associated with the reaction scheme were fitted to measured integral composition-reaction time data using the Marquardt-procedure (refs. 7,9). In Fig. 1.2 pre-
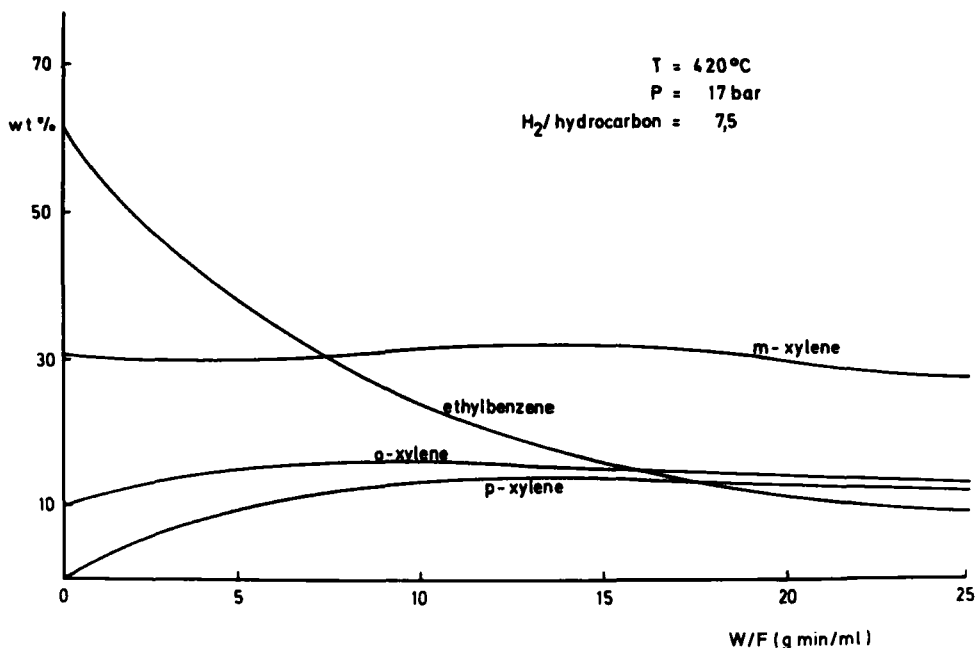
Fig. 1.2. Predicted C_8-aromatic distributions at different reaction times in a continuously operated isothermal fixed bed reactor (ref. 9).

dicted C_8-aromatic compositions at different reaction times are plotted, indicating optimal reaction times for o- and p-xylene production. Scheme 1.1 shows the calculated reaction rate coefficient together with the reaction scheme. The only simplification was that side reactions (ring opening, cracking and hydrogenation), which occur only to a limited extent, were taken into account by a single irreversible first-order reaction.

The next example illustrates that the same experimental data can lead to different results if a different method of calculation is used (ref. 10). Scheme 1.1 contains cyclical reaction paths. The free energy change around a cycle must be zero and this implies that, in any cyclical isothermal reaction sequence, the following equation must be valid:

$$K_{12} \cdot K_{23} \cdots K_{n1} = 1 \tag{1.1}$$

where K_{ij} is the equilibrium constant for the reaction

$$A_i \rightleftharpoons A_j \tag{1.2}$$

and
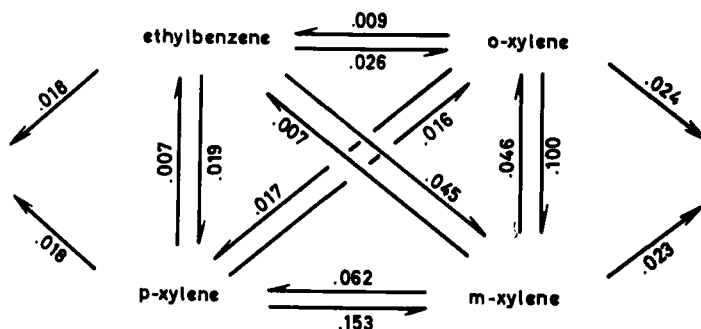
Scheme 1.1

$$K_{ij} = k_{ij}/k_{ji} \qquad\qquad\qquad (1.3)$$

where k_{ij} and k_{ji} represent respectively the pseudo first-order forward and backward rate coefficients for reaction (1.2). Three independent cycles can be found in Scheme 1.1; the data published in (ref. 7) result in the cycle products listed in Table 1.1.

Table 1.1

Products of Equilibrium K-values Around the Cycles of Scheme 1.1 (Data after ref. 7; the table reproduced by permission from ref. 10)

Cycle Number	Cycle Description	Cycle Product
1	ethyl—ortho—para—ethyl	1.13
2	para—meta—ortho—para	1.21
3	ethyl—meta—para—ethyl	0.96

Anselmo and Upadhye (ref. 10) re-evaluated these k-values by minimizing the sum of the squares of the relative errors between the model predictions and the constraint that the cycle product must equal unity. Their results are shown in Scheme 1.2. The irreversible reaction rates were fixed at values given in (ref. 6). The differences are not significant and the difference between K-values for individual reactions, obtained by the two methods of calculation, is between 0.08 and 11%.

ethylbenzene .00835 o-xylene
.0245

.018 .0063 .0184 .0066 .0130 .0487 .104 .024

.0128 .0422

.018 .023

p-xylene .0626 m-xylene
.1374
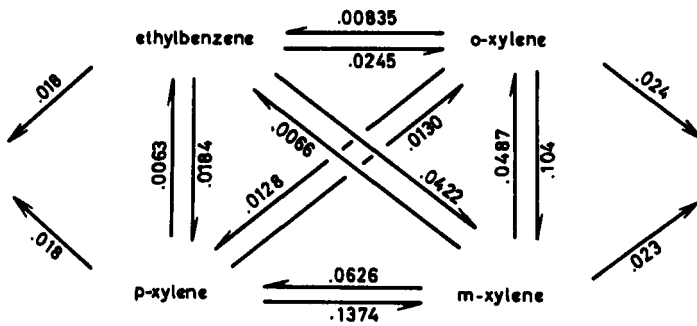
Scheme 1.2

REFERENCES

1 Froment, G.F. and Bischoff, K.B., Chemical reactor analysis and design, Wiley, New York, 1979.
2 Thomas, C.L., Catalytic Processes and Proven Catalysts, Acad. Press, New York, 1970, pp. 21-24.
3 H. Heinemann, Catal. Rev.-Sci. Eng., 23 (1981) 315.
4 N.Y. Chen and W.J. Reagan, U.S.P. 4,101,595 (Jul. 1978).
5 M. Nitta and P.A. Jacobs, in Catalysis by Zeolites (B. Imelik et al. ed.) Stud. Surf. Sci. Catal. Vol. 5, Elsevier, Amsterdam, 1980, p. 251.
6 Röbschläger, K.H. and Christoffel, E.G., Ind. Eng. Chem. Prod. Res. Dev., 18 (1979) 347.
7 Röbschläger, K.H. and Christoffel, E.G., Can. J. Chem. Eng., 58 (1980) 517.
8 N.H. Orr, D.L. Cresswell and D.E. Edwards, Ind. Eng. Chem. Proc. Des. Dev., 22 (1983) 135.
9 Röbschläger, K.H., Ph.D. thesis, Bochum, 1979.
10 K.J. Anselmo and R.S. Upadhye, Can. J. Chem. Eng., 61 (1983) 129.

Chapter 2

BASIC PHENOMENA AND CONCEPTS IN CATALYSIS

In chemical reactions bonds between certain atoms are broken and others formed. There are usually many possibilities for this to give a large number of products. However, in biological systems as well as in mass transformations performed by man certain single products are desired. This aim is achieved by the presence of a further substance, a catalyst, within the reactive system.

2.1 HISTORICAL

The term "catalysis" was coined by Berzelius in 1835 when writing his annual report on advances in physical sciences and used to cover a number of physiological and chemical reactions, discovered at that time, all with the common feature that they proceeded in the presence of a further substance which did not itself alter during the course of the reaction. Among these reactions were the oxidation of ethyl alcohol yielding acetic acid and the combustion of hydrogen, both of which take place in the presence of platinum at room temperature, the decomposition of ammonia and hydrogen peroxide in the presence of different metals, the conversion of starch into sugar in the presence of acids or ferments and the cleavage of amygdaline in the presence of emulsine.

Berzelius defined a catalyst as a substance which by its mere presence evokes chemical actions which would not take place in its absence. This definition simply described the observation of the phenomenon, "catalysis", without making any attempt to interpret or explain its nature. The word was formed from a combination of two Greek words, κατα (kata) = down and λυδειν (lysein) = to split or break. 'By "awaking affinities which are asleep" (Berzelius), a catalyst breaks down the normal forces which inhibit the reactions of molecules' (ref. 2). The same word was also used by the ancient Greeks for a riot; perhaps this was one of the reasons why one of Berzelius' colleagues, J. von Liebig strongly argued against this definition, fearing that German authors would put the idea of the catalytic force, which in his mind favoured indolence and laziness, into the heads of the young people (ref. 1). The Chinese word "tsoo mei" (cui mei) which means "marriage broker" perhaps describes more correctly the idea behind what is commonly thought

of as the phenomenon of catalysis (ref. 2). After Berzelius, it took some sixty years until a new definition of catalysis was given by W. Ostwald, based on the knowledge of chemical equilibrium, that all chemical reactions proceed via a number of more or less stable intermediates.

From the point of view of natural philosophy, Ostwald realized that, in the case of catalysis, the "release causality" is valid as opposed to "causal causality". For example, when hydrogen and oxygen combine, the free energy difference causes the liberation of a well-defined amount of energy which is equivalent to the difference of the latent energy of the components and can be exactly calculated ("causal causality"). However, hydrogen and oxygen can exist as a gaseous mixture at ambient temperature for centuries and nothing happens until a burning match or a platinum black catalyst is introduced into the system. This additional, but negligible, effect releases the process ("release causality") which, however, takes place due to the inherent thermodynamics and is not caused by the introduction of the catalyst (or match).

The above chain of ideas has been taken from Schwab's deeply philosophical essay on "History of Concepts in Catalysis" (ref. 3). He correctly remarks "it is unimportant if the releasing substance actually enters into the reaction sequence, e.g. if platinum forms an intermediate oxide or if it remains unchanged and acts merely by its presence". That is the reason why we shall not dwell excessively on the development of ideas in the history of catalysis but will concentrate in forthcoming chapters on how to obtain a deeper insight into this phenomenon of Nature*.

According to Ostwald the phenomenon catalysis can be understood as an acceleration of a thermodynamically feasible reaction through the presence of a substance, the catalyst, which itself is neither essentially altered nor consumed by this chemical action. Further, from thermodynamics it is obvious that a catalyst which increases the rate of the forward reaction of a reversible reaction must also

---

*An interesting recent essay on "The Development of Theories of Catalysis" /K.J. Laidler, Archive for History of Exact Sciences, 35 (1986) 345/ adds much to the above-mentioned sources. It concentrates mainly on pre-Berzelius ideas; on Ostwals's contributions to understanding of catalysis and on the development of theories of homogeneous acid-base catalysis.

increase the rate of the reverse process. Within the frame of this definition the mode of action of a catalyst is suggested in the following way: Rates of homogeneous gaseous reactions are usually expressed according to the Law of Mass Action in the following way:

$$\frac{da_i}{dt} = k(T) \ f(a_i) \qquad (2.1)$$

where $f(a_i)$ is a power function of the individual concentrations, a_i, and k is the rate coefficient. The temperature dependence of k is given by the Arrhenius equation

$$k = A \ . \ exp \ (-A_E/RT) \qquad (2.2)$$

where A is the pre-exponential factor, A_E the activation energy and R the gas constant. The rate coefficient k can, at least in principle, be calculated on the basis of collision or transition state theory. From collision theory, the rate coefficient is given by

$$k = P \ . \ Z_{AB} \ exp \ (-A_E/RT) \qquad (2.3)$$

where P is an empirical steric factor, and Z_{AB} the number of collisions between reactant molecules. The activation energy A_E is that critical energy the reactant molecules must possess to enable the reaction to take place. This is usually depicted as shown in Fig. 2.1, where the potential energy is plotted against the reaction co-
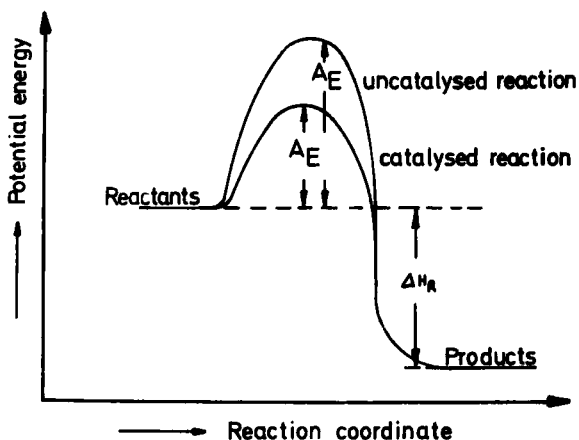
Fig. 2.1. Potential energy profile for a catalyzed and uncatalyzed exothermic reaction.

ordinate. Between the average potential energies of reactants and products an energy barrier exists which can only be surmounted by a small fraction of reactant molecules for which the total colli- sion energy exceeds the activation energy.

The action of the catalyst according to this theory is to dec- rease the activation energy barrier for a certain reaction thus increasing the rate of this reaction because a larger fraction of reactant collisions now hastens product formation (Fig. 2.1). Contrary to the collision theory, the transition state theory con- siders the potential energy of the configuration of the transition state. A reaction sequence is suggested which for a bimolecular reaction is written in the following way:

$$A + B \rightleftharpoons (AB)^{\ddagger} \longrightarrow products$$
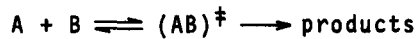
The overall rate of this reaction sequence is obtained assuming steady-state, which means that both reactions proceed at the same rate, and the decomposition of the transition state complex is rate determining. This, together with the first assumption, signi- fies that the first step of the sequence is practically at thermo- dynamic equilibrium. The decomposition rate of the activated comp- lex is expressed in terms of a decomposition frequency

$$\nu = k \cdot T/h$$

where h is Planck's constant and k the Boltzmann constant. The concentration of the activated complex is replaced by reactant concentrations resulting in the following rate equation

$$r = k \cdot T/h \cdot K_P^{\ddagger} \cdot P_A \cdot P_B \qquad (2.4)$$

where $K^{\ddagger}$ is the equilibrium constant

$$K_P^{\ddagger} = \frac{P^{\ddagger}_{AB}}{P_A \cdot P_B} \cdot$$

Introducing

$$-\Delta G^{\ddagger} = \Delta H^{\ddagger} - T\Delta S^{\ddagger} = RT \ln K_P^{\ddagger} ,$$

where $\Delta H^{\ddagger}$ is the standard enthalpy and $\Delta S^{\ddagger}$ is the standard acti- vation entropy, the rate coefficient is given by

$$k = (k \cdot T)/h \cdot \exp(\Delta S^{\ddagger}/R) \cdot \exp(-\Delta H^{\ddagger}/RT). \qquad (2.5)$$

The action of the catalyst within this theory is to decrease the activation enthalpy with respect to the uncatalyzed reaction, which must overcompensate the usually lower activation entropy in the case of the catalyzed reaction.

The definition of catalysis according to Ostwald focuses too strongly upon the rate increasing action of a catalyst in a thermodynamically feasible reaction, because in most cases homogeneous reactions, analogous to the catalyzed reactions, are not observed and therefore homogeneous and catalyzed reactions cannot be compared with one another. Thus uniting both catalysis definitions, that of Berzelius and of Ostwald, we may describe a catalyst as a substance which evokes chemical reactions that would not take place without it and which controls the direction of chemical reactions within the framework of thermodynamic rules.

In addition to this thermodynamic definition of catalysis, several other approaches have been put forward during the last 100 years, including the concept of "intermediate chemical compounds" by Sabatier (a view strongly opposed by Ostwald). We have seen, however, that this concept returns in a modified version in the activated complex theory. The "active site theory" suggested by Taylor in 1925 (ref. 4) postulates that distinct sites on a catalytic surface can interact with the reactants; he also expressed a view that "the amount of surface which is catalytically active is determined by the reaction itself". This implies that different surface complexes have different degrees of binding to the catalyst (see later, in the bond strength requirement in Section 2.2.3.). The geometric theory (ref. 5) attributed the active sites to geometric formation of what were assumed to be perfect crystal planes whereas earlier formulations of the electronic theory regarded surface energetics as more important (in terms of energies of solid state electrons) than surface atoms, as distinct geometric entities. As far as further theories and concepts are concerned the reader is referred to Schwab's historical essay (ref. 3) (where the underlying philosophy is stressed rather than a sequence of dates). A volume concentrating on the history of catalysis (theory and practice) in the United States has also been published (ref. 6).

The achievements in surface science during the last 20-30 years have favored a pragmatic approach to catalysis: instead of proposing new general theories, the accumulation of much detailed data has taken place. A happy exception is Sachtler's recent treatise

(ref. 7) discussed in detail in Section 2.2.3.

Most of the transformations of stable reactants into stable products do not proceed in one step but via highly reactive intermediates through a sequence of "elementary" steps. According to Boudart (ref. 8) these "elementary" steps are single irreducible acts at the molecular level, usually where one bond is opened or formed or simultaneously one bond is formed while another one is opened. Highly reactive intermediates are, for example, carbocations, free radicals and, in catalytic reactions, complexes of reactant molecules with the active centers on the catalyst. The special feature of catalytic reactions is that the active centers are reproduced in the sequence of "elementary" steps through which reactants are converted into products; this means that the same active centers, which are fixed on the catalyst, permanently govern the single events of reactant transformations.

From the concepts described so far, a measure of the activity of catalysts can be indicated by so called turnover-numbers: the number of molecule transformations realized by one active center per unit time. Use of this activity measure presupposes that the total number of active centers per unit weight of the catalyst is known. If there is a distribution of turnover numbers for the single active centers on the catalyst, only mean turnover numbers for the catalyst may be obtained. In reactive catalytic systems, where the number of active centers on the catalyst is constant, the rate of reactant transformations is limited by the sum of turnover numbers of the single active centers. Thus, with increasing reactant concentration in the system, a saturation phenomenon is observed. This means that the reaction rate cannot be increased beyond a certain limit.

Another important feature of catalytic systems is the temporal stability of the active centers. Usually the ability of active centers to converting reactant molecules decreases with the operation time of the catalyst. This deactivation may be caused by impurities in the reactive system or by products which either block active centers, thus decreasing the total number of active centers, or adsorb in the vicinity of active centers, thus changing the energetic configuration around these centers. In addition the catalyst can undergo structural changes.

As was pointed out above, catalysis is the basic principle behind the transformation of matter. There are two large domains for

transformation of matter, energy storage and transformation through chemical reactions, and the transformation of matter with the aim of producing other, new products. Two large systems on earth where matter is converted are the biosphere and man-made chemical reactions. The total energy transformation in the biosphere is approximately 20x10 exp (20) kjoules per annum and that in man-made systems is calculated to be about 12 percent of the energy transformation in the biosphere in 1970 (ref. 9).

The man-made energy flux on earth is mainly chemical based on the conversion of mineral oil, coal, natural gas and uranium. In 1980 the conversion of natural gas reached 1620 billion (10^9) m^3, that of coal 2.8 billion tons, brown coal 0.965 billion tons and mineral oil 3.07 billion tons. The largest part of this energy flux (nearly 75%) is used for heating, with about 20% for transport, while about 7% of the mineral oil is used to produce new materials. Mineral oil is thus one of the most important raw-materials for the chemical industry. The main areas of chemical activity are in agriculture, with the production of fertilizers, plant preservatives and animal food; the petroleum industry, with the production of raw-materials for the petrochemical industries (*e.g.* ethylene, propylene, butene, butadiene, isoprene, aromatics, synthesis gas, gasoline, fuels, tars and lubricants), the food, fine chemicals, detergent and heavy inorganic chemicals industries as well as in pollution control.

It is interesting to note that first industrial catalytic processes (alcoholic fermentation and soap making, known since ancient times) used homogeneous catalysts or enzymes without knowing anything of catalysis. The first "modern" process also used a homogeneous catalyst: nitric oxide to oxidize SO_2 to SO_3 in the earlier ("lead chamber") sulfuric acid manufacture. Heterogeneous commercial processes followed in the twentieth century: first "contact" H_2SO_4 production, then ammonia synthesis, the latter being the first process to utilize the achievements of scientific catalyst development as well as high pressure engineering in the early 1900--s. We may agree with Heinemann (ref. 10) that the major breakthroughs in modern large-scale industrial catalytic processes, that produce presently over 20% of all industrial products, occurred in the last 50 years, starting with catalytic cracking of petroleum products in 1936. An excellent outline of the most important 20-25 industrial catalytic processes (mostly heterogeneous) have been

given in Heinemann's work (ref. 10); it is sufficient to quote his observation that the yearly product values of several processes may each reach 10^9 \$ per year.

The discussion of individual industrial processes in their historical context would be far beyond the scope of this book, but it can be pointed out that the breakthrough started in the 1930's has proceeded since then more or less uninterrupted. All developments were of a slow evolutionary character: developing new, more active, more stable or more selective catalysts for existing processes or finding another product which could be more economically produced by a new, catalytic route. Even the most spectacular development of the last 20-30 years: the introduction of zeolites as large--scale industrial catalysts occurred in this way. "It is a rare event when a whole new field of catalytic applications opens up" (ref. 10). This happened when catalytic automotive exhaust control had to be developed. Exhaust control represents a new class of technological achievement: it applies three-function catalysts which have to operate reliably over a wide range of temperature and gas flow and must possess exceptional stability.

Whereas in biological systems all reactions are catalytic reactions, in man-made systems catalytic reactions prevail only where old materials are transformed to produce new ones. Chemical energy conversion is mainly accomplished by burning the raw materials oil, coal and natural gas; electro-catalytic chemical energy transformation in fuel cells at present is of no importance, but may represent an important future trend. Another potentially important surface process is photochemical fuel production, the tremendous possibilities of which are still dormant (refs. 10,11).

Catalytic systems can be divided into three distinct categories, homogeneous catalysis, where reactants and catalysts are present in the same phase, heterogeneous catalysis, where the catalyst and reactants are present in different phases and enzyme catalysis. Enzymes are catalysts which are produced in living cells and evoke and control a large variety of biochemical reactions. As enzymes retain their activity independently of living organisms they also can be used as catalysts in man-made systems. Irrespective of these categories, the majority of catalytic reactions can be associated with two types of reactions, one where the characteristic step is the transfer of an electron from reactant to catalyst or *vice versa* and the other where the characteristic step is the transfer of pro-

tons or the formation of heteropolar donor-acceptor pairs.

2.2 CATALYTIC SYSTEMS

Of the three kinds of catalytic systems heterogeneous catalytic reactions, on which this book is focused, are by far the most important reactions in man-made chemical conversions. In order to understand in more detail the advantages and disadvantages of heterogeneous catalytic reactions a short survey of the different catalytic systems will be presented in this section. There are three features which determine predominantly the suitability of catalysts in chemical reactions: activity, selectivity and stability. The activity indicates the reactivity of catalytic systems, *i.e.* the rate at which reactants are transformed into products, the selectivity is a measure of the ability of a catalyst to preferentially catalyse one of a number of possible reactions and the stability indicates how long a catalyst will be able to fulfil its action. There are large differences in these characteristic features with the different catalytic systems.

2.2.1 Enzyme catalysis

Enzymes are proteins. The most striking feature of these biocatalysts, which are responsible for all chemical reactions in living systems, is their exceptional selectivity and activity. This can be understood from protein structure (ref. 12). The primary structure of a protein is specified by covalent peptide bonds which link the single amino acids and covalent disulfide bonds which join different parts of the protein chain. Besides these covalent bonds, noncovalent interactions like electrostatic and van der Waals attractions, π-electron stacking and hydrogen bonding, in which the peptide main chain and the amino acid side chains are involved, determine the spatial structure of a protein. Although single noncovalent interactions in proteins are weak the total energy involved is very large because many such interactions exist. The significance of these interactions lies in the fact that they are related to each other by a phenomenon named "cooperativity" which means that the individual noncovalent interactions influence each other in such a way that the second interaction occurs more readily than the first and so on. Through this effect a stable structure of the enzyme is obtained which can also be modified by

further cooperative interactions.

The catalytic function of many enzymes is supported by prosthetic groups (coenzymes) which are generally metal ions or complex organic molecules and which are either weakly or covalently bound to the protein structure. The catalytically active sites in enzymes are specific binding sites which have geometric shapes - very often pockets or grooves - which complement the shapes of the reactants (substrates) converted by this enzyme. Thus, besides the principle of catalysis, molecular shape also plays an important part in biochemical reactions; this is also responsible for the high selectivity of these reactions. The high rate of enzyme-catalyzed reactions is achieved by the conformational adaptability of the enzyme to each of the intermediate steps through which reactants are transformed into products.

Kinetic modelling of enzyme catalyzed reactions usually starts with quite a simple mechanism

$$E + S \underset{k_{-1}}{\overset{k_1}{\rightleftharpoons}} E - S \underset{k_{-2}}{\overset{k_2}{\rightleftharpoons}} E + P$$

where S = substrate, E = enzyme, E - S = enzyme-substrate-complex and P = product. Assuming steady-state and that the second step is rate determining, the so-called Michaelis-Menten equation is obtained

$$v = - \frac{d[S]}{dt} = \frac{k_2 \cdot [E][S]}{K_M + [S]} \tag{2.6}$$

where

$$K_M = \frac{k_{-1} + k_2}{k_1}.$$

At constant enzyme concentration, with increasing substrate concentration, a limiting value, v_{max}, of the reaction rate is obtained, which can be used to eliminate the enzyme concentration. In this case $[S] \gg K_M$ and eq. 2.6 reduces to

$$v_{max} = k_2 \cdot [E]. \tag{2.7}$$

Combining eq. 2.6 and 2.7 we obtain

$$v = \frac{v_{max} [S]}{K_M + [S]}. \tag{2.8}$$

For the evaluation of v_{max} and K_M from experimental data linearized forms of eq. 2.8 are used:

$$\frac{1}{v} = \frac{K_M}{v_{max}} \frac{1}{[S]} + \frac{1}{v_{max}} \tag{2.9}$$

$$v = -\frac{v}{[S]} K_M + v_{max}. \tag{2.10}$$

Eq. 2.9 is the Lineweaver-Burk relation and eq. 2.10 the Eadie-Hof-stee equation. Although the model described so far can be used for the kinetic analysis of single enzyme catalysed reactions, in real biological systems the underlying reaction networks are much more complicated due to mixed culture systems or feed-back or feed-forward control of key enzyme systems which often give rise to bistability or sustained composition oscillations.

Enzyme catalysts are not classified with respect to their chemical nature but according to their catalytic action. In man-made systems enzyme catalysis is used in fermentation processes. A fermentation can be viewed as an enzyme-catalyzed chemical reaction, where the cellular material is the catalyst support. The main applications of these reaction systems are in the production of antibiotics like penicillins, streptomycin, chloramphenicol, erythromycin and nystatin; vitamins, like riboflavin, ascorbic acid and cyanocobalamin and enzymes. Furthermore a continuously growing number of very specific changes in complicated chemical molecules is performed by enzyme catalysts. Other important future areas for the use of microorganisms in man-made systems are the production of proteins for solving food problems on earth, the treatment of industrial and urban waste, the replacement of less selective catalysts in heterogeneous or homogeneous catalytic reaction systems by highly selective enzymes which have been immobilized in insoluble polymers or in membranes or gels, and the storage and transformation of energy.

2.2.2 Homogeneous catalysis

With respect to overall mass transformations in man-made systems enzyme catalytic reactions are at present of little importance: of more importance are homogeneous catalytic reactions which are used nowadays in about 20 major industrial processes (some typical examples being given in Table 2.1) and in numerous small-scale reactions. With homogeneous catalytic reactions the catalysts and reactants are present in one phase and, from an engineering viewpoint, a major disadvantage of this arises from the difficulty in

Table 2.1

Typical industrial homogeneous catalytic reactions.

Reactants	Catalyst	Products	Reaction conditions
Ziegler-Natta process			
$CH_2=CH_2$	$TiCl_4/Al\ R_3$	polyethylene	10-160 atm, 130-270°C
$CH_3CH=CH_2$	$TiCl_3/Al\ R_3$	polypropylene	20-40 atm, 50-85°C
Wacker process			
$CH_2=CH_2+O_2$	$PdCl_2/CuCl_2/HCl_{aq}$	CH_3CHO	4 atm, 120-130°C
Oxo-process			
$CH_2=CH_2+CO+H_2$	$Co_2(CO)_8$	CH_3CH_2CHO	100-200 atm, 140-170°C
$CH_3CH=CH_2+ROOH$	$Mo(CO)_6$	$CH_3CH\overset{}{\underset{O}{\diagdown\diagup}}CH_2$	1 atm, 110°C
CH_3OH+CO	$RhCl_3/CH_3J$	CH_3COOH	30-40 atm, 180°C
C_6H_{12} + air	$Co(OAc)_2$	cyclohexanone + cyclohexanol	10-15 atm, 125-165°C
$ArCH_3$ + air	Co(II) salt	benzoic acid (COOH)	2-3 atm, 120-130°C
p-Xylene + air	$Co(OAc)_2/Mn(OAc)_2/NaBr$	terephthalic acid	15 atm, 225°C
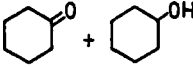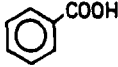
separating the product from the catalyst; this is a particular problem in large-scale conversions with open reaction systems.

Homogeneous catalytic reactions are classified according to the type of catalytically active species and an idealized scheme which also includes enzymes, has been proposed by Nakamura and Tsutsui (ref. 13) and is given in Scheme 2.1. Although there are some examples of homogeneous catalytic gaseous reactions, like SO_2-oxidation in the presence of NO_2 or the decomposition of acetaldehyde in the presence of iodine, most reactions are in the liquid phase and a great deal of scientific research is concerned on the inves-
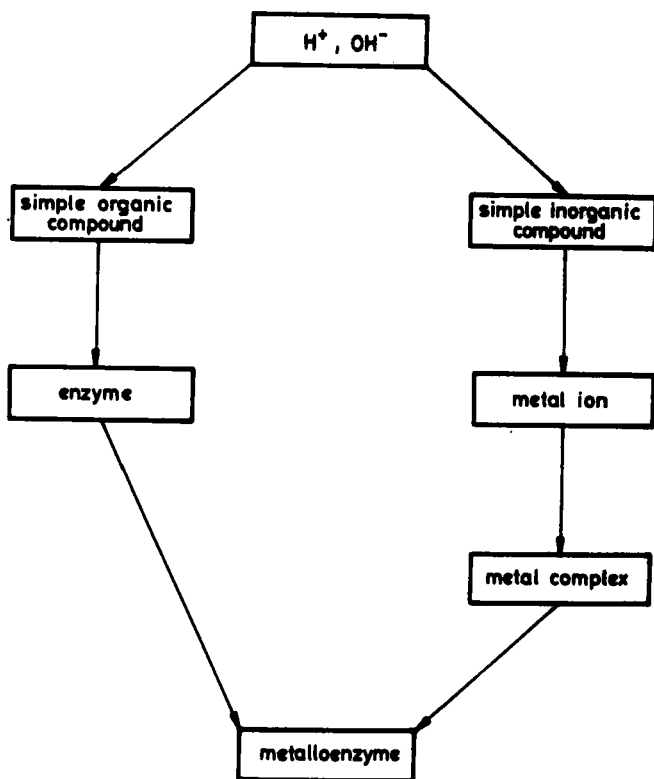
Scheme 2.1

tigation of the mechanisms of transition metal complex catalyzed
reactions. Usually these mechanisms are written in a "clock"-nota-
tion, which clearly indicates the cyclic nature of the catalytic
processes, where in closed sequences the active centers which enter
the reaction sequence are reproduced again during the course of the
series of elementary steps through which reactants are transformed
into products.

One of the characteristics of homogeneously catalyzed reactions
arises from the fact that the catalytically active species may
first be formed in the reaction mixture through a number of preca-
talytic reactions and often an induction period will be required
before conversion begins. The bonding capacity of transition metal
ions and the stability of coordination compounds can be predicted
by the "18-electron-rule" which states that if the nine outer or-
bitals of a transition metal accommodate 18 electrons a stable
complex will be obtained. Donor ligands such as methyl and hydrido
are considered to contribute one, carbon monoxide and phosphines
two, π-allyl-ligands three and π-arene six electrons. The reacti-

vity of transition metal complexes for a large number of olefin polymerization, addition and oxidation reactions and CO-insertion and decarbonylation reactions can be understood in terms of a 16- and 18-electron rule (refs. 14,15) which describes the underlying reaction mechanisms by a series of dissociations and associations of ligands during which the catalytically active species passes through intermediates with 16 and 18 electrons in the nine outer orbitals of the transition metal.

Recently attempts have been made to find analogies between the way the reactant is held in the ligand field of a complex and its adsorption on a heterogeneous surface (refs. 16,17). Alloys provide especially good models, since active metal atoms are surrounded by inactive alloying atoms and thus a limited number of active metal atoms are available for sorption. Various crystal surfaces can be compared with cluster complexes containing more than one metal atom (ref. 17). Further efforts are in progress to elucidate the simi- larities and differences between these systems.

To describe and explain the reactivity - the rate at which homo- geneously catalyzed reactions proceed - a detailed picture is needed which takes into consideration steric and electronic factors like the stereochemistry around a particular atom or ion and the exchange interactions between metal and ligand orbitals as well as generalized donor-acceptor interactions during electron transfer from the highest occupied molecule orbital of the donor to the lowest unoccupied molecule orbital of the acceptor. Although very suitable for discussing in a qualitative way the individual reac- tivities of different catalytic systems, these concepts up to now have not been used for quantitative modelling of the dynamic beha- vior of homogeneous catalytic reactions. For this purpose, one can use either the concept of the rate of elementary steps, which builds up the rate of change of concentrations of stable species measured in the liquid phase, or else a less sophisticated concept where the rate of disappearance of reactant molecules is expressed via power functions of concentrations of stable species in the reaction mixture. In cases where the concentration of the cataly- tically active species is kept constant and the rate of a single homogeneous catalyzed reaction is measured as a function of reac- tant concentrations, as in enzyme catalysis, a saturation phenome- non will be observed due to the limited overall turnover numbers of active centers.

A special feature of homogeneous catalytic transition metal
complex reactions is the enhanced selectivity compared with hetero-
geneous catalytic reactions. This is attributed to the characteris-
tic substrate selectivity which means complex formation with one
compound in preference others; this is less pronounced than with
enzymes but more pronounced than with heterogeneous catalysts. The
different important effects are described in terms of regioselec-
tivity which accounts for effects like the formation of branched
product molecules in favor of unbranched, of enantioselectivity
which accounts for the ability of chiral catalysts (with an asym-
metric carbon) to differentiate between enantiofaces and of dia-
stereoselectivity which accounts for reactions at diastereotopic
sites or on diastereofaces.

Future developments in homogeneous catalysis are, on the one
hand, concerned with the demands of the chemical and energy trans-
formation industries and on the other with the continuous search
for more active and more selective catalysts and the combination of
advantages of the different catalytic systems. Thus the feedstock
basis for the application of homogeneous catalytic conversions
changed in the past from acetylene to olefins and synthesis gas and
will also incorporate in the future the conversion of biomass (ref.
15). To combine the advantages of homogeneous and heterogeneous
catalytic reaction systems, (high selectivity and ease of preser-
ving and reactivating the catalysts), homogeneous catalysts and
heterogenized by anchoring the homogeneous catalysts through coor-
dinating groups like phosphins to polymers like cross-linked poly-
styrene or even to traditional oxidic supports (see, *e.g.* refs.
17,18).

2.2.3 Heterogeneous catalysis

Heterogeneous catalytic reaction systems, in which fluid reac-
tants are passed over solid catalysts, are at present the most
widely used catalytic processes in the man-made transformation of
matter. A number of these processes are listed in Table 2.2. A com-
parison with the results of Table 2.1 indicates that much higher
temperatures are used in heterogeneous catalytic reactions than in
homogeneous catalytic ones. Enzyme catalyzed reactions, on the
other hand, are usually performed at or just above room temperature.
The optimal temperature for penicillin production, for example, is
$25^{o}C$ and above $26^{o}C$ a deactivation of the enzyme system Penicillium
chrysogenum is observed (ref. 20).

Solid catalysts are classified according to their chemical

Table 2.2

Industrial heterogeneous catalytic processes

Processes/ Reactants	Catalyst	Products	Reaction conditions
Petroleum refining processes			
Catalytic re-forming/naphtha	Pt/Al_2O_3-Cl or $Pt/Re/Al_2O_3$-Cl	naphtha with increased octane number	15-30 bar, 470-510°C
Hydrodesulfuri-zation/petroleum fractions	sulfided Co-Mo/Al_2O_3 or sulfided Ni-W/Al_2O_3	sulfur-free petroleum fractions	30-200 bar, 300-430°C
Catalytic cracking large petroleum molecules	Zeolite/silica-alumina	smaller petroleum molecules	3-5 bar, 500-550°C
Petrochemical processes			
ethylene, O_2	supported Ag	ethylene oxide	10-20 bar, 250-300°C
$H_2C=CH_2$,HCl,O_2	supported $CuCl_2$	$ClCH_2$-CH_2Cl	2-4 bar, 220-240°C
benzene, O_2	V_2O_5-MoO_3-H_3PO_4	maleic anhydride	2-5 bar, 350-450°C
Inorganic chemical processes			
N_2, H_2	Fe/Al_2O_3/K_2O/CaO	NH_3	200 bar, 380-550°C
SO_2, O_2	V_2O_5	SO_3	500°C, 1 bar
NH_3, O_2	Pt/Rh	NO	1-10 bar, 850-900°C
CO, H_2	ZnO-Cr_2O_3	CH_3OH	100-350 bar, 240-380°C

nature into metals, semiconductors, insulators and solid acids
(ref. 2), Table 2.3.

Table 2.3

Classification of heterogeneous catalysts (ref. 2).

Class	Catalyzed reactions	Examples
Metals	hydrogenation dehydrogenation hydrogenolysis isomerization cyclization	Pt, Pd, Fe, Ni
Semiconductors	oxidation dehydrogenation desulfurization denitrogenation	NiO, ZnO, MnO_2, Cr_2O_3, Bi_2O_3-MoO_3, WS_2, NiS, CoS, MoS_2
Insulators	dehydration	Al_2O_3, SiO_2, MgO
Solid acids	polymerization cracking isomerization alkylation	zeolites amorphous SiO_2-Al_2O_3

Heterogeneous catalytic reaction systems are preferred for
large-scale industrial conversions which are usually operated as
open reaction systems, *i.e.* as reaction systems with continuous
exchange of matter and energy with the environment. The four basic
reactor types for performing heterogeneous catalytic reactions, the
fixed bed reactor, the fluidized bed reactor, the trickle bed-
-reactor and the slurry reactor, are depicted in Fig. 2.2. In such
systems mass and energy fluxes are coupled with chemical reactions
which occur on the active centers of the catalyst surface. Hence,
a kinetic analysis of these systems must include the concurrence
of rates of surface reactions, the adsorption and desorption rates
of reactant molecules on active sites at the surface and the rates
of physical mass and energy transport processes. Usually with
isothermal reaction systems the following steps are considered;
   1. Diffusion of reactants from the bulk fluid to the external
     surface of the catalyst particle.
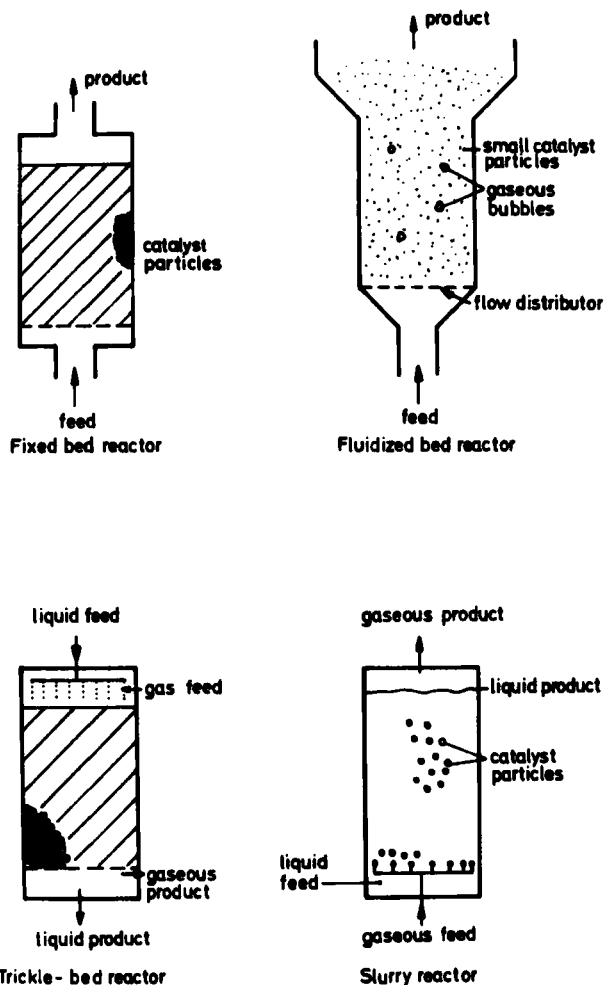
Fig. 2.2. Industrial reactors for performing heterogeneous cataly-
tic reactions

  2. Diffusion of reactants into pores.
  3. Adsorption of reactants on the surface of the solid catalyst.
  4. Surface reaction.
  5. Desorption of products.
  6. Diffusion of products out of the pores.
  7. Diffusion of products from the external surface of the cata-
     lyst particle to the bulk fluid.

In what follows, some basic approaches to the analysis of the dif-
ferent steps are discussed. The first two steps can be understood
in terms of the chaotic kinetic motion of molecules in systems with

and without walls. On a molecular level the surfaces of the cata-
lyst particles are rough. During the flux of molecules, caused by
pressure gradients, along these rough surfaces molecules preferen-
tially collide with surface faces opposite to the direction of
flux. Assuming elastic collisions, where the angle of incidence is
equal to the angle of reflection, after such collisions a fraction
of the molecules near the walls has momentum opposite to the momen-
tum along the direction of flow and thus, by further collisions,
the average velocity of the molecules near the catalyst particle
decreases and a boundary layer is formed around it.
In reactive systems concentration gradients of reactant and product
molecules through this boundary layer occur giving rise to a diffu-
sive flux the rate of which can be described by Fick's law

$$J_1 = -D_{12} \cdot \frac{dc}{dx} \tag{2.11}$$

where J_1 is the diffusive flux [mole/L^2t] and D_{12} the molecular
diffusivity of species 1 in 2 [L^2/t].

In catalytic reaction systems the maximum overall rate of mass
conversion is limited by the total amount of reactant molecule
transformations realized by the sum of the single active centers.
In order to obtain large space-time yields with open reaction sys-
tems it is desirable to use solid catalysts with a large number of
active centers per unit volume. In many cases this is realized by
using highly porous solid materials which are often prepared by
pressing small crystallites into larger catalyst pellets thus gi-
ving rise to a bidisperse pore distribution, with small primary
pores (radii up to 100 or 200 Å) in the original crystallites and
larger secondary pores. Some of the porous materials have surface
areas up to 500 m^2/g. For reactant and product molecules, such ca-
talyst pellets are like a sponge with a complicated interconnected
pore system. Unlike the first step to be considered, the diffusion
through the boundary layer around the catalyst pellet, the second
step, diffusion into the pore system, is a parallel process,
because the individual molecules can always either diffuse into the
pore system or adsorb on the surface. Due to the presence of walls,
in addition to the molecular diffusion transport process which
occurs through molecule-molecule collisions, other transport mecha-
nisms will occur. In pores where the pore diameter is small compa-
red with the mean free path between molecule-molecule collisions,
mass transport through molecule-wall collisions prevails and is

called Knudsen-transport. Molecules which adsorb at the walls and diffuse along the surfaces are transported via a surface diffusion process. In two- or multi-component systems with concentration gradients, where the individual species have different diffusivities, a pressure gradient always develops which is opposite to the concentration gradient of the faster diffusing species and which is balanced by convective flow. In porous systems this is called D'Arcy-flow. Thus in porous systems four different transport mechanisms can be identified.

To use Fick's law to describe the molecular diffusion flux in porous systems, the molecular diffusion coefficient, D_{12}, is multiplied by the porosity, ϵ, of the catalyst pellet and divided through a tortuosity factor, τ,

$$D_{12eff} = \frac{D_{12} \cdot \epsilon}{\tau} \qquad (2.12)$$

to account for the smaller free volume in the porous medium and the longer diffusion distances due to the pore network by which an effective molecular diffusivity is obtained. In a similar way an effective Knudsen diffusivity, $D_{K\ eff}$, can be defined.

An analysis of the superposition of diffusive flux and surface reactions in porous catalysts usually does not consider the different flux mechanisms and structure of the pore network but is based on an effective diffusivity, D_{eff}, which is defined as the ratio of flux through the total cross section (normal to the diffusion direction) to the concentration gradient. Assuming that molecular diffusion and Knudsen diffusion are the only mass fluxes in the porous catalyst and that both processes are in series, the effective diffusivity, D_{eff}, can be related to the effective molecular and the effective Knudsen diffusivity by the Bosanquet equation:

$$\frac{1}{D_{eff}} = \frac{1}{D_{12\ eff}} + \frac{1}{D_{K}\ eff} . \qquad (2.13)$$

The initial step in the adsorption process involves the collision of a gaseous molecule with the surface. The Hertz-Knudsen equation

$$Z = P/(2\pi mkT)^{1/2} \qquad (2.14)$$

relates the impact rate, Z, usually expressed as molecules $s^{-1}\ cm^{-2}$, to the gas pressure, P, with k the Boltzmann constant, T, the gas temperature and, m, the mass of the gaseous molecule. In general, there are about 10^{15} atoms per cm^2 of surface. Assuming that the

sticking probability is unity with nitrogen at 300 K and a pressu-
re of 1 Pa, each surface site will be impinged 3.10^3 times per
second. The sticking probability, which is defined as the ratio of
the rate of molecule capture in the adsorbed state to the impact
rate on the surface, is for many surfaces considerably less than
unity and decreases further with increasing surface coverage. The
amount adsorbed per unit area of the catalyst surface is uniquely
determined by the temperature and equilibrium pressure of the gase-
ous molecules. Under isothermal conditions the amount adsorbed can
be directly related to the pressure of the gaseous phase.

Adsorption and surface reaction are processes occurring in
series. Thus, in cases where surface reactions are rate determi-
ning, at steady-state conditions the adsorption step is practically
at equilibrium and to model the overall rate we need to know the
equilibrium relationship between the concentration of gaseous mo-
lecules and amount adsorbed. The Langmuir model is the simplest
for deriving a theoretical isotherm. Assuming that (i) the catalyst
surface is energetically uniform, (ii) adsorption is restricted to
a monolayer, (iii) there is no interaction between adsorbed mole-
cules and (iv) the total number of adsorption sites is constant
under all experimental conditions, the adsorption rate can be ex-
pressed as

$$r_{ad} = k_{ad} \cdot p \cdot (1 - \theta)$$

and the desorption rate as

$$r_{des} = k_{des} \cdot \theta.$$

At equilibrium both rates are equal and the Langmuir isotherm is
obtained

$$\theta = \frac{K_{ad} \cdot p}{1 + K_{ad} \cdot p} \qquad (2.15)$$

where θ is the fraction covered by adsorbed molecules and

$$K_{ad} = \frac{k_{ad}}{k_{des}}$$

is the adsorption equilibrium constant. If equilibrium adsorption
is followed by a surface reaction the overall rate is given by

$$r = k_s \cdot \theta = \frac{k_s \cdot K_{ad} \cdot p}{1 + K_{ad} \cdot p} \qquad (2.16)$$

where k_s is the rate constant of the surface reaction. Eq. (2.16)
corresponds to eq. (2.8), derived for the kinetics of single enzy-
me reactions, because both equations follow from equivalent under-
lying reaction mechanisms, assuming that steady-state has been
achieved and that the second step is rate determining. With an ad-
sorption-surface reaction the reaction mechanism is

$$A + l \rightleftharpoons Al \rightleftharpoons Bl \rightleftharpoons B + l$$
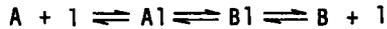
where l represents a free active center on the surface and Al and
Bl are surface complexes. With the third step, the desorption of B,
the active center, l, is regenerated.

Replacing the assumption of the Langmuir model, that the surface
is energetically uniform, by the assumption that the adsorption
heat decreases linearly with increased coverage the Temkin isotherm
is obtained

$$\Theta = k_1 \cdot \ln(p \cdot k_2) \qquad (2.17)$$

where k_1 and k_2 are constants at a given temperature. A further
frequently used adsorption heat decreases logarithmically with
increased coverage.

$$\Theta = k \cdot p^{1/n}. \qquad (2.18)$$

The single steps in heterogeneous catalytic reactions discussed so
far may disguise the actual surface reaction mechanism. The most
important step in the sequence, however, is the chemical transform-
ation step of reactants on the surface. The concept of adsorption-,
desorption- or diffusion-disguised surface reactions stems from the
fact, that very often only the rate of change of species concent-
ration in the fluid phase is accessible to measurement and no in-
formation can be obtained regarding the concentrations of the ac-
tual surface complexes. In investigating mechanisms of surface reac-
tions due to this "disguise", reaction step(s) may appear in the
fluid phase which do not actually occur on the surface. A striking
example of this adsorption/desorption "disguise" was described by
Weisz (ref. 21) who considered the following reaction scheme

$$
\begin{array}{ccccc}
A+l & & B+l & & C+l \\
\updownarrow & & \updownarrow & & \updownarrow \\
Al & \rightleftharpoons & Bl & \rightleftharpoons & Cl
\end{array}
$$
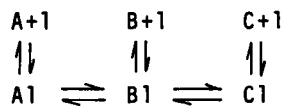
where Al, Bl, Cl are surface complexes. In cases where the rates of

the surface reactions are small, compared with the rates of adsorption and desorption in the gaseous phase, a reaction in series is observed similar to that taking place on the catalyst surface. If the surface reaction rates are fast, compared with the rates of adsorption and desorption in the gaseous phase, a parallel reaction is observed

$$A \underset{C}{\overset{B}{\lessgtr}}$$

because in this case equilibrium between the surface complexes is established.

A detailed understanding of surface reactions needs information about the active centers on the solid catalyst and the structure of the surface complexes formed during conversion of reactant molecules to product molecules. Even identifying the active centers is a difficult task because their concentration is usually 10^{-3} or less of the total surface atoms. For example an impurity in the bulk of solid material at a concentration of 1 ppm will give rise to about 20 monolayers when distributed on the surface of a solid of volume 1 cm^3. Much progress in both identifying active centers and determining the structure of actual surface complexes has been made with the development of improved UHV-techniques and techniques for preparing clean surfaces and also by applying a large number of different spectroscopic methods to the investigation of solid surfaces and the structure of surface complexes.

The systematic studies of Somorjai and his group have to be mentioned here; they combined the catalytic chemist's views with several high vacuum methods of the surface scientist in order to obtain new information from both sides of the problem (see, *e.g.*, refs. 22-24). They developed a combined system to study catalytic reactions in a sealed chamber at pressures of between 10^{-7} and 10^2 Torr *i.e.* over almost ten orders of magnitude (ref. 22). Mostly single crystals were studied this way. Before and after reaction, the reaction chamber was removed, the space evacuated, and the sample subjected to common ultrahigh vacuum measurements, including LEED and Auger-electron spectroscopy. In this way reaction rates, selectivities, *e.g.* transformations of cyclohexane or n-hexane over Pt single crystal faces (ref. 24), as well as concomitant changes in surface structure and composition could be followed without removing the sample from the closed apparatus. Although detailed

discussion of such works is beyond the scope of the book, some
recent important achievements will be quoted when appropriate.

The selectivity of solid catalysts is usually analyzed in terms
of electronic and geometric factors. In considering reactant mole-
cule-catalyst surface interactions, Sachtler (ref. 7) classified
into four main categories the requirements a catalyst must fulfil
in order to catalyze one reaction path among a number of thermo-
dynamically feasible reactions: bond strength, coordination, en-
semble and template requirement. The benefit of such a classifica-
tion lies in the separation of the different effects although, in
reality, the reaction path is determined by the combined action of
all these effects resulting finally in a low activation energy
barrier, and an increase in the rate of this particular reaction
step.

The bond strength requirement considers the strength of the
chemisorptive bond which is determined by the electronic characte-
ristics of the atoms and molecules involved in forming the surface
complex and thus combines the older electronic factor concept with
the energetic aspects of the multiplet model (ref. 25). The other
three requirements account for geometric demands. The coordination
requirement considers the coordination sites per surface atom which
may be classified by ^1M, ^2M, ^3M, where the superscipt indicates the
degree of coordinative unsaturation. The ensemble requirement con-
siders whether a single surface atom or ensemble of several adja-
cent atoms is involved in the surface reaction and the template
requirement accounts for the stereochemical properties of an active
center which must be satisfied in order to produce stereo-specific
products (see also Section 3.1.3).

Solid catalysts, when used in chemical reactions, must usually
be activated to display the desired activity and selectivity; the
actual activity and selectivity under operational conditions
depends not only on this activation procedure but also on the total
history of the catalyst including all preparation procedures. Thus
with man-made solid catalysts it is rather difficult to attain a
certain catalyst activity and selectivity which is the same for
differently produced catalyst charges.

Enzymes for example in biological systems are synthesized with
a very high degree of reproducibility. In biological systems
usually hundreds of enzyme-catalyzed reactions proceed simultaneo-
usly and these must be harmonized with one other. Besides control-
ling a single enzyme activity by regulating its quantity, there are

three main ways of regulating enzyme activity, through multienzyme complexes, through energy-dependent covalent modification of enzymes and through the binding of small molecules to the enzymes to act either as activators or inhibitors.

In heterogeneous catalytic reaction systems the analogous phenomenon to enzyme inhibition is catalyst deactivation; this, however, usually serves not to establish a certain desired activity and selectivity, but to determine the long-term stability of a catalyst. One of the aims in investigating the characteristics of solid catalysts is to find catalysts with long-term stability or find procedures that will restore the original activity and selectivity of solid catalysts after some degree of deactivation. Catalyst deactivation is caused either by changes in the catalyst structure due to extreme (or even normal) operating conditions, by impurities in the reactant feed, or by side or following reactions during reactant conversion. Like mass and energy transport processes, deactivation reactions superimpose the occuring surface reactions, but in most industrial applications deactivation reactions proceed over a much longer time-scale than the desired surface reactions. It was just such time scale differences that served as the basis for a novel analysis of catalytic processes using three time scales: the fastest time scale applies for adsorption--desorption-surface reaction phenomena; the second for the residence time of molecules in the catalytic reactor and the third and longest time scale for slow processes like slow overlayer accumulation on the surface, frequently associated with irreversible changes of the catalyst, *e.g.* deactivation (ref. 26). A quantitative parameter space analysis has been reported using an extended Langmuir-Hinshelwood reaction scheme (ref. 27).

2.3 LABORATORY STUDIES OF HETEROGENEOUS CATALYTIC PROCESSES

As outlined in the previous section, the majority of large-scale processes in chemical and refinery industries are based on heterogeneous catalytic reactions. Improvement in existing processes or the introduction of new ones is mostly a result of the development of new catalysts or the modification of existing ones. The four main tasks of laboratory studies in this context (catalyst preparation, catalyst screening, scale-up from laboratory equipment to pilot and industrial plants and process optimization) are depicted

TASKS OF LABORATORY   COMPLEX REACTION   LABORATORY REACTORS
INVESTIGATIONS OF
HETEROGENEOUS
CATALYTIC PROCESSES

o catalyst preparation
                                  o species   o microcatalytic pulse reactor
o catalyst screening
    o catalytic activity   o gaschromatographic reactor
    o selectivity   o reaction mechanism
    o stability   o single pellet diffusion reactor

o scale-up   o reaction kinetics   o catalytic fixed bed reactor

o process optimization   o recycle reactor

Scheme 2.2

in Scheme 2.2 (ref. 28). For straightforward catalyst preparation
detailed information about the reaction mechanism, by which the
reactive species are interconverted, is needed and that means know-
ledge of the nature of the active sites, of the structure of surfa-
ce complexes and of reaction trajectories through which the surface
complexes are transformed. In principle, reaction mechanisms can be
investigated by both kinetic and nonkinetic methods. The great
problem with kinetic methods is how to find correlations between
the empirical rate model and the true kinetic model and/or the
underlying mechanism (ref. 29). Using kinetic methods for the eva-
luation of heterogeneous catalytic reaction mechanisms, the rate
at which all individual elementary reactions - the physical steps
involved - contribute to the overall rates of macroscopically ob-
servable changes of species concentration in the fluid phase will
have to be measured. This presupposes the application of non-
-steady-state operation conditions and sophisticated experimental
equipment which not only allow the rates of change of concentra-
tions in the fluid phase but also the rate of change in concentra-
tions of surface intermediates to be obtained. Until now only a
few such studies have been completed (ref. 30). Frequently non-ki-
netic methods are employed as very often a large number of species
occur in the reaction mixture. Among these are the spectroscopic
methods by which either single steps like the chemisorption of a
species are usually investigated or samples are withdrawn from the
reactive system at certain times and conclusions obtained from the
comparison of the different results. Another non-kinetic method is

the method of model compound reactions, where product distributions
from model compounds are compared with product distributions assu-
ming certain reaction mechanisms.

The next three tasks of laboratory studies, catalyst screening,
scale-up from laboratory equipment to large-scale industrial pro-
cesses and process optimization are the main topics of chemical
engineering studies. To perform these studies much attention is
focused on mathematical modeling and on model predictions of the
characteristics of the reactive system under consideration and of
the performance of larger scale reactors on the basis of data from
laboratory reactors, for which parameter estimation procedures and
statistical evaluations of obtained parameters and models are
needed. Quite often, however, these mathematical models are applied
in a very formal manner without sufficient consideration of the
basic chemical transformation steps in the catalytic reactions.

Screening of catalysts takes place in order to find the most
suitable catalyst for use in a given industrial process; this means
that the most active, stable and selective catalyst has to be se-
lected. Although access to quantitative and reproducible experimen-
tal results is indispensable in every case, catalyst screening
demands a degree of comparison which means that standardization of
all procedures, under which certain properties of the catalyst are
measured, must be carried out. Several research groups are engaged
in this field (refs. 31-34); the progress, however, achieved so far
is not great and depends mainly on the complex concurrence of mass
and energy fluxes with adsorption and reaction on the catalyst sur-
face in multicomponent reaction systems and also on the fact that
the actual activity and selectivity of any catalyst will depend on
its history. The activity of the European Research Group on Cata-
lysis (ref. 34) resulted in the preparation of a standard SiO_2
supported Pt catalyst ("EUROPT-1") which has been characterized by
several methods (refs. 35-38) and also used in various catalytic
reactions. For characterizing the activity of solid catalysts three
kinds of measurement can be used. The most reasonable means of
determining the activity and selectivity of a catalyst is to use
turnover numbers which indicate the number of molecules converted
per unit time by an active center. Despite the great progress made
in the last few decades to adapt spectroscopic methods to the
investigation of catalytically active solid surfaces under reaction
conditions, reliable turnover numbers are very difficult to obtain
under the conditions encountered in industrial processes. The

two kinds of measurement are (i) rate constants and ratios of rate
constants of a suitable reaction scheme, by which the dynamic beha-
vior of the reactive system can be described over a range of ope-
rating conditions, and (ii) the temperature at which a certain con-
version is obtained or the conversion which is obtained at a cer-
tain temperature. Measures of the last kind, although frequently
applied in industry, are rather unreliable, especially in case of
catalysts with widely varying activity, because, for example, the
reaction mechanisms may change with increasing temperature or the
rates of physical transport processes may contribute in a different
manner to the obtained product distributions, and thus rather comp-
lex phenomena are compared on the basis of a single point in the
reaction space. In contrast to this, rate constants are collected
over a larger range of operating conditions and therefore enable a
better-founded indication of catalyst activity and selectivity to
be obtained.

There are three approaches to study chemical kinetics. The
first is based on a knowledge of the stability and reactivity of
atoms and molecules involved in the chemical reaction; in practice,
however, excessive computing expense is required especially with
complex reaction networks. The second is based on the concept of
elementary reactions which, weighted by a set of stoichiometric
coefficients, provide a framework for dynamic modeling of the ob-
servable rate of change of the mixture composition. The elementary
reactions are defined by a set of stoichiometric coefficients and
a rule which relates the reaction rate to species concentration and
temperature. The third concept directly relates the rate of change
of composition of the mixture to the concentration of the indivi-
dual species in the reaction mixture usually by power law functions,
the relation being limited only by stoichiometric requirements. As
the second approach considers the underlying reaction mechanism it
is to be preferred for characterizing catalyst activity and selec-
tivity.

For catalyst screening, as well as for scale-up and process op-
timization, information is needed on catalyst activity, selectivity
and stability. The necessary measurements are usually obtained in
laboratory reactors which mostly represent scaled-down versions of
large industrial ones. In accordance with the foregoing considera-
tions, the kinetic analysis should be performed in three steps (de-
picted in Scheme 2.3, ref. 28). Firstly, the underlying reaction
mechanism is examined. The way of doing this is to begin by ana-

```
                        ┌─────────────────────┐
                        │ Kinetic Investigation │
                        └─────────────────────┘

┌──────────────────┐      ┌──────────────────┐      ┌──────────────────────┐
│ Evaluation of the │──────│ Constructing of a │──────│ Parameter estimation │
│ reaction mechanism │      │ mathematical model │      └──────────────────────┘
└──────────────────┘      └──────────────────┘
```
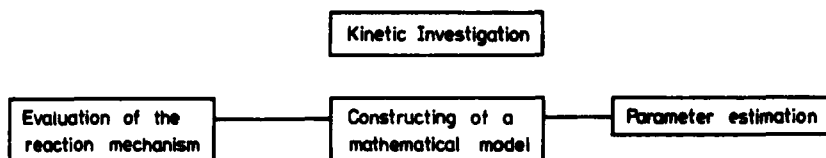
Scheme 2.3

lyzing the reaction mixture and then find out the directed graphs
by which the single species are connected. Very simple reaction
schemes are frequently used for mathematical modeling, as the reac-
tor models of catalytic reforming process simulations reveal (refs.
39-41) for example. Nevertheless, more extensive knowledge of the
actual reaction mechanism is preferable, to demonstrate the condi-
tions by which the complex underlying reaction mechanism can be
broken down into a simple reaction scheme which is sufficient for
modeling reactor dynamics and for understanding the physical mea-
ning of model parameters which are derived from these simple
schemes.

A major problem connected with the evaluation of reaction mecha-
nisms is catalyst deactivation. In industrial processes catalysts
are normally activated by a given procedure, reaction conditions
are only varied to a small extent, and catalyst deactivation pro-
ceeds on a much longer time scale than any interconversion of reac-
tants. In contrast, laboratory studies involve the change of reac-
tion conditions over a wide range where catalyst deactivation is a
more difficult problem and quite often rates of deactivation and
reactant conversion are on the same time scale. As reaction mecha-
nisms provide the framework for constructing the kinetic model to
describe the dynamics of the reactive system, the question is
whether and how to incorporate the deactivation reaction steps into
this system. There are two possibilities to be considered: either
by some tedious running-in procedures an activity and selectivity
level of the catalyst is obtained which is constant over a certain
reaction time and remains the same with different catalyst charges,
or, where no constant activity and selectivity level of the cata-
lyst can be achieved, an arbitrary activity level of the catalyst
is chosen and the data are recalculated for this activity level.
In the first situation there is always a large uncertainty as to
whether the activity and selectivity level of the catalyst in a
certain reactor configuration is the same as in other reactor confi-
gurations or in larger-scale reactors. In the second situation only

poor quality kinetic data can be obtained. If a reaction mechanism
without deactivation steps is considered then, with nonseparable
kinetics, the data will be inconsistent in every case (refs. 42,43)
and, even if deactivation steps are incorporated into the reaction
network, the rate constants may be concentration-dependent and thus
usually are not amenable to quantitative evaluation. The concept of
separable complete rate equations was introduced by Szépe and
Levenspiel (ref. 42). According to them the reaction rate of deac-
tivating reaction systems can be described by an equation of the
form:

$$\text{rate} = f \text{ (present conditions, past history).} \qquad (2.19)$$

If eq. (2.19) can be rewritten into the form

$$\text{rate} = f \text{ (present conditions).q (past history)} \qquad (2.20)$$

it is called separable, which means that the kinetics of the reac-
tion under consideration is unchanged by deactivation.

The second step involves a suitable mathematical model, which
consists of two parts: selection of a reaction rate model and deri-
vation of a reactor model. To model the reaction rate either power
function or hyperbolic models are usually employed which account
for competitive adsorption. The advantage of hyperbolic or Langmuir-
-Hinshelwood-Hougen-Watson (LHHW) models over power function models
was discussed by Boudart (ref. 44) who pointed out that these
LHHW-models enable a better description of the dependence of over-
all reaction rates on temperature and partial and total pressures.
In cases where the denominators of the LHHW-models are the same for
all rate equations, they can be factorized and pseudo-mass action
rate equations obtained (ref. 45). If the denominators are diffe-
rent in the individual rate equations, they can be described by the
reaction time and the selectivity behavior of the catalyst follo-
wing from pseudo-mass action rate equations. Concentration profiles
along the length of the reactor can be obtained from a relation
between the real and the fictive reaction time (ref. 46). Thus, as
with heterogeneous catalytic reactions, pseudo-mass action kinetics
may play an important role. The laboratory reactors listed in
Scheme 2.2 are usually operated as open reaction systems. The reac-
tor model considers the effects of rates of physical processes on
the measured conversions. As the kinetic analysis, especially of
complex reaction networks, is considerably simplified if the reactor

model is quasi-identical with the reaction rate model, the time variable only being replaced by a space variable, the operating conditions are frequently chosen in such a way that concentration and temperature gradients in the catalyst pellet and at the phase boundary are negligible and the dispersion effects in the fluid phase can be ignored. In Table 2.4 some criteria are listed which enable tests for transport limitations in experimental catalytic reactors to be carried out (refs. 47,48). Some of these criteria are connected with the effectiveness factor usually symbolized by η, which is defined as

$$\eta \equiv \frac{\text{rate of reaction with pore diffusion influence}}{\text{rate of reaction with surface conditions}} . \qquad (2.21)$$

Madon and Boudart (ref. 54) recently developed a further criterion, suggested first by Koros and Nowak (ref. 55), to assess whether measured catalytic activity is independent of the influence of transport phenomena. This criterion states that

$$\frac{\text{rate of reaction}}{\text{concentration of catalytically active material}} = \text{constant} \quad (2.22)$$

when no transport phenomena govern the observed values. The concentration of the catalytically active material can be expressed as the mass fraction of active material, its surface area or the number of surface moles per unit mass of the whole catalyst. The last of these gives the most exact definition in terms of turnover number; the experimental determination of the true active surface represents, however, the most difficult experimental problem. Madon and Boudart (ref. 54) consider the Koros-Nowak criterion for cases of mass or heat transport, interphase and intraparticle transport, for liquid and gas phase reactions.

The last step of kinetic analysis involves the estimation of model parameters; today this is most frequently carried out using computer programs which contain parameter estimation procedures of suitable objective functions and statistical testing procedures. A comparison of results obtained from different parameter estimation methods can be made on the basis of the cost of determining the set of experimental data, of the goodness of fit of the calculated to the experimental data and of the uniqueness of the model parameters which is affected by model, numerical and experimental errors.

Some laboratory reactors, listed in Scheme 2.2 are better suited than others to perform the single steps of kinetic analysis. Their

advantages and disadvantages will be discussed in more detail in Chapter 4.

A final word on the basic concepts in catalysis will be devoted to mathematical modeling. It has been pointed out earlier that mathematical models are used for catalyst screening, scale-up and process optimization procedures. With these aims, the main interest

Table 2.4

Criteria for testing transport limitations in experimental catalytic reactors (refs. 43,44)*.

Rate limiting phenomenon	Criterion	Literature
Intraparticle transport		
isothermal pellet $\eta \geq 0.95$ if:	$\dfrac{r \cdot R_p}{C_s \cdot D_{eff}} < 1$	Weisz and Prater (ref. 49)
no temperature gradients in particle if:	$\dfrac{\lvert \Delta H \rvert \cdot r \cdot R_p^2}{\lambda \cdot T_s} < \dfrac{T_s \cdot R}{A_E}$	Anderson (ref. 50)
with endothermic or exothermic reactions and power-law kinetic $\eta = 1 \pm 0.05$ if:	$\dfrac{r \cdot R_p^2}{C_s \cdot D_{eff}} < \dfrac{1}{(n - \dfrac{A_E}{R \cdot T_s} \cdot \dfrac{(-\Delta H) D_{eff} \cdot C_s}{\lambda T_s})}$	Kubota and Yamanaka (ref. 51)
Interphase transport		
absence of heat transport limitation in the film round the particle if:	$\dfrac{-\Delta H \cdot r \cdot R_p}{h \cdot T_b} < 0.15 \dfrac{R \cdot T_b}{A_E}$	Mears (ref. 52)
absence of mass transport limitation through film for isothermal cases and first-order reactions if:	$\eta \cdot k/k_c \cdot a < 0.1$	Carberry (ref. 53)
Interparticle transport		
absence of significant dispersion effects if:	$\dfrac{L}{d_p} > 20 \dfrac{k_b \cdot \tau}{Pe_a}$	Mears (ref. 47)

*) Meaning of symbols

r = observed reaction rate per unit particle volume

R_p = particle diameter

D_{eff} = effective diffusion coefficient

C_s = concentration at external surface of catalyst particle

T_s = absolute temperature at catalyst surface

A_E = activation energy

R = gas constant

ΔH = heat of reaction

λ = thermal conductivity of particle

n = integer exponent in power law rate expressions

h = heat transfer coefficient

T_b = temperature in bulk fluid

k = intrinsic rate constant per unit particle volume

k_c = mass transfer coefficient between fluid and particle

a = external surface area of catalyst particle per unit particle volume

Pe_a = axial Peclet number (= ratio of convective to dispersive transport)

τ = space time

d_p = particle diameter

L = length of catalyst bed

k_b = apparent rate constant per unit bulk catalyst volume

in mathematical modeling is focused on obtaining values of the model parameters by fitting experimental data because, otherwise, no quantitative comparison of activity and selectivity of catalysts or model predictions of the behavior of the reactive system in other reactor configurations is possible. Quite often the need to be able to determine the model parameters results in severe modification of the original models; this is achieved by simplifying assumptions by which, for example, large reaction networks can be resolved into quite simple reaction schemes.

On the other hand, mathematical modeling can also be a tool to increase our understanding of the space-time structure of reactive catalytic systems as documented, for example, in the work of Prigogine and co-workers (refs. 56-58). By considering possible conservations of symmetry of the space-time structures of reactive systems against transformations in space and time the usual chemi-

cal approach to understanding chemical reactions, on the basis of
atom and molecule properties, can be decisively extended and shape
principles can be incorporated. One of the fundamental ideas in the
history of mathematics was the introduction of space coordinates
as a reference system in the Middle Ages. This concept has also
been used to describe chemical reactions, replacing the space
coordinates by species coordinates by which a composition space is
obtained. This can be illustrated by the reversible triangle
network:

Assuming monomolecular reactions among the three species A_1, A_2
and A_3, the network gives rise to dynamic behavior which is descri-
bed by the following set of differential equations:

$$\frac{da_1}{dt} = -(k_{21} + k_{31})a_1 + k_{12}a_2 + k_{13}a_3$$

$$\frac{da_2}{dt} = k_{21}a_1 - (k_{12} + k_{32})a_2 + k_{23}a_3 \qquad (2.22)$$

$$\frac{da_3}{dt} = k_{31}a_1 + k_{32}a_2 - (k_{13} + k_{23})a_3.$$

Using matrix and vector notation eq. (2.22) can be rewritten.
We put

$$\alpha(t) = \begin{bmatrix} a_1(t) \\ a_2(t) \\ a_3(t) \end{bmatrix} \text{ and } K = \begin{bmatrix} -(k_{21}+k_{31}) & k_{12} & k_{13} \\ k_{21} & -(k_{12}+k_{32}) & k_{23} \\ k_{31} & k_{32} & -(k_{13}+k_{23}) \end{bmatrix}$$

and obtain

$$\dot{\alpha}(t) = K \cdot \alpha(t). \qquad (2.23)$$

For geometrical representation of eq. (2.23) two constraints must
be considered which are connected with chemical reactive systems:
(i) the Law of Mass Conservation applies and this means that

$$\sum_{i=1}^{n} a_i = 1 \qquad (2.24)$$

where a_i is the mole fraction of the species A_i and (ii) no nega-
tive.species concentrations can arise

$$a_i \geq 0. \qquad\qquad (2.25)$$

Furthermore the reactive system contains a thermodynamic equilib-
rium which is an attractor to all non-equilibrium states. This
means that, with progress in reaction time, the composition of the
reactive system will vary until the equilibrium point is attained.

   In the composition space described by eq. (2.24) and (2.25) all
possible compositions of the reactive three-component system are
restricted to a triangle which can be constructed through the com-
position points (1, 0, 0), (0, 1, 0) and (0, 0, 1) (Fig. 2.3.).
The entries of the composition vector α, which is directed from
the origin to the reaction plane where all possible composition
points are located, are the single concentrations expressed as mole
fractions of the species from which the reactive system is built
up. Thus a point in the composition space represents a composition
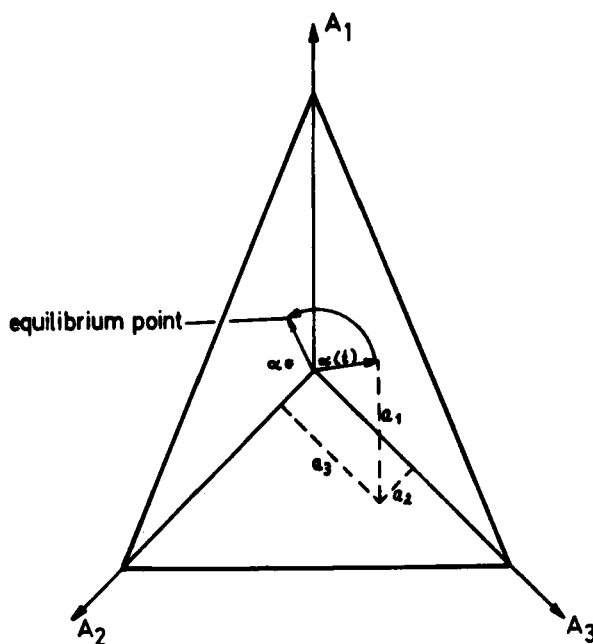
Fig. 2.3. Reaction plane of a three-component reactive system in
the composition space, α^* denotes the equilibrium composition vec-
tor.

of the reactive system. The geometrical meaning of eq. (2.23) is, that an operator K, the rate constant matrix, acts upon an arbitrary initial composition, causing a rotation and a change in length of the composition vector until the equilibrium point is attained. Some reaction paths on the reaction plane of a reversible three component system are depicted in Fig. 2.4. There are some directions in the composition space where the action of the rate constant matrix operator only causes a change in length without rota-
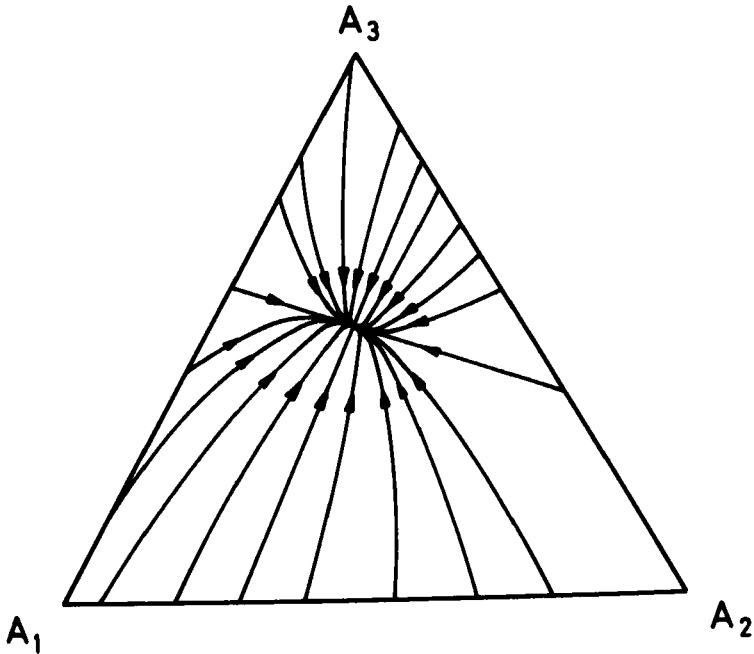
Fig. 2.4. Reaction paths on the reaction plane of a reversible three-component system.

ting the composition vectors; this means that the application of the operator, K, on these composition vectors results in the same vectors multiplied by a constant. These vectors are called eigenvalues or characteristic roots of the operator K. In reversible n-component systems there always exist n such eigenvectors (ref. 45). With the reactive system under consideration one eigenvector is the equilibrium vector which can be observed experimentally, and which has an eigenvalue of zero, whereas the two other eigen-

vectors do not represent realizable compositions. Initial compositions, however, which are located in a plane spanned by the equilibrium vector and one of the other eigenvectors of K, remain in this plane while shifting with time to the equilibrium point thus producing straight line reaction paths on the reaction plane. The proof of this follows directly from the eigenvalue equations. The mathematical analysis described so far, predicts the occurence of straight line reaction paths on the reaction plane and it will be demonstrated in later sections that these straight line reaction paths can also be observed with reactive chemical systems.

Of course, the reaction trajectories cannot move arbitrarily in the composition hyperplane: they should always approach an equilibrium concentration. Thus, a region of the composition triangle can be defined as the area of "accessible composition" with a given feed composition. Thermodynamic analysis has also shown that even the direction of reaction trajectories cannot be arbitrary: they should be directed in such a way that the free energy along them should always decrease (ref. 59). Intermediates in a catalytic system, which are often present in very small amounts (like surface species the concentration of which may be well below detection limits), may <u>couple</u> reactions which are apparently linear and independent of each other. For example, the reactions $A \rightleftharpoons B$; $A \rightleftharpoons C$ represent a pair of separate reactions the sum of which results in $2A \rightleftharpoons B+C$. However, if these processes occur via an intermediate, M: $2A \rightleftharpoons M \rightleftharpoons B+C$, reaction trajectories are possible that otherwise would be forbidden thermodynamically. Changing reaction temperatures would shift the equilibrium points, thus the area of accessible composition could be expanded. Shape-selectivity imposes another constraint in terms of diffusivity: If, for example, the diffusivity of B in the set of reactions $A \rightleftharpoons B$; $B \rightleftharpoons C$ is close to zero in the pore, then the overall reaction outside the pore will be $A \rightleftharpoons C$. This is permissible in terms of free energy but cannot be realized with equally accessible sites for A, B and C. In a sense, shape selective catalysts can be (hypothetically) substituted by a semipermeable membrane which does not let product B pass. The authors (ref. 59) remind the reader of the fact that shape selective catalysts imitate Nature: where, for example, enzymes are embedded in semipermeable membranes in living tissues. There is still a lot to discover about how selective diffusion can modify accessible compositions and kinetic trajectories.

REFERENCES

1   A. Mittasch, Chemische Novitäten, (1935), Heft 4/5, 169.
2   G.C. Bond, Heterogeneous Catalysis, Principles and Applicati-
    ons, Oxford University Press, 2nd ed., 1986. The quotation has
    been taken from p. 2.
3   G.-M. Schwab, in J.R. Anderson and M. Boudart (Editors),
    Catalysis Science and Technology, Vol. 2, Springer, Berlin,
    1981, p. 1.
4   H.S. Taylor, Proc. Royal Soc., London, A108 (1925) 105.
5   A.A. Balandin, Z. phys. Chem., B2 (1929) 289.
6   B.H. Davis and W.P. Hettinger, Jr. (Editors), Heterogeneous Ca-
    talysis. Selected American Histories, ACS Symp. Series No. 222,
    American Chemical Society, Washington, 1983.
7   W.M.H. Sachtler, Faraday Disc. Chem. Soc., 72 (1981) 8.
8   M. Boudart, Kinetics of Chemical Processes, Prentice Hall,
    Englewood Cliffs, 1968.
9   A.L. Lehninger, Ber. Bunsenges. Phys. Chem., 84 (1980) 943.
10 H. Heinemann, in J.R. Anderson and M. Boudart (Editors), Cata-
    lysis Science and Technology, Vol. 1, Springer, Berlin, 1981,
    p. 1.
11 J.-M. Lehn, in Proc. 8th Internat. Congr. Catal., Berlin
    (West), 1984, Vol. 1, p. 63.
12 G.G. Hammes, Enzyme Catalysis and Regulation, Academic Press,
    New York, 1982.
13 A. Nakamura and M. Tsutsui, Homogeneous Catalysis, John Wiley
    and Sons, New York, 1980.
14 C.A. Tolman, Chem. Soc. Rev., 1 (1972) 337.
15 G.W. Parshall, Homogeneous Catalysis, John Wiley and Sons, New
    York, 1980.
16 E.L. Muetterties, T.N. Rhodin, E. Bard, C.F. Brucker and W.R.
    Pretzer, Chem. Rev., 79 (1979) 91.
17 J.K.A. Clarke and A.C.M. Creaner, Ind. Eng. Chem. Prod. Res.
    Dev. Chem. Rev., 20 (1981) 574.
18 Yu.I. Yermakov, B.N. Kuznetsov and V.A. Zakharov, Catalysis by
    Supported Complexes, Stud. Surf. Sci. Catal. Vol. 8, Elsevier,
    Amsterdam, 1981.
19 Yu.I. Yermakov and L.N. Arzamaskova, in L. Cerveny (Editor)
    Catalytic Hydrogenation, Stud. Surf. Sci. Catal. Vol. 27,
    Elsevier, Amsterdam, 1986, p. 459.
20 S. Aiba, A.E. Humphrey and N.F. Millis, Biochemical Engineer-
    ing, Academic Press, New York, 1973.
21 P.B. Weisz, Adv. Catal., 13 (1962) 137.
22 G.A. Somorjai, Chemistry in Two Dimensions: Surfaces, Cornell
    Univ. Press, Ithaca, 1981.
23 G.A. Somorjai and F. Zaera, J. Phys. Chem., 86 (1982) 3070.
24 G.A. Somorjai, in Proc. 8th Internat Congr. Catal. Berlin
    (West), 1984, Vol. 1, p. 113.
25 A.A. Balandin, Adv. Catal., 19 (1969) 1.
26 H.S. Chang and M. Aluko, Chem. Eng. Sci., 39 (1984) 37.
27 M. Aluko and H.S. Chang, Chem. Eng. Sci., 39 (1984) 51.
28 E.G. Christoffel, Cat. Rev.-Sci. Eng., 24 (1982) 159.
29 J.M. Smith, Ind. Eng. Chem. Fundam., 21 (1982) 327.
30 K. Tamaru, Dynamic Heterogeneous Catalysis, Academic Press,
    London, 1978.
31 A.H. Neal, in B. Delmon *et al.* (Editors) Preparation of Cata-
    lysts, Stud. Surf. Sci. Catal. Vol. 3, Elsevier, Amsterdam,
    1979, p. 719.
32 G.K. Boreskov, Ibid., p. 723.
33 G.C. Bond, R.L. Moss, R.C. Pitkethly, K.S.W. Sing and R.
    Wilson, Ibid., p. 715.

34 E.G. Derouane, Ibid., p. 727.
35 G.C. Bond and P.B. Wells, Appl. Catal., 18 (1985) 221;
18 (1985) 225.
36 J.W. Geus and P.B. Wells, Appl. Catal., 18 (1985) 231.
37 A. Frennet and P.B. Wells, Appl. Catal., 18 (1985) 243.
38 P.B. Wells, Appl. Catal., 18 (1985) 259.
39 H.G. Krane, A.B. Groh, B.L. Schulman and J.H. Sinfelt, in Proc.
5th World Petrol. Congr., 1959, p. 39.
40 W.S. Kmak, AICHE Meeting, Texas, March 1971.
41 M.P. Ramage, K.R. Graziani and F.J. Krambeck, Chem. Eng. Sci.,
35 (1980) 41.
42 S. Szépe and O. Levenspiel, Proc. 4th Europ. Symp. Chem. React.
Engineering, Pergamon Press, London, 1971, p. 265.
43 A. Löwe, Chem. Ing. Tech., 52 (1980) 777.
44 M. Boudart, AICHE J., 2 (1956) 62.
45 J. Wei and C.D. Prater, Adv. Catal., 13 (1962) 203.
46 A.M. Kugelmann and J.C. Bonacci, J. Catal., 39 (1975) 10.
47 D.E. Mears, Ind. Eng. Chem. Proc. Des. Develop., 10 (1971) 541.
48 J.J. Carberry, Ind. Eng. Chem., 56 (1964) 39.
49 P.B. Weisz and C.D. Prater, Adv. Catal., 6 (1954) 143.
50 J.B. Anderson, Chem. Eng. Sci., 18 (1963) 147.
51 H. Kubota and Y. Yamanaka, J. Chem. Eng. (Japan), 2 (1969) 238.
52 D.E. Mears, J. Catal., 20 (1971) 127.
53 J.J. Carberry, AICHE J., 7 (1961) 351.
54 R.J. Madon and M. Boudart, Ind. Eng. Chem. Fundam., 22 (1982)
470.
55 R.M. Koros and E.J. Nowak, Chem. Eng. Sci., 22 (1967) 470.
56 I. Prigogine, C. George, F. Henin and L. Rosenfeld, Chemica
Scripta, 4 (1973) 5.
57 P. Glansdorff and I. Prigogine, Thermodynamics of Structure,
Stability and Fluctuations, John Wiley, New York, 1971.
58 I. Prigogine, Vom Sein zum Werden, Piper, Munchen 1979.
59 R. Shinnar and C.A. Feng, Ind. Eng. Chem. Fundam., 24 (1985)
153.

This Page Intentionally Left Blank

Chapter 3

INVESTIGATION OF HETEROGENEOUS CATALYTIC REACTION SYSTEMS

The objectives of investigating heterogeneous catalytic reaction systems are twofold: for fundamental reasons, so that a better understanding of the basic phenomena of catalytic reactions may be obtained and why they occur or for more practical reasons, such as applying catalytic reactions in man-made transformations of matter and to study in detail how matter is converted by means of catalytic reactions. The following presentation is mainly concerned with methods for studying heterogeneous catalytic reactions that can be carried out with the laboratory reactors listed in Scheme 2.1 (Chapter 2), and with the underlying theoretical concepts and therefore focuses on practical aspects. For the same reason, spectroscopic and temperature-programmed methods will only be very briefly considered. Of the several techniques used today for the investigation of surfaces, these few examples were selected as being potentially suitable for detecting surface intermediates.

3.1 INVESTIGATION OF REACTION MECHANISMS

The methods for studying reaction mechanisms of heterogeneous catalytic reactions encompass a large number of more or less sophisticated approaches from the application of surface spectroscopies to the investigation of gas-solid interfaces and the mathematical analysis of concentration versus space velocity data from continuously operated fixed bed reactors. In an attempt to classify the different methods, model compound reactions are considered, where product distributions, obtained from model compound conversions, are compared with theoretical product contributions derived by assuming certain reaction mechanisms.

3.1.1 Spectroscopic Methods
In the last few decades a large number of spectroscopic methods for the analysis of solid surfaces have become available. This can be seen in the "Probst diagram" (Fig. 3.1), where the excitation of the sample by various probes is represented by ingoing arrows, and possible responses to these excitations by outgoing ones. Each combination of arrows constitutes, in principle, at least one
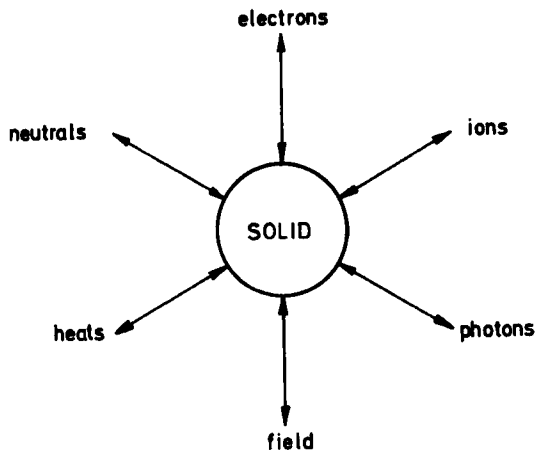
Fig. 3.1. The "Probst diagram".

method for studying the solid surface. There are many more possible
techniques, however, because single combinations of in and out
arrows may give rise to different spectroscopies depending on the
properties of the probe and the emitted particle. A number of
these spectroscopic techniques are listed in Table 3.1 (refs. 1-5).

In order to understand in detail reaction mechanisms of reactant
molecule transformations through surface complex intermediates, it
is necessary to elucidate the microscopic processes on the surfa-
ces. As indicated in Table 3.1 with spectroscopic methods the sur-
face structure, surface topography and surface composition of solid
materials can be determined. Furthermore the structure of adsorbed
molecules and the binding between solid surface and adsorbents can
be evaluated. Thus surface spectroscopy provides the means of stud-
ying   heterogeneous catalytic reaction mechanisms at the molecu-
lar level. However, for elucidating the mechanisms of "real" hete-
rogeneous catalytic systems, *i.e.* of man-made catalytic transform-
ations, surface spectroscopic methods so far only provide an
approach, which is restricted to the investigation of clean, well-
-defined, and mostly non-reactive systems under low pressures,
whereas industrial catalytic systems deal with solid surface com-
positions, that are unknown, and polycrystalline surfaces and
pressures $>10^5$ Pa, as delineated in Table 3.2 (ref. 6).

As outlined in previous sections, catalysis is a dynamic pro-
cess which proceeds through different intermediates and therefore
direct information about these intermediates should be obtained

under non-steady state reaction conditions. A further difficulty in identifying reactive intermediates on solid surfaces stems from the fact that stable adsorbed molecules are much more abundant on these surfaces than reactive intermediates, and the surface concentration of the latter species may be too low to be observed. Thus the application of spectroscopic methods has contributed very much to the investigation and understanding of the nature of active centers on solid catalysts. However, until now, unambiguously identified reactive intermediates on solid surfaces have only rarely been obtained.

Of all spectroscopic methods, those which can be termed "vibrational spectroscopies" can be regarded as the most promising in catalytic studies. These methods (infrared- or IR-, Raman, electron energy loss spectroscopies, neutron scattering *etc*.) generate excitations in the vibrations of interatomic bonds. In this way, surface active groups, like surface hydroxyls, acidic sites *etc*. can be studied, and probe molecules can be used whose adsorption on characteristic surface sites (often thought to be identical to "active sites") may give useful information about surface states. Two valuable reviews summarizing the literature up to the early 1980's have been published recently (refs. 7,8). *In situ* observations of surface intermediates proper occupy little space in these reviews. Such data start to appear more frequently in the mid-1980's.

IR spectroscopy has a great advantage compared with other spectroscopic processes, namely it does not require a high vacuum. However, it has its disadvantages, too. For example, some reactant and surface species do not present infrared bands in a wavelength range where most catalytic materials and/or supports are transparent. Also, the preparation of sufficiently thin wafers of catalysts - which often have to be self-supporting and should contain enough catalytically active material - is not a simple task. Several types of infrared cell have been constructed (refs. 9-12), permitting *in situ* measurements during catalytic reactions. They are usually suitable for measurements between high vacuum (10^{-6} Torr) and near-ambient pressures. A high-pressure system has been reported recently (ref. 11); it applies a cylindrical IR-reflecting crystal embedded in the high pressure reactor. The IR beam enters the cylinder and undergoes total reflectance several times. At each point of reflection the penetration depth into the surrounding solution is 1...1.5 μm and this short cell pathlength collects

TABLE 3.1

Surface spectroscopies (refs. 1-4).

Spectroscopy (acronym)	Probe (input)	Measurement (output)	Information on
Emission: electron spectroscopy			
- Ultraviolet photoemission spectroscopy (UPS)	monochromatic UV-photon beam ($\sim$20 eV)	electron emission $vs.$ energy	surface states, direction of bonds, valence state of ion
- X-ray photo-emission spectroscopy (XPS or ESCA)	monochromatic X-ray ($\sim$1,5 keV)	electron emission $vs.$ energy	surface composition, valence state of ion
- Auger electron spectroscopy (AES)	electron beam ($\sim$3 keV)	derivative electron emission $vs.$ energy	surface composition, valence state of ion
- Ion neutralization spectroscopy (INS)	helium ions (5 eV)	electron emission $vs.$ energy	surface states
- Field emission spectroscopy (FES)	electric field ($\sim$3x10^7 V/cm)	electron emission $vs.$ energy	surface states, direction of bonds, crystal structure
Scattering electron spectroscopy			
- Energy loss spectroscopy (ELS)	monoenergetic electrons ($\sim$1 keV)	derivate electron emission $vs.$ energy loss	transitions between surface states
- Soft X-ray appearance potential spectroscopy (SAPS)	monoenergetic electrons ($\sim$10-1000 eV)	derivative total X-ray yield $vs.$ incident electron energy	surface states, composition, valence state of ion
Electron diffraction			
- Low energy electron diffraction (LEED)	monoenergetic electrons (10-1000 eV)	angular distribution of elastically scattered electrons	surface crystallography

Spectroscopy (acronym)	Probe (input)	Measurement (output)	Information on
Photon spectroscopy			
- Infrared spectroscopy (IR)	monochromatic infrared photons $[(2-50) \times 10^{-2}$ eV]	absorption $vs.$ wavelength	occupied surface states, structure of adsorbed molecules
- Optical spectroscopy	monochromatic photons (0.5-6.5 eV)	absorption $vs.$ wavelength	occupied surface states, structure of adsorbed molecules
- Extended X-ray absorption fine structure (EXAFS)	monochromatic X-ray photons (few keV from a synchrotron)	modulation of the absorbed photon intensity $vs.$ energy	coordination number, atomic distances, nature of surrounding atoms (heavy nuclei)
Ion back scattering spectroscopy			
- Secondary ion mass spectroscopy (SIMS)	ions (~1 keV)	sputtered ion current $vs.$ mass-to-charge ratio	surface composition (as function of depth)
- Rutherford back-scattering spectroscopy (RBS)	helium ions (few MeV)	backscattered He^+ ions $vs.$ energy	surface states and composition

TABLE 3.2

Relation between surface science and catalysis

	Surface science	Industrial catalysis
Surface composition	clean surface	undefined surface (promotors?)
Surface structure	single crystal	polycrystalline ("active sites"?)
Pressure	$<10^{-2}$ Pa	$>10^5$ Pa

information on what happens on the other side of the reflecting cylinder, *i.e.* in the reactor space. Homogeneous catalytic reactions such as cobalt-catalyzed carbonylations as well as zeolite syntheses have been followed this way. Of course, the reflected beam represents a rather noisy and weak signal and hence a Fourier-transform IR spectrometer with a data collection is a prerequisite for proper data processing. Most *in situ* infrared catalytic studies reported so far involve reaction partners having intense IR bands in easily detectable regions: NO or CO*. When evaluating these data one has to be careful to remember that the surface species we see is not necessarily identical with the intermediate responsible for the chemical reaction. Other additional measurements are necessary to confirm the information obtained.

The performance of *in situ* infrared spectroscopy will now be illustrated by a few examples. When CO_2 is hydrogenated over supported Rh (ref. 13) or Ru (ref. 14) the vibrations of surface formate ions, C-H groups, surface hydrocarbonate and adsorbed CO can be identified in the IR spectrum. The presence of Rh is necessary for the formation of surface formate; however, its surface concentration was higher on Rh/Al_2O_3 than that corresponding to the number of surface metal atoms and was zero on Rh/SiO_2 (ref. 13). This means that surface formate is a by-product which migrates to the alumina support from Rh (ref. 13) and Ru (ref. 14); the situation is similar with supported Pd (ref. 15). The wavenumber of adsorbed CO is characteristic of linear CO adsorption on Rh and Ru; in addition, bridged CO also appears on Pd. CO is a dissociation product of CO_2; if CO_2 is removed from the gas phase, the absorption band of adsorbed CO also disappears. The wavenumber values of this CO are shifted to lower values compared with the pure M - CO band; the authors suggest that this is due to the formation of an H - Rh - CO type surface species, because the same shift is observed when CO_2

---

*Of the 472 papers that appeared on vibrational spectroscopy on catalysts in 1985, 187 deal with transmission IR spectroscopy; of these, CO is the probe molecule in 75 and NO in 16 which represents about 50% of the total. Carbonyl vibrations represent a large fraction of the probe molecules in the remaining 50%. In addition, the vast majority of HREELS papers (45 out of 58 items) deal also with CO. /J. Mink, Plenary Lecture, Sixth International Conference on Fourier-Transform Spectroscopy, Vienna, August 1987; Microchim. Acta (1988) in press./

and H_2 are coadsorbed. This may be the precursor of surface carbon, another, IR-inactive, intermediate of methane formation. The presence of the latter could be demonstrated by its hydrogenation off the catalyst.

In another study of the same group, the role of surface isocyanate was studied in the reaction between NO + CO (refs. 10,16). This species - showing an intense IR band - does not play an important role in catalytic NO reduction. It migrates to the SiO_2 support from the Pt (ref. 10) or Rh catalyst (ref. 16) and decomposes above about 400 K. However, its IR spectrum demonstrates that chemisorbed oxygen increases its thermal stability, thus, the possibility that it is a real surface intermediate under dynamic conditions, in excess oxygen, cannot be excluded.

An *in situ* kinetic and IR study of CO oxidation on Group VIII metal/SiO_2 (ref. 17) involved temperature programming of the catalysts after various pretreatments and monitoring the IR spectra of adsorbed CO and simultaneous reaction rate measurements. With increasing temperature on Rh/SiO_2, linearly adsorbed CO predominated. The intensity of its IR band decreased and, upon ignition, a very small band corresponding to CO, adsorbed in all likelihood on a higher oxidation state of Rh, remained. Upon cooling, all IR bands reappeared, that corresponding to linear CO decreased, and the doublet of the dicarbonyl species became noticeably more intense. The position of the CO bands also indicated the predominant oxidation state of Rh. Simultaneous rate measurements indicated that the CO oxidation rate decreased according to the sequence Rh(0)>Rh(I)>Rh(I-III). In addition formation of surface oxides strongly inhibited CO oxidation on Ru and Pd.

In transient response studies (for details, see Section 4.5), changes following a step-change in the concentration of one of the reactants have been monitored. For IR studies, an extremely low volume IR cell was constructed (ref. 12). When a He flow through a wafer of Pt/SiO_2 catalyst was replaced by a mixture of 5% O_2/He, adsorbed CO_2 showed a further slight increase whereas the intensity of adsorbed CO decreased. At steady-state (after 10 s!) the bands of adsorbed CO_2 disappeared, those of adsorbed CO reached a higher constant intensity. Thus, this step-change resulted in the formation and abrupt desorption of a "slug" of CO_2 which was in a vibrationally hot state. Upon passing CO_2 alone, the above transient phenomena were not observed (ref. 12). Another IR cell for transi-

ent studies is shown in Fig. 4.37.

3.1.2 Temperature Programmed Methods

These methods are typically non-steady-state methods involving heating of the catalyst sample according to a - usually linear - temperature programme. The sample is placed in a stream of inert gas or the temperature programme is applied to a single crystal sample under vacuum. Information is usually obtained by detecting mass signal(s).

If a gas is adsorbed previously on the catalyst, gradual heating causes its desorption. With increasing temperature, the desorption rate increases, reaches a maximum and then decreases as the surface is depleted of adsorbate (ref. 18). (Temperature Programmed Desorption, TPD, or Thermal Desorption Spectroscopy, TDS.) If the same gas has more than one adsorbed form on the surface, the number of such "desorption peaks" will correspond to the adsorbed forms. For example, four types of adsorbed hydrogen were identified on platinum black (ref. 19); the number of desorption peaks and their exact position is still a matter of debate. The method can be used for, *e.g.*, reducing the catalyst (Temperature Programmed Reduction, TPR); then the gas flow contains hydrogen and its consumption is detected. Also, Temperature Programmed Oxidation, TPO, is often applied.

There are ample data in the literature describing how quantitative information - adsorption energy, kinetic order, energy of activation, preexponential factor of desorption *etc.* - can be obtained from TPD spectra (ref. 18). TPD, TPR, TPO and other versions are very often used for catalyst characterization. From our point of view, *i.e.* for investigating reaction mechanisms, the various methods of Temperature Programmed Reaction Spectroscopy, TPRS, are more interesting. Here, one gas can be adsorbed and a second reactive gas (or its mixture with an inert gas) can be used as a carrier (Temperature Programmed Reaction, TPR). In the Temperature Programmed Surface Reaction, TPSR, two gases are coadsorbed and their surface reaction is monitored while the catalyst is heated in an inert atmosphere (ref. 18). TPRS proper involves the adsorption of a relatively complex molecule on a catalyst. This is then heated in an inert atmosphere or vacuum and the desorption of various species - reactant itself and various products - is monitored (ref. 20). For example, when n-hexane is adsorbed on a Pt-containing catalyst and then heated, unchanged n-hexane, unsaturated C_6-hydro-

carbons fragments and benzene can be detected by mass spectrometry (refs. 20-22). The situation is analogous to other n-C_6 reactants; Fig. 3.2 shows the desorption spectra observed with n-1,4-hexadiene
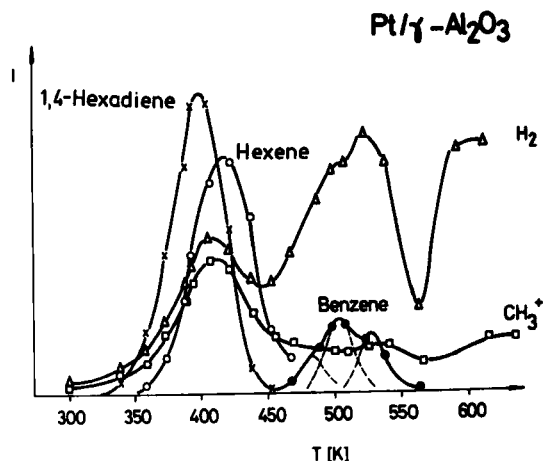
Fig. 3.2. Temperature Programmed Reaction Spectra obtained with adsorbed 1,4-hexadiene. Reproduced with permission from (ref. 21).

reactant (ref. 21). Here hexenes appear as hydrogenation products. Note that hydrogen leaving the surface exhibits peaks parallel to those of benzene. This does not indicate that the $C_6H_{10} \rightarrow C_6H_6$ + + $2H_2$ occurs simultaneously at the temperatures of desorption but that both products of this reaction leave the catalyst simultaneously, even if the reaction took place on the surface at lower temperatures. If perdeuterated n-heptane is adsorbed, only the third peak in the triple benzene peak system was accompanied by the desorption of D_2 (ref. 20) indicating that hydrogen gas may also have originated from the "hydrogen pool" on the catalyst surface. Benzene gives a single desorption peak with n-hexane and a triple desorption peak system with n-hexene, n-hexadienes as reactants on Pt/Al_2O_3. Pt-black gives a triple peak system with n-hexane, too. The desorption temperatures are 483, 503, 527 K on Pt/Al_2O_3 (n-hexane gives a peak at 503 K) and 428, 448, 467 K on Pt-black (ref. 21). This indicates a common rate-determining step in aromatization for each starting open-chain hydrocarbon. The peak systems of benzene obtained after adsorption of cyclohexane, cyclohexene and cyclohexadiene were different from those of open-chain reactants and

also differed from each other (ref. 22). Thus, benzene formation
from n-hydrocarbons and C_6-cyclics should have different rate-de-
termining steps and the formation of C_6-cyclics from n-hexene or
n-hexane as surface intermediates is unlikely.

TPRS spectra can also supply quantitative values for the surface
process: energies of activation, preexponential factors and even
turnover numbers can be calculated (ref. 23).

The method of TPRS provides evidence about what happens on the
surface proper but, in addition to being a non-steady-state process,
it has another disadvantage: the adsorbed phase reacts in the ab-
sence of gas-phase reactants and astoichiometric components often
influencing the observed reactions - as hydrogen does in the pro-
cess of aromatization - are also absent. This latter disadvantage
has been overcome by introducing Scanning Kinetic Spectrometry
(SKS; ref. 24) which, in its design, is related to the TP methods
carried out in high vacuum systems: single crystal surfaces are
used for adsorption and/or reaction and the mass signal is obtained
by a mass spectrometer placed in the vicinity of the active surfa-
ce. SKS uses a crystal, which, prior to the experiments has been
completely saturated with reactant. A molecular beam of reactant is
then directed at the catalytic crystal under a definite angle - $60°$
from the surface normal in (ref. 24) - whose temperature is then
raised according to a pre-selected programme. A multiplex quadru-
pole mass spectrometer is mounted normal to the crystal surface
and detects products and reactants leaving the surface. The main
disadvantage of the conventional TP methods is thus eliminated by
providing a continuous reactant supply to the surface. Reactant
consumptions are indicated by negative peaks; the appearance of
products (due to chemical reactions) or that of the reactant (due
to desorption processes) by positive peaks. Figure 3.3 shows spect-
spectra of CD_3OH, CD_3OD, D_2 and CO arising when CD_3OH flux was di-
rected to a Ni(111) crystal. Peak α corresponds to the desorption
of unchanged CD_3OH; β to a recombinative desorption of methanol
(note that this is the only peak in the CD_3OD spectrum). The pre-
cursor of CD_3OD must be a CD_3O adspecies ($cf.$ γ_1 on the CD_3OH
spectrum). This decomposes into CO and H adsorbed on the surface;
recombination and desorption of H-atoms corresponds to the γ_2 nega-
tive peak, the desorption of CO, corresponds most likely to the γ_3
peak of the CD_3OH spectrum. It can be estimated that - at a speci-
fic CD_3OH flux of 4×10^{12} cm^{-2} s^{-1} - 16% of the surface species
gives CD_3OH, 23% CD_3OD, whereas 61% decomposes into CO and D. On a
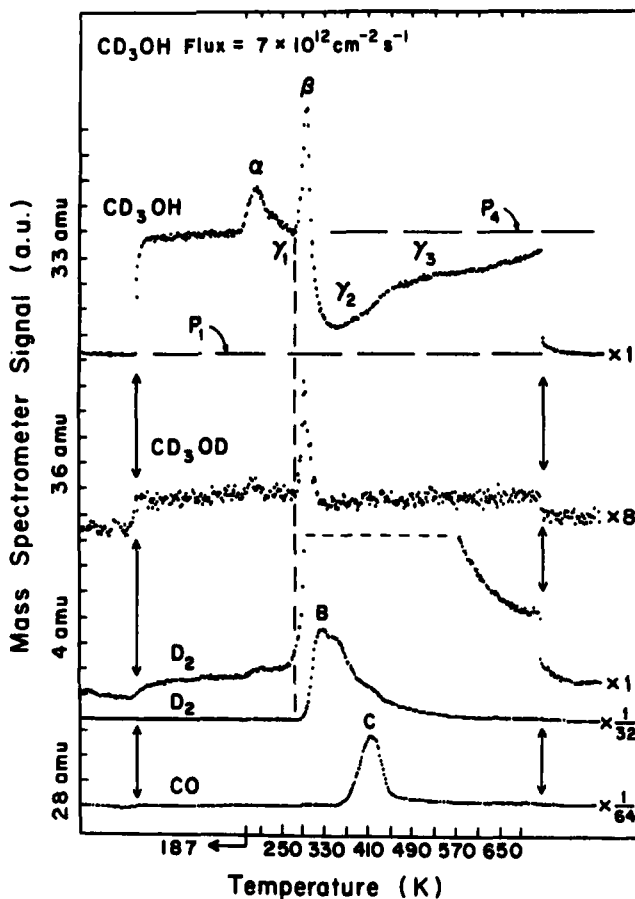
Fig. 3.3. Scanning Kinetic Spectra for CD₃OH incident on Ni(111). The crystal was exposed to 10^{16} cm^{-2} CD₃OH at 187 K prior to experiment. Reproduced with permission from (ref. 24).

Cu(111) crystal, a selective decomposition into CD_2O could also be observed.

3.1.3 Model Compound Reactions

Model compound reactions are very frequently used to investigate reaction mechanisms of heterogeneous catalytic reactions, to classify the activity and selectivity of catalysts under non-deactivating and deactivating conditions and to study the nature of active centers and reactive surface complexes. The procedure is the following: taking account of all available knowledge regarding the chemical reaction under consideration, possible theoretical reaction trajectories are formulated. In the second step, model

compounds are chosen in such a way that the obtained product dist-
ributions enable discrimination among rival mechanisms, and finally,
theoretical and experimental product distributions are compared.
Quite often these experiments are carried out using micro-pulse
reactors (see Chapter 4) where 100-500 mg of catalyst is placed in
a small tube reactor and reactant pulses of 0.1 - 5 µl size are
swept through the catalyst bed by the continuous flux of carrier
gas. The analysis of the products is performed by gas chromatog-
raphy or gaschromatograph-mass spectrometer systems to which the
micropulse reactor is coupled. The application of this method will
now be demonstrated by some examples:

Example 3.1: Mechanism of methylcyclopentane ring opening on acidic
catalysts. Conversions of hydrocarbons on bifunctional noble
metal/acidic carrier-catalysts or on acidic zeolite or amorphous
Al_2O_3-SiO_2-catalysts belong to the largest scale catalytic processes
in the petroleum refinery industry. The transformations of hydro-
carbons on acidic catalysts are discussed in terms of mechanisms
with carbocations as the reactive intermediates. Two classes of
carbocations exist which are designated as threefold-bonded
"classic" carbenium ions or fivefold coordinated "nonclassical"
carbonium ions. While nonclassical carbocations have been identi-
fied in superacids by NMR-spectroscopy their existence has not been
proved in heterogeneous catalytic gaseous reactions, although
mechanisms with carbonium ion intermediates have been postulated
in a number of investigations to account for measured product dist-
ributions. According to Olah (ref. 25), the attack of a proton
from the acidic catalyst on a -C-C- or a -C-H-sigma bond of the
hydrocarbon may result in a two-electron--three-center bonding,
Scheme 3.1, and this protonolysis will be the first step in isomeri-
zation and C-C-bond scission on acidic catalyst centers.
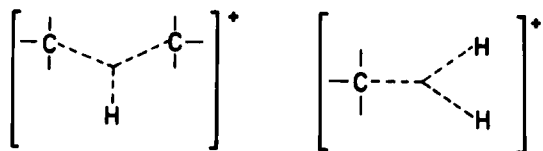
Scheme 3.1

Protonolysis of C-C-bond results in cleavage of the C-C-bonds with
formation of a smaller alkane and a carbenium ion whereas C-H-bond
protonolysis is followed by splitting off the hydrogen and reforma-

tion of a carbenium ion. Carbenium ions either undergo cleavage at the β-position, or react with C-H- or C-C-bonds or isomerize *via* C-C or C-H delocalizations.

The most important differences between mechanisms in which carbenium ions and carbonium ions are involved and the classical formulations of carbenium ion mechanisms are (1) direct scission of protonolyzed C-C-bonds, (2) direct formation of carbenium ions from alkanes via C-H-bond protonolysis and subsequent cleavage of H_2 (with the classical formulations it was difficult to explain the formation of carbenium ions from alkanes by proton attack. Usually it was assumed that the carbenium ions were formed from interaction of olefins with the acidic catalyst), (3) formation of protonated cyclopropanes in the transition state of carbenium ion rearrangements, which are more stable than primary carbenium ions.

An indication of the type of carbocation intermediate can be obtained from product distributions of C_5-ring naphthenes as model compounds. In Figure 3.4 (ref. 26) we see histograms of the methylcyclopentane product distributions from its conversion on a 0.5 wt% Pt/γ-Al$_2$O$_3$ catalyst, a partially deactivated 0.5 wt% Pt/γ-Al$_2$O$_3$ (where the platinum function, due to a pretreatment procedure with hydrocarbon conversions at 530°C has lost its isomerization, cyclization and hydrogenolysis activity) and the acidic γ-Al$_2$O$_3$ carrier of these catalysts. Over highly dispersed platinum a nonselective or statistical cleavage of the methylcyclopentane takes place (refs. 27-29), by which n-hexane, 2-methylpentane and 3-methylpentane are formed in a molar ratio of 2:2:1, whereas acid catalyzed ring opening of methylcyclopentane yields n-hexane as the main product. This latter result can be interpreted in terms of a mechanism in which a C-C-ring bond is directly protonolyzed by a proton (ref. 30). Due to the stabilizing effect of the methyl group, the most probable transition state is as shown in Scheme 3.2, which further reacts with the formation of a secondary carbenium ion with n-hexane structure. This carbenium ion either stabilizes through proton abstraction, by which n-hexene is formed, or through hydride ion abstraction from an alkane, by which n-hexane is formed. Thus the experimental observation, that n-hexane is the main product of acidic catalyzed methylcyclopentane ring opening, can be accounted for by assuming a nonclassical carbocation intermediate. However, the above experimental findings also fit with a mechanism which involves classical carbenium ions and their β-scissions (ref. 31). There are four possible carbenium ions with a methylcyclopentane
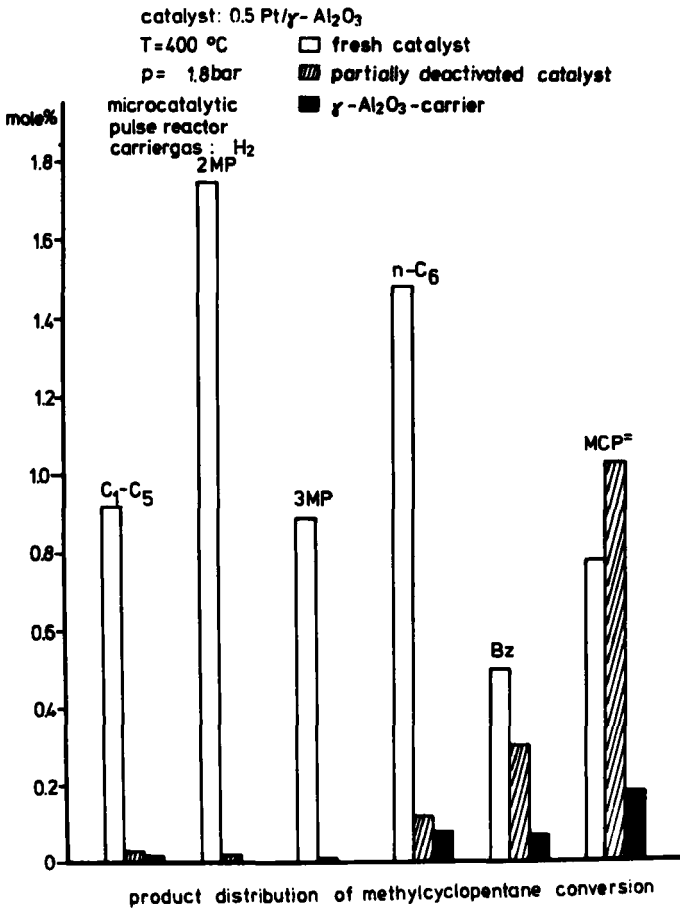
Fig. 3.4. Methylcyclopentane conversion on a 0.5 wt% Pt/Al_2O_3 cata-lyst, a partially deactivated 0.5 wt% Pt/Al_2O_3 catalyst and the aci-dic Al_2O_3-carrier. Reproduced with permission from (ref. 26). Copyright 1978 by American Chemical Society.
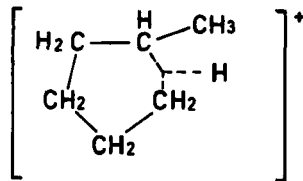
Scheme 3.2

structure, Scheme 3.3. With the two assumptions, (i) that the rate--determining steps are the bond ruptures in the carbenium ions and

Scheme 3.3

(ii) that β-cleavages, by which secondary and tertiary carbenium
ions are converted into primary ones, are energetically unfavoured,
only two out of the six possible transformations of the above car-
benium ions remain where n-hexane is formed. Thus, with methyl-
cyclopentane as model compound, discrimination between the two
acid-catalyzed C-C-bond scission mechanisms cannot be achieved.
    The two mechanisms can, however, be distinguished on the basis
of product distributions from 1,2-dimethylcyclopentane conversion
(ref. 32). The possible carbenium ions with the 1,2-dimethylcyclo-
pentane structure and the ring opening reaction products, *via* the
β-cleavage routes, are depicted in Scheme 3.4. With the same as-
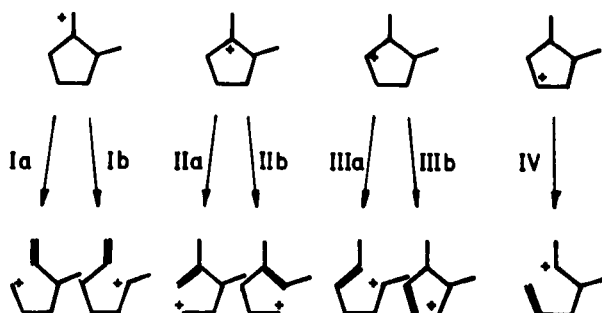
Scheme 3.4

sumptions used for the methylcyclopentane ring opening, 3-methyl-
hexane and n-heptane are expected from 1,2-dimethylcyclopentane
ring cleavage. Direct protonolysis of 1,2-dimethylcyclopentane, on
the other hand, should result in ring rupture yielding mainly
n-heptane, because the transition state is thermodynamically favou-
red where the C-C-bond between the two methyl groups is protonoly-
zed. As the results in Fig. 3.5 reveal, n-heptane is the main
product of acid catalyzed ring cleavage of 1,2-dimethylcyclopentane,
indicating direct C-C-bond protonolysis followed by C-C-bond
scission.

T= 400 °C   ☐ fresh 0.35 Pt/Al$_2$O$_3$
p= 1.8 bar ▨ partially deactivated 0.35 Pt/Al$_2$O$_3$
microcatalytic
pulse reactor
carriergas: H$_2$

mole %

2.0—

1.0—

2,3DMP   3MH

n-Hp

0—

ring opening products from 1,2 DMCP conversion
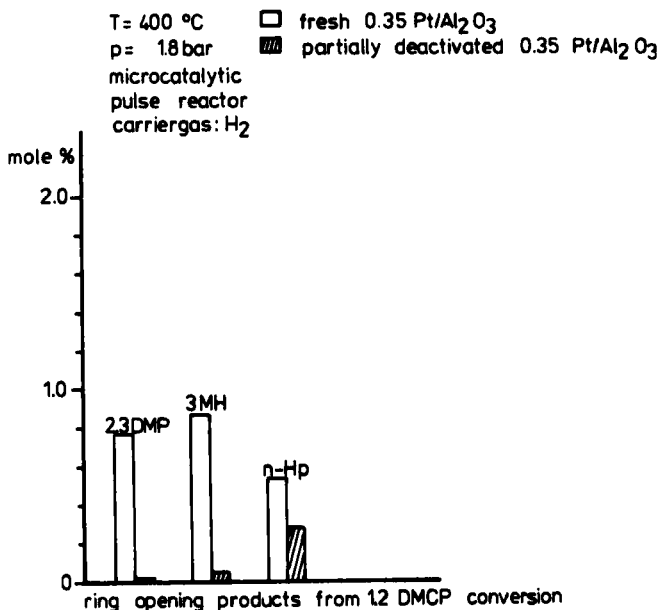
Fig. 3.5. Ring opening products from 1,2-dimethylcyclopentane con-
version.

Example 3.2: Reaction mechanism of ethylbenzene isomerization. The
main source of industrial production of xylenes is the C$_8$-aromatic
cut of the product stream of catalytic reforming plants. Typical
product distributions of the C$_8$-aromatics are 17 wt% ethylbenzene
(EBZ), 18 wt% p-xylene, 43 wt% m-xylene and 22 wt% o-xylene. If
pyrolysis benzene is used as feed, the fraction of ethylbenzene in
the mixture accounts for up to 60 wt%. The particularly important
p- and o-xylenes are obtained from this feed by a combined process,
consisting of catalytic isomerization and thermal separation.
Whereas xylenes undergo isomerization on acidic catalysts, as for
instance amorphous and crystalline aluminosilicates, HF/BF$_3$ or
various zeolites (refs. 33,34), ethylbenzene undergoes transalkyla-
tion (disproportionation) over acidic catalysts, like ZSM-5 zeolite
(ref. 35). It isomerizes *via* hydrogenated intermediates over bi-
functional catalysts (ref. 36), containing a (de)-hydrogenation and
an acidic function (see also Chapter 1). Isomerization of an ethyl-
cyclohexenyl group, yielding dimethylcyclohexenyl groups, requires
at least two reaction steps, which have been shown to consist of a

ring contraction to a cyclopentenyl structure followed by ring
expansion to a cyclohexenyl one (ref. 37 and references therein).

Over a weakly acidic Pt/Al$_2$O$_3$-F catalyst, o-xylene was the main
product from ethylbenzene isomerization. From this and the additi-
onal experimental result (that over the acidic carrier ethylcyclo-
hexane no isomerization, yielding dimethylcyclohexanes, took place)
a reaction mechanism involving nonclassical carbocations via ethyl-
cyclohexene - 1-ethyl-2-methyl-cyclopentene-1,2-dimethylcyclohexene
to o-xylene (which further isomerizes to m- and p-xylene) was pos-
tulated (ref. 38). Further evidence for this reaction mechanism
can be obtained from product distributions of conversions of the
model compounds ethylcyclohexene, 1,2-methylethylcyclopentene,
1,3-methylethylcyclopentene and 1,1-dimethylcyclohexane on a weakly
acidic Pt/Al$_2$O$_3$ catalyst, Table 3.3 (ref. 26). Conversions of

TABLE 3.3

C$_8$-aromatic distributions from conversions of C$_8$-naphthenes over
Pt/Al$_2$O$_3$. After (ref. 26). Copyright 1979, American Chemical Society.

Feed[a]	C$_8$-aromatic products			
	ethyl-benzene	o-xylene	m-xylene	p-xylene
ethylcyclohexene	98.9	0.6	0.4	0.1
1,2-methylethylcyclopentene	19.5	43.6	27.7	9.2
1,3-methylethylcyclopentene	4.1	5.7	49.3	40.9
1,1-dimethylcyclohexane	1.1	98.9	-	-
equilibrium concentrations	8.0	22.5	47.0	22.5

[a] Reaction conditions: 400°C, 1.8 bar, 120 mg 0.5 wt% Pt/Al$_2$O$_3$-cata-
lyst, pulse microreactor, hydrogen carrier gas velocity:
150 ml/min, pulse size 0.1 μl.

1,1-dimethylcyclohexane have been considered to account for possib-
le isomerization routes via 1,2-methyl shifts. From ethylcyclo-
hexene and 1,2-methylethylcyclopentene conversion, o-xylene is the
main product among the xylene isomers. Ethylbenzene formation from
1,2- and 1,3-methylethylcyclopentene conversion is quite different.
Dehydroisomerization products, which result from a single skeletal
rearrangement, are o-, m-xylene and ethylbenzene in the case of
1,2-methylethylcyclopentene conversion and p-, m-xylene and ethyl-
benzene in the case of 1,3-methylethylcyclopentene conversion;
whereas the formation of p-xylene, from 1,2-methylethylcyclopentene,

and of o-xylene, from 1,3-methylethylcyclopentene, requires at
least two skeletal rearrangements.

Predictions from classical carbenium ion mechanisms do not agree
with all the experimental results discussed so far. From 1,3-methyl-
ethylcyclopentene two tertiary carbenium ions are formed by proton
addition. These tertiary carbenium ions undergo skeletal rearrange-
ments yielding m- and p-xylene *via* secondary carbenium ions and
ethylbenzene *via* primary carbenium ions; this is in agreement with
reported results because the transformations through secondary
carbenium ions should be faster than the transformation through a
primary carbenium ion intermediate, Scheme 3.5. The main products
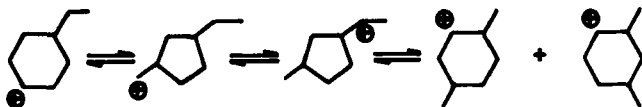
Scheme 3.5

expected from 1,2-methylethylcyclopentene conversion are o- and
m-xylene and from 1,3-methylethylcyclopentene conversion, ethylben-
zene in similar amounts, Scheme 3.6. This does not agree, however,

Scheme 3.6

with the experimental product distributions given in Table 3.3.
Assuming C-H-delocalized protonated cyclopropanes (ref. 25) as
intermediates of skeletal isomerizations, the obtained product
distributions from the different model compound conversions can be
explained. Different amounts of ethylbenzene are predicted for
dehydroisomerization of the two methylethylcyclopentenes, because,
in the case of 1,3-methylethylcyclopentene a secondary carbenium
ion is transposed into a secondary one, Scheme 3.7, whereas in
case of 1,2-methylethylcyclopentene a <u>tertiary</u> carbenium ion is
transposed into a tertiary one, Scheme 3.8.

Similar considerations apply to the formation of the xylenes
from the two methylethylcyclopentenes. Besides the transformation
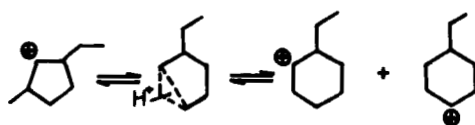
Scheme 3.7
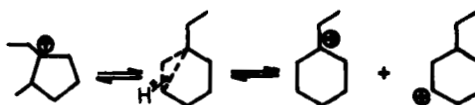
Scheme 3.8

Scheme 3.9

of 1,2-methylethylcyclopentene into o-xylene, Scheme 3.9, all other skeletal rearrangements of methylethylcyclopentene structures into dimethylcyclohexene structures and *vice versa* involve formation of at least one secondary carbenium ion intermediate. Regarding the ethylbenzene isomerization, the reaction sequence ethylcyclohexene - 1,2-methylethylcyclopentene - 1,2-dimethylcyclohexene (Scheme 3.10) is the only one in the total C_8-five-ring and six-ring system
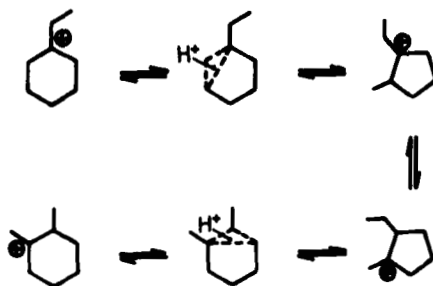
Scheme 3.10

which only involves skeletal rearrangements of tertiary carbenium
ions through C-H-delocalized protonated cyclopropane-structures.
Thus the experimental results obtained correspond with predictions
from theoretical reaction mechanisms assuming "classical" and
"nonclassical" carbocation intermediates.

Example 3.3: Identification of the actual activity and selectivity
of a bifunctional platinum reforming catalyst. In cases where the
underlying reaction network of a reactive catalytic system provides
the frame for constructing kinetic equations by which the reaction
rates are described (which are the entries for the dynamic reactor
model), an activity and selectivity level of the catalyst is
required which is reproducible and constant at least for a certain
reaction time. Usually in heterogeneous catalytic reaction systems,
single reactions do not occur, rather a number of different reac-
tions, the contribution of each to the observed product distribu-
tions being dependent on the operating conditions and on the actual
state of the catalyst. Model compound reactions can provide a means
of indicating this activity and selectivity state of the catalyst,
as will be demonstrated with hydrocarbon conversions on a bifunc-
tional Pt-catalyst; these play an important part in petroleum
refining processes such as catalytic reforming and C_8-aromatic iso-
merization.
    The concept of bifunctional catalysis involves combining two
different functions in one catalyst. For example, the first might
be a metal which catalyzes (de)-hydrogenation reactions of
paraffins into olefins or naphthenes into aromatics and their
reverse reactions, and the second an acidic function which cataly-
zes skeletal rearrangements of the olefins formed on the metal
through carbocation mechanisms (refs. 39,40) (although the exact
nature of the cyclization steps is still disputed (ref. 41)). This
picture seems to be consistent with the macroscopic phenomena ob-
served in the catalytic reforming process. However, dehydrocycli-
zation, skeletal isomerization, closure and opening of five- and
six-membered rings, as well as hydrogenolysis of n-alkanes, can be
catalyzed by the metallic function alone. Similarly, the acidic
function alone can catalyze ring opening, ring closure, isomeriza-
tion and ring contraction and expansion reactions (ref. 42). Thus
hydrocarbon species are interconverted by means of a large number
of consecutive or parallel elementary reactions on bifunctional ca-
talysts. The analysis of this complex reaction network is further

impeded by changing activity and selectivity during operation of the catalyst by which, for example, hydrogen partial pressure dependences of individual hydrocarbon conversion rates, or the portions which certain reactions contribute to the measured overall conversions, are drastically changed; in addition new reactions occur in the reactive system due to carbonaceous deposits on the metal function of the catalyst. Thus the hydrogen partial pressure dependences of n-hexane isomerization and cracking rate may be either -1 or -1.5 and less, depending on whether the products are mainly formed *via* the classical bifunctional mechanism or *via* platinum catalyzed reactions (ref. 43). In the case of the formation of carbonaceous deposits on the surface of platinum particles, the platinum catalyzed isomerization mechanism may change from the "C_5-cyclic" mechanism (by which for example n-hexane is interconverted to the methylpentanes *via* a methylcyclopentyl-surface complex), to the "bond-shift" mechanism (by which alkane isomerization proceeds *via* intermediate structures with a cyclopropane ring). As indicated in Table 3.4 (ref. 44), with

TABLE 3.4

Hydrogenolysis product distribution and 2-methylpentane/3-methylpentane ratio from n-hexane conversions on Pt/Al_2O_3 as a function of hydrogen partial pressure. After (ref. 44).

Carrier gas	Feed pulse	$C_1/\Sigma(C_2-C_5)$ mole%/mole%	2-methylpentane/3-methylpentane
H_2	n-hexane	0.3	1.9
80% H_2 - 20% He	n-hexane	0.32	1.86
60% H_2 - 40% He	n-hexane	0.35	1.7
40% H_2 - 60% He	n-hexane	0.4	1.55
20% H_2 - 80% He	n-hexane	0.5	1.5
He	n-hexane	0.9	-
H_2^a	n-hexane[b]	5.7/4.4/3.6	1.27

Reaction conditions: pulse micro reactor, 400°C, 1.8 bar, 0.3 μl pulses, 150 mg, 0.35 wt% Pt/Al2O3 catalyst; carrier gas velocity 150 ml/min.

[a] n-hexane conversion after switching from H2/He mixtures and He carrier gas to H2 carrier gas.

[b] C1/Σ(C2-C5) - ratio from the first three pulses after switching from He to H2 carrier gas.

decreasing H_2-partial pressure at constant total pressure, this
means that, under deactivating reaction conditions, the mole ratio
of 2-methylpentane/3-methylpentane formation from n-hexane conver-
sion changes from 1.9 (which corresponds closely to the theoretical
value expected from the "C_5-cyclic" mechanism) to 1.27 (which is
closer to the value expected from the acid-catalyzed mechanism
due to deactivation of the metallic function). Like the isomeriza-
tion mechanism, the hydrocarbon hydrogenolysis mechanism will also
depend on clean platinum surfaces or platinum surfaces covered with
carbonaceous deposits, as indicated in Table 3.4. On deactivated
platinum, hydrogenolysis reactions yield mainly methane whereas on
clean platinum surfaces statistical C-C-bond cleavage is observed.
Perhaps removal of residual surface CH_x species by hydrogenating
them off the surface also contributes to enhanced methane yield
after switching to hydrogen carrier gas (last row of Table 3.4).
Such species may, and do, contribute to the formation of carbonace-
ous residues (ref. 45).

   To derive a suitable reaction scheme for mathematically modeling
the platforming process and to determine the model parameters by
use of a set of consistent experimental data, as stated above, it
is necessary to obtain a constant and reproducible activity and
selectivity level of the catalyst and to establish that this acti-
vity and selectivity level is the same with different reactor con-
figurations. For this a model compound reaction is needed which in-
dicates the actual activity and selectivity of the catalyst. In the
case of the hydrogen - hydrocarbon - Pt/Al_2O_3 system, methylcyclo-
pentane can be used as a model compound. As the results plotted in
Fig. 3.6 reveal, in the case where platinum catalyzed reactions
mainly contribute to the observed product distributions, statisti-
cal cleavage of the methylcyclopentane C-C-bonds is observed: in
the case where platinum only displays (de)-hydrogenation activity,
reactants are transformed into products mainly *via* a bifunctional
mechanism and n-hexane is the main product of methylcyclopentane
ring opening. On platinum, with large platinum crystallites, selec-
tive methylcyclopentane ring opening occurs yielding mainly methyl-
pentanes. With a platinum surface covered by carbonaceous deposits,
platinum reactions still mainly contribute to the observed product
distributions. The main product of C-C-bond cleavages is methane.

   *Obviously monitoring the activity and selectivity state of a
catalyst will not decrease the problems connected with obtaining a
constant and reproducible activity and selectivity state for the*
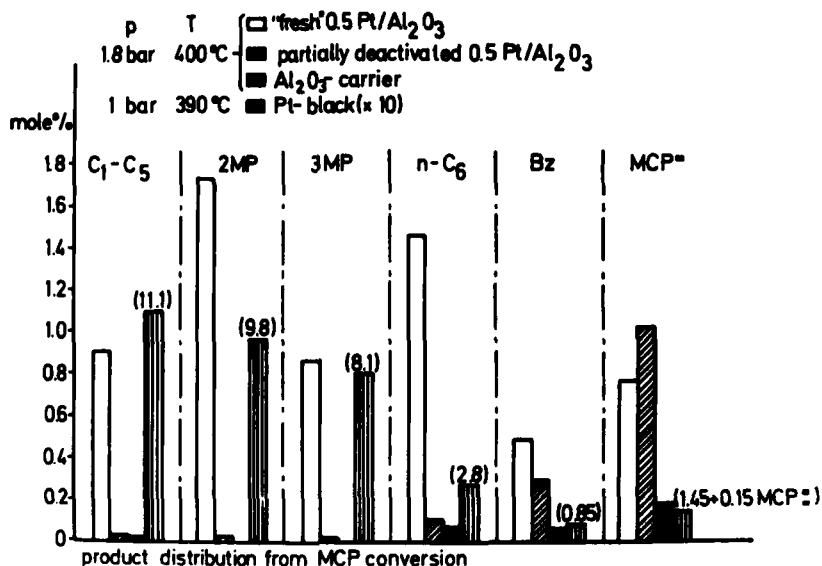
Fig. 3.6. Catalytic activity and selectivity of 0.5 wt% Pt/Al₂O₃ and Pt-black in methylcyclopentane conversions. Apparatus: pulse microreactor, carrier gas: H₂. Reproduced with permission from (ref. 44).

catalyst; nevertheless a chemical characterization of the actual state of the catalyst, under real reaction conditions, will be of considerable help in producing suitable running-in procedures.

The examples presented so far show how to use model compound reactions to evaluate reaction mechanisms and determine the actual activity and selectivity of a catalyst. The nature of the active sites can also be studied by use of model compound reactions which shall be expressed in terms of the different requirements a catalyst must fulfil to selectively catalyze specific reactions.

The bond strength requirement accounts for formation and rupture of chemical bonds between atoms of the reactant and the catalyst surface. Thus a characterization of different catalytically active centers directly follows from the occurence or non-occurence of suitable model compound reactions. Difficulties with this procedure arise from the assignment of the reactions to the active centers which might be either surface atoms of the investigated catalytic active phase or surface impurities. Great progress has been made, however, in the last few decades in the preparation and identification of clean surfaces.

The coordination requirement accounts for coordination sites per

surface atom which may be classified by [1]M, [2]M, [2]MH, [3]M, [3]MH where
the superscript indicates the degree of coordinative unsaturation
and MH an active center, where a hydrogen atom is adsorbed (refs.
46,47), Scheme 3.11. Active centers [2]MH, [3]MH are formed by adsorp-
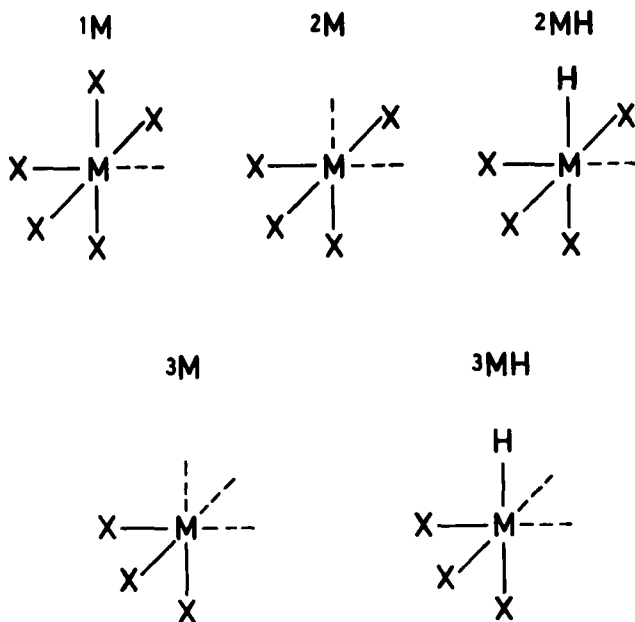
Scheme 3.11

tion of H_2 on active centers [2]M and [3]M followed by transfer of ato-
mic hydrogen to an adjacent site or to the interior of the crystal.
An investigation of the coordinative unsaturation can be accomplis-
hed by characterizing adsorptions of probe molecules like CO, C_2H_4
and H_2, and specific reactions like H_2-D_2-equilibration, alkene
hydrogenation and ethylene-deuterium exchange reactions as outlined
in Table 3.5 (ref. 46).

The ensemble requirement considers whether a single surface atom
or an ensemble of several adjacent atoms is involved in the surface
reaction. A large amount of work has focused on this principle.
Indirect approaches to the investigation of this requirement are
(i) the determination of partial pressure dependencies of the ra-
tes of model compound reactions, as exemplified in the work of
Frennet et al. (ref. 48), with the methane-deuterium exchange

TABLE 3.5

Characterizing reactions for determining coordinative unsaturation of active sites. Reproduced with permission from (ref. 46).

Characterizing reaction	Surface sites				
	^1M	^2M	^2MH	^3M	^3MH
adsorption of CO or C_2H_4	+	+	+	+	+
adsorption of H_2	-	+	-	+	+
H_2-D_2 equilibration	-	-	-	-	+
alkene hydrogenation	-	-	-	+	+
C_2H_4-D_2 exchange	-	-	-	+	+
C_2H_4-C_2D_4 exchange or alkene isomerization	-	-	+	-	+

reaction on rhodium or conversion measurements of specific reactant molecules and (ii) comparison of observed and theoretically expected product distributions as exemplified in the work of Gault (ref. 29) and Paål (ref. 49) with alkane cyclization, isomerization and hydrogenolysis reactions on noble metals. A more direct approach to the study of ensemble requirement is to dilute a catalytically active metal surface by alloying with a chemically inert metal and then observing changes in catalyst selectivity towards characteristic reactions (refs. 50-52). By measuring actual surface compositions and the corresponding product distributions in the gaseous phase for specific model compound conversions, single reactions can be assigned to ensembles of different size on the surface. Thus, for example, with hydrocarbon reactions on Pt-Au alloys it was found that of hydrogenolysis, isomerization and dehydrocyclization, hydrogenolysis reactions require the largest ensembles, whereas different routes for isomerization reactions should exist requiring ensembles of different size (ref. 53).

To sum up, model compound reactions are feasible for the study of all the detailed requirements needed for a certain reaction path to occur. Spectroscopic methods, adapted to the investigation of the constitution and morphology of catalytically active surfaces, have greatly improved the possibility of assigning reactions, observed in the gaseous phase, to active centers on the catalyst surface.

3.1.4 Determination of reaction mechanisms from conversion *versus* reaction time and related data

The simplest analysis of concentration versus reaction time data from continuously operated fixed bed reactors, with respect to obtaining information on underlaying reaction mechanisms, considers the shape of these curves. An example is given in Fig. 3.7 where
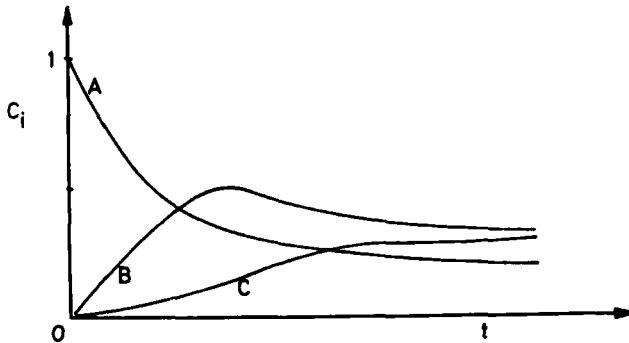
Fig. 3.7. Concentration *versus* reaction time data from a continuously operated fixed bed reactor.

changes in concentration of three stable species in the fluid reaction mixture are plotted against reaction time, t. The concentration of component A decreases to a final value, the concentration curve of B passes through a maximum, has a finite slope at the origin of the coordinate system and reaches a finite final value, whereas the concentration curve of component C displays a zero slope at the origin of the coordinate system but also finally reaches a finite value. From the zero slope of the concentration C at the origin it is concluded that C is not directly formed from A, because in this case the decrease in concentration of A would be directly connected with an increase in concentration of C and a finite slope of the concentration *vs.* reaction time curve, at time zero, would be expected. Thus, species C is assumed to be formed in a consecutive reaction. As all component concentrations reach finite values with increasing reaction time, it is concluded that the reactions are reversible. The concentration of species B passes through a maximum by which species B is assumed to be an intermediate product and the following reaction scheme is postulated:

$$A \rightleftharpoons B \rightleftharpoons C.$$

Better information on the underlying reaction mechanisms from continuously operated fixed bed reactors follows either from an analysis of data obtained with a differential or an integral reactor. For an ideal isothermal catalytic flow reactor, the following continuity equation is obtained

$$F_{Ao} dX = r \, dW \qquad (3.1)$$

where W is the weight of catalyst (kg), F_{Ao} the molar flow rate (mole/h), r the overall reaction rate and X the conversion. With low conversions (under 5-10%) the catalytic flow reactor is called a differential reactor and for dynamic modeling the differentials in eq. 3.1 can be replaced and the continuity equation takes the following form

$$F_{Ao} \cdot \Delta X = r \cdot W \qquad (3.2)$$

where the rates are obtained directly from measured feed and product concentrations. With catalytic reactions the rate expressions which are the entries into equations 3.1 and 3.2 are, even for single reactions, rather complicated, because they account for adsorption, surface reaction and desorption. For example, with the reaction

$$A \rightleftharpoons B + C$$
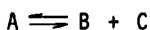
with the individual steps

$$A + 1 \rightleftharpoons A1$$
$$A1 \rightleftharpoons B1 + C$$
$$B1 \rightleftharpoons B + 1$$
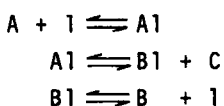
where 1 is again a free active center on the catalyst surface, the following rate equations result, assuming steady state conditions and that the free enthalpy drop of the overall reaction is nearly attained in only one of the three reaction steps (*i.e.* one of the three steps is rate determining)
(1) adsorption is rate determining:

$$r = [k(P_A - P_B P_C/K)]/(1 + K_B P_B) \qquad (3.3)$$

(2) surface reaction is rate determining:

$$r = [k(P_A - P_B P_C/K)]/(1 + K_A P_A + K_B P_B) \qquad (3.4)$$

(3) desorption is rate determining:

$$r = [k(P_A - P_B P_C/K)]/(1 + K_A P_A + K_B P_B + K_C P_C). \qquad (3.5)$$

The parameters in these equations are estimated either by fitting

equation (3.1) to conversion *versus* space velocity W/F data, or
equation (3.2) directly to the rates. Equations (3.3)-(3.5) can
also be used for discrimating among rival reaction rate models,
that means to identify whether adsorption, desorption or surface
reactions are rate determining or whether two surface sites or only
one are involved in the surface reactions.

The classic method of evaluating reaction mechanisms on the ba-
sis of the ideal reactor models, eq. (3.1) and (3.2), with the
reaction rate models, eq. (3.3)-(3.5) originates from Yang and
Hougen (ref. 54) who demonstrated that the reaction rate equations
can be drastically simplified by using initial reaction rates at
W/F = 0. With differential reactors the initial rates are obtained
directly because, in this case, the reaction rate is assumed to be
constant over the length of the catalyst bed. With integral reac-
tors, the initial rates are obtained from the slopes of tangents to
the conversion *versus* space velocity data at W/F = 0. Considering
initial rates, r_0, equations (3.3)-(3.5) reduce to

$$r_0 = k \cdot P_A \qquad\qquad (3.6)$$
$$r_0 = k \ P_A / (1 + K_A \cdot P_A) \qquad\qquad (3.7)$$
$$r_0 = k'. \qquad\qquad (3.8)$$

From plots of the initial rates *versus* the total pressure, the rate
determining step can be identified. As indicated in Fig. 3.8, the
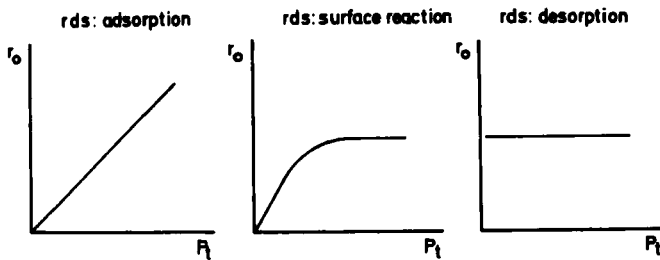
Fig. 3.8. Initial rates as function of total pressure, P_t.

initial rate is a linear function of total pressure if the adsorp-
tion is rate determining and independent of total pressure if de-
sorption is the rate determining step. If the surface reaction is
the rate determining step of the reaction mechanism considered, the
initial rate increases with increasing pressure until a saturation

value is reached. In the case of a dual site reaction being rate determining, the initial rate as a function of total pressure would pass through a maximum.

Besides this graphical approach to determining the reaction mechanisms of heterogeneous catalytic reaction, reaction mechanisms are frequently evaluated by mathematical analysis of the conversion *versus* space velocity data. The procedure adopted is as follows: first different reaction mechanisms are postulated which provide the framework for deriving kinetic reaction models. Then, the model parameters are determined by fitting to experimental conversion *versus* space velocity data or, in case of data from a differential reactor, directly to the rates at different partial pressures. In the last step the "goodness of fit" of the theoretical models to the experimental data is evaluated by statistical methods and the theoretical model which best describes the experimental data is selected as being adequate. The procedure will be illustrated by a model discrimination for dehydrogenation of 1-butene into butadiene on a chromium-alumina catalyst in a differential reactor as repor- ted by Dumez and Froment (refs. 55,56). The following five mecha- nisms were postulated:

Mechanism 1: atomic dehydrogenation, surface recombination of
hydrogen
reaction steps: 1. $B + 1 \rightleftharpoons B1$
2. $B1 + 1 \rightleftharpoons M1 + H1$
3. $M1 + 1 \rightleftharpoons D1 + H1$
4. $D1 \rightleftharpoons D + 1$
5. $2H1 \rightleftharpoons H_2 1 + 1$
6. $H_2 1 \rightleftharpoons H_2 + 1$
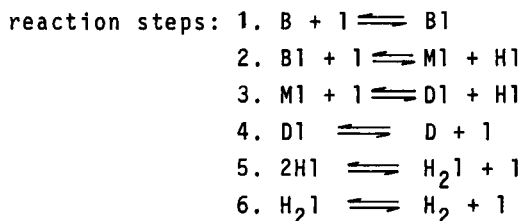
where B = butene, 1 = free active center of catalyst, M = hydrogen deficient butene - surface complex, D = butadiene.

Mechanism 2: atomic dehydrogenation, gas phase hydrogen recombina-
tion
reaction steps: 1. $B + 1 \rightleftharpoons B1$
2. $B1 + 1 \rightleftharpoons M1 + H1$
3. $M1 + 1 \rightleftharpoons D1 + H1$
4. $D1 \rightleftharpoons D + 1$
5. $2H1 \rightleftharpoons H_2 + 21$.
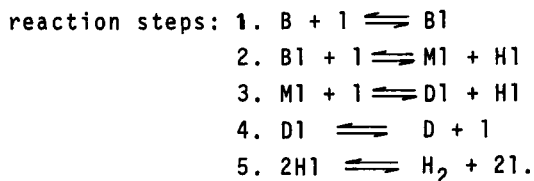
Mechanism 3: molecular dehydrogenation
reaction steps. 1. $B + 1 \rightleftharpoons B1$

2. $B1 + 1 \rightleftharpoons D1 + H_2 1$
3. $D1 \rightleftharpoons D + 1$
4. $H_2 1 \rightleftharpoons H_2 + 1.$
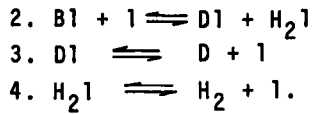
Mechanism 4: atomic dehydrogenation, intermediate complex with short lifetime, surface recombination of hydrogen

reaction steps: 1. $B + 1 \rightleftharpoons B1$
2. $B1 + 21 \rightleftharpoons D1 + 2H1$
3. $D1 \rightleftharpoons D + 1$
4. $2H1 \rightleftharpoons H_2 1 + 1$
5. $H_2 1 \rightleftharpoons H_2 + 1.$
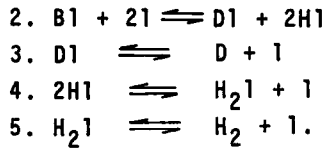
Mechanism 5: as mechanism 4, but with gas phase hydrogen recombination

reaction steps: 1. $B + 1 \rightleftharpoons B1$
2. $B1 + 21 \rightleftharpoons D1 + 2H1$
3. $D1 \rightleftharpoons D + 1$
4. $2H1 \rightleftharpoons H_2 + 21.$
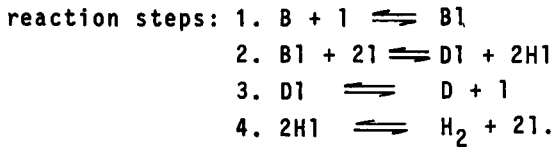
On the basis of these five mechanisms, rate equations are deduced under the assumptions of steady state. This means that all the reaction steps in a sequence proceed at the same rate, and one of the individual steps of a sequence is rate determining. The assumption of a rate determining step means that the rate constant of this step is much smaller than the rate constants of the other steps. The assumption that all steps in a sequence proceed at the same rate then signifies that the rate determining step is far from thermodynamic equilibrium, whereas the other steps are close to it; this can be understood in terms of the rate expressions of chemical reactions $r_i = k_i(T) \cdot f(c_i)$. If the k_i of a step is small, $f(c_i)$ must be large to ensure that this step proceeds at the same rate as the others and *vice versa*. The steps which are nearly at equilibrium are handled as if equilibrium had been achieved. On the basis of the five mechanisms, Dumez and Froment derived 15 rate equations assuming different adsorption, surface reaction and desorption steps as rate determining. The following rate equation was found to give the best fit for the experimental data

$$r = \frac{k_1 \cdot K_1 \cdot C_t (P_B - \frac{P_H \cdot P_D}{K})}{(1 + K_1 P_B + \frac{P_D}{K_3} + \frac{P_H}{K_4})^2} \qquad (3.9)$$

where P_i are partial pressures of hydrogen (H), butane (B) and bu-

tadiene (D), K_i equilibrium constants of the i-th reaction step, C_t, total concentration of active sites and, k_1, the rate constant of the rate determining step. Equation (3.9) was derived from mechanism 3 with the second reaction step being rate determining. The discrimination among the 15 models necessary to arrive at eq. (3.9) was based on a sequential discrimination procedure by which an optimal experimental design was achieved and also on a statistical testing procedure of the current adequacy of the rival models. For the sequential choice of experimental conditions, the following design criterion was used

$$D_{i,n} = \sum_{k=1}^{m} \sum_{l=k+1}^{m} (\hat{y}_i^{(k)} - \hat{y}_i^{(1)})^2 \tag{3.10}$$

where $D_{i,n}$ is the divergence between estimates of the function, $\hat{y}$, for each of the models, k and l stand for the models and the index i for the grid point which is actually tested. The model adequacy was also tested by using a criterion which, in cases where the experimental error variance σ^2 is exactly known, takes the following form (ref. 57)

$$\chi^2 = \frac{(n - p_i)S_i^2}{\sigma^2} \tag{3.11}$$

where $(n - p_i)$ represents the degrees of freedom, n the number of experiments, p_i the number of parameters in the i-th model and S_i^2 an unbiased estimate of the error variance.

At first glance the mathematical analysis of experimental conversion *versus* space velocity data described so far seems to offer information on heterogeneous catalytic reaction mechanisms at the molecular level. Thus, it would be the reverse of the procedure for kinetic analysis described in Scheme 2.2, Section 2.3. The three steps were there: (1) investigation of the network by which the species in the reaction mixture are linked together; (2) deriving a mathematical model based on the obtained reaction mechanism and (3) parameter estimation by fitting to conversion *versus* space velocity data obtained under reaction conditions which are similar to those of the reaction system for which model predictions shall be obtained. The analogy is, however, only apparent.

Conversion *versus* space velocity data measured in the fluid phase only supply very restricted information about the actual surface mechanisms at a molecular level, independent of the mathematical complexity by which the analysis of the experimental data has been performed. The reasons why these informations are restricted

comprise that (i) usually steady-state operation of the fixed bed reactor is applied; (ii) the simplifying assumptions are introduced to express surface concentrations in terms of the experimentally accessible fluid phase concentrations and (iii) the complex reaction networks is decomposed into reaction schemes which can be mathematically handled. The simplifying assumptions that are commonly made are (1) that the catalyst is a constant entity over the total range of compositions in the gaseous phase, (2) that there is a rate determining step and (3) that there is a most abundant surface intermediate. The notion of the most abundant surface intermediate means that the concentrations of other surface species can be neglected compared with the concentrations of the most abundant surface intermediate.

With the latter two assumptions Boudart (ref. 58) illustrated the ambiguity of simplified kinetics using an isomerization reaction $A \rightleftharpoons B$ which takes place in three steps (1) adsorption on an empty surface site; (2) surface reaction; (3) desorption of product B. Assuming four different situations with different rate determining steps and different most abundant surface intermediates, the same rate law

$$r = C_t \frac{k_1 \cdot C_A}{1 + k_2 C_A}$$

(which described the kinetics in all the four situations) was derived; however, the constants k_1 and k_2 had quite different physical meanings.

The assumption that the catalyst is a constant entity over the total range of compositions is quite often not fulfilled and this frequently restricts the kinetic analysis to considering only one reaction trajectory on the reaction hyperplane in the composition space, because starting with different initial compositions would result in different activity and selectivity levels of the catalyst. Obviously, the kinetic analysis with respect to the aims discussed in previous sections is more suitable if reaction trajectories on the total reaction hyperplane are considered. If just one reaction trajectory is used for kinetic analysis - in most cases as initial composition only the reactant feed is considered instead of mixtures containing also stable intermediate products or final products - quite often a large number of experimental points are measured on this single reaction trajectory; this, however, cannot improve the model discrimination procedure, because a single reaction trajectory is usually sufficiently determined by a small

number of experimental points.

As a result, the mathematical analysis of composition *versus* space velocity data, with respect to model discrimination, simply verifies the statement, that Langmuir-Hinshelwood-Hougen-Watson models are better suited to model the dynamics of heterogeneous catalytic reactions than are power-law-models (ref. 59). The main use of these models is to predict the dynamic behaviour of the investigated reaction system. If only composition *versus* space velocity data are available for kinetic analysis, with no independent information about the underlying reaction network or about the importance of the rate of adsorption/desorption steps, a discrimination among different rival rate models is necessary in order to find the rate model which best describes the experimental data over the range of the applied reaction conditions. The statistical testing procedures for the different models only ensure, however, the adequacy of the final rate model and do not provide evidence that a certain reaction mechanism operates. Thus, the mathematical analysis discussed so far delivers a suitable reaction scheme which will provide a framework for deriving an adequate dynamic rate model. The problems of identifying the underlying reaction mechanism and proving how it can be transformed into a simplified reaction scheme are not tackled.

3.1.5 Graph theory and reaction mechanisms

A formal linear combination of species on the reactant or the product site of an elementary reaction is called a complex (ref. 60); it is completely characterized by the m-tuple of the stoichiometric coefficients of the set of m species which make up the complex. A reaction network which consists of complexes and reactions which link the complexes together can be associated with directed graphs (digraphs), where the nodes of a digraph are the complexes of the reactive mass-action systems and the arcs are the "reacts-to" relations between the complexes. Based on such a description of reactive chemical systems, Happel and Sellers (ref. 61) discussed a method for unambiguous generation of all reaction mechanisms by which a set of species is linked together, giving rise to the observed overall production and consumption of reactants and terminal products. Chemical reactive systems can be viewed within two vector spaces, an S-dimensional space of the mechanisms and a Q-dimensional space of the chemical reactions. The mechanisms are linear combinations of the simplest kinds of mecha-

nisms, the elementary steps giving rise to the elementary reactions
which form the basis for the space of all reactions. The transfor-
mation of mechanisms to reactions is linear because, in a chemical
system, the reactions are additive. In reactive systems two kinds
of species occur, intermediates and terminal species. Steady-state
mechanisms are those whose reactions only involve terminal species.
The set of all reaction vectors, which contain only these terminal
species, constitutes the overall reaction space. The question to
be considered now, given a specified reaction vector and a set of
possible elementary steps, is to find all mechanistic vectors which
produce this specified reaction vector. With the method proposed,
the S-dimensional space of all mechanisms is changed to a basis
which separates this space into three parts: a subspace of all
cycles which are the kernels of the mechanism space, a subspace of
steady-state mechanisms which does not yield cycles by linear combi-
nations and a subspace of non-steady-state mechanisms which does
not yield steady-state mechanisms by linear combinations of single
mechanisms. This is obtained from the diagonalized form of an S x A
matrix where A is the number of species in the reactive chemical
system and S the dimension of the mechanism space, which determines
the linear transformation of the mechanism vectors to the reaction
vectors

$$
\begin{array}{l} S_1 \\ S_2 \\ \cdot \\ \cdot \\ \cdot \\ S_S \end{array}
\begin{bmatrix}
\alpha_{11} & \cdots & \alpha_{1I} & \alpha_{1,I+1} & \cdots & \alpha_{1,I+T} \\
\alpha_{21} & & \alpha_{2I} & \alpha_{2,I+1} & & \alpha_{2,I+T} \\
\cdot & & \cdot & \cdot & & \cdot \\
\cdot & & \cdot & \cdot & & \cdot \\
\cdot & & \cdot & \cdot & & \cdot \\
\alpha_{S1} & & \alpha_{SI} & \alpha_{S,I+1} & & \alpha_{S,I+T}
\end{bmatrix}
\tag{3.12}
$$

where S_i are the i-th steps in the chemical system, T = A-I the
number of terminal species, I the number of intermediate species
and α_{ij} the stoichiometric coefficients of species a_j in the ele-
mentary reaction r_i. Since the overall reaction vector involves
only terminal species, mechanistic vectors have to be determined
which recycle all intermediates involved. The explicit basis for
the space of overall reactions can be characterized by corresponding
rows in the diagonalized form of the matrix (3.12). The mechanisms
which give rise to the specified overall reaction are called the
direct mechanisms and are defined in the sense, that if one step of
the mechanism is omitted, no mechanism can be formed by linear

combination to produce the specified overall reaction rate. According to Happel and Sellers (ref. 61), these direct mechanisms are obtained by determining the maximal cycle-free subsystems from the set of mechanistic steps of the given chemical system and then evaluating the unique direct mechanism contained in each of the cycle-free subsystems. The Q-step cycle-free subsystems which are formed from Q linearly independent reactions are obtained by removing C appropriate steps from the total system of mechanistic steps, where C is the dimension of the cycle space; it can be obtained from the diagonalized form of matrix eq. (3.12).

Thus the method described so far provides a procedure for deriving a suitable reaction scheme for mathematical modeling from a set of known possible elementary reactions.

Different approaches have now been presented to enable the determination of reaction networks by which species in heterogeneous catalytic systems are linked together. Spectroscopic methods offer the possibility of studying heterogeneous catalytic reactions at the molecular level. Until now this approach has been confined to clean, frequently low pressure, systems which are operated far removed from industrial catalytic reactions. Temperature Programmed methods can give information on real catalysts, too. This is, however, an indirect one. Model compound reactions present also an indirect approach to studying surface reactions using product distributions obtained in the gaseous phase. However, with specific compounds, either from their structure or by isotope labelling (refs. 29,49,62). it is possible to chemically characterize the activity and selectivity of catalysts. With mathematical evaluation of composition *versus* space time and related data the situation resembles the cave parable of Platon where, the original objects have to be recognized from only their shadows. Therefore the main use of this method is to provide a suitable mathematical model for describing the actual dynamic behavior and for predicting the behavior of a system in larger scale reactors or other reactor configurations and not to gain insight into the molecular events on the catalyst surface. The last method discussed starts to fill the gap between complex underlying reaction mechanisms and much simpler reaction schemes which are used to modell the dynamics of the investigated chemical systems.

3.2 DYNAMIC MODELING

Within the framework of laboratory studies of heterogeneous ca-
talytic reactions, dynamic modeling provides a suitable chemical
reaction rate model and a reactor model. In cases where the acti-
vity and selectivity of solid catalysts are characterized by rate
constants, obtained from conversion - space velocity data in open
reaction systems, operating conditions are frequently chosen in
such a way that the reactor model is identical with the chemical
reaction rate model, which considers adsorption, surface reaction
and desorption steps, only the time variable being replaced by a
spatial one. For process optimization and scale-up from laboratory
reactors to industrial ones, a mathematical model of the chemical
reactor is needed to account for the concurrence of mass, heat and
momentum transport processes with adsorption, surface reaction and
desorption of reactive species on the catalyst. As we are dealing
with open reactive systems far from thermodynamic equilibrium, the
regions over which mass, heat and momentum balances are formed are
usually differential volumes for which the mathematical models are
sets of linear or nonlinear differential equations.

3.2.1 Rate models of heterogeneous catalytic reactions

According to the concept of elementary reactions which, weighted
by a set of stoichiometric coefficients, provide the frame for
dynamic modeling of the observable rate of change of the composition
of the mixture, the first step in deriving rate models of hetero-
geneous catalytic reactions is the evaluation of the underlying
reaction mechanism. Typical reaction mechanisms for acid-catalyzed
and platinum-catalyzed hydrocarbon isomerization are outlined in
Schemes 3.12 and 3.13. The reactive intermediates in these two
examples are different carbocations bound to the surface of acidic
metal oxides. Adsorption and desorption steps which lead to forma-
tion of the surface complexes and re-formation of active centers
on the catalyst surface are incorporated within the network of
elementary reactions which contribute to the observed product dist-
ributions.

The kinetic description of chemical reactions in closed systems
with underlying reaction mechanisms, as plotted in Schemes 3.12
and 3.13, is completely consistent with the requirements of thermo-
dynamics and stoichiometry if the following conditions are satis-
fied:
(1) the catalyst is a constant entity over the total range of com-

+H₂ | -H₂   Pt

-H* | +H*

H₃C-CH₂-CH₂-CH₂-CH₂-CH₃

-H* | +H*

H₃C-CH₂-CH₂-CH-CH₂-CH₃   +H₂ / -H₂   [H₃C-CH₂-CH₂-CH-CH₂-CH₃]⁺ (H---H)

[H₃C / HC---H / H₂C   CH-CH₂-CH₃]⁺

[H₃C / H---CH / H₂C   CH₂-CH₂-CH₃]⁺

[H₃C / C---H / H₂C   CH₂-CH₂-CH₃]⁺

H₃C-CH-CH₂-CH₂-CH₃
       |
       CH₃

-H* / +H*   +H* / -H*
      -H₂
      +H₂

Scheme 3.12

C   C   C   C   C
 \ /   \ /   \
  C   + M →   C   → H₂C   C
 / \   / \   / \
C   C   C   C   M   CH₂
              \ /
               M
                              ↕

C   C   CH₂
 \ /   /
  C   C---C---CH₂
 / \   / | \
C   M   ←   C   C   M---CH₂
 \ /
  M + ⟍Y   ←

Scheme 3.13

position, only one type of active center contributes to chemi-
cal conversions and the rate parameters are independent of the
concentrations of reacting species;

(2) each elementary reaction gives rise to a rate function of the
    mass action form;
(3) the mass is conserved in each elementary reaction;
(4) the rate constants in the rate functions are constrained by the
    principle of detailed balancing;
(5) the stoichiometric coefficients are non-negative integers.

   By relaxing condition (3), Horn and Jackson (ref. 60) showed
that open reaction systems can also be described within the formal
structure of mass action kinetics. To achieve this, further pseudo-
-elementary reactions are added to the set of elementary reactions
which account for supplying species to and removing them from the
reactor. If, for instance, a species is supplied to the reactor at
a constant rate or a species is removed from the reactor at a rate
proportional to its concentration in the reactor, the reactions
$0 \rightarrow A_i$ and $A_j \rightarrow 0$ are added to the set of elementary reactions.
Apparently, with these reactions the mass is not conserved. If, for
example, a reaction $A_1 \rightarrow A_2$ takes place in a continuously operated
stirred tank reactor, the underlying reaction network is

$$0 \underset{v}{\overset{v \cdot a_{01}}{\rightleftharpoons}} A_1 \overset{k}{\longrightarrow} A_2 \underset{v}{\overset{v \cdot a_{02}}{\rightleftharpoons}} 0$$

where k is the rate constant, v the flow rate per unit volume and
a_{01} and a_{02} time invariant concentrations of species A_1 and A_2 in
the feed.

   Chemical reactions can be visualized as transformations of
reaction vectors with time in the composition space. Following
Feinberg and Horn (ref. 63), mechanisms are classified according to
their number of complexes, and linkage classes, the dimension of
the stoichiometric subspace, the deficiencies of the mechanisms and
their weak reversibility. In Table 3.6 some examples of reaction
mechanisms are shown. Complexes are the entities which appear before
and after arrows in the mechanism. For example, the complexes in
mechanism 7, Table 3.6, are A_1, $2A_1$, $A_1 + A_2$, $2A_2$, A_2, 0 and in
mechanism 8, Table 3.6, 0, A_1, $A_1 + A_2$, $A_3 + A_4$, $A_3 + A_2$, $A_4 + A_5$,
$A_4 + A_6$, $A_7 + A_6$. The number of complexes is denoted by n. Linkage
classes in a mechanism, denoted by l, are sets in the mechanism,
where complexes are directly or indirectly lined to all other comp-

lexes of this set and not linked to other complexes of the mechanism outside this set. Hence, for mechanism 5, the linkage classes are $\{A_2, A_4\}$, $\{A_1 + A_3, A_5 + A_6\}$ and $\{2A, A_2 + A_3, A_7\}$ and for mechanism 8, Table 3.6, $\{0, A_1\}$, $\{A_1 + A_2, A_3 + A_4\}$, $\{A_3 + A_2, A_4 + A_5\}$ and $\{A_4 + A_6, A_7 + A_6\}$. For a mathematical description of the mechanisms a species space $V = R^m$ is introduced which is an M-dimensional vector space with basis $\{e_1, e_2...e_m\}$ where $e_1 = \{1, 0, 0...0\}$, $e_2 = \{0, 1, 0, 0 ...0\}$ *etc*. Complexes are represented in the species space by corresponding species basis vectors. Hence, for mechanism 6 the complex vectors are e_1, $2e_2$, e_3 $e_3 + e_4$, e_5 and $e_6 + e_7$. Reactions are represented in the species space by subtracting the vector of the reactant complex from the corresponding product complex vector. For mechanism 6, for example, the set of reaction vectors is given by $\{e_1 - 2e_2, e_3 - 2e_2, e_5 - (e_3 + e_4), e_6 + e_7 - (e_3 + e_4), e_5 - (e_6 + e_7), e_6 + e_7 - e_5\}$. The stoichiometric subspace for a mechanism with a dimension denoted by s is spanned by its set of reaction vectors. For determination of s, use is made of an equivalent statement which defines s as the number of elements of the largest linearly independent set formed from the reaction vectors of the reaction mechanism. Hence, s is obtained by determining the rank of an $r \times M$ matrix composed of the reaction vectors, where r is the number of reactions in the mechanism and M the dimension of the species space.

A further characteristic of reaction mechanisms is their reversibility which, in some cases, is weak. A reaction mechanism is reversible if, for every reaction leading from reactant to product, there is a reverse reaction leading from product to reactant. A mechanism is weakly reversible if, for any pair of complexes which are connected by a directed arrow pathway, there exists a further directed pathway consisting of one or more directed arrows leading back from the product complex to the reactant complex. Hence the mechanism
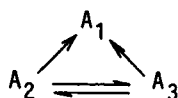
is not weakly reversible because there exists a directed arrow from A_2 to A_1 but no pathway back from A_1 to A_2; whereas the mechanism

TABLE 3.6

Examples and classification of reaction mechanisms. After (ref. 63); for denotions, see text. Copyright 1974, Pergamon Journals Ltd.

Mechanism	n	l	s	δ
1) $2A_1 \longrightarrow A_2 \rightleftharpoons A_3 + A_4$	3	1	2	0
2) $A_3 + A_4 \rightleftharpoons \overset{2A_1}{\diagup} \diagdown A_2$	3	1	2	0
3) $A_3 + A_4 \longrightarrow \overset{2A_1}{\diagup} \diagdown A_2$	3	1	2	0
4) $A_1 \longrightarrow A_2$ $A_1 + A_3 \longrightarrow A_4$ $A_2 + A_5$	5	2	3	0
5) $A_2 \rightleftharpoons A_4$ $A_2 + A_3 \rightleftharpoons A_5 + A_6$ $2A_1 \rightleftharpoons A_2 + A_3$ A_7	7	3	4	0
6) $A_1 \longleftarrow 2A_2 \longrightarrow A_3$ $A_3 + A_4 \longrightarrow A_5$ $A_6 + A_7$	6	2	4	0
7) (Lotka-mechanism) $A_1 \longrightarrow 2A_1$ $A_1 + A_2 \longrightarrow 2A_2$ $A_2 \longrightarrow 0$	6	3	2	1
8) (Glycolysis-mechanism) $0 \longrightarrow A_1$ $A_1 + A_2 \longrightarrow A_3 + A_4$ $A_3 + A_2 \longrightarrow A_4 + A_5$ $A_4 + A_6 \longrightarrow A_7 + A_6$	10	4	5	1

TABLE 3.6 (continued)

Mechanism	n	l	s	δ
9) (Brusselator) $0 \rightleftharpoons A_1 \longrightarrow A_2$ $2A_1 + A_2 \longrightarrow 3A_1$	5	2	2	1

is weakly reversible because for every directed arrow pathway there is a directed pathway leading back to the reactant complex.

From the number of complexes, the number of linkage classes and the dimension of the stoichiometric subspace, the deficiency (ref. 63) of the mechanism under consideration is given by

$$\delta = n - l - s.$$

Usually the characteristics of the dynamic behaviour of reactive systems are analysed in terms of the stability of the solutions of the set of differential equations which describe the reactive system mathematically. As these differential equations are derived from the underlying reaction mechanism, the dynamic behaviour of reactive systems should also be qualitatively predicted by the framework of the structure of the reaction network. Feinberg and Horn (refs. 60,63,64) suggested the "zero-deficiency"-theorem, which, for mechanisms with deficiency zero states that
(1) for mechanism not weakly reversible with arbitrary kinetics, the dynamic equations cannot give rise to an equilibrium point in the positive orthant of the species space;
(2) for mechanisms not weakly reversible with arbitrary kinetics, the corresponding dynamic equations cannot give rise to a cyclic composition trajectory which passes through a composition point in the positive orthant of the species space V^+;
(3) for weakly reversible mechanisms with mass action kinetics, the induced dynamic equations cannot give rise to composition cycles in the positive orthant of the species space and, with any choice of positive rate constants in each stoichiometric compatibility class in V^+, there exists one asymptotically stable equilibrium composition.

If every reaction in the reaction network is assigned with a scalar-valued rate function $r_{i,j}$, which only takes non-negative

values, a description of the dynamic behavior of the network is obtained. The kinetics are termed "mass-action" if the individual rate functions are of the form

$$r_{ij} \equiv k_{ij} \prod_{l=1}^{N} a_l^{\alpha_{il}} \tag{3.13}$$

where k_{ij} is a positive rate constant and a_l the molar concentration of species A_l. The actual state of the reaction mixture in the species space is represented by the vector $\alpha(t)$ which is defined by

$$\alpha(t) = a_1(t) \, e_1 + a_2(t) \, e_2 + \dots a_M(t) \, e_M. \tag{3.14}$$

The time derivative of $\alpha(t)$, $\dot{\alpha}(t)$ expresses vectorially the rate of change of composition of the reactive mixture and is defined by

$$\dot{\alpha}(t) = \dot{a}(t) \, e_1 + \dot{a}_2(t) \, e_2 + \dots \dot{a}_M(t) \, e_M. \tag{3.15}$$

For isothermal closed reactive systems, it is generally assumed that $\dot{\alpha}(t)$ is completely determined by $\alpha(t)$, which means that

$$\dot{\alpha}(t) = r\,(\alpha(t)) \tag{3.16}$$

where $r\,(\alpha(t))$ is the overall rate function and is constructed by taking a linear combination of all reaction vectors of the mechanism, each multiplied by the corresponding individual rate function. For example, for the following network (ref. 64)
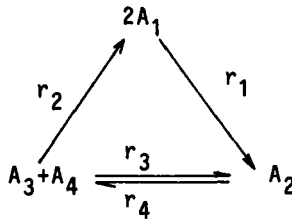
the overall rate function is
$$r\,(\alpha(t)) \equiv r_1\,[2e_1 - (e_3 + e_4)] + r_2\,[e_2 - 2e_1] +$$
$$+ r_3\,[e_2 - (e_3 + e_4)] + r_4\,[e_3 + e_4 - e_2] \tag{3.17}$$

or in component form
$$\dot{a}_1\,(t) = 2r_2 - 2r_1$$
$$\dot{a}_2\,(t) = r_1 + r_3 - r_4 \tag{3.18}$$
$$\dot{a}_3\,(t) = r_4 - r_3 - r_2$$

where $r_1 = k_1 \, a_1^2$, $r_2 = k_2 \, a_3 \, a_4$, $r_3 = k_3 \, a_3 \, a_4$ and $r_4 = k_4 \, a_2$ and k_1, k_2, k_3 and k_4 are positive rate constants. Composition trajectories cannot wander arbitrarily with time through the species space. They are constrained to remain in parallels of the stoichiometric subspace. This can be realized in the following way (ref. 64): If the set of vectors representing the complexes in the mechanism under consideration is denoted by $\{y_1, y_2, \ldots, y_2\}$ and the rate functions of the individual reactions from the i-th to the j-th complexes are denoted by r_{ij}, the overall rate function is given by

$$r(\alpha) \equiv \sum_{i,j=1}^{n} r_{ij}(\alpha) \, (y_i - y_j). \qquad (3.19)$$

The rate of change of composition of the reaction mixture is given by

$$\dot{\alpha}(t) = \sum_{i,j=1}^{n} r_{ij}(\alpha(t)) \, (y_i - y_j). \qquad (3.20)$$

The right-hand side of eq. 3.20 is a linear combination of the reaction vectors from which the reactive system is build up and therefore lies in the stoichiometric subspace S of the species space. Integration of eq. 3.20 yields

$$\alpha(t) = \alpha(0) + \sum_{i,j=1}^{n} \{ (\int_0^t r_{ij} (\alpha) \, dt) \, (y_i - y_j) \} \qquad (3.21)$$

where $\alpha(0)$ is the initial composition at $t = 0$ and $\alpha(t)$ are compositions on the corresponding trajectory. The second term on the right-hand side of eq. 3.21 is an element of the stoichiometric subspace S for the mechanism and hence all compositions on a composition trajectory are the sum of an initial composition and a time-dependent vector of the stoichiometric subspace and thus are confined to parallels of the stoichiometric subspace $\alpha(t) = \alpha(0) + S$. In other words, compositions $\alpha(t)$ are transformed into compositions $\alpha(t')$ only in a manner compatible with the stoichiometric constraints imposed by the underlying reaction network and, hence, all possible compositions are partitioned into stoichiometric compatibility classes exemplified by the mechanism

$$2A_1 \underset{k_{-1}}{\overset{k_1}{\rightleftharpoons}} A_2$$
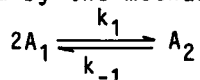
given in Fig. 3.9 (see also the last section of Chapter 2). The
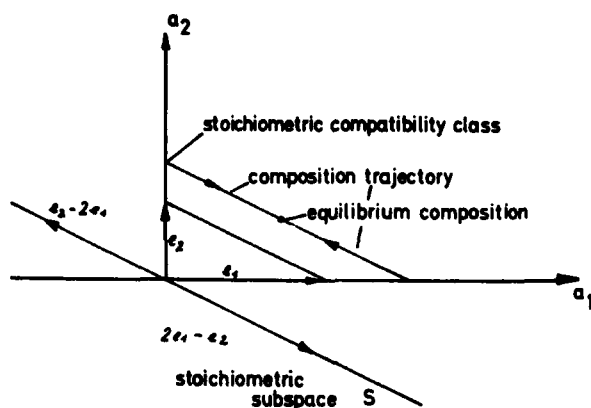
Fig. 3.9. Stoichiometric subspace and stoichiometric compatibility classes for mechanism $2A_1 \rightleftharpoons A_2$. Reproduced with permission after (ref. 63).

dynamic equations in component form for this mechanism are

$$\dot{a}_1 = -2k_1 a_1^2 + 2k_1 a_2 \quad \text{and}$$
$$\dot{a}_2 = k_1 a_1^2 - k_{-1} a_2. \tag{3.22}$$

So far dynamic equations have been derived on the basis of the underlying reaction networks by which the species are linked and comprise the reaction steps of reactive intermediates, bound to the catalyst surface, reaction steps by which the reactive intermediates on the surface are formed and the active centers are reproduced. Furthermore, it has been assumed that all these steps follow mass action kinetics. While this assumption is widely applied when modeling the dynamics of homogeneous gaseous phase reactions, in the case of heterogeneous catalytic gas-solid reactions it is inadequate for the phenomena occuring. The geometric and electronic characteristics of an active center on the catalyst surface (which, summarized over all active centers, determine the activity and selectivity of the catalyst) are strongly dependent on the actual state of the solid and also on adsorption of reactant and product molecules on the solid surface in the vicinity of the active centers. Thus, the rate constants of surface complex formation, transformation and desorption of products will usually be concentration-dependent, that means the catalyst cannot be considered as a constant entity over the total range of composition. However, in practice, with industrial heterogeneous catalytic reactions, partial

pressures of reactants and total pressures are often only varied to
a small extent and stable reactant and product molecules display a
similar adsorption behavior, by which, over a certain range of com-
position, the catalyst can be assumed to be a constant entity and
the rate coefficients independent of the amounts of reacting spe-
cies. Although this assumption introduces a model error, model
predictions and investigations on the structure of the underlying
reactive systems are more easily performed with systems of diffe-
rential equation having constant model parameters.

   Complex networks like those depicted in Schemes 3.12 and 3.13
give rise to multiparameter systems with largely varying parameter
values. Furthermore, a kinetic analysis of such networks presuppo-
ses knowledge of the rate of change of concentration of all species
in the network which, in most cases, is not available. Hence the
kinetic description of the reactive system is not usually based on
the original reaction network, but on a simplified reaction scheme.
The reduction of the original reaction network to a simplified
reaction scheme is realized using the steady-state approximation
and the assumption of a rate determining step in reaction sequences.
The procedure is illustrated (ref. 65) with a bimolecular reversible
reaction

$$A + B \underset{k-}{\overset{k+}{\rightleftharpoons}} C + D \qquad (3.23)$$

which is assumed to proceed in the following sequence;

step 1: $\qquad A + 1 \underset{k_{-1}}{\overset{k_1}{\rightleftharpoons}} A1$

step 2: $\qquad B + 1 \underset{k_{-2}}{\overset{k_2}{\rightleftharpoons}} B1$

step 3: $\qquad A1 + B1 \underset{k_{-3}}{\overset{k_3}{\rightleftharpoons}} C1 + D1$ $\qquad (3.24)$

step 4: $\qquad C1 \underset{k_{-4}}{\overset{k_4}{\rightleftharpoons}} C + 1$

step 5: $\qquad D1 \underset{k_{-5}}{\overset{k_5}{\rightleftharpoons}} D + 1.$
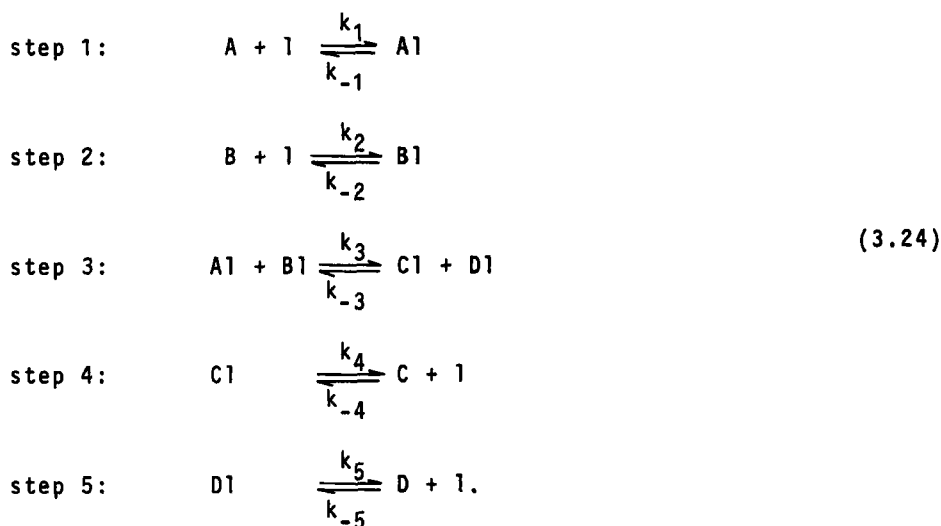
The steady-state approximation signifies that the rates of all the five steps of the reaction sequence are the same. If the bimolecular surface reaction (step 3) is the rate-determining step, the overall rate of the reaction is determined by the rate of this step

$$r = k_3 a_{A1} a_{B1} - k_{-3} a_{C1} a_{D1}. \tag{3.25}$$

As all the steps proceed at the same rate, steps 1, 2, 4 and 5 must be near the thermodynamic equilibrium composition points and it is usually assumed for these steps that thermodynamic equilibrium is established. This means that the ratio of products and reactants of these steps is time invariant. Hence, the surface concentrations which are the entries to the overall rate equation 3.25 can be replaced by experimentally accessible gas phase concentrations

$$
\begin{array}{lll}
\text{step 1} & \dfrac{a_{A1}}{a_A \, a_1} = K_1 & \\[2mm]
\text{step 2} & \dfrac{a_{B1}}{a_B \, a_1} = K_2 & \\[2mm]
\text{step 4} & \dfrac{a_{C1}}{a_C \, a_1} = K_4 & \tag{3.26} \\[2mm]
\text{step 5} & \dfrac{a_{D1}}{a_D \, a_1} = K_5 &
\end{array}
$$

where K_1, K_2, K_4, K_5 are adsorption equilibrium constants. Substituting the surface concentrations in eq. 3.25 by eq. 3.26 the following rate equation is obtained:

$$r = k_3 \cdot K_1 \cdot K_2 \left(a_A \cdot a_B - \frac{K_4 \cdot K_5}{K_{eq} \cdot K_1 \cdot K_2} \cdot a_C \cdot a_D \right) a_1^2 \tag{3.27}$$

where $K_{eq} = k_3/k_{-3}$ is the overall equilibrium constant. The concentration of the free active centers a_1 (which is also usually not directly amenable to experimental determination) can be replaced in the following way:
The total concentration of active centers a_{1t} is given by

$$a_{1t} = a_1 + a_{A1} + a_{B1} + a_{C1} + a_{D1}. \tag{3.28}$$

Substituting eq. 3.26 in eq. 3.28 we find

$$a_{1t} = a_1 + a_1 K_1 a_A + a_1 K_2 a_B + a_1 K_4 a_C + a_1 K_5 a_D \tag{3.29}$$

or

$$a_1 = \frac{a_{1t}}{1 + K_1 a_A + K_2 a_B + K_4 a_C + K_5 a_D} \quad . \tag{3.30}$$

The ratio a_1/a_{1t} is the fraction of unoccupied active centers

$$\frac{a_1}{a_{1t}} = \frac{1}{1 + \Sigma\, K_i a_i} \quad . \tag{3.31}$$

Correspondingly the fractional coverage of species A is given by

$$\frac{a_{A1}}{a_{1t}} = \Theta_A = \frac{K_1 a_A}{1 + \Sigma\, K_i a_i} \quad . \tag{3.32}$$

Rewriting eq. 3.25 in terms of fractional coverages, the following equation is obtained

$$r = k_3' \, \Theta_A \Theta_B - k_{-3} \, \Theta_C \, \Theta_D \tag{3.33}$$

where $k_3' = k_3 \cdot a_{1t}^2$. Substituting eq. 3.32 in eq. 3.33 results in

$$r = k_3 \cdot K_1 \cdot K_2 \cdot a_{1t}^2 \cdot \frac{a_A \cdot a_B - a_C \cdot a_D \cdot K_{eq} \cdot K_1 \cdot K_2/(K_4 \cdot K_5)}{(1 + \Sigma\, K_i a_i)^2} \quad . \tag{3.34}$$

Equation 3.34 can be further simplified by assuming a "most abundant surface intermediate" (masi).

With the procedure described so far, arbitrarily long sequences of consecutive reactions can be kinetically treated like one-step reactions. Concentrations of intermediates which are not usually accessible to experimental observation can be replaced by stable gas phase concentrations. In the case of heterogeneous catalytic reactions, this replacement introduces a number of adsorption equilibrium constants into the rate equation which, however, do not account for the equilibrium state between gaseous phase molecules and molecules adsorbed at the solid surface. However, they do account for reactive adsorption/desorption of reactant molecules on active centers, which are far less abundant on the solid surface than adsorption centers. Hence, these adsorption equilibrium constants cannot usually be determined by independent adsorption experiments. They are obtained from curve-fitting procedures on the basis of equations such as eq. 3.34. Combining the constants, which appear in products of different constants in eq. 3.34, into one constant in each case, a rate expression results which can be deri-

ved from different underlying reaction mechanisms as demonstrated by Boudart (ref. 59). Thus, in replacing the original reaction mechanism by a simplified reaction scheme for dynamic modeling, an ambiguity is introduced into the dynamic model equations derived from this simplified reaction scheme.

With the overall reaction given in eq. 3.23 and the assumed reaction sequence eq. 3.24, all steps take place only once to produce the overall conversion indicated in eq. 3.23 and the ratio of the overall forward to overall backward rate constant is given by

$$\frac{k_+}{k_-} = K \qquad (3.35)$$

where K is the thermodynamic equilibrium constant. In reaction sequences where the rate determining step must be repeated several times to produce the overall conversion, the ratio of the overall forward to backward rate constant is given by

$$\frac{k_+}{k_-} = K^{1/s_r} \qquad (3.36)$$

where s_r is the stoichiometric number of the rate determining step. This equation, which was first proposed by Horiuti (ref. 66), can be visualized in the following way (ref. 67). If a reaction, *e.g.* ammonia synthesis

$$N_2 + 3H_2 \; \underset{k_-}{\overset{k_+}{\rightleftharpoons}} \; 2NH_3 \qquad (3.37)$$
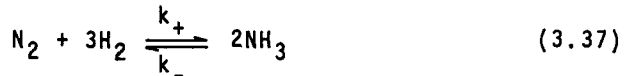
takes place *via* the following steps:

$$
\begin{array}{llll}
 & & & s \\
\text{step 1:} & N_2 + 2l \; \underset{k_{-1}}{\overset{k_{+1}}{\rightleftharpoons}} \; 2 \; Nl & & 1 \\[1em]
\text{step 2:} & H_2 + 2l \; \underset{k_{-2}}{\overset{k_{+2}}{\rightleftharpoons}} \; 2 \; Hl & & 3 \\[1em]
\text{step 3:} & Nl + Hl \; \underset{k_{-3}}{\overset{k_{+3}}{\rightleftharpoons}} \; NHl & & 2 \\[1em]
\text{step 4:} & NHl + H_2 \; \underset{k_{-4}}{\overset{k_{+4}}{\rightleftharpoons}} \; NH_3 + l & & 2 \\
\end{array}
\qquad (3.38)
$$
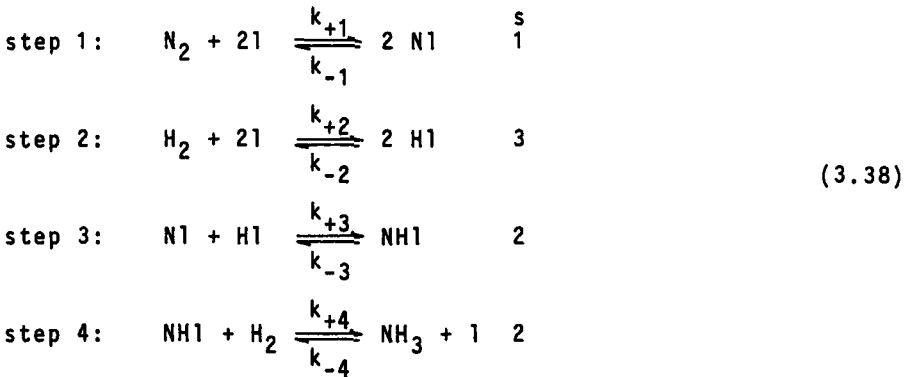
then step 1 takes place once, step 2 thrice and step 3 and 4 twice in order to obtain the stoichiometric conversion given by eq. 3.37.

At steady-state the rate of the overall reaction can be expressed
in terms of each of the rates of the individual steps divided by
their stoichiometric number. Hence, the overall reaction rate R of
reaction 3.37 is expressed as follows:

$$R = (r_{+1} - r_{-1}) = 1/3 \ (r_{+2} - r_{-2}) = 1/2 \ (r_{+3} - r_{-3}) =$$
$$= 1/2 \ (r_{+4} - r_{-4}) \tag{3.39}$$

where r_{+i} and r_{-i} are the forward and backward rates of the i-th
step. At equilibrium, the principle of microscopic reversibility is
assumed to hold and for step 1 for example, the equilibrium cons-
tant K_1 is equal to k_{+1}/k_{-1}

$$K_1 = k_{+1}/k_{-1} = \frac{a^2_{N1_{eq}}}{a_{N_2,eq} \ a^2_{1_{eq}}} = \exp(-\Delta G_0/RT) \tag{3.40}$$

where $a_{i_{eq}}$ are the equilibrium concentrations and ΔG_0 the standard
free energy change of the reaction under standard conditions. Under
the reaction conditions for step 1,

$$-\Delta G = \Delta G_0 + RT \ \ln \frac{a^2_{N1}}{a_{N_2} \cdot a^2_1} \tag{3.41}$$

where $-\Delta G$ is the free reaction enthalpy. Introducing the equilib-
rium constant into eq. 3.41 the following equation is obtained:

$$-\Delta G = -\Delta G_0 + RT \ \ln \ (\frac{a_{N_2} a^2_1}{a^2_{N1}} \cdot \frac{k_{+1}}{k_{-1}} \cdot \frac{1}{K_1}) =$$
$$\tag{3.42}$$
$$= -\Delta G_0 + RT \ \ln \frac{r_{+1}}{r_{-1}} - RT \ \ln K_1$$

where r_{+1} and r_{-1} are the forward and backward rates of step 1 of
eq. 3.38. For a reaction sequence the total free energy drop is
the sum of the free energy differences for each single step mul-
tiplied by its stoichiometric number. In the case where one step
is rate-determining, the free energy change of the overall reaction
ΔG is given by

$$\Delta G = s_r \cdot \Delta G_r \ \text{ or } \ \Delta G_r = \Delta G/s_r \tag{3.43}$$

where ΔG_r is the free energy change for the rate-determining step

and the overall rate follows from

$$R = \frac{1}{s_r} (r_{+r} - r_{-r}) = \frac{r_{+r}}{s_r} [1 - \exp(\Delta G/s_r RT)];$$ (3.44)

while at equilibrium,

$$\frac{R_+}{R_-} = \frac{k_+}{k_-} = \exp(-\Delta G/s_r RT) = K^{1/s_r}.$$ (3.45)

Hence, the ratio of the overall forward and backward rate constants of a reaction sequence is equal to K^{1/s_r}.

With the assumptions discussed so far, reaction sequences can be dynamically treated like one-step reactions. Another procedure for reducing complex reaction networks has been proposed by Wei and Kuo (refs. 68,69) for monomolecular reaction systems. By this procedure species are lumped into a few groups; this is exemplified in Scheme 3.14 by means of a four-component system which is lumped
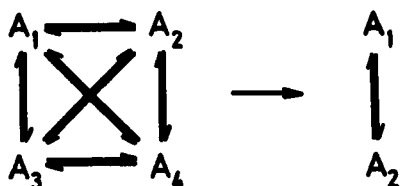
Scheme 3.14

into a two-component one. Wei and Kuo partitioned mathematical lumping into two categories, exact lumping and approximate lumping. Exact lumping can be further divided into proper lumping, semiproper lumping and improper lumping. With proper lumping, the chemical species of the system can be parcelled into several independent classes; with semiproper and improper lumping, each chemical species may belong to different lumping classes of species. In terms of composition vectors, lumping is the transformation of an n-tuple composition vector α into an $\hat{n}$-tuple vector $\hat{\alpha}$ (which has a smaller dimension than the original composition vector), by means of an $\hat{n}$ x n matrix M of rank $\hat{n}$:

$$\hat{\alpha} = M \cdot \alpha.$$ (3.46)

Monomolecular reaction systems, which give rise to the following
dynamic equation

$$\dot{\alpha}(t) = -K \, \alpha \, (t),\qquad (3.47)$$

are only exactly lumpable by a matrix M if a matrix $\hat{K}$ exists such
that the kinetic behavior of the lumped system can be described by

$$\frac{d\hat{\alpha}}{dt} = -\hat{K}\hat{\alpha}.\qquad (3.48)$$

The necessary and sufficient condition for a reaction system to be
exactly lumpable is (ref. 68)

$$M \cdot K = \hat{K} \cdot M.\qquad (3.49)$$

Considering the consequences of lumpability on the eigenvectors and
eigenvalues of the system, by the lumping procedure some of the
eigenvectors of the coefficient matrix K, eq. 3.47, are crossed
off and the remaining eigenvectors are projected into a correspon-
dingly lower dimensional space. If x_i and λ_i are the eigenvectors
and eigenvalues of the rate constant matrix K then for n - $\hat{n}$ eigen-
vectors of K, the vector Mx_i vanishes and, for the remaining eigen-
vectors of K, the vector Mx_i is an eigenvector of the rate constant
matrix of the lumped system $\hat{K}$ with the same eigenvalue λ_i. Hence

$$M = (\hat{X} \; \vdots \; 0) \, X^{-1}.\qquad (3.50)$$

Where $\hat{X}$ is the $\hat{n}$ x $\hat{n}$ nonsingular eigenvector matrix of $\hat{K}$ and 0 an
$\hat{n} \cdot (n - \hat{n})$ null matrix.

   The eigenvectors that remain, under mapping the original A-spe-
cies space into the lumped $\hat{A}$-species, are linear combinations of
the row vectors of the matrix MA. The theoretical lumping procedu-
res require knowledge of the rate constant matrix K. If the rate
constant matrix is not available in advance, the decision whether
the system is lumpable or not can be performed using experimental
methods based on either the definition, that systems are exactly
lumpable if and only if each pair of M-equivalent initial vectors
remains M-equivalent under motion with time along the reaction
trajectories, or on the theorems that the $\hat{A}$-subspace of the species
space is spanned by the row vectors of the matrix MA and that the
initial compositions in the $\hat{A}$-space will remain in this space while
converging on the equilibrium composition.

With the assumptions and theorems discussed so far, complex reaction networks can be reduced to more simplified reaction schemes, providing an adequate framework for deriving dynamic models. These kinetic models are the entries into the reactor models, which are considered in the following section.

3.2.2 Reactor models

Systems consist of the contents of a definite region in space. Usually systems are partitioned into (i) isolated systems, to or from which no mass, heat or work transfer can take place, (ii) adiabatic systems, to or from which no heat can be transferred, (iii) closed systems, across the boundaries of which no mass transfer can take place, and (iv) open systems which are defined as regions of space through which mass, heat or work flows. As non-isolated systems interact with other systems including reservoirs, the whole assembly of systems is considered as a global one. Reservoirs are idealized environments of the systems, assumed to be sufficiently large so that changes in all intensive properties, caused by interaction with the system, are negligible. Systems may be either at an equilibrium state, a steady-state or a non-steady state.

Themodynamic equilibrium systems are described using state functions, defined as properties which unequivocally determine the state of the system, independent of the way in which the equilibrium state is attained. The state functions are related to each other by an equation of state which defines a hyperplane in the coordinate system of the state functions to which all possible equilibrium states are restricted. Thermodynamic processes have taken place if, between two times, at least one of the properties of the system has changed. Usually they are considered to take place under reversible conditions, *i.e.* an infinitesimal change of driving force will reverse the direction of the process. The theoretical model for performing thermodynamic processes by passing at every stage through equilibrium states drastically simplifies their mathematical description because the state vector is restricted to the hyperplane defined by the equation of state.

Industrial chemical reactions are mostly accomplished in open systems with a continuous exchange of mass and energy with the environment. There are two limiting reactor types, the continuously operated stirred-tank reactor (CSTR) and the plug-flow reactor. In the following, only fixed bed reactors are considered and these, in

their idealized version, are mathematically modeled like plug-flow
reactors, because most heterogeneous catalytic reactions are
carried out in this type of reactor.There are also fluidized bed
and trickle bed processes. The mathematical description of these
reaction systems, however, is achieved in the same way as those of
fixed bed reactors. In deriving the mathematical models the variab-
les, by which the process under consideration is described, must
be known and an equation formulated for each dependent variable.
For example, with steady-state gaseous flow through a channel, the
four dependent variables are the pressure p, the density ρ, the
temperature T and the flow velocity u: the independent variable is
the area A of the cross-section of the channel. The model equations
are:

mass flux balance

$$\frac{dm}{dt} = A \cdot \rho \cdot u = \text{const.} \tag{3.51}$$

force balance

$$-A dp - A \cdot \rho \cdot u du - A \cdot \rho \cdot g dz - dF_w = 0 \tag{3.52}$$

energy balance

$$\frac{dU}{dt} + d(A \cdot p \cdot u) + \dot{m}\, d(\frac{v^2}{2}) + A \cdot dl \cdot \rho \cdot g \cdot v\, \frac{dz}{dT} - dQ_{ext} = 0 \tag{3.53}$$

and the equation of state of the gas

$$p = \rho \cdot RT. \tag{3.54}$$

The balances are formed over a differential volume element. The
terms in the force balance account for the resulting pressure force
on the volume element, the resulting inertia force, the axial com-
ponent of gravity force and the resulting resistance force. The
terms in the energy balance, where U is the internal energy of the
volume element, account for the increase in internal energy with
time in the volume element, the resulting energy flux against the
pressure force, the resulting kinetic energy flux, the increase of
potential energy with time and the external supplied energy flux.
Equations 3.51 to 3.54 describe gaseous dynamic processes and, in
general, also describe thermodynamic processes without any assump-
tions concerning the manner in which these processes take place.
In the case of all chemical reactors, chemical reactions must
also be considered within the model equations. This, however, does

not change the set of model equations. These are only extended by terms which account for the chemical reactions. The balances over differential volume elements dV in case of once-through-flow reactors (or over finite volumes ΔV in case of systems where the state functions are space invariant) always take the following form as specified, for example, for the mass balance for a species i, where the conservation principle requires that

$$\begin{matrix} \text{rate of } i \\ \text{into dV} \end{matrix} - \begin{matrix} \text{rate of } i \\ \text{out of dV} \end{matrix} - \begin{matrix} \text{rate of production} \\ \text{of } i \text{ in dV} \end{matrix} =$$

$$= \begin{matrix} \text{rate of accumulation} \\ \text{of } i \text{ in within dV.} \end{matrix} \tag{3.55}$$

The flux of i into or out of the volume element may be caused by convective or diffusive fluxes. In case of convective fluxes, the rate of accumulation of i in dV, Fig. 3.10, equals the differences
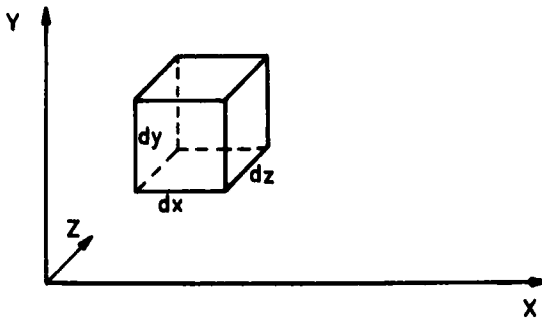
Fig. 3.10. Derivation of the mass balance.

of the fluxes in the directions along the axes of the spatial coordinate system in and out of the volume element.

$$\frac{\partial a}{\partial t} \cdot dxdydz = dydz \left[u_x \cdot a \big|_x - u_x \cdot a \big|_{x+dx} \right] + dxdz \left[u_y a \big|_y - u_y \cdot a \big|_{y+dy} \right]$$

$$+ dxdy \left[u_z a \big|_z - u_z \cdot a \big|_{z+dz} \right] \tag{3.56}$$

where u is the flow rate and a the concentration. The convective fluxes through the planes at x+dx, y+dy and z+dz are expanded into Taylor series around x, y and z and, as we deal with differential volume elements dV, all derivations of second and higher order are neglected. Hence the terms $u_x a \big|_{x+dx}$, $u_y a \big|_{y+dy}$ and $u_z a \big|_{z+dz}$ can be replaced by

$$dydz \ (u_x a|_{x+dx}) = [u_x a|_x + \frac{\partial u_x a}{\partial x} \ dx] \ dydz$$

$$dxdz \ (u_y a|_{y+dy}) = [u_y a|_y + \frac{\partial u_y a}{\partial y} \ dy] \ dxdz \qquad (3.57)$$

$$dxdy \ (u_z a|_{z+dz}) = [u_z a|_z + \frac{\partial u_z a}{\partial z} \ dz] \ dxdy.$$

Combining eq. 3.56 and 3.57 and introducing

$$\nabla = \frac{\partial f}{\partial x} + \frac{\partial f}{\partial y} + \frac{\partial f}{\partial z} \ ,$$

the rate of accumulation of species i by the convective flux is given by

$$\frac{\partial a}{\partial t} = -\nabla(u \cdot a). \qquad (3.58)$$

Correspondingly the diffusive flux through the volume element is given by

$$\frac{\partial a}{\partial t} \ dxdydz = dydz \ (I_x - I_{x+dx}) + dxdz \ (I_y - I_{y+dy}) +$$
$$+ \ dxdy \ (I_z - I_{z+dz}) \qquad (3.59)$$

where I is the diffusive flux defined by Fick's law

$$I = -D \ \frac{da}{dx} \ . \qquad (3.60)$$

Replacing the diffusive fluxes through the planes at x+dx, y+dy and z+dz by

$$I_{x+dx} = I_x + \frac{\partial I_x}{\partial x} \ dx \qquad \text{and so on,}$$

the rate of accumulation of species i in the volume element by the diffusive flux will be

$$\frac{\partial a}{\partial t} = \nabla(D \cdot \nabla a) \qquad (3.61)$$

where D is the diffusion coefficient. Hence, the overall rate of accumulation of species i in the volume element, caused by convective and diffusive fluxes, of a homogeneous nonreactive system follows from eq. 3.61 and 3.58

$$\frac{\partial a}{\partial t} = -\nabla(u \cdot a) + D \ \nabla^2 a. \qquad (3.62)$$

In the case of reactive systems, a further term is added to equation 3.62, which considers the rate of change of concentration of species i by chemical reaction.

Fixed bed reactor models are classified as shown in Table 3.7 (ref. 56). The pseudo-homogeneous models do not account for the

TABLE 3.7
Classification of fixed bed reactor models

	Pseudo-homogeneous models	Heterogeneous models
One-dimensional	plug flow reactor model	plug flow model
		+ interfacial gradients
	+ axial mixing	+ intraparticle gradients
Two-dimensional	+ radial mixing	+ radial mixing

presence of a solid catalytic phase in the reactor, this is considered with heterogeneous models, where separate conservation equations are derived for the fluid phase and the solid phase. With the basic reactor model, the flux of the fluid through the reactor is assumed as a plug flow by which all entering molecules will reside in the reactor for the same residence or contact time. If the reaction conditions are adjusted in such a way that isothermal plug flow prevails in the reactor, the analysis of conversion *versus* contact time data with respect to evaluating the kinetics of the chemical reactions is largely simplified and this is the reason why the basic reactor model has been used until now in most of the laboratory studies of heterogeneous catalytic processes.

If axial mixing and a diffusive flux are superimposed on the convective plug flow, a dispersion term is considered within the reactor model. Two-dimensional models account for radial gradients of concentration and temperature in the reactor and the mass and energy fluxes coupled with these gradients. With the basic heterogeneous model the flux of the fluid phase is assumed to be plug flow but different temperatures and concentrations are distinguished in the fluid and solid phase. More complex heterogeneous models consider interfacial and intraparticle gradients and nonideal flow of the fluid phase. In the following some fixed bed reactor models are delineated.

The ideal tubular-flow reactor is usually operated under steady-state and isothermal conditions and also under conditions where
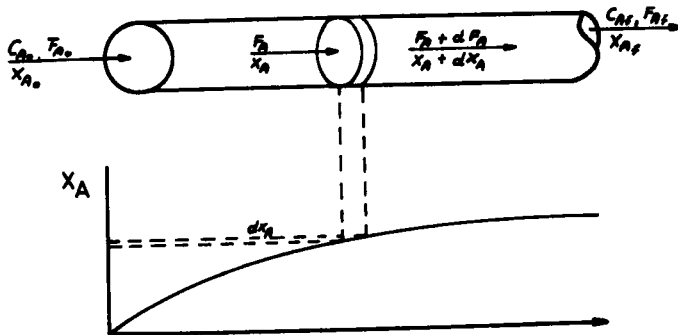
Fig. 3.11. Mass balance for the ideal plug flow reactor.

any pressure drop over the length of the reactor can be neglected. Steady-state conditions signify that the state functions are time--invariant at any position within the reactor. Applying eq. 3.55 to these operating conditions, the following equation is obtained (Fig. 3.11):

$$F_A - (F_A + dF_A) + r_A dV = 0 \qquad (3.63)$$

where F_A is the molar flux of species A (mol/sec), r_A the rate of the reaction based on volume of fluid and X_A the fraction of reactant A converted into product. Introducing

$$dF_A = -F_{A0} dX_A,$$

equation 3.63 can be rewritten

$$F_{A0} \, dX_A = (-r_A) dV$$

or

$$\int_0^V \frac{dV}{F_{A0}} = \int_0^{X_{Af}} \frac{dX_A}{(-r_A)} . \qquad (3.64)$$

In most of the laboratory studies of heterogeneous catalytic processes this is used for evaluating the kinetics of the underlying reaction mechanisms based on either the differential method of kinetic analysis or on the integral one.

If the reaction system is not isothermal and pressure drops over the length of the reactor have to be accounted for, besides the

mass balance, e.q. 3.63, an energy and a momentum balance is deri-
ved over the differential volume element and the following set of
differential equations is used for reactor simulation:

mass balance

$$-u \frac{da_A}{dz} = \rho_c \cdot r_A \qquad (3.65)$$

energy balance

$$u \cdot \rho_g \cdot c_p \frac{dT}{dz} = -(\Delta H)\rho_c \cdot r_A - \frac{4U}{d_t} (T - T_r) \qquad (3.66)$$

momentum balance

$$-\frac{dp}{dz} = \frac{2 \, f\rho_g \cdot u^2}{g \cdot d_p} \qquad (3.67)$$

where u is the linear velocity, z the length variable of the reac-
tor tube, ρ_c and ρ_g the catalyst and the gas density, c_p the speci-
fic heat of the fluid phase d_t and d_p the tube and the catalyst
particle diameter, f the friction factor and U an overall heat
transfer coefficient for the heat transfer from outside the reactor
tube into the catalyst bed. $\frac{1}{U} = \frac{1}{\alpha_i} + \frac{d}{\lambda} + \frac{1}{\alpha_u}$ where α_i and α_u are the
heat transfer coefficients outside and inside the tube, d the
thickness of the tube wall and λ the heat conductivity of the wall
material. The initial conditions of eq. 3.65-3.67 are $a_A = a_{A0}$,
$T = T_0$ and $p = p_0$ at $z = 0$.

Operation conditions of fixed-bed reactors which give rise to
model equation 3.64 (*i.e.* to a situation, where the reactor model
and the reaction rate model are quasi-identical) are frequently
applied to evaluate the kinetics of heterogeneous catalytic reac-
tions in order to analyze underlying reaction mechanisms *i.e.* to
identifying the reaction network and rate determining steps in that
network. The set of model equations 3.65-3.67, on the other hand,
is used for reactor simulation, *i.e.* for answering questions concer-
ning the length of the reactor, to obtain a certain conversion,
pressure drops, wall temperatures of the reactor tube, the determi-
nation of runaway criteria of the reactive system or process opti-
mization.

If the flow patterns in the reactor are more complicated, or lar-
ge gradients exist in the generalized forces between the phase
boundaries or within the single phases (which give rise to mass,
energy and momentum fluxes), additional terms are added to the set
of differential equations 3.65-3.67; alternatively the set of diffe-

rential equations is enlarged to account for these effects. In
cases where the flow pattern deviates from ideal plug flow axial
and/or radial dispersion is considered. The model equations for
situations with negligible pressure drop along the length of the
reactor then take the following form for steady-state conditions:
mass balance

$$\varepsilon \cdot D_a \frac{d^2 a_A}{dz^2} - u \frac{da_A}{dz} - \rho_c \cdot r_A = 0 \qquad (3.68)$$

energy balance

$$\lambda_a \frac{d^2 T}{dz^2} - \rho_g \cdot u \cdot d_p \frac{dT}{dz} + (-\Delta H)\rho_c \cdot r_A - \frac{4U}{d_t} (T - T_r) = 0 \qquad (3.69)$$

with the boundary conditions

$$\text{at } z = 0 : u (a_{A0} - a_A) = \varepsilon \cdot D_a \frac{da_A}{dz}$$

$$\rho_g \cdot uc_p (T_0 - T) = -\lambda_a \frac{dT}{dz} \qquad (3.70)$$

and at $\qquad z = L : \frac{da_A}{dz} = \frac{dT}{dz} = 0$

where T_r is the temperature of surroundings, ε is the bed porosity
(void fraction of packing), λ_a the effective thermal conductivity
in the packed bed in the axial direction and D_a the axial disper-
sion coefficient, which accounts for axial diffusion and axial
mixing due to nonideal flow. Model equations 3.68 and 3.69 predict
uniform concentrations and temperatures in a cross-section of the
reactor tube. If reactions with pronounced heat effects are invol-
ved, this may be too much of a simplification and terms which con-
sider radial heat and mass fluxes are incorporated in the model
equations 3.68 and 3.69. Detailed analysis of this is outside the
scope of the present book. Various approximations have been sugges-
ted but, as pointed out by Paterson and Carberry (ref. 70) they
often result in poor agreement between theory and experiment. These
authors also consider axial heat dispersion because radial heat
conductivity is not constant along the reactor bed. Similarly, the
ratio of tube diameter to particle diameter should be taken into
account in order to obtain a better fit to experimental data.

In contrast to the pseudo-homogeneous models, in heterogeneous
models of fixed bed reactors the differential volume over which
mass, energy and momentum balances are derived is partitioned into

a fluid and a solid phase and mass and energy fluxes, through the phase boundary and within the single phases, are also considered. The coupling of concentrations in the fluid and the solid phase is performed by either use of the concentration gradient in the solid phase boundary or by use of the concentration gradient through the boundary layer around the solid particles. Under steady-state conditions, the mass transport rate through the boundary layers around the catalyst particles equals the rate of chemical reactions within the catalyst particles and, with the same assumptions for the basic pseudohomogeneous model, model equations for the basic heterogeneous model are given by:

fluid phase

$$-u \cdot \frac{da_A}{dz} = k_g A_v (a_A - a_A^S) \tag{3.71}$$

$$u \cdot \rho_g \cdot c_p \frac{dT}{dz} = h_f A_v (T^S - T) - \frac{4U}{d_t} (T - T_r) \tag{3.72}$$

solid phase

$$\rho_B \cdot r_A = k_g \cdot A_v (a_A - a_A^S) \tag{3.73}$$

$$(-\Delta H) \rho_B r_A = h_f \cdot A_v (T^S - T) \tag{3.74}$$

boundary conditions

at z = 0 $a_A = a_{A0}$ and $T = T_0$

where k_g is the gas phase mass transfer coefficient, A_v the external catalyst particle surface area per unit catalyst mass, h_f the heat transfer coefficient for the heat transfer through the boundary layer around the solid particles, a_A^S, the molar concentration of fluid reactant in front of the catalyst particles and T^S the temperature at the solid surface.

The terms $k_g A_v (a_A - a_A^S)$ and $h_f \cdot A_v (T^S - T)$ follow from the film model for mass and heat transfer from the fluid to the solid phase, where concentration and temperature gradients are restricted to a boundary layer around the solid. Mass and heat transfer through the boundary layer are described by Fick's law, respectively:

$$I = -D \cdot A_v \frac{da}{dx} \quad \text{and} \quad Q = -\lambda A_v \frac{dT}{dx} \tag{3.75}$$

where x is the distance coordinate through the boundary layer.

Replacing the differentials da/dx and dT/dx by $\Delta a/\Delta x$ and $\Delta T/\Delta x$, and compressing $D/\Delta x$ to k_g and $\lambda/\Delta x$ to h_f the terms given above are obtained.

If mass and heat transfer rates inside the catalyst particle have to be considered and the reaction rate is not uniform throughout the catalyst particle, the set of reactor model equations takes the following form:

fluid phase

$$-u \frac{da_A}{dz} = k_g \ A_v \ (a_A - a_A^s) \tag{3.76}$$

$$u \cdot \rho_g \ c_p \ \frac{dT}{dz} = h_f \cdot A_v \ (T^s - T) - \frac{4U}{a} \ (T - T_r) \tag{3.77}$$

solid phase

$$\frac{D_{eff}}{r^2} \frac{d}{dr} \ (r^2 \frac{d\bar{a}_A}{dr}) - \rho_s \ r_A \ (\bar{a}_A, \ \bar{T}) = 0 \tag{3.78}$$

$$\frac{\lambda_{eff}}{r^2} \frac{d}{dr} \ (r^2 \frac{d\bar{T}}{dr}) + \rho_s \ (-\Delta H) \cdot r_A \ (\bar{a}_A, \ \bar{T}) = 0 \tag{3.79}$$

with the boundary conditions

at $\quad z = 0 : a_A = a_{A0}, \quad T = T_0$ (3.80)

at $\quad r = 0 : \frac{d\bar{a}_A}{dr} = \frac{d\bar{T}}{dr} = 0$ (3.81)

at $\quad r = R : k_g \ (a_A^s - a_A) = -D_{eff} \frac{d\bar{a}_A}{dr}$

$$h_f \ (T^s - T) = -\lambda_{eff} \frac{d\bar{T}}{dr} \tag{3.82}$$

where D_{eff} and λ_{eff} are respectively the effective diffusion coefficient and the effective thermal conductivity in the catalyst, R the radius of the catalyst particle, r the radial coordinate in the catalyst pellet and $\bar{a}$ and $\bar{T}$ concentration and temperature within the catalyst particle.

In the model equations 3.76-3.82 heat and mass transfer rates inside the catalyst pellet and at the solid/fluid phase boundary are considered. Quite often, even with strongly exothermic reactions, the catalyst particles are practically isothermal due to the comparatively large heat conductivity of solids, whereas temperature gradients occur at the phase boundary between solid particles and fluid. On the other hand, effective diffusivities of species in porous media are much smaller than corresponding bulk

diffusivities through the boundary layer around the catalyst particles. Hence, concentration gradients are expected inside the catalyst particles with only small concentration gradients in the boundary layer around them.

With the reactor models discussed so far, continuum models have been used for the interstitial fluid. In the case of pseudo-homogeneous models the catalyst particles have been assumed to be small enough to ensure that the concentration and temperature fields, with which the particles interact, are uniform. In the case of heterogeneous models for fluid and solid phase, continuum models have been applied and concentrations and temperatures in both fields are coupled by the mass and energy fluxes through the phase boundaries. In contrast to these models, with the so-called cell models the interstitial fluid is described by connected cells in each of which the fluid has uniform properties. The cells may only be connected axially. If radial fluxes in the reactor tube have to be considered, the cells are also connected in a radial direction. Furthermore, feed-back mechanisms can be incorporated in the models.

The cell models are compared with a continuous model, satisfying the experimentally verified conditions that in a fixed bed there is practically no backmixing and that signal propagation speed is finite (ref. 71). Although a solution of the continuous hyperbolic equation, satisfying the physically exact inlet boundary conditions, can be obtained, it has been pointed out (ref. 71) that for design purposes, no one model has an outstanding advantage over any other. So, the simpler "standard dispersion model", with the obviously incorrect conditions of backmixing and infinite signal propagation speed, can be used for reactor design with an accuracy sufficient for practical purposes provided one keeps in mind its inadequacy when fine structures (*e.g.*, accurate concentration at a specified point) are to be determined. The common characteristic of all the models presented so far, except the steady-state cell models, is that they consist of a set of ordinary or partial nonlinear or linear differential equations. The applications of these reactor models, however, are quite different.

In the epistomological application of dynamic models the aim is to understand the space-time structure of real catalytic reactive systems and for this the existence and stability of solutions of the set of differential equations is investigated.

In the industrial application of dynamic models the aims are to quantitatively compare the activity, selectivity and long-time sta-

bility of catalysts and to simulate chemical reactors with respect
to scale-up from laboratory reactors to industrial ones, to optimi-
ze chemical processes and to investigate the stability of the che-
mical reactors. For these latter aims the model parameters have to
be determined by fitting to suitable experimental data and, using
further statistical procedures, the reliability of the estimated
parameters must be evaluated. Usually the model parameters cannot
be determined by performing independent experiments or calculated
with suitable correlations. Once the model parameters have been
evaluated, quantitative model predictions are feasible. In the
following section a short survey is given of the structure of
linear and nonlinear systems and of parameter estimation procedures.

3.2.3 Linear systems

Usually in kinetic investigations the temperature is kept cons-
tant within a set of experiments and the model coefficients are
assumed to be constant. Thus an autonomous system of differential
equations of the form

$$\dot{a} = f \, (a_i) \qquad\qquad (3.83)$$

is obtained.

Heterogeneous catalytic reaction systems are frequently kineti-
cally modelled using the hyperbolic Langmuir-Hinshelwood-Hougen-
-Watson (LHHW)-models

$$-r = \frac{-k \; \Pi \; a_i^{n_i}}{[1 + \Sigma \; K_i a_i^{m_i}]^0} \; . \qquad\qquad (3.84)$$

With hyperbolic reaction rate models, two situations may arise: in
the first the denominator of the LHHW-model is the same for all
rate equations and can be factorized to yield pseudo mass action
rate equations. In the case of pseudomonomolecular systems, equation
3.84 then takes the form

$$\frac{da_i}{dt} = \Phi[- \sum_j k_{ji} \, a_i + \sum_j k_{ij} \, a_j] \qquad\qquad (3.85)$$

where Φ is a function of composition and time, which is the same
for all rate equations in the system. The conditions under which
heterogeneous catalytic reaction systems follow pseudo-mass-action
kinetics have been discussed in previous sections.

If the denonimators are not the same, in the individual rate

equations they can be compressed with the reaction time and the selectivity behavior of the catalyst following from pseudo mass-action rate equations. For this analysis, which has been proposed by Kugelmann et al. (ref. 72) and Ramage et al. (ref. 73), equation 3.85 may be rewritten using matrix and vector notation. We put

$$\alpha(t): = \begin{bmatrix} a_1(t) \\ \cdot \\ \cdot \\ \cdot \\ \cdot \\ a_n(t) \end{bmatrix}$$

and

$$K: = \begin{bmatrix} -\sum\limits_{j=1}^{n} k_{ji} & k_{12} & \cdots & k_{1n} \\ \cdot & & & \\ \cdot & & & \\ \cdot & & & \\ \cdot & & & -\sum\limits_{j=1}^{n} k_{jn} \\ k_{n1} & k_{n2} & \cdots & \end{bmatrix}$$

and obtain $\dot{\alpha}(t) = \Phi \cdot k_{lm} \cdot K'\alpha(t)$,   (3.86)

where $\Phi = \dfrac{1}{1 + P \cdot g^{T} \cdot \alpha(t)}$, P the total pressure, g a row vector with elements g_i, g_i the adsorption isotherm for the i-th species, k_{lm} the lm-th element in the rate constant matrix K and $K = k_{lm} \cdot K'$. Introducing a fictitious time scale defined by

$$d\tau = \dfrac{1}{1 + P \cdot g^{T} \cdot \alpha(t)} \cdot k_{lm} \cdot dt$$ (3.87)

equation 3.86 can be rewritten

$$\dfrac{d\alpha}{d\tau} = K' \cdot \alpha(t).$$ (3.88)

From the solution of equation 3.88 the selectivity behavior of the reaction system is obtained in terms of relative rate constants for the individual reactions. If the conversion in the reactor is to be determined, absolute rate constants and the terms g_i must be known and these are obtained by integration of equation 3.87.

If the kinetic analysis is performed with a fixed bed reactor, operated under steady-state and isothermal conditions with plug flow of the fluid phase, the time variable in equation 3.86 is replaced by the liquid hourly space velocity S_{LH}, defined as volume

liquid feed/volume catalyst time and equation 3.86 takes the following form

$$\frac{\rho_1}{M_f \cdot \rho_s} \cdot \frac{d\alpha}{d(1/S_{LH})} = \Phi \cdot k_{lm} \cdot K' \cdot \alpha(t) \qquad (3.89)$$

where ρ_1 and ρ_s are the liquid and bulk catalyst densities, respectively and M_f the molecular weight of the feed. Again introducing a fictitious time τ'

$$d\tau' = \frac{M_f \cdot \rho_s}{\rho_1} k_{lm} \Phi \, d \, (1/S_{LH}) \qquad (3.90)$$

equation 3.89 becomes monomolecular with respect to τ'

$$\frac{d\alpha}{d\tau'} = K' \cdot \alpha. \qquad (3.91)$$

Now the selectivity behavior of the catalytic systems is described by the solution of equation 3.91 and the activity behavior by integration of equation 3.90.

The considerations presented so far indicate that, even with heterogeneous catalytic reactions, pseudomonomolecular systems play an important part. The well-known general solution to a system of coupled linear first order differential equations (eq. 3.91) is

$$a_1 = c_{11} e^{-\lambda_1 t} + \ldots c_{1n} e^{-\lambda_n t}$$
$$\vdots$$
$$a_n = c_{n1} e^{-\lambda_1 t} + \ldots c_{nn} e^{-\lambda_n t} \qquad (3.92)$$

where c_{ji} and λ_i are constant parameters related to the rate constants k_{ij}. Using this form of the general solution for estimating the rate constants of the individual "elementary reactions" from experimental data, difficulties arise firstly from the curve fitting techniques by which a set of model parameters (c_{ij}, λ_i) is determined from a set of experimental data, and secondly in deriving the rate constants k_{ij} from the model parameters (c_{ij}, λ_i).

It is well known, however, from the basic theory of linear differential equations that the system of coupled linear differential equations 3.91 can be transformed into an uncoupled system, the solution of which easily allows the determination of the desired rate constant matrix K. For this purpose, we introduce new

functions

$$a_i(t) = \sum_{j=1}^{n} x_{ij} \, b_j(t) \qquad i = 1 \ldots n$$

or, again using matrix and vector notation,

$$\alpha(t) = X \cdot \beta(t) \tag{3.93}$$

where

$$X: = \begin{bmatrix} x_{11} & \cdots & x_{1n} \\ \cdot & & \\ \cdot & & \\ \cdot & & \\ \cdot & & \\ x_{n1} & \cdots & x_{nn} \end{bmatrix} \text{ and } \beta(t): = \begin{bmatrix} b_1(t) \\ \cdot \\ \cdot \\ \cdot \\ \cdot \\ b_n(t) \end{bmatrix} .$$

The coefficients x_{ij} in eq. 3.92 are chosen in such a way that the original coupled system of differential equations 3.90 is transformed into the following uncoupled set

$$\dot{b}_1(t) = -\lambda_1 \, b_1(t)$$
$$\cdot$$
$$\cdot \tag{3.94}$$
$$\cdot$$
$$\dot{b}_n(t) = -\lambda_n \, b_n(t)$$

or, again in matrix and vector notation,

$$\dot{\beta}(t) = -\Lambda\beta(t) \tag{3.95}$$

where Λ is the diagonal matrix

$$\Lambda = \begin{bmatrix} \lambda_1 & \cdots\cdots & 0 \\ \cdot & \cdot & \\ \cdot & & \cdot \\ \cdot & & \cdot \\ 0 & \cdots\cdots & \lambda_n \end{bmatrix} .$$

For proper determination of the parameters x_{ij} we differentiate eq. 3.93

$$\dot{\alpha}(t) = X \cdot \dot{\beta}(t) . \tag{3.96}$$

Introducing eq. 3.93 and eq. 3.96 into eq. 3.91 we obtained

$$X \cdot \dot{\beta}(t) = K \cdot X \cdot \beta(t) . \tag{3.97}$$

Multiplying from the left by X^{-1}, the inverse of X results in

$$\dot{\beta}(t) = X^{-1} \cdot K \cdot X \cdot \beta(t) . \tag{3.98}$$

Eq. 3.98 and eq. 3.95 are identical provided $X^{-1} \cdot K \cdot X$ represents a diagonal matrix, *i.e.* X must be chosen in such a way, that K is diagonalized. From matrix calculus (ref. 74) we know that each matrix with n linear independent eigenvectors x_i is transformed into the diagonal matrix

$$-\Lambda = -\text{Diag}(\lambda_i)$$

of its eigenvalues by a transition to the coordinate system of the eigenvectors of the matrix, which immediately follows from the eigenvalue equations. Hence, if the condition is satisfied that K possesses n linearly independent eigenvectors, the transformation matrix X must be formed from the n eigenvectors of K to diagonalize K. The proof that this condition holds was given by Wei and Prater (ref. 75) for n-component reversible monomolecular reaction systems. In the case of reaction systems with irreversible and reversible reaction steps it is not always possible to diagonalize K. Solutions to eq. 3.94 are easily obtained:

$$
\begin{aligned}
b_1(t) &= C_1\, e^{-\lambda_1 t} \\
&\ \vdots \\
b_n(t) &= C_n\, e^{-\lambda_n t} \ .
\end{aligned}
\tag{3.99}
$$

Introducing eq. 3.99 into eq. 3.91 we obtain the general solution to the system of linear differential eq. 3.91

$$
\begin{aligned}
a_1(t) &= C_1\, x_{11}\, e^{-\lambda_1 t} + \ldots C_n\, x_{1n}\, e^{-\lambda_n t} \\
&\ \vdots \\
a_n(t) &= C_1\, x_{n1}\, e^{-\lambda_1 t} + \ldots C_n\, x_{nn}\, e^{-\lambda_n t} .
\end{aligned}
\tag{3.100}
$$

Rewriting eq. 3.100 in vector and matrix notation yields

$$\alpha(t) = X\, e^{-\Lambda t}\, C \tag{3.101}$$

where the vector C can be determined from the initial value of α at $t = 0$

$$\alpha(0) = X \cdot C$$

hence
$$C = X^{-1}\, \alpha(0) \qquad \text{and}$$

$$\alpha(t) = X\, e^{-\Lambda t}\, X^{-1} \alpha(0) \tag{3.102}$$

which is the general solution to eq. 3.91.

Combining all the eigenvalue equations

$$K \cdot x_i = -\lambda_i \, x_i \qquad\qquad (3.103)$$

results in the following equation

$$K \cdot X = -X\Lambda \qquad\qquad (3.104)$$

from which the rate constant matrix K can be obtained by multiply-
ing with the inverse of X from the right

$$K = -X\Lambda X^{-1} . \qquad\qquad (3.105)$$

Hence, the rate constant matrix can easily be computed as long as
the eigenvectors and eigenvalues of the rate constant matrix are
known. In the following section some procedures are described which
enable the determination of the eigenvectors and eigenvalues of the
rate constant matrix.

3.2.4 Parameter estimation procedures with linear differential equations

Estimation of the parameter matrix in the mathematical models of
open reactive systems is now usually performed using computer prog-
rams which contain parameter estimation procedures *via* optimization
of suitable objective functions and statistical testing procedures
which indicate the reliability of the obtained set of model para-
meters. With reactive systems, which can be kinetically described
by a set of linear differential equations, other procedures are
feasible. As discussed so far the action of the rate constant
matrix on the state vector $\alpha(t)$, which comprises the concentrations
of the individual species, causes in most cases a rotation and a
variation in length of the state vector. There are directions of
the state vector, however, in the composition space where the ac-
tion of the rate constant matrix only causes a variation in length
of the state vector. If these directions are denoted by x_i the
following equation holds:

$$K \cdot x_i = -\lambda_j \cdot x_i . \qquad\qquad (3.106)$$

The vectors x_i are the eigenvectors and the scalar constants $-\lambda_j$
the eigenvalues of the matrix K. Equation 3.106 implies that the
model parameters can be obtained by simple matrix operations as
long as the eigenvectors and eigenvalues of the parameter matrix
are known. The eigenvectors and eigenvalues of the rate constant
matrix K can be determined from equation 3.102, or by use of proce-
dures proposed by Gavalas (ref. 76) and Wei and Prater (ref. 75).

(i) <u>Two-point-method.</u> This method uses the general solution to systems of linear differential equations. In order to use eq. 3.102 for determining the eigenvectors and eigenvalues of K, we must rewrite this equation. Eq. 3.102 still holds if we replace the single composition vectors $\alpha(t)$ and $\alpha(0)$ by concentration matrices A(T) and A(0), formed from a set of composition vectors $\alpha_i(0)$ and $\alpha_i(t)$

$$A(t) = (\alpha_1(t) \ \cdots \ \alpha_n(t))$$
$$A(0) = (\alpha_1(0) \ \cdots \ \alpha_n(0)).$$

(3.107)

To obtain invertible matrices, the number n of the composition vectors in A(0) and the corresponding matrix A(t) must equal the number n of the components in the state vector α and the initial vectors $\alpha_i(0)$ must be linearly independent. If a larger number m>n of experiments is used for the kinetic analysis, the matrices A(t) and A(0) will have to be multiplied by the transpose of the matrix A(t) (ref. 77). Substituting A(t) and A(0) for $\alpha(t)$ and $\alpha(0)$ in eq. 3.102 and multiplying by $A(0)^{-1}$ and X we obtain

$$[A(t) \ A(0)^{-1}] \ X = X \ e^{-\Lambda t}$$

(3.108)

showing that the matrix $[A(t) \ A(0)^{-1}]$ has eigenvectors x_i, which are, at the same time, the eigenvectors of the rate constant matrix K, and eigenvalues $e^{-\lambda_i t}$, from which the eigenvalues $-\lambda_i$ of the rate constant matrix can easily be calculated. For this calculation, however, the state vectors $\alpha_i(t)$ must all be obtained at the same time t. If the experiments are performed in a batch-operated stirred tank reactor or in a continuously operated fixed bed reactor, this means that the composition vectors $\alpha_i(t)$ must be obtained at equal reaction times or space velocities, respectively. To circumvent this exprerimental difficulty, concentration *versus* reaction time or space velocity data are measured and from the resulting graphs initial concentration vectors and state vectors at a certain reaction time or space velocity are determined.

The foregoing analysis indicates that two composition points on different linearly independent reaction trajectories in the composition space are always needed to determine the rate constant matrix. The analysis can also be applied to linear diffusion-reaction systems as, for example, in the evaluation of experimental data from the diffusion reactor (ref. 78) which is described in more detail in Chapter 4. In this case the change of composition with

time is described by the following set of differential equations

$$\nabla^2 \alpha - [(L^2 A)\; D^{-1}\; K]\; \alpha = 0 \qquad (3.109)$$

where α is again the composition vector, L the length of the catalyst pellet, A the catalytically active area per unit volume of pellet and D the diagonal matrix of the effective diffusivities of the species in the porous pellet. With the boundary conditions

$$\nabla \alpha = 0 \qquad \text{at} \quad \eta = 1$$

and

$$\alpha = \alpha(1) \qquad \text{at} \quad \eta = 0$$

where η is a dimensionless position variable through the pellet, the solution is

$$\alpha(0) = X\; [1/\cosh\,(h_\lambda)]\; X^{-1}\alpha(1) \qquad (3.110)$$

where X and h_λ are the eigenvectors and the eigenvalues of the matrix $[(L^2 A)\; D^{-1} K]$. Introducing again concentration matrices A(1) and A(0) formed from corresponding bulk and centerplane concentration column vectors, and multiplying by the inverse of A(1) and the eigenvector matrix X, the following equation is obtained

$$[A(0)\; A(1)^{-1}]\; X = X\; [1/\cosh\,(h_\lambda)]. \qquad (3.111)$$

Hence, from the experimentally determined matrix $[A(0)\; A(1)^{-1}]$, eigenvectors and eigenvalues are computed by which the eigenvector matrix X and - after calculation of $[1/\cosh\,(h_\lambda)]$ - the eigenvalue matrix of the original matrix $[(L^2 A)\; D^{-1}\; K]$ are obtained. The rate constant and diffusivity matrix can be separated by making use of the reaction rates in the bulk phase measured simultaneously with corresponding sets of bulk and centerplane concentrations.

Recently an initial value approach has been suggested which converts the two-point boundary value problem into an initial value one. It is claimed that the performance of the method is equivalent to that of the two-point method. The transformations are presented for three types of Langmuir-Hinshelwood equations (*cf.* Eq. 3.84 in the simplest cases when $i=1$ or 2 and also, for the case when the denominator is raised to the n-th power). Simple power law rate equations and autocatalysis are also tackled (ref. 79).

(ii) <u>The method of Gavalas.</u> In contrast to the "two-point" method described so far, Gavalas (ref. 76) gave another approach for estimating the matrix in linear systems with constant coefficients

and real eigenvalues in which an arbitrary number of measured compositions along reaction trajectories are taken into account. The only restriction is, that composition points on the different trajectories, at the same reaction times or space velocities, are needed. Gavalas begins with the general solution to systems of linear differential equations, eq. 3.102. After some rearrangements of this equation the following expression is obtained.

$$\sum_{l=1}^{n} \gamma_l(j) \ [\alpha_l(k,\beta) - \alpha_l(1,\beta) \ e^{-\lambda_j t_k}] = 0 \qquad (3.112)$$

where $\gamma(j)$ is the j-th row of the inverse of the eigenvector matrix X^{-1}, $k = 1 \ldots N$ (N = number of measurement times), $\beta = 1 \ldots m$ (m = = number of initial states), $l = 1 \ldots n$ (n = number of components in the state vector). The form of eq. 3.112 corresponds to least square problems, which belong to the classic applications of symmetric matrices (ref. 80) and thus suggests the formulation of a sum for error squares

$$J = \sum_{k=1}^{N} \sum_{\beta=1}^{m} \sum_{l=1}^{n} \left\{ \gamma_l(\alpha_l(k,\beta) - \alpha_l(1,\beta) \ e^{-\lambda t_k} \right\}^2 \qquad (3.113)$$

where λ is now a variable. Eq. 3.113 can be rewritten in quadratic form

$$J = \gamma^T \ W(\lambda) \gamma \qquad (3.114)$$

where $W(\lambda)$ is a symmetric matrix and J is a scalar. The quadratic form is positive definite for all $\lambda \neq \lambda_j$ and positive semidefinite for $\lambda = \lambda_j$. The proof that $J(\lambda)$ is positive semidefinite for all $\lambda = \lambda_j$ follows directly from Eq. 3.113. For $\gamma_l(j) = 0$, the bracket amounts to zero for $\lambda = \lambda_j$ and from this $J(\lambda) = 0$. For any given λ, the minimum $\mu(\lambda)$ of the quadratic form with respect to λ and γ is the smallest eigenvalue of $W(\lambda)$ which can be proved by

$$\mu(\lambda) = \min_{|\gamma|=1} \gamma^T \ W(\lambda) \gamma = \min_{\gamma} \frac{\gamma^T}{|\gamma|} \ W(\lambda) \ \frac{\gamma}{|\gamma|} = \min_{\gamma \neq 0} \frac{\gamma^T W(\lambda) \gamma}{\gamma^T \gamma} \ , \qquad (3.115)$$

introducing a new variable $\gamma = \gamma_0 + t\zeta$, where $\zeta \in R^n$ and $t \in R$. A function

$$f(t) = \frac{(\gamma_0 + t\zeta)^T \ W(\lambda) \ (\gamma_0 + t\zeta)}{(\gamma_0 + t\zeta)^2} \qquad (3.116)$$

is obtained which reaches a minimum at $t = 0$ and can be differentiated to yield

$$f'(0) = \frac{2}{\gamma_0^2} [\zeta^T W(\lambda)\gamma_0 - \frac{\gamma_0^T W(\lambda)\gamma_0}{\gamma_0^2} \zeta^T\gamma_0] \qquad (3.117)$$

rearranging yields

$$\zeta^T (W(\lambda) \gamma_0 - \mu(\lambda) \gamma_0) = 0 \qquad (3.118)$$

for all $\zeta \in R^n$ or

$$W(\lambda)\gamma_0 - \mu(\lambda)\gamma_0 = 0. \qquad (3.119)$$

The function $\mu(\lambda)$ reaches minimum values at points $\lambda_1, \ldots, \lambda_n$, which are the eigenvalues of the matrix K. The corresponding vectors $\gamma(\lambda_1), \ldots, \gamma(\lambda_n)$ are the rows of the matrix X^{-1} and the rate constant matrix is again calculated by

$$K = X\Lambda X^{-1}. \qquad (3.120)$$

The procedure for determining the rate constant matrix is the following: starting from a number of initial states which must span the reaction space, paths in the composition space are measured at equal reaction times. From this data the matrix $W(\lambda)$ is computed for any given λ. With standard routines like the Householder-Givens method, the smallest eigenvalue of $\mu(\lambda)$ is calculated. Then λ is varied over a special range and for each λ the smallest eigenvalue is computed. A plot of the smallest eigenvalues of $W(\lambda)$ against λ yields a graph which has local minima at $\lambda_1, \ldots, \lambda_n$. This is demonstrated in Fig. 3.12 for the reaction network of Scheme 3.15 (ref. 42). The original problem of estimating a set of parameters from experimental data is thus replaced by a one-dimensional computer search.
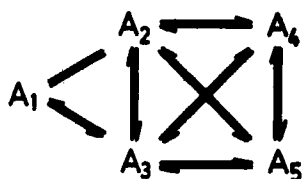
Scheme 3.15
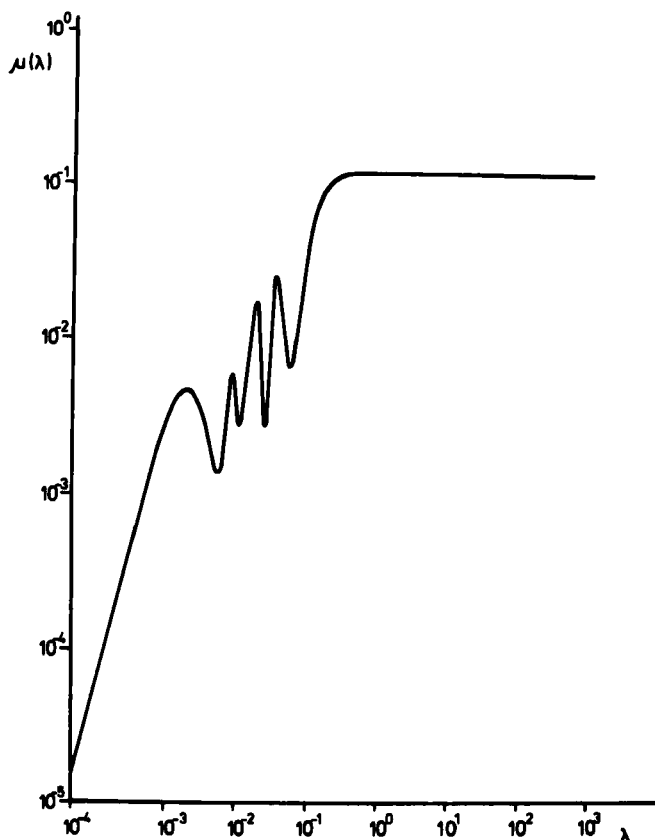
Fig. 3.12. Evaluation of eigenvalues of the rate constant matrix for a reversible five-component system with the method of Gavalas. Reproduced with permission from (ref. 42), p. 174, by courtesy of Marcel Dekker, Inc.

(iii) The method of Wei and Prater. Unlike the two methods discussed so far, Wei and Prater (ref. 75) described an experimental procedure of determining the eigenvectors and eigenvalues of the parameter matrix K in eq. 3.91. In their approach they consider a class of reaction mechanisms where all species are linked together by reversible or irreversible monomolecular reactions. In the case of reversible reaction systems they proved that the rate constant matrix K possesses real eigenvalues, which are all non-positive, and that there exists a basis of eigenvectors of K. These properties of the rate constant matrix K followed directly from a transformation of the original rate constant matrix into a symmetric matrix by making use of the principle of detailed balancing:

$$k_{ji}\alpha_i{}^* = k_{ij}\alpha_j{}^* \quad \text{or with matrix notation} \ (KD)^T = KD \quad (3.121)$$

where $\alpha_i{}^*$ and $\alpha_j{}^*$ are equilibrium concentrations and D is the diagonal matrix of the equilibrium concentrations. The real nonpositive eigenvalues of the rate constant matrix imply that compositions on the reaction hyperplane do not oscillate about the equilibrium point. As stated above, the action of the rate constant matrix on composition vectors in the composition space causes a rotation and a change in length of the composition vectors, except those composition vectors in the direction of the eigenvectors of the rate constant matrix. These latter ones do not undergo rotation. The further development of the method is demonstrated with the class of reaction mechanisms where all species are linked together by reversible monomolecular reactions. In such systems all composition vectors are fixed to a [1,1,1, ...]-hyperplane in the composition space due to the laws of conservation of mass: $\sum_{i=1}^{n} a_i = 1$, and no negative amounts can arise: $a_i \geq 0$. Starting with arbitrary initial compositions, with progress in reaction time all reaction paths $\alpha(t)$ move towards equilibrium. The equilibrium composition must be one of the characteristic directions because the action of the rate constant matrix on this composition neither causes a rotation nor a change in length. As all the mass of the reaction system is contained in the equilibrium vector, the other eigenvectors must contain also negative amounts and thus do not represent realizable compositions. Wei and Prater demonstrated, however, that composition vectors $\alpha(t)$ located on a plane spanned by the equilibrium vector and one of the other eigenvectors will remain on this plane while moving - with progress in reaction time - to the equilibrium vector, thus forming straight line reaction paths on the reaction-hyperplane. By vector addition of the initial composition vector of a straight line-reaction path on the edge of the reaction hyperplane and the quilibrium vector, the other eigenvectors are obtained.

The experimental search for the straight line reaction paths will be outlined for a reversible three-component system and for reversible and irreversible n-component systems which contain only one linkage class. In the case of reversible three-component systems the procedure is straightforward. The reaction paths in the composition plane of a reversible three-component system have been plotted in Fig. 2.4 (Chapter 2). All reaction trajectories approach the equilibrium composition with progress in reaction time, thereby

asymptotically joining the second eigenvector. Hence, the second eigenvector can be experimentally determined by repeatedly taking intersecting points of the tangents to the reaction paths near the equilibrium composition, with the edges of the composition triangle as new initial compositions, until the straight-line reaction path is located. The third eigenvector is obtained from orthogonality relations between the characteristic vectors.

The rate constant matrix for the characteristic species system can be determined from any curved reaction path on the reaction simplex. Measured compositions $\alpha(t)$ of such a reaction path are transformed into the composition $\beta(t)$ of the hypothetical system by $\beta = X^{-1}.\alpha$, where X^{-1}, the inverse of the eigenvector matrix X, has been computed by conventional methods, and β is the vector of concentrations of the hypothetical species

$$\beta = \begin{bmatrix} b_0 \\ b_1 \\ b_2 \end{bmatrix} .$$

Plotting $\ln b_j$ versus the reaction time, straight lines are obtained and from their slopes the eigenvalues $-\lambda_i$ can be determined. If the reaction time is not available, relative rate constants of the change in composition of the characteristic species can be determined from graphs $\ln b_i$ versus $\ln b_j$. The slopes of the obtained straight lines are the ratios λ_i/λ_j.

The method of Wei-Prater will be illustrated by the example of xylene isomerization. When only the interconversion of the three xylene isomers is to be considered, the reactions can be described by the following triangular scheme:

o-xylene

k_{13} k_{31} k_{12} k_{21}

k_{23}
p-xylene ⇌ m-xylene
k_{32}
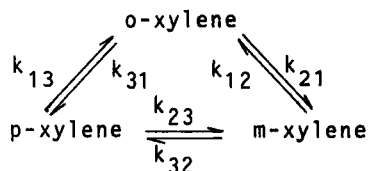
The actual rate coefficients are very strongly catalyst-dependent. Data calculated by the Wei-Prater technique are shown in Table 3.8 (ref. 81). The relative importance of 1,3-methyl shifts (o   p conversion) is negligible over La Y and amorphous silica-alumina but important on ZSM-5. This results in Wei-Prater diagrams where there is very little difference between the actual reaction paths,

TABLE 3.8

Relative rate constants for xylene isomerization calculated by the Wei-Prater technique. Reproduced with permission from (ref. 81).

Rate	Catalyst		
	La Y 623 K	H-ZSM-5 523 K	Silica-Alumina (ref. 83)
k_{21}	10.9	2.15	21.2
k_{12}	4.79	0.82	13.0
k_{23}	8.08	3.27	37.1
k_{32}	3.61	1.43	17.3
k_{13}	1.00	1.00	1.00
k_{31}	1.02	1.15	1.03

starting from pure isomers, and the ones obtained by assuming that xylene products are formed in equilibrium ratios from the pure reactant (Fig. 3.13). On the other hand, with selective catalysts,
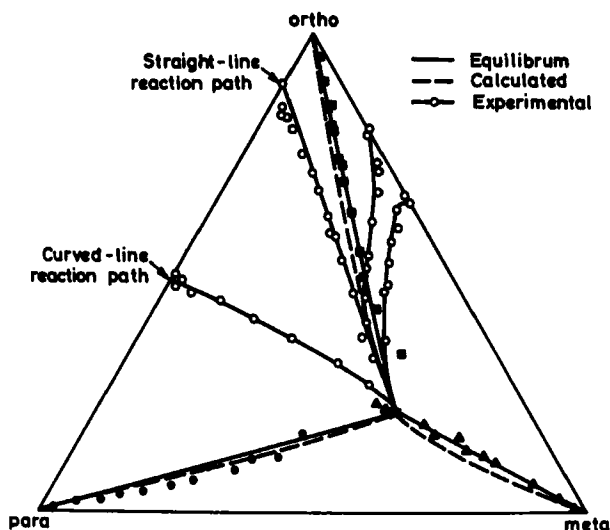
Fig. 3.13. Wei-Prater diagram for xylene isomerization at 523 K with a ZSM-5 catalysts. Equilibrium line results if products within a pore are in equilibrium regardless of total conversion; calculated curve is obtained using Wei-Prater rate coefficients (Table 3.8). Reproduced with permission from (ref. 81).

123

like La Y (ref. 82), silica-alumina (ref. 83) or ferrierite (a ten-
-ring window zeolite) (ref. 84) very marked curvature is seen in
the reaction paths. The enhanced para-selectivity of the ferrierite
catalyst is especially favorable from a practical point of view
(see Chapter 1). The question may arise whether formation of an
isomer in amounts greater than equilibrium is, in principle, possib-
le or a violation of thermodynamics. It can be shown that reaction
rate coefficients are strictly coupled by the equilibrium constant
in two-component systems only; in multicomponent systems, the only
thermodynamic constraint is that the overall free energy of the
system must decrease (ref. 85). If thermodynamic contours are
plotted around the equilibrium point in the Wei-Prater diagram of
xylenes, it can be seen that the curved pathway of m-xylene isome-
rization, giving excess para-isomer, in fact fulfils this condi-
tion. Of course, at the equilibrium point, where all three isomers
are in equilibrium, no other composition is possible (Fig. 3.14).
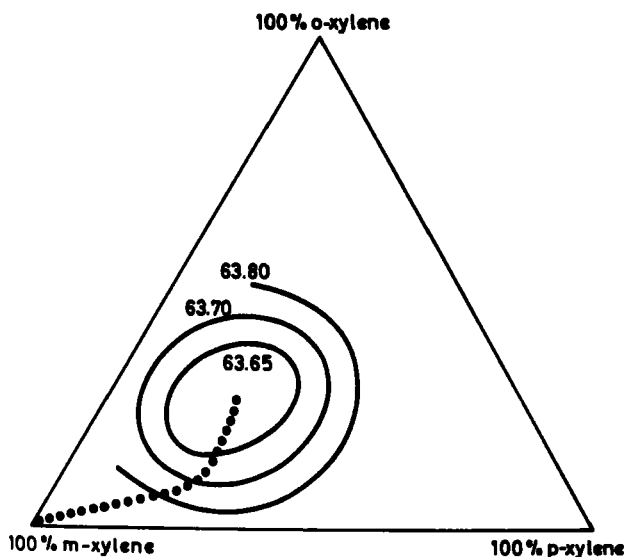
Fig. 3.14. Free energy contours for xylene isomers in the region
between pure m-xylene and the equilibrium at 723 K. Plotted course
is for m-xylene isomerization over ferrierite catalyst, determined
at various space velocities. Reproduced with permission from
(ref. 85).

Such behaviour can be interpreted in terms of "shape selectivity",
namely that the intermediate for p-xylene is formed more easily in
the zeolite channel than that for o-xylene. Also, the relative

diffusion rate for the p-xylene molecule (with smaller cross sec-
tion) is higher. Therefore it is easy to see that xylene loss
(which is observed experimentally) would consume first of all o-xy-
lene isomers or their precursors by, for example, coking or dis-
proportionation reactions.

With a decaying reversible three-component system, Scheme 3.16,
the experimental determination of the eigenvectors is more compli-
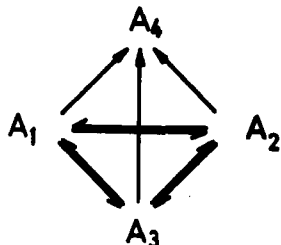
Scheme 3.16

cated. In this case all reaction paths move towards the origin for-
ming thereby a set of curves which envelops the only straight line
reaction path located in the positive orthant, Fig. 3.15 (Ref. 86);
this has been called the ray vector, x_r, by Prater et al. (ref. 87).
The other two characteristic vectors, x_1 and x_2, do not directly
correspond to observable straight line reaction paths. Composition
vectors $\alpha_x(t)$, however, located in a plane encompassed by one cha-
racteristic vector and the ray vector will remain in this plane
while decaying to zero according to the following equation (ref. 88)

$$\alpha_x(t) = b_r(t)\ x_r + b_i(t)\ x_1. \qquad (3.122)$$

In this equation b_i and b_r are amounts of the characteristic spe-
cies B_i in the transformed coordinate system. A projection of this
composition vector onto the triangle plane yields an "artificial
straight line reaction path" which can be located experimentally.
Hence, the procedure for evaluating the rate constant matrix results
in the following: the end point of the ray vector on the reversible
reaction simplex and the end point of an artificial straight line
reaction path, located on an edge of the reaction simplex, are de-
termined experimentally. By linear combination of this composition
vector and the ray vector

reaction scheme:

x_r, x_1, x_2 : characteristic vectors
———→ : reaction path
— – — : parallel projected reaction path
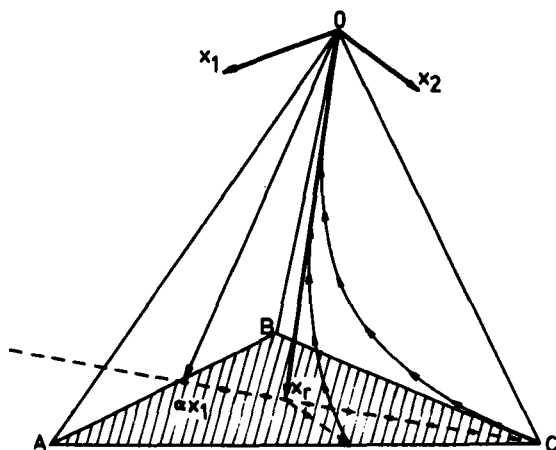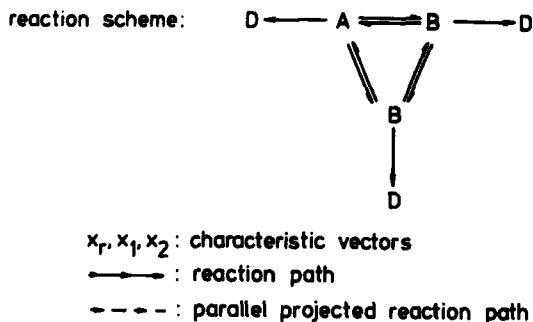
Fig. 3.15. Reaction simplex of a three-component system containing reversible and irreversible reaction steps. Reproduced with permission from (ref. 86).

$$x_1 = \alpha_{x_1}(0) - \gamma x_r \qquad (3.123)$$

and the orthogonality relation between the two characteristic vectors

$$x_r^T D^{-1} x_1 = 0, \qquad (3.124)$$

a second eigenvector is obtained. In this equation x_r^T is the transposed ray vector, D^{-1}, a diagonal matrix from the reciprocal equilibrium concentrations (without irreversible steps) and γ is a scalar which is obtained from equations 3.123 and 3.124

$$\gamma = \frac{x_r^T \ D^{-1} \ \alpha x_1(0)}{x_r^T \ D^{-1} x_r} \ . \qquad (3.125)$$

The third eigenvector is computed again from an orthogonality rela-
tion. Following the evaluation of the eigenvectors, the eigenvalues
are determined from any curved reaction path as in the reversible
three-component system.

Applying the foregoing procedure to n-component systems, diffi-
culties arise in locating the (n-1) required straight-line reaction
paths; this can be demonstrated with an n-component reversible reac-
tion system containing one linkage class. In this case the general
solution of the set of linear differential equations, by which the
dynamics of the reactive system is described, is given by

$$\alpha(t) = C_1 \ x_0 + C_2 \ x_1 e^{-\lambda_1 t} + C_3 \ x_2 e^{-\lambda_2 t} + \ldots \qquad (3.126)$$

where $0<\lambda_1<\lambda_2<\ldots$, $x_i \in R^n$, $C_i \in R$. The assumption of $0<\lambda_1<\lambda_2<\ldots$ holds
for reaction systems with different rate constants.

With progress in reaction time all reaction paths $\alpha(t)$ are mo-
ving asymptotically to the equilibrium composition vector x_0, there-
by joining the second eigenvector x_1. This can be demonstrated by

$$\dot{\alpha}(t) = e^{-\lambda_1 t} (-\lambda_1 \ C_2 \ x_1 - \lambda_2 \ C_3 \ x_2 \ e^{(\lambda_1 - \lambda_2)t} - \ldots) \qquad (3.127)$$

$$\text{with} \quad t \to \infty \quad \dot{\alpha}(t) \approx - \lambda_1 C_2 \ x_1 \ e^{-\lambda_1 t} \qquad (3.128)$$

$$\text{and} \quad \frac{\dot{\alpha}(t)}{||\dot{\alpha}(t)||} \approx x_1 . \qquad (3.129)$$

This means, that starting with arbitrary initial compositions, the
same straight-line reaction path on the reaction hyperplane will
always be found. Hence, with reversible systems the equilibrium
vector and one further eigenvector can be experimentally located.
In the case of pseudomonomolecular n-component systems containing
one linkage class and reversible and irreversible reaction steps
the general solution is given by

$$\alpha(t) = C_1 \ x_r \ e^{-\lambda_r t} + C_2 \ x_1 \ e^{-\lambda_1 t} + \ldots C_{n+1} \ x_n \ e^{-\lambda_n t}. \qquad (3.130)$$

In a reaction system like this, starting with arbitrary initial
compositions, all reaction paths move towards the origin thereby
enveloping the only directly observable straight-line reaction path

x_r. In this case the procedure for experimentally locating the required artificial straight line reaction paths is the following (refs. 89,90). Firstly, the ray vector is determined starting with different initial compositions on the reaction plane of the reversible system, near the foot point of the ray vector. The second eigenvector is determined by a projection of measured composition paths parallel to the ray vector onto the reaction plane of the reversible n-component system. All reaction paths on this reaction plane will asymptotically join the second eigenvector x_1 while being transformed to the foot point of the ray vector on this plane with progress in reaction time, which can thus be located by repeatedly taking intersecting points of tangents to the reaction trajectories, near the ray vector composition, with the edges of the reaction plane as new initial compositions.

Further characteristic directions are determined in the same way, by purging the initial compositions and all further compositions along the measured reaction trajectories of portions of already determined eigenvectors. By this procedure the reaction trajectories are projected onto reaction planes in the composition space on which the eigenvectors with the smallest eigenvalue, are asymptotically approximated with progress in reaction time. Mathematically this procedure may be described in the following way

$$\alpha(t) - C_1 \, x_r - C_2 \, x_1 \, e^{-\lambda_1 t} = \delta(t) = C_3 \, x_2 \, e^{-\lambda_2 t} +$$

$$+ \, C_4 \, x_3 \, e^{-\lambda_3 t} + \dots + C_{n-1} \, x_n \, e^{-\lambda_n t} \tag{3.131}$$

where $\delta(t)$ is a reaction path on the reaction plane in the n-dimensional species space purged of portions of the eigenvectors x_r and x_1.

In the foregoing three parameter estimation procedures have been described which can be applied to linear systems. In Chapter 4 some examples will be given of the use of these methods for data evaluation in suitable experimental set-ups for the investigation of the dynamics of pseudomonomolecular reactive systems. Besides these methods, library parameter estimation computer programs can also be used for data evaluation. Usually with library programs the experimental part and the parameter estimation part may be separated and carried out independently of each other; this is not the case, however, if sequential experimental designs are used for parameter estimation.

The method proposed by Li (ref. 91) may represent a transition
to optimization methods treated in the next Section. It is, howe-
ver, mentioned here because it is based on searching natural
straight-line reaction paths (NSLRP) and artificial straight line
reaction paths (ASLRP) by a computer optimization process. The
solution is presented for first-order n-component reaction systems
with reversible and/or irreversible steps. Any reaction path can
be obtained by linear combination of n-reaction paths with linearly
independent initial compositions; in principle, they need not be
located in the positive orthant of the composition space. The cur-
vature of these arbitrary reaction paths is characterized by the
area between them and the straight-line reaction paths. Thus, the
straight-line paths are sought by minimizing the area between them
and the arbitrary reaction paths. The areas are projected on the
two-dimensional coordinate planes and evaluated by numerical integ-
ration. Then an optimization process is carried out. If the NSLRP
is not surrounded by arbitrary reaction paths, the error of compu-
ting will be larger than the experimental error. This can occur if
the NSLRP has no segment in the positive orthant. Then ASLRP-s are
produced by projection with finite segments in the positive
orthant. These will be surrounded by artificial reaction paths and,
hence, can be calculated accurately. In addition to the reversible
triangular reaction and the irreversible sequence

$$A_1 \longrightarrow A_2 \longrightarrow A_3,$$
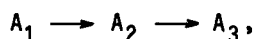
three other networks shown in Scheme 3.17 have been evaluated
(ref. 91).

$$
\begin{array}{ccc}
A_1 \rightleftharpoons A_2 & A_1 \rightleftharpoons A_2 & A_1 \rightleftharpoons A_2 \\
\downarrow \quad\quad \downarrow & \Updownarrow \quad\quad \Updownarrow & \downarrow\ \diagdown\diagup\ \downarrow \\
A_4 \quad\quad A_3 & A_4 \rightleftharpoons A_3 & A_3 \rightleftharpoons A_4
\end{array}
$$
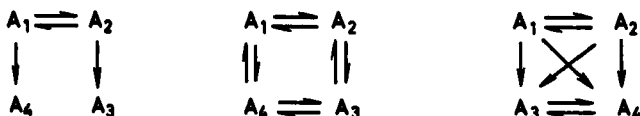
Scheme 3.17

3.2.5 Parameter estimation via optimization of objective functions
As opposed to the methods discussed so far, parameter estimation
via optimization of objective functions can be performed with models
which have linear or nonlinear parameters. The mathematical model

relates the observed variables, which are actually measured in each experiment, to independent variables, which are known for each experiment, and the parameters. For example, in a chemical reaction the rate of reaction may be the observed variable, the reactant concentrations the independent variables and the rate constants the parameters. In implicit form the model can be written as

$$g(y_u, a_u, \Theta) = 0 \qquad (3.132)$$

where g is a vector of functions which are specified by the model, y_u is the vector of observed variables for the u-th experiment, a is the vector of independent variables for the u-th experiment and Θ the vector of model parameters. Rewriting eq. 3.132 we obtain explicit equations

$$y_u = f(a_u, \Theta). \qquad (3.133)$$

The aim is now to find values of Θ that will satisfy exactly equation 3.133. However, due to experimental, model and computational error, it will not be possible to determine values of Θ that exactly fit equation 3.133. For this purpose, equation 3.133 is rewritten in the form

$$u_u = y_u - f(a_u, \Theta) \qquad (3.134)$$

where u_u are vectors, representing the difference between observed and predicted values at the u-th experiment, called residuals. With appropriate parameter estimation procedures values of Θ have to be found which minimize or maximize suitable functions of the residuals. The most commonly employed functions are least squares where

$$S = \sum_{u=1}^{n} [y_u - f(a_u, \Theta)]^2 \qquad (3.135)$$

is minimized for selection of parameter values. For models which are linear in the parameters for u observations, the following set of equations can be written

$$
\begin{aligned}
y_1 &= \Theta_1 a_{11} + \Theta_2 a_{12} + \cdots \Theta_m a_{1m} + u_1 \\
y_2 &= \Theta_1 a_{21} + \Theta_2 a_{22} + \cdots \Theta_m a_{2m} + u_2 \\
&\;\vdots \\
y_n &= \Theta_1 a_{n1} + \Theta_2 a_{n2} + \cdots \Theta_m a_{nm} + u_n .
\end{aligned}
\qquad (3.136)
$$

Applying the least squares principle, the sum of squares of the unobservable errors is minimized with respect to the parameters

$$S(\Theta) \equiv \sum_{u=1}^{n} u_u^2 = \sum_{u=1}^{n} (y_u - f(a_u, \Theta))^2 \overset{\Theta_i}{\to} Min. \qquad (3.137)$$

Using matrix notation, equation 3.137 can be rewritten, with

$$Y = \begin{vmatrix} y_1 \\ y_2 \\ \cdot \\ \cdot \\ \cdot \\ y_n \end{vmatrix} \qquad\qquad A = \begin{vmatrix} a_{11} & a_{12} & \cdots & a_{1m} \\ a_{21} & a_{22} & \cdots & a_{2m} \\ \cdot \\ \cdot \\ \cdot \\ a_{n1} & a_{n2} & \cdots & a_{nm} \end{vmatrix}$$

$$U = \begin{vmatrix} u_1 \\ u_2 \\ \cdot \\ \cdot \\ \cdot \\ u_n \end{vmatrix} \qquad\qquad \Theta = \begin{vmatrix} \Theta_1 \\ \Theta_2 \\ \cdot \\ \cdot \\ \cdot \\ \Theta_m \end{vmatrix}$$

to obtain
$$Y = A \cdot \Theta + U. \qquad (3.138)$$

The least square estimates of the Θ_i for eq. 3.137, computing $\frac{\delta S(\Theta)}{\delta \Theta_i} = 0$, become

$$\Theta = (A^T A)^{-1} A^T \cdot Y. \qquad (3.139)$$

Many kinetic model equations can be linearized in the form of equation 3.136. For example, for a heterogeneous catalytic reaction $A_1 \longrightarrow A_2 + A_3$ with the steps

step 1: adsorption of A_1 $\qquad A_1 + l \longrightarrow A_1 l$

step 2: surface reaction $\qquad A_1 l + l \overset{k_2}{\longrightarrow} A_2 l + A_3 l$

step 3: desorption of A_2 $\qquad A_2 l \longrightarrow A_2 + l$

step 4: desorption of A_3 $\qquad A_3 l \longrightarrow A_3 + l,$
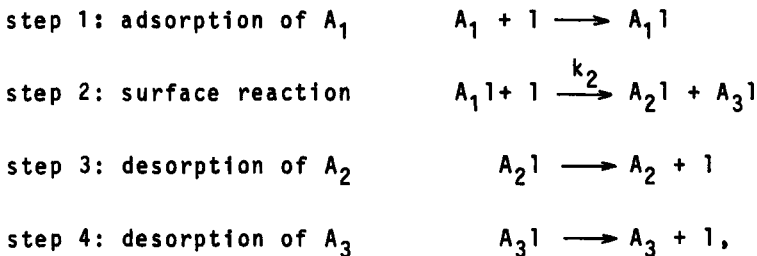
assuming that the surface reaction is the rate determining step, the following rate expression is obtained

$$r = \frac{k \cdot K_{A_1}(P_{A_1} - P_{A_2}P_{A_3}/K)}{(1 + K_{A_1}P_{A_1} + K_{A_2}P_{A_2} + K_{A_3}P_{A_3})^2} \qquad (3.140)$$

where K is the overall equilibrium constant, K_{A_i} the adsorption equilibrium constants, $k = k_2$. L the global rate coefficient and P_{A_i} the partial pressures. Linearizing eq. 3.140, the following equation is obtained:

$$\sqrt{\frac{P_{A_1} - P_{A_2} \cdot P_{A_3}/K}{r}} = \frac{1}{\sqrt{kK_{A_1}}} + \frac{K_{A_1}}{\sqrt{kK_{A_1}}} P_{A_1} +$$

$$+ \frac{K_{A_2}}{\sqrt{k \cdot K_{A_2}}} P_{A_2} + \frac{K_{A_3}}{\sqrt{k \cdot K_{A_3}}} \cdot P_{A_3} . \qquad (3.141)$$

In cases where some of the observed variables are known with less reliability than others or where the observed variables are measured on different scales or represent entities with different physical dimensions, weighted least squares are used for the estimation of the model parameters by assigning a non-negative weight factor, b_i, to each u and minimizing the weighted sum of squares

$$S(\Theta) = \sum_{u=1}^{n} \sum_{i=1}^{k} b_i [Y_{ui} - f_i (a_u, \Theta)]^2 . \qquad (3.142)$$

Many models are nonlinear in their parameters. In these cases too, objective functions like least squares are minimized. The parameter estimation procedure now, however, is an iterative procedure due to the non-linear parameter surface in the parameter space. For the iterative process initial estimates of the model parameters are needed and an efficient optimization strategy is required. Complications may arise if the least-squares surface contains multiple or flat minima. A typical example of a sum-of-least-squares surface is given in Fig.3.16 (ref. 92) for the following rate equation for iso-octene hydrogenation at fixed values of K_s and K_u

$$r = \frac{k \cdot K_H \cdot K_u \cdot P_H \cdot P_u}{(1 + K_H \cdot P_H + K_u \cdot P_u + K_s \cdot P_s)^2} . \qquad (3.143)$$

Here k is the forward rate constant of isooctene hydrogenation and K_H the hydrogen adsorption constant.
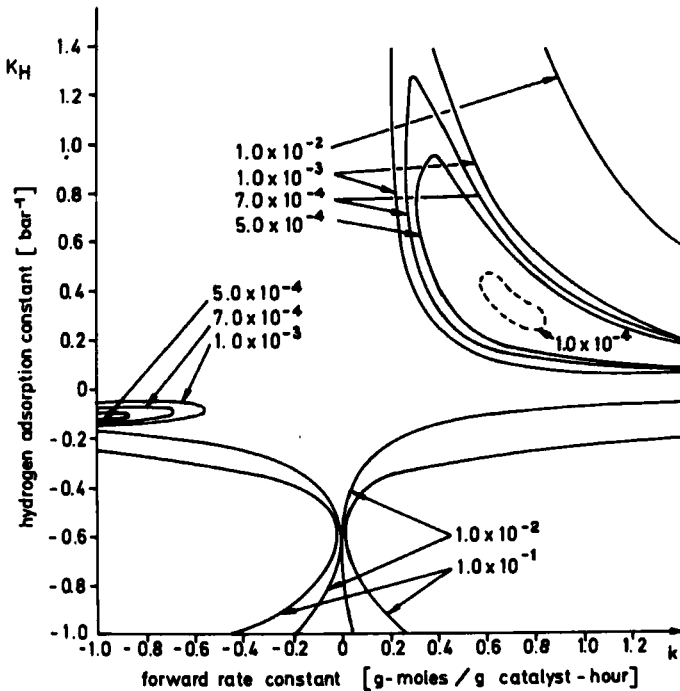
Fig. 3.16. Contour of sums of least squares of residual rates for isooctene hydrogenation. Reproduced with permission from (ref. 92).

There are three basic types of optimization methods (refs. 92-95). With the <u>linearization method</u> the non-linear model equations are linearized in Taylor series around the initial estimates for the parameters, neglecting all derivatives of second and higher order. The iteration procedure involves repetitive evaluation (ref. 63) of

$$\Delta t_{i+1} = (J_i^T J_i)^{-1} J_i u_i \qquad (3.144)$$

$$t_{i+1} = t_i + \Delta t_{i+1} \qquad (3.145)$$

until convergence is achieved where

$$J_i = \{\frac{\delta f (a_u, \Theta)}{\delta\Theta_i}\Big|_{\Theta=t_i}\}$$

and $\qquad u_i = y - f(a, t_i)$

is a vector of residuals $y - f(a, t_i)$ with respect to the $(i + 1)$--th iteration and t_i are estimates of Θ_i.

With the steepest-descent method a first-order design in the pa-
rameter space is set up about the initial estimates of the parame-
ters. Calculating the sum of squares at each point, the direction
of the steepest-descent is determined and in this direction of the
parameter space a new set of parameters is selected and the total
procedure repeated until the sums of squares start to increase.
With a second order design the precise location of the minimum is
then determined.

Steepest-descent methods are very stable for initial iterations
but may converge slowly for multiparameter systems, while lineari-
zation methods are more efficient for the final iterations (ref.
92). Hence, compromise methods have been suggested which use
steepest-descent procedures for initial iterations and the lineari-
zation method in the final stages. With these procedures the correc-
tions of the parameters are calculated by means of

$$\Delta t_{i+1} = (J_i^T J_i + \lambda_i I_i)^{-1} J_i^T u_i \qquad (3.146)$$

where I is a matrix of unity diagonal terms and zero off-diagonal
terms, $J_i^T u_i$ the vector of steepest-descent and λ_i is a Lagrange
multiplier which continually decreases with an increasing number of
iterations.

Fitting carried out by nonlinear least squares, is efficient
only when the sample size approaches infinity. Ratkowsky (ref. 96)
advised a "close-to-linear" model where a good fit can also be ob-
tained with small samples. Thus, the general Hougen-Watson equation
can be re-written in such a way that all Θ parameter estimators are
placed in the denominator of equations like Eq. 3.143. These esti-
mators are claimed to be much closer to linearity than those dist-
ributed in the numerator and denominator. Six catalytic kinetic
systems are evaluated, all having different forms of rate equation,
including isomerization of pentane, hydrogenation of isooctenes
etc.

Once the optimization procedure has been performed and the model
parameters have been estimated, information about the precision of
the estimates is required. If the errors in the dependent variable
have constant variance σ^2, and are normally and independently dist-
ributed, t is an unbiased estimate of Θ and the variance-covariance
matrix is given by

$$V(t) = (A^T A)^{-1} \sigma^2. \qquad (3.147)$$

For linear models the $(1 - \alpha)$ 100% confidence intervals for the individual parameters t_i are given by

$$t_i \pm t (n - p, 1 - \alpha/2) [v(t_i)]^{\frac{1}{2}} \qquad (3.148)$$

where $t(n - p, 1 - \alpha/2)$ is the $\alpha/2$ percentage point of the t-distribution with $(n - p)$ degrees of freedom and $v(t_i)$ the i-th diagonal element of the variance-covariance matrix $V(t)$. From the off-diagonal terms of the variance-covariance matrix, the correlation among the parameter estimates is determined; it is usually high for hyperbolic models. This leads to joint confidence regions of the estimates t_i which enclose the region of joint parameter uncertainty. The joint confidence region, which represents a p-dimensional ellipsoid in the parameter space, is defined by

$$(t - \theta)^T A^T (\theta - t) = s^2 p F (p, n - p) \qquad (3.149)$$

where s^2 is an independent estimate of the experimental error variance δ^2 which, in the case of adequate models, can be calculated by the minimum residual sum of squares divided by the corresponding number of degrees of freedom, p is the number of parameters and $F (p, n - p)$ is the $(1-\alpha)$ 100% point of the F-distribution. For the reliability analysis of parameters in non-linear models, the non--linear models are linearized by a Taylor expansion neglecting second and higher order derivatives and the statistical testing procedures, discussed so far, applied.

Quite often the model equations contain not only dependent and independent variables but also derivatives of the dependent variables with respect to the independent variables. For parameter estimation in differential equations, for which no analytical solution can be obtained, the calculation of the residuals for the single observations requires numerical integration of the set of model equations. Problems with parameter estimation in differential equations may arise when the nature of the solutions to a given set of equations changes with the values of the parameters. The solutions may be stable and converge to equilibrium points or unstable and diverge to infinity: they may enter into stable limit cycles or spiral away from limit cycles or oscillate around equilibrium points. Furthermore steady states of the state variables may be attained which are independent of some of the parameters.

3.2.6 Nonlinear systems

In the foregoing sections parameter estimation procedures have been discussed. In the case of parameter estimation in nonlinear differential equations, which cannot be analytically integrated, the optimization of appropriate objective functions requires numerical solution of the model differential equations. To-day, with the computer facilities available numerical solutions of any solvable differential equation or system of differential equations can be obtained with acceptable accuracy.

Although an analytical solution has recently been proposed (ref. 97) for some simple cases, like a power law type chemical reaction in a catalyst pellet or a Langmuir-Hinshelwood type reaction, numerical approximations of the solutions still prevail in present day calculations. These are frequently based on Runge-Kutta-procedures or on finite difference methods. Once the model parameters have been determined, model predictions can be realized. Quite often, however, if space-time structures of reactive systems are investigated, the questions under consideration can be answered from descriptive properties of the solutions such as stability or periodicity, *i.e.* from qualitative investigations of differential equations without actually solving them. This procedure can be delineated with the following system

$$\frac{dx_1}{dt} = f(x_1, x_2)$$

$$\frac{dx_2}{dt} = g(x_1, x_2)$$

(3.150)

where f and g are functions possessing continuous first partial derivatives. As the independent variable does not appear explicitly in f and g, the system 3.150 is said to be autonomous. The $x_1 x_2$-plane is called the phase plane and the arc defined parametrically by any solution $x_1 = x_1(t)$ and $x_2 = x_2(t)$ is called a trajectory or orbit of eq. 3.150. The $x_1 x_2$-equation of the trajectories through a point (x_1^0, x_2^0) can be found by eliminating the independent variable from the system eq. 3.150 by dividing the two equations by one another

$$\frac{dx_2}{dx_1} = \frac{f(x_1, x_2)}{g(x_1, x_2)} .$$

(3.151)

Eq. 3.151 represents the slope of the trajectory at the point

(x_1, x_2). If, at a given point, $f(x_1, x_2)$ and $g(x_1, x_2)$ are si-
multaneously zero, the slope is indeterminate, and such a point is
said to be an equilibrium point or critical or singular point. Iso-
lated equilibrium points have the property that there exists a
circle around this point which only contains this equilibrium point
and no other. A qualitative analysis of the solutions of eq. 3.150
describes the nature of trajectories in the vicinity of equilibrium
points. For a two-dimensional linear homogeneous system eq. 3.150
takes the following form

$$\frac{dx_1}{dt} = a_{11} x_1 + a_{12} x_2$$

$$\frac{dx}{dt} = a_{21} x_1 + a_{22} x_2$$

(3.152)

where a_{11}, a_{12}, a_{21} and a_{22} are real constants. Assuming that

$$\det \begin{bmatrix} a_{11} & a_{12} \\ a_{21} & a_{22} \end{bmatrix} \neq 0$$

(3.153)

the only equilibrium point of the system eq. 3.152 is (0,0). Eq.
3.152 can be rewritten in matrix notation

$$\dot{x} = A x.$$

(3.154)

With constant coefficients, a_{ik}, the solution to eq. 3.154 is given
by

$$x = c\, e^{\lambda t}.$$

(3.155)

Introducing eq. 3.155 into eq. 3.154 the following equation is ob-
tained

$$(A - \lambda I)\, x = 0.$$

(3.156)

Nontrivial solutions for eq. 3.156 are obtained under the condition

$$\det (A - \lambda I) = 0.$$

(3.157)

Hence, the characteristic equation of the coefficient matrix simul-
taneously represents the characteristic equation of the system equa-
tion 3.152. If $\lambda = \lambda_i$ is a characteristic root, then equation 3.156
has non-trivial solutions which are the components of characteris-
tic vectors corresponding to that characteristic root. The charac-
teristic roots are obtained from the characteristic equation of the
coefficient matrix A

$$\lambda^2 - (a_{11} + a_{22})\,\lambda + (a_{11}a_{22} - a_{12}a_{21}) = 0. \qquad (3.158)$$

The characteristic roots determine the form of the solutions for x_1 and x_2 and, hence, the nature of the trajectories of the system 3.152.

Five cases can be identified and are presented in Fig. 3.17 (ref. 98). The arrows along the trajectories indicate the direction
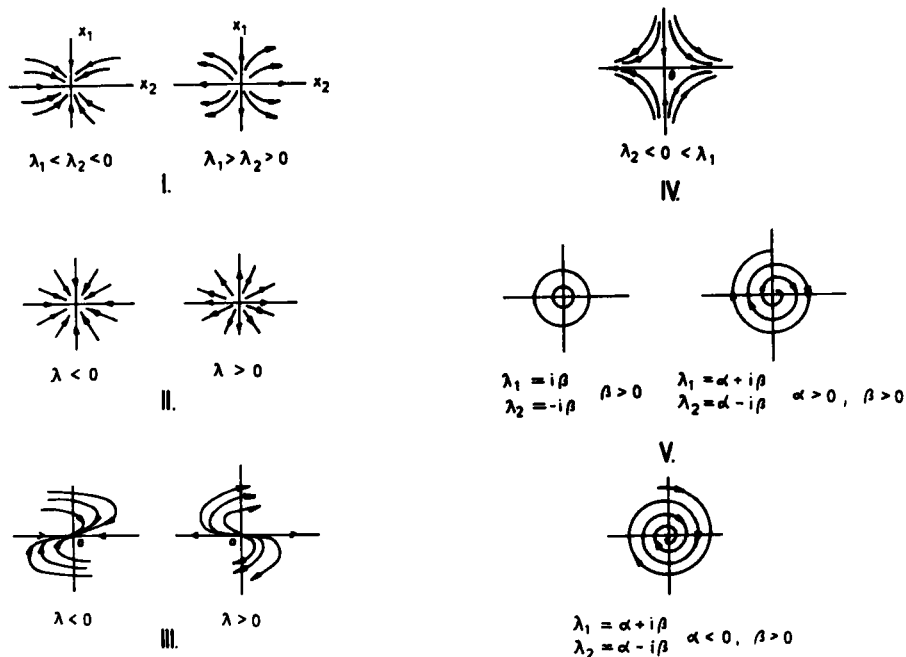
Fig. 3.17. Typical trajectories around the equilibrium point of the linear system $dx_1/dt = a_{11}x_1 + a_{12}x_2$, $dx_2/dt = a_{21}x_1 + a_{22}x_2$ whose characteristic equation is $\lambda^2 - (a_{21} + a_{22})\lambda + (a_{11}a_{22} - a_{12}a_{21}) = 0$. Reproduced with permission from (ref. 98), p. 128, by courtesy of Marcel Dekker, Inc.

of increasing time. In Case I the characteristic roots are real, unequal and of like sign. The equilibrium point is called a node which is asymptotically stable for negative eigenvalues and unstable for positive eigenvalues; this means that every trajectory which is sufficiently close to the equilibrium point actually approaches. In Case II the characteristic roots are real and equal. With negative eigenvalues the node is asymptotically stable and with positive eigenvalues unstable. In Case III the eigenvalues are real and

equal and the canonical form is A = $\begin{vmatrix} \lambda & 1 \\ 0 & \lambda \end{vmatrix}$. Here the equilibrium point is an asymptotically stable node if the roots are negative, and unstable if the roots are positive. In Case IV the characteristic roots are real, unequal and of unlike sign. The equilibrium point is called a saddle point, which is unstable. In Case V the roots are complex conjugate numbers $\lambda_1 = \alpha + i\beta$ and $\lambda_2 = \alpha - i\beta$. If the roots are purely imaginary, then the equilibrium point is called a center, *i.e.* in the neighbourhood of the equilibrium point there exists an infinite set of closed trajectories and the equilibrium point is in the center of them. If $\alpha \neq 0$ then the equilibrium point is a spiral point which is asymptotically stable if the real part of the root is negative and unstable if the real part is positive.

The treatment of nonlinear systems with respect to the nature and stability of solutions corresponds to that of the linear system considered so far. In a first approach approximately linear autonomous systems are investigated which can be written in the following form

$$\frac{dx_1}{dt} = a_{11} x_1 + a_{12} x_2 + f(x_1, x_2)$$

$$\frac{dx_2}{dt} = a_{21} x_1 + a_{22} x_2 + g(x_1, x_2)$$

(3.159)

where the functions g and f are nonlinear but small compared with the linear terms. If this is the case the system, in sufficiently small neighbourhoods of equilibrium points, behaves essentially like a linear system. If functions on the right-hand side of eq. 3.159 do not contain linear terms in Taylor expansions of these functions around the equilibrium point, the system is not approximately linear and qualitative descriptions of solutions of such systems are no longer concerned with the nature of trajectories around equilibrium points but with the stability and periodicity of solutions, *i.e.* under what conditions solutions approach or stay close to given solutions. Frequently the analysis of stability properties of a given solution is based on the Lyapunov second method (ref. 98). For these, a differentiable function V is defined throughout a domain S containing the equilibrium point (x_1^0, x_2^0). The function V is said to be positive definite on domain S if V $(x_1^0, x_2^0) = 0$ and if V $(x_1, x_2) > 0$ at all other points of S; to be positive semidefinite on domain S if V $(x_1^0, x_2^0) = 0$ and if

$V(x_1, x_2) \geqq 0$ at all other points of S; to be negative definite on S if $V(x_1^0, x_2^0) = 0$ and if $V(x_1, x_2) < 0$ at all other points of S; and finally to be negative semidefinite if $V(x_1^0, x_2^0) = 0$ and $V(x_1, x_2) \leqq 0$ at all other points of S. The Lyapunov theorem states for autonomous systems with an isolated equilibrium point at the origin

$$\frac{dx_1}{dt} = F(x_1, x_2) \qquad \frac{dx_2}{dt} = G(x_1, x_2)$$

if the functions F and G have continuous first partial derivatives in a domain S containing the equilibrium point and if a function V, with continuous first partial derivatives, exists which is positive definite in S, that the equilibrium point is asymptotically stable if the derivative of V with respect to the given system is negative definite on S. The equilibrium point is at least stable if the derivative of V is negative semidefinite on domain S. The isolated equilibrium point is unstable if, in its neighbourhood, there is at least one point where V is positive and the derivative of V is positive definite on S or where V is negative and the derivative of V is negative definite on S. Application of the Lyapunov second method requires determination of an appropriate function V which is frequently difficult to construct.

With the linear system discussed above either no periodic solutions infinitely many periodic solutions with pure imaginary characteristic roots are observed. For nonlinear autonomous systems, on the other hand, only one periodic solution, *i.e.* a limit cycle may be observed, which is either approached spirally from inside or from outside the limit cycle by trajectories with increasing time. A simple autonomous system which exhibits such behavior is (ref. 99)

$$\frac{dx_1}{dt} \quad x_1 + x_2 - x_1 (x_1^2 + x_2^2)$$

$$\frac{dx_2}{dt} \quad x_1 + x_2 - x_2 (x_1^2 + x_2^2).$$

(3.160)

Other systems where limit cycles may occur are non-linear second order differential equations like

$$\frac{d^2x}{dt^2} + k_1(x) \frac{dx}{dt} + k_2(x) = 0$$

which is equivalent to the autonomous system of first order differential equations

$$\frac{dx_1}{dt} = x_2$$

$$\frac{dx_2}{dt} = k_1(x_1)\ x_2 - k_2(x_1). \tag{3.161}$$

The existence of limit cycles is stated by the Poincaré-Bendixson theorem for autonomous systems of differential equations

$$\frac{dx_1}{dt} = F\ (x_1,\ x_2)$$

$$\frac{dx_2}{dt} = G\ (x_1,\ x_2)$$

where F und G are continuous functions and satisfy local Lipschitz conditions. Reaction mechanisms which, among others, give rise to periodic solutions or limit cycles include the "Lotka"-mechanism (ref. 100)

$$A_1 + B \xrightarrow{k_1} 2A_1$$

$$A_1 + A_2 \xrightarrow{k_2} 2A_2 \tag{3.162}$$

$$A_2 \xrightarrow{k_3} D$$

for which the dynamic equations take the following form assuming the species concentrations B and D are time-invariant

$$\frac{da_1}{dt} = k_1\ a_1 - k_2\ a_1\ a_2$$

$$\frac{da_2}{dt} = k_2\ a_1\ a_2 - k_3\ a_2. \tag{3.163}$$

The trajectories for this system on the phase plane are presented in Fig. 3.18. The equilibrium point is a center. Other mechanisms are given in eq. 3.164 (ref. 101).

$$A_2 + B \xrightarrow{k_1} A_1$$

$$A_1 + A_2 \xrightarrow{k_2} C \tag{3.164}$$

$$A_1 + D \xrightarrow{k_3} 2A_1 + A_3$$
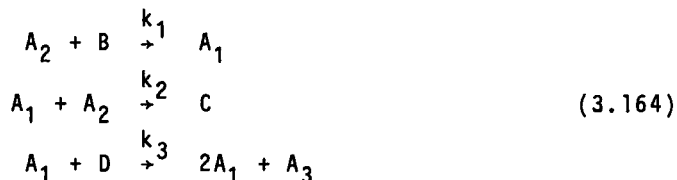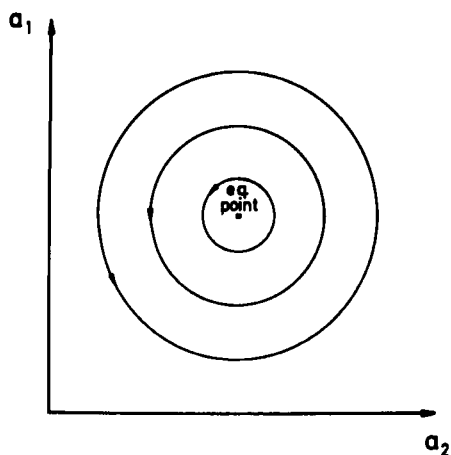
Fig. 3.18. Typical trajectories around the center of the system
$\dot{a}_1 = k_1 a_1 - k_2 a_1 a_2$, $\dot{a}_2 = k_2 a_1 a_2 - k_3 a_2$.

$$
\begin{aligned}
2A_1 &\xrightarrow{k_4} E \\
A_3 &\xrightarrow{k_5} 2A_2
\end{aligned}
\tag{3.164}
$$

and 3.165 (ref. 68)

$$
\begin{aligned}
B &\xrightarrow{k_1} A_1 \\
2A_1 + A_2 &\xrightarrow{k_2} 3A_1 \\
A_1 + C &\rightarrow A_2 + D \\
A_1 &\rightarrow E
\end{aligned}
\tag{3.165}
$$
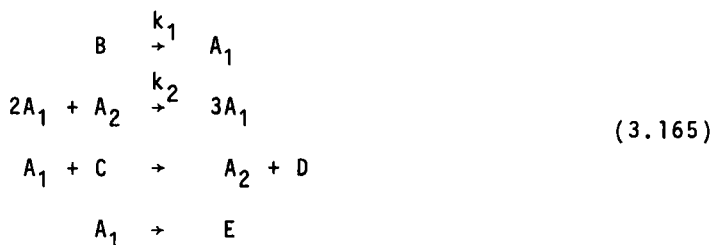
where B, C, D and E are species concentrations which are kept cons-
tant. The reaction mechanism eq. 3.164 is used for modeling the
Belousow-Zhabotinsky reaction. The equilibrium point of this system
is unstable and, for certain values of the rate constants, periodic
solutions are obtained. The dynamic equations derived from mecha-
nism eq. 3.165 which has been used for extensive theoretical consi-
derations (ref. 102), give rise to an unstable equilibrium point
surrounded by a stable limit cycle.

The nonlinear reactive systems presented so far have been main-
ly used for qualitatively investigating the time-space-structures
of these systems. Even more complex situations arise, if the chemi-

cal reactions are coupled with diffusive fluxes.

3.3 MASS TRANSPORT IN POROUS MEDIA

In the following section some mathematical models of diffusion
processes in gaseous systems, with and without walls, are presen-
ted. Gaseous diffusion can be either visualized in the framework
of kinetic theory or of thermodynamics of irreversible processes.
The presence of walls in gaseous systems gives rise to molecule-
-wall collisions and hence, to Knudsen and surface diffusion in
addition to bulk diffusion or, in cases where the molecular size is
of the same order of magnitude as the pore diameters, to configu-
rational diffusion.

3.3.1 Diffusion in gaseous systems without walls

The characteristics of irreversible processes is an entropy in-
crease of the global system and a simultaneous exergy decrease,
the rates of both being related by the following equation

$$-\dot{\epsilon} = T_0 \, \dot{S} > 0 \qquad\qquad (3.166)$$

where $-\dot{\epsilon} \equiv -d\epsilon/dt$ is the rate of exergy dissipation, and $\dot{S} = dS/dt$
the rate of entropy creation. The exergy of a system is the maximum
useful work which the system can produce at constant temperature
and pressure of an idealized environment (reservoir) without cau-
sing permanent changes in other systems. In cases where system and
idealized reservoir have identical pressures and temperatures the
exergy is equal to the Gibbs free energy function. For systems
which are not too far from equilibrium, the flows of given proper-
ties are linear functions of the driving forces. The generalized
driving force $_\Delta X_i$ conjugated to the flow Γ_i of a given property is
defined as the rate of entropy production due to the flow Γ:

$$_\Delta X_i \equiv \frac{S_i}{\Gamma_i} = -\frac{\dot{\epsilon}_i}{T_0 \, \Gamma_i} \; . \qquad\qquad (3.167)$$

Eq. 3.167 holds for well-defined systems of dimension ΔV. With
open flow systems differential generalized driving forces X_i are
used and defined as

$$X_i \equiv \frac{\dot{s}_i}{J_i} \qquad\qquad (3.168)$$

where $\dot{s}_i$ is the rate of entropy production per unit volume and J_i
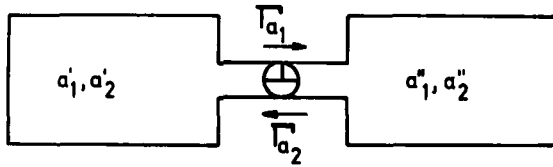
Fig. 3.19. Isothermal interdiffusion of ideal gases

the flow per unit surface (amount of i s^{-1} cm^{-2}) or flux. For iso-
thermal interdiffusion of two ideal gases, Fig. 3.19, the entropy
change for expansion of the gaseous species A_1 and A_2 from partial
pressures P'_{A_1} to P''_{A_1} and P'_{A_2} to P''_{A_2}, respectively, is

$$\Delta S = R \ln \frac{P'_{A_1}}{P''_{A_1}} + R \ln \frac{P'_{A_2}}{P''_{A_2}} = R \ln \frac{a'_1}{a''_1} + R \ln \frac{a'_2}{a''_2} \qquad (3.169)$$

where a_1 and a_2 are the concentrations of species A_1 and A_2. Hence,
the rate of entropy creation due to diffusion, $\dot{S}_d$, for this sys-
tem is

$$\dot{S}_d = \Gamma_{A_1} R \ln \frac{a'_1}{a''_1} + \Gamma_{A_2} R \ln \frac{a'_2}{a''_2} \qquad (3.170)$$

where Γ_{A_1} and Γ_{A_2} are the molar flows of the gaseous species A_1 and
A_2 [mol s^{-1}]. Introducing chemical potentials,

$$\mu_a = \mu^0 + RT \ln a \qquad (3.171)$$

where μ^0 is the standard potential which depends on temperature but
not on concentration, into eq. 3.170 the following equation is ob-
tained

$$\dot{S}_d = \frac{1}{T} \cdot \Gamma_{A_1} (-\Delta\mu_{a_1}) + \frac{1}{T} \Gamma_{A_2} (-\Delta\mu_{a_2}). \qquad (3.172)$$

From eq. 3.167 and 3.172 the generalized force for the diffusion of
the i-th component is

$$\Delta X_{d,i} = \dot{S}_{d,i}/\Gamma_{A_i} = -\Delta\mu_{a_i}/T \qquad (3.173)$$

and the differential generalized driving force

$$X_{d,i} = -\frac{1}{T}\left(\frac{d\mu_{a_i}}{dz}\right).$$ (3.174)

From the continuity equation the steady state flux is given by

$$J_i = u_i \cdot a_i.$$ (3.175)

If the velocity u_i is proportional to the driving force the mobility m_i, defined as the ratio of velocity and driving force, can be introduced into equation 3.175 resulting in

$$J_i = m_i \cdot a_i \left(-\frac{d\mu_{a_i}}{dz}\right)$$ (3.176)

for the isothermal diffusion flux. Substituting the concentration for the chemical potential and introducing the diffusion coefficient for $m_i \cdot R \cdot T$, an expression identical with Fick's diffusion law is obtained

$$J_i = -D_i \frac{da_i}{dz}.$$ (3.177)

The considerations presented so far do not reveal anything about the diffusion coefficient D_i itself. The coefficients appearing in eq. 3.177 are phenomenological and in the general case, where the flux of a given property can be produced by different kinds of driving forces, only a few relationships between the transport coefficients can be obtained by use of the Onsager reciprocal relations.

The considerations presented so far provide the basis for the experimental determination of diffusion coefficients. For calculation and prediction of the binary and multicomponent diffusion coefficients the functional dependence of these coefficients must be known; this can be derived from the kinetic theory.

The underlying thinking model of the kinetic theory of gases describes a gaseous medium by a large number of spheres which move arbitrarily and collide with one another or with surrounding walls. From a knowledge of the instantaneous values of the position vector x and momentum vector ω of each of the molecules, from which the system is built, during the course of time the macroscopic properties of the system should be completely determinable. As systems are built from huge numbers of molecules giving rise to equally large numbers of coupled equations of motion, distribution functions are used for the mathematical description, and they express

the probability that at time t, molecules with a momentum $d\omega$ about ω are in certain volume elements of the phase space. Introducing probabilities, the phase space in the mathematical model is continuous. The distribution functions are further simplified by assuming diluted gases *i.e.* that all the molecules are identical and a given molecule can occupy every position in the phase space regardless of the positions of the other molecules. Expressions for the calculation of diffusion coefficients can be either derived from the simplified kinetic theory (where it is assumed that the perturbation of the equilibrium state, which gives rise to mass, momentum or heat fluxes, is so small that the equilibrium distribution function is not altered), or from the so-called rigorous kinetic theory (where the distribution function of a gaseous system removed from equilibrium is derived and the transport coefficients are then obtained from approximate solutions to this distribution function).

Gaseous systems in equilibrium (*i.e.* systems in which the state functions are invariant in space and time), can be mathematically modelled by the Maxwell-Boltzmann distribution function $F^{(0)}$ (ref. 103), which relates the fraction of molecules with energy $E(x,\omega)$ to the spatial coordinates between x and x + dx and with momenta between ω and ω + dω.

$$F^{(0)}(x,\omega) \, dx \, d\omega = \frac{dn}{n} = \frac{\exp(-E/kt) \, dx \, d\omega}{\int\limits_{-\infty}^{+\infty} \cdots \int\limits_{-\infty}^{+\infty} \exp(-E/kt) \, dx \, d\omega} \quad (3.178)$$

where k is the Boltzmann constant. Assuming small deviations from the equilibrium state and that the mean free paths (*i.e.* the average distances between two successive collisions), are only determined by molecular collisions in the gaseous phase, the net-diffusive flux in a given direction can be determined. Hence, the molecular binary diffusion coefficient is described by the equation

$$D_{12} = D_{21} = 1/3 \ \bar{u} \ \lambda \quad (3.179)$$

where $\bar{u}$ is the average velocity of the molecules in the system and λ the mean free path. A similar expression can be obtained for the Knudsen diffusion coefficient

$$D_K = 2/3 \ R \cdot \bar{u} \quad (3.180)$$

where R is the pore radius.

Gaseous systems removed from equilibrium can be mathematically described by the Boltzmann distribution function which can be derived by considering a group of molecules in a differential volume element of the phase space at times t and t + dt and taking into account the effect of collisions of molecules with molecules of the same or another species. One approximate solution to the Boltzmann equation was given by Chapman and Enskog (ref. 103), who used the perturbation technique, *i.e.* they replaced the distribution function in the Boltzmann equation of every component by the sum of the equilibrium distribution function and a perturbation term which, in the case of a small perturbation, was assumed to be linear. The expression for the functional dependence of binary diffusion coefficients obtained from the Chapman-Enskog theory is given in equation 3.181

$$D_{12} = 0.0018583 \frac{T^{3/2}(1/M_1 + 1/M_2)^{1/2}}{p \ \sigma_{12}^2 \ \Omega_{12}} \tag{3.181}$$

where M_1 and M_2 are molecular weights of gaseous species 1 and 2, p the total pressure, σ_{12} the collision diameter for unlike molecules and Ω the collision integral, which has the dimension of area and depends on temperature and the intermolecular potential. Multicomponent diffusivities D_{ij}^m can be approximately calculated from binary diffusion coefficients (ref. 104) or obtained experimentally using the generalized Fick's law suggested by Onsager (ref. 105).
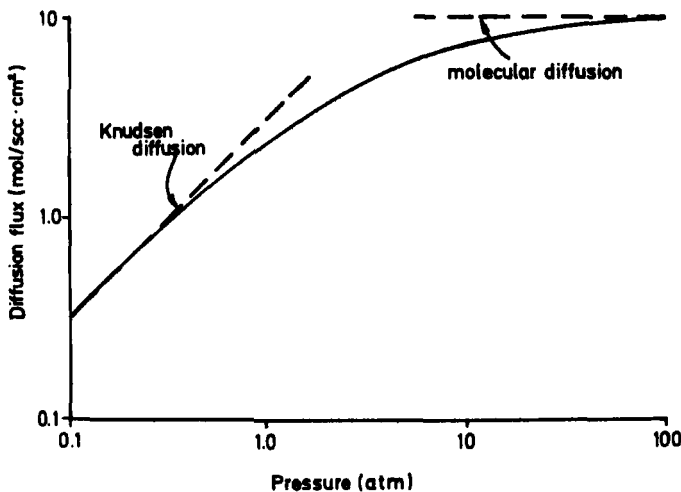
Fig. 3.20. Dependence of the steady-state diffusion flux of total pressure.

According to the Chapman-Enskog theory, binary diffusion coefficients are independent of composition, inversely proportional to
the pressure and depend on the temperature according to the relationship $T^{3/2}/\Omega_{12}(T)$. The Knudsen diffusion coefficient, on the
other hand, is independent of the system pressure. Hence, the
diffusion flux due to Knudsen-transport increases linearly with
increasing pressure whereas the diffusion flux due to molecular
diffusion is independent of total pressure (as Fig. 3.20 reveals).

3.3.2 Diffusion in gaseous systems with walls

Diffusion in gaseous systems with walls can be formally treated
like molecular diffusion by passing two gases under isobaric and
isothermal conditions past opposite faces of a catalyst pellet and
measuring the flux of one gas into the other and applying Fick's
law

$$J = -D_{eff} \frac{dc}{dx} . \qquad (3.182)$$

Hence, an effective diffusivity through the catalyst pellet is defined as the ratio of the flux through the total cross section,
normal to the diffusion direction, to the concentration gradient
through the pellet. D_{eff} is merely phenomenological and can only be
obtained using eq. 3.181. For prediction of D_{eff}, assumptions about
the mass transport mechanism and the structure of the porous medium
have to be introduced. In the simplest case diffusion is first considered in a cylindrical pore. Two transport mechanisms are assumed
to occur in series: bulk diffusion and Knudsen diffusion. At
steady-state the rates of the two fluxes in series are equal and
the overall molar flux can be represented as

$$J = -D \frac{dc}{dx} \qquad (3.183)$$

where

$$D = \frac{1}{1/D_{12} + 1/D_k} \qquad (3.184)$$

is a combined diffusion coefficient defined by eq. 3.184. Then D is
converted into D_{eff} by use of geometrical models of the pore system.
The geometrical models suitably approximate the voids in the porous
media which can be expressed in terms of the physical properties of
the catalyst which are accessible to experimental determination
(*e.g.* the total porosity, distribution of pore sizes or surface
area per gram catalyst). Some widely used models are the parallel-

-pore model (ref. 106), capillary models (ref. 107), or random pore models (refs. 108-110).

In the parallel pore model, the porous pellet is replaced by a two- or three-dimensional pile of parallelepipeds with radius $\bar{R}$ which is the mean pore radius obtained from

$$\bar{R} = 2V_g/S_g, \qquad (3.185)$$

where V_g is the pore volume of catalyst and S_g the pore surface area of catalyst per unit mass. Expressing the length of the diffusion paths through the pellet by means of a tortuosity factor τ, the effective diffusivity D_{eff} is obtained from

$$D_{eff} = D \cdot \varepsilon/\tau, \qquad (3.186)$$

where ε is the porosity of the pellet (void /pore/ volume of particle/total volume of particle). The porosity can be determined from the weight difference of a dry catalyst sample and a sample immersed in a liquid such as water or carbon tetrachloride or by using the helium-mercury method (ref. 111).

Several up-to-date methods for catalyst characterization have been summarized in a recent volume (ref. 112).

The tortuosity factor, which accounts for elongated diffusion distances in the porous medium as well as for dead-end pores and varying pore sections, can be obtained from the rate of replacement of a liquid within the void volume of porous pellets compared with a surrounding liquid, where both liquids have similar molar volumes (ref. 113). In the case of diffusion of liquids in porous structures, the mean free paths are usually small compared with pore radii and the combined diffusivity, eq. 3.184, is replaced by the molecular diffusion coefficient. For the mole fraction x_1 of a component 1 diffusing out of an isotropic pellet, as function of time t, the following approximate solution to nonstationary diffusion can be derived

$$x_1/(x1)_\infty = 2(1 + \beta) \ t/\pi \cdot \omega \qquad (3.187)$$

where $(x_1)_\infty$ is the equilibrium mole fraction of component 1, $\beta =$ = volume of pores/volume of surrounding liquid and

$$\omega = \left(\frac{R \cdot L}{R+L}\right)^2 \cdot \frac{\tau}{4 \cdot D_{12}} \qquad (3.188)$$

R and L are the radius and the length of the cylindrical pellets.

The tortuosity factor follows from the initial slope of a plot of $x_1/(x_1)_\infty$ *versus* t, which is depicted in Fig. 3.21 for the system n-hexane, n-heptane, 20 wt% Ni/Al$_2$O$_3$ (ref. 114).
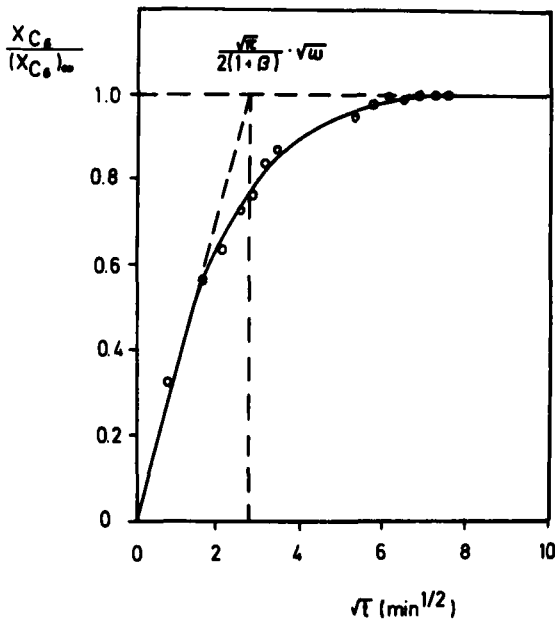
Fig. 3.21. Determination of the tortuosity factor for a commercial Ni/Al$_2$O$_3$ catalyst. Reproduced with permission from (ref. 114).

Models of porous media, which are based on the distribution of pore sizes are the capillary, random pore and network models. In the capillary models, the geometry of the porous medium is approximated by randomly oriented capillaries or parallel oriented bundles of capillaries where each capillary has a uniform radius and the bundle exhibits a distribution of radii. The model of Johnson and Stewart (ref. 107) results in the following relation for the effective diffusivity

$$D_{eff} = \frac{\rho}{\tau} \cdot \sum_{r=0}^{r=\infty} \frac{\Delta V_g}{(1 - \alpha_1 x_1)/D_{12} + 1/D_{K_1}} \qquad (3.189)$$

where ρ is the solid density, $\alpha_1 = 1 + N_2/N_1$, N = molar flux [mol m^{-2} s^{-1}], ΔV_g the pore volume fraction and x the mole fraction. The random pore model of Wakao and Smith (refs. 108,109) considers diffusion in the secondary pore structure (formed by pressing small

crystallites into pellets), diffusion in the small crystallites and a series diffusion, involving macro- and micropores. The voids in the pellet are imagined as short void regions surrounding and between individual particles. According to this model, the effective diffusivity can be predicted by the following relation

$$D_{eff} = \frac{\varepsilon_M^2}{(1-\alpha_1 y_1)/D_{12}+1/D_{K_M}} + \frac{\varepsilon_\mu(1+3\varepsilon_M)}{1-\varepsilon_M} \cdot \frac{\eta_i}{(1-\alpha_1 y_1)D_{12}+1/D_{K_\mu}} \quad (3.190)$$

where ε_M and ε_μ are the void fractions of macro and micro regions, η_i the micropore effectiveness factor, D_{12} the molecular diffusion coefficient and D_{K_M} and D_{K_μ} the Knudsen diffusion coefficients in macro- and micropores. Macro- and microregions are represented as short straight, cylindrical pores of average radii $\bar{R}_M$ and $\bar{R}_\mu$.

In addition to diffusion, finite adsorption and desorption rates as well as surface diffusion of adsorbates can contribute to the transport of a substance through a slab of porous solid. All these processes can give a resulting diffusivity defined by Aris (ref. 115) as "apparent diffusivity" D_a, as opposed to "effective diffusivity" D_{eff} discussed so far. The ratio D_a/D_{eff} is plotted in (ref. 115) as a function of such parameters as the ratio of pore diffusivity to surface diffusivity, the adsorption equilibrium constant, and the ratio of adsorption rate to diffusion rate. For transport, it is assumed that the sorption process is not in equilibrium; equilibrated sorption and no surface diffusion represent limiting cases. In contrast to the approach of characterizing mass transport through porous media by an effective diffusivity D_{eff} as discussed so far, the dusty-gas model considers the influence of walls in diffusive systems and clarifies the nature of the overall diffusive flux and the nature of the coupling between diffusive and viscous fluxes in porous media. With the dusty-gas model the porous medium is represented as an accumulation of suspended spherical, uniform, distributed particles which are much heavier and larger than the gas molecules and, hence, are at rest and do not contribute to the thermal conductivity and viscosity of the gaseous components (refs. 116, 117). The overall transport is divided into three independent transport mechanisms: Knudsen flow, in which the gas density is so low that only collisions of gaseous molecules with the walls contribute to the mass flow, molecular diffusion, where the mass transport is caused by gaseous molecule-molecule collisions and viscous flux which is caused by a pressure gradient. Surface diffusion is not considered. The combination of the different mecha-

nisms is achieved in the following way: the partial pressure gradient causes the molecular-diffusive flux through molecule-molecule collisions and the Knudsen diffusion flux through molecule-wall collisions and hence, the driving force for the overall diffusive flux can be considered to be made up of two separate contributions. The viscous flux is then simply added to the diffusive flux for each species giving

$$
J_1 = [\frac{-D_{K_1,eff} D_{12,eff}}{(x_2 \cdot D_{K_1,eff} + x_1 D_{K_2,eff})p + D^0_{12,eff}}] \frac{p}{RT} \frac{dx_1}{dy} -
$$

$$
- [\frac{D_{K_1,eff}(D_{K_2,eff} \cdot p + D^0_{12,eff})}{(x_2 D_{K_1,eff} + x_1 D_{K_2,eff} + D^0_{12,eff})} + \frac{B_0 \cdot p}{\mu}] \frac{x_1}{RT} \cdot \frac{dp}{dy}
$$

(3.191)

where $D^0_{12,eff} = D_{12,eff} \cdot p$, J_1 = molar flow of species 1, $D_{K_i,eff}$ = = effective Knudsen diffusion coefficient, $D_{12,eff}$ = effective molecular binary diffusion coefficient, P = pressure, x_i = mole fraction, y = spatial coordinate, μ = viscosity and B_0 = viscous flow parameter. The four effective parameters in the model equation $D_{12,eff}$, $D_{K_1,eff}$, $D_{K_2,eff}$ and B_0/μ are experimentally determined by permeability and isobaric counter diffusion measurements. In the case of permeability measurements the molar flow of a single gaseous species through the porous medium is monitored at different total pressures and different pressure drops over the pellet and eq. 3.191 reduces to

$$
J = -[D_{K,eff} + (B_0/\mu) P] \frac{1}{RT} \frac{dP}{dy} ,
$$

(3.192)

which yields upon integration

$$
JRTL/\Delta P = D_{K,eff} + (B_0/\mu)P
$$

(3.193)

i.e. $D_{K,eff}$ and B_0/μ can be determined from the ordinate intercept and the slope, respectively, of the straight line which is obtained by plotting JRTL/ΔP against the average total pressure in the porous medium.

In the case of isobaric counter diffusion measurements, eq. 3.191 reduces to

$$J = \frac{-D_{K_1,eff} \, D^0_{12,eff}}{(x_1 D_{K_2,eff} + x_2 D_{K_1,eff})P + D^0_{12,eff}} \, \frac{p}{RT} \, \frac{dx}{dy} \qquad (3.194)$$

which upon integration yields

$$JRTL \equiv \frac{D_{K_1,eff} \, D^0_{12,eff}}{D_{K_1,eff} - D_{K_2,eff}} \cdot$$

$$\cdot \ln \left[\frac{(D_{K_2,eff} - D_{K_1,eff})Px_1(1) + D_{K_1,eff} P + D^0_{12,eff}}{(D_{K_2,eff} - D_{K_1,eff})Px_1(0) + D_{K_1,eff} P + D^0_{12,eff}} \right] \qquad (3.195)$$

where $x_1(0)$ and $x_1(1)$ are the mole fractions of species 1 at each front of the porous medium. $D_{12,eff}$ can be computed by means of an trial and error procedure. The diffusion reactor which will be presented in Section 4.2 is a suitable laboratory reactor for experimentally determining an effective diffusivity according to eq. 3.192, as well as an effective Knudsen diffusivity on the basis of permeability measurements and also an effective molecular diffusivity as defined by eq. 3.195.

In the formulation of the dusty-gas model the structure of the porous medium is contained by three parameters which correspond to the three transport mechanisms considered: the porosity-tortuosity factor ε/τ for molecular diffusion, the Knudsen flow parameter K_0 and the viscous flow parameter B_0. In cases where the actual structure of the porous medium is represented by simple geometries, the structural parameters are simply related to measurable physical properties of the porous medium. Thus, for a long circular capillary of radius R,

$$K_0 = R/2, \qquad B_0 = R^2/8, \qquad \varepsilon/\tau = 1. \qquad (3.196)$$

For isotropic media, geometrically modelled with bundles of straight pores of mean radius $\bar{R}$,

$$K_0 = (2\bar{R}\varepsilon)/(3\tau) \quad \text{and} \quad B_0 = \frac{\varepsilon}{\tau} \cdot \frac{2}{9\pi^2} \cdot (\bar{R})^2. \qquad (3.197)$$

For geometric models which represent the actual voids in the porous medium, more realistic relationships for the structural parameters are more complicated or difficult to derive. In these cases the parameters have to be obtained from suitable experimental data.

The simultaneous occurence of diffusion and chemical reaction

complicates the picture; even more so for cases of multistep reactions which represent the overwhelming majority of catalytic processes.

The simplest two-step reactions:

$$A_1 \longrightarrow A_2 \longrightarrow A_3$$

and

$$A_1 \begin{array}{c} \nearrow A_2 \\ \searrow A_3 \end{array}$$
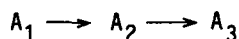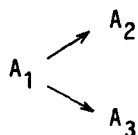
were analyzed in isothermal symmetrical catalyst pellets (slab, cylinder and sphere) using the dusty-gas model (ref. 118). Analytical solution of the corresponding equations was possible for some particular physical cases (*e.g.*, equal Knudsen and/or binary diffusivities for all components or with infinite Knudsen or binary diffusivities). Theoretical concentration profiles can thus be calculated. The method was applied to the methanol synthesis reaction with two parallel linearly-independent chemical processes:

$$CO + 2H_2 \longrightarrow CH_3OH$$
$$CO_2 + 3H_2 \longrightarrow CH_3OH + H_2O$$
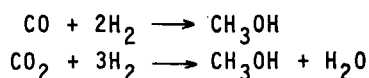
occurring on a spherical catalyst pellet (ref. 119). A maximum CO_2 concentration inside the pellet was reported.

3.4 CATALYST DEACTIVATION

The actual activity and selectivity of a catalyst depend on the history of the catalyst, beginning with the first preparation step and as a rule changing with time on stream. A new batch of catalyst may require a "running-in" period to reach the desired level of activity and selectivity. This time is often reduced by additives. Two examples can be mentioned here: supported Pt/Al_2O_3 catalysts of naphtha-reforming possess excess and undesirable hydrogenolysis activity in their fresh state. This can be tempered by their deliberate poisoning by controlled dosing of sulfur (ref. 120) or by the first portions of the reactant itself causing carbon accumulation on the surface (ref. 121). After this period, a constant activity is expected from practical catalysts; however, a decreasing activity is usually observed called catalyst deactivation. Its time scale varies considerably and may correspond to those of the desi-

red chemical surface reactions or deactivation may be very slow compared with the main reactions. Catalyst deactivation is a severe problem in the case of laboratory studies of heterogeneous catalytic processes, with respect to catalyst screening, scale-up from laboratory to industrial reactors and process optimization. For all of these tasks kinetic parameters, which characterize the activities and selectivities, are needed. These are estimated by using fitting procedures, starting with a set of experimental composition *versus* space velocity data, preferably covering the total reaction hyperplane in the composition space and which are usually obtained at different temperatures.

A few years ago it was still true that, compared with the total number of related scientific investigations, deactivation was only the subject of a rather small number of studies (refs. 78,122,123). However, in the 1980's both the number of papers and the depth of treatment increased rapidly (refs. 124-127). A series of conferences started in Berkeley in 1978 the latest being organized in Antwerpen, in 1987. Their proceedings have been published as separate volumes (refs. 127,128). It is still true, however, that no uniform and general treatment of catalyst deactivation has been published.

Investigations of the mechanism of the deactivation processes can be assigned to catalytic chemistry/surface science and to a reaction kinetics/chemical engineering approach. In the following, some deactivation mechanisms and principles for deriving dynamic model equations are discussed.

3.4.1 Deactivation mechanisms: chemical models

Within the concept of active centers, catalyst deactivation can be understood either as a decrease in the number of active centers per unit surface area with time on stream or as a decrease in the ability of individual active centers to convert reactant into product molecules (*i.e.* as a decrease in the turnover-numbers on individual active centers per unit time). There are many theoretically possible processes which may cause deactivation which we shall not consider in detail. Usually these are divided into several main classes (refs. 122-124,129):

(i) Structural changes (reconstruction) in the catalyst and on the surface of the catalyst, which may be caused, for example by sintering of originally finely dispersed crystallites, restructuring of crystallite planes, volatilization of surface metal

atoms, metal-support interactions, alloying, and segregation of
alloys.

(ii) <u>Strong chemisorption</u> of reactants, products or impurities on
active centers; this is termed <u>poisoning.</u>

(iii) <u>Deposition of residues;</u> for example, layers of carbonaceous
material formed in consecutive reactions from hydrocarbon sur-
face complexes or from other residues built up from fluid phase
species on the catalyst surface; this is termed <u>coking</u> or <u>fou-
ling.</u>

A few selected examples will now be given for all three classes.
Surface spectroscopic methods for studying active centers and their
surroundings on catalytically active surfaces, under deactivating
(or analogous) conditions, will be mentioned here. Such methods can
be independent of kinetic methods (ref. 128) although the rigid
separation of the two types of approach is not correct. Together
with examples of deactivation, some running-in processes will be
treated, too. These usually belong to the first two classes. Fou-
ling, in general, produces a deposit representing a separate phase
and is beyond the running-in period of the life of a catalyst.

(i) <u>Reconstruction.</u> Although structural changes may be thermally
induced, they depend mostly upon the chemical environment on the
solid surfaces, therefore frequently combined effects are observed.
For example, the recrystallization of the Pt-wire net used as a ca-
talyst for ammonia oxidation has long been recognized; in spite of
this, the catalyst preserves its activity until a mechanical failure
occurs. H_2S impurities may enormously accelerate the recrystalliza-
tion of Pt wire used for ammonia oxidation (ref. 130). Another
example has been presented by Galwey *et al.* (ref. 131) who heated
a Pt-wire up to 1800 K in O_2 until the electron micrograph showed
a quite smooth surface. When the wire was used as a catalyst for
CO oxidation at 500 K, a major faceting occurred exposing several
small pyramids on the surface. Obviously, a phenomenon called
"corrosive chemisorption" occurred, the catalyst-adsorbate bond
strength being so large that removal of the adspecies took with it
catalyst atoms from their original position thus inducing surface
restructuring. Somorjai (ref. 132) interpreted the <u>sulfur</u> poisoning
of a platinum surface in terms of its recrystallization from (111)
symmetry to (100) planes and the subsequent changes in structure
sensitivity. The effect of <u>hydrogen</u> in recrystallization and/or
sintering of Pt powder has also been reported (ref. 133).

(ii) <u>Poisoning.</u> Deposition of deeply dehydrogenated species on to

a Pt/Al$_2$O$_3$ reforming catalyst during the initial stages of methyl-
cyclohexane (MCH) dehydrogenation may be termed as poisoning in the
strictest ·sense since it is completely reversible: the deposit can
be removed by hydrogenation (ref. 134). During this period, an
equilibrium can be assumed between active and reversibly deactiva-
ted sites, through a simple dehydrogenation step. This period lasts
until about 20-40% of the original activity is lost; then a long-
-term deactivation follows which is, at most, partly reversible
and may be termed "fouling" (the authors, in fact, use this expres-
sion). Increasing hydrogen pressure slowed down this poisoning.
Kinetic aspects of this process will be discussed later.

The structure of the carbonaceous overlayers and their effect
on the activity of various single crystal faces has been studied
extensively by Somorjai and associates (ref. 135). A complete car-
bonaceous overlayer formed during the first few minutes (or even
seconds) of contact with the reaction mixture at cyclohexane pre-
ssures as low as 10^{-6} Torr (ref. 136). This deposit selectively
covered edge and kink sites and suppressed hydrogenolysis. Constant
activity was observed in dehydrogenation/dehydrocyclization reac-
tions in the presence of 0.1 to 1 monolayer of this overlayer. This
layer can store hydrogen and may show a marked catalytic activity
in hydrogenation/hydrogen transfer reactions (refs. 135,136).
Multilayer carbon buildup and eventual graphitization, with exten-
sive deactivation, takes place above 700 K. Reacting [^{14}C]-label-
led 3-methylpentane on Pt-black showed that, at a surface atomic
ratio C/Pt = 0.8, about 70% of the aromatizing/dehydrogenating ac-
tivity remained; at the same time, only 30% of the original hydro-
genolysis activity was observed (ref. 137). This selective poiso-
ning of hydrogenolysis by carbonaceous deposits was also observed
with Pt/Al$_2$O$_3$ and Pt-Re/Al$_2$O$_3$ (ref. 121). A fresh Pt/Al$_2$O$_3$ catalyst
showed a conversion and a methane selectivity of about 100%. This
situation persists in a flow reactor using a n-heptane feed of 1
Torr in 1 bar H$_2$. Increasing the n-heptane pressure to 10 Torr,
methane selectivity drops to below 10% rapidly, with increasing
aromatic selectivity (up to 90%). At this partial hydrocarbon pressu-
res, accumulation of carbonaceous deposits must have been sufficient
to poison sites for excessive hydrogenolysis: however, aromatization
sites remained intact. Increasing the heptane pressure to 56 Torr,
aromatization activity started to drop. Here accumulation and migra-
tion of the deposits to the support were claimed to compete (ref.
45). Here obviously, a selective poisoning occurred which is regar-

ded as useful because aromatics are valuable products from n-hepta-
ne while methane is not. It is clear, however, that "usefulness" is
a question of economic and not chemical definition.

Several experiments indicate that aromatization requires small
Pt-ensembles (ref. 138) and is promoted by conditions when the Pt-
-surface is divided by additives into smaller separated areas. This
can be done by inactive alloying elements; such as Cu, Au (refs.
52,138), Sn or Pb (refs. 52,121). Carbonaceous deposits can, to
some extent, substitute the latter type of additives and so can the
addition of sulfur. Hydrogenolysis on n-pentane dropped to zero
over a Pt/Al$_2$O$_3$ with a surface atomic ratio S/Pt = 1 (ref. 120).
This sample did not chemisorb hydrogen indicating no "free" Pt-
-atoms on the surface; still, the activity and selectivity for the
n-hexane reforming reaction was retained. A similar result can be
achieved by high temperature hydrogen pretreatment (ref. 139). The
sulfur tolerance of Pt-Re/Al$_2$O$_3$ is much lower: the same amount of
S added resulted in an initial activity of a bimetallic catalyst
six times lower than that of the monometallic supported Pt-sample
(ref. 140). Sulfur atoms are bound selectively to surface Re-atoms,
the resulting Re-S species being very effective in dividing Pt-sur-
faces into ensembles favoring aromatization (refs. 41,135,141).

Sulfur on a Pt(100) crystal face can completely suppress the
oxidation of CO by NO (ref. 142). Using Auger-electron spectroscopy
to determine the chemical composition of the surface and low energy
electron diffraction to analyze the surface structure, the forma-
tion of sulfur overlayers when exposing Pt(100) surfaces to H$_2$S at
10^{-8} Torr and the oxidation of CO on clean and sulfided Pt-surfa-
ces have been investigated. Together with the suppression of CO
oxidation, sulfur forms centered (2 x 2) or primitive (2 x 2) su-
perlattices on the platinum surface.

(iii) Fouling. As a rule, this process, is accompanied by the build-
up of an overlayer or deposit representing a separate phase on a
much larger scale than poisons attached to the catalyst, sometimes
in an atomically dispersed state. Fouling is observed, for example,
in the hydrodesulfurization of residual oil feedstocks where vana-
dium and nickel sulfides, present in asphaltenes and resins are
deposited via an autocatalytic reaction in the superficial regions
of the catalyst pellets (ref. 143). Thus the regions in the cata-
lyst with metal deposition do not contribute to reactant conversion,
however, with metal deposition a further related effect also occurs
with coking. Due to the deposition of residues on the internal sur-

face of porous catalysts, the pore diameters change and hence also
the diffusivities. In the case of hydrodesulfurization, with inc-
reased metal sulfide deposits in the superficial regions of the
catalyst pellets the interior of the catalyst pellets become less
and less accessible to the large reactant molecules until the pores
are fully blocked and the activity rapidly declines to almost zero.
Two processes are competing here: the formation of deposits mainly
on the outer surface of the pellets by heavy metal-containing mo-
lecules and surface poisoning within the pores. If the first pro-
cess is more rapid, the pore mouths will be physically blocked be-
fore the deposits reach the center of the catalyst pellet. The ac-
tivity is then lost, although catalytically active surfaces are
still present, but in accessible. A mathematical analysis of the
process (assuming uniform pore-size distribution and first-order
kinetics for both demetallization and desulfurization) has been pre-
sented by Ahn and Smith (ref. 144). A similar coupling with mass
transport rates within the porous structure is also expected in ca-
ses of structural changes in the catalyst.

3.4.2 Kinetic and chemical engineering approach to catalyst deac-
tivation

In terms of the active center concept, deactivation processes
accompanying surface reconstruction [class (i)] change the electro-
nic and geometric characteristics of active centers and their en-
vironment. Hence, it cannot be expected that the rates of corres-
ponding surface reactions can be mathematically modelled with
differential equations having constant coefficients, if it is not
assumed that, for transforming a certain reactant into a product,
the active centers must be provided with a certain electronic and
geometric environment; any slight change of this environment will
cause a total loss of the ability of the active center to convert
reactants into products. With Class (ii) and (iii) deactivation
processes (poisoning and fouling) the number of active centers is
decreased by blocking or strong chemisorption. Adsorption of spe-
cies of the fluid phase in the vicinity of active centers, however,
will also change the electronic and geometric characteristics of
active centers.

Deactivation can be taken into account in kinetic analysis as
follows:
1. Deactivation steps are incorporated into the reaction network
   and the dynamic model equations are derived from the complete

reaction network.

2. Experimental provisions are taken to decouple rates of deacti-
vation steps and other surface reactions at constant temperatu-
re and reaction mixture composition in cases where the complete
rate equation can be separated into a product of a term descri-
bing the present conditions and a term describing past history;
these provisions can also be used to discriminate among rival
deactivation mechanisms on the basis of simplified reaction
schemes, where deactivation steps are incorporated.

3. Following thoroughly accomplished running-in procedures an acti-
vity and selectivity level of the catalyst can be found, which
is constant during a series of measurements on the same catalyst
sample and for different catalyst samples. The experimental data
required to determine the coefficient matrix in the dynamic mo-
del equations are then obtained at this activity and selectivi-
ty level of the catalyst and hence the coefficient matrix only
characterizes this single catalyst activity and selectivity le-
vel. This may severely limit the possibility of predicting the
activity and selectivity of the same catalyst in other labora-
tory reactor configurations or in larger scale reactors and
further experiments will have to be performed to examine the
actual activity and selectivity level of the catalyst in these
different reactors. Obviously the usefulness of such data is
rather restricted.

4. The set of experimental data for determining the coefficient
matrix is obtained at different catalyst activity/selectivity-
-levels. A certain activity/selectivity-level of the catalyst
is assumed and all the data are "corrected" for this value by
use of a further set of reference-measurements made under stan-
dard conditions at different times-on-stream. In the case of
nonseparable kinetics, the set of data obtained in this way is
inconsistent and of no use in the laboratory studies claimed
above.

Of the four cases considered, in the first two, deactivation
reactions are investigated and are incorporated into the reaction
network on different levels. With the other two, deactivation is
dealt with like a phenomenon which has to be circumvented in order
to obtain a required set of experimental data. The most usual pro-
cedure for studying the dynamics of reactive catalytic systems is
that described in Case 3.

With the aim of mathematically modeling the dynamics of deacti-

vating catalytic reaction systems, reaction schemes are required
for the formulation of the model equations. Reaction schemes which
have been frequently considered in the literature are (W is the
poison deposited on the catalyst):
Impurity or side-by-side deactivation

$$A_1 \longrightarrow A_2$$
$$P \longrightarrow W.$$

(3.197)

Parallel self-poisoning

$$A_1 \longrightarrow A_2 \quad \text{or} \quad A_1 \longrightarrow A_2 + W$$
$$A_1 \longrightarrow W$$

(3.198)

Series self-poisoning

$$A_1 \rightarrow A_2 \longrightarrow W$$

(3.199)

and triangular self-poisoning

$$A_1 \longrightarrow A_2$$
$$\searrow W \nearrow$$

(3.200)

The kinetics of self-poisoning also has its effect on deactivation
rate. First-order and Langmuir-Hinshelwood kinetics have been con-
sidered to describe parallel and series fouling, respectively, in
a fixed-bed adiabatic catalytic reactor. It turned out that Lang-
muir-Hinshelwood fouling may be much more severe than when it takes
place according to first-order kinetics. Again, the time scale of
fouling should be very large compared with that of the catalytic
reactions; solutions could be obtained for this pseudo-steady sta-
te (ref. 145).

   As was stated above, in man-made catalytic conversions the main
aim is to obtain high space-time yields and hence (unlike biologi-
cal systems where inhibition of enzyme activity is a regulating
mean for the rate of single reaction), with man-made reactive sys-
tems deactivation mechanisms are investigated in order to reduce
considerably or slow down deactivation reactions, or to discover
procedures for regenerating the original activity and selectivity
of the catalyst. Table 3.9 shows typical stability periods and
factors which determine the long-term stability of some important
industrial catalysts according to Denny and Twigg (ref. 146). The
rate of the "useful" reaction and that of catalyst deactivation de-
termines the operational strategy to be adopted commercially when
using catalytic processes. At present, these strategies are mostly
based on empirical correlations of catalyst deactivation rather
than the exact incorporation of deactivation functions in the over-
all kinetics. Theory has still a long way to go before a scienti-

TABLE 3.9

Typical stability periods and factors determining the long-time stability of industrial catalysts (ref. 145).

Reaction	Operation conditions	Catalyst	Typical stability period [years]	Deactivation process affecting standing time
Ammonia synthesis $N_2 + 3H_2 \longrightarrow 2NH_3$	450-550°C 200-500 atm	$Fe/K_2O/Al_2O_3$	5-10	slow sintering
Methanation $CO + 3H_2 \rightarrow CH_4 + H_2O$	250-350°C 30 atm	Ni/Al_2O_3	5-10	slow poisoning (S, As-compounds)
Methanol synthesis $CO + 2H_2 \rightarrow CH_3OH$	200-300°C 50-100 atm	$Cu/Zn/Al_2O_3$	2-8	slow sintering
Hydrodesulfurization light petroleum	300-400°C 35-70 atm	$CoS/MoS_2/ /Al_2O_3$	5-10	slow coking
Heavy petroleum, residua	340-425°C 55-170 atm	$CoS/MoS_2/ /Al_2O_3$	0.5-1	fouling (metal sulfide deposits)
Ammonia oxidation $2NH_3 + 5/2O_2 \rightarrow 2NO + 3H_2O$	800-900°C 1-10 atm	Pt-alloy gauze	0.1-0.5	loss of Pt, poisoning
Catalytic cracking of oils	500-560°C 2-3 atm (fluidized bed)	Zeolite	0.000002	rapid coking (continuous regeneration)
Benzene oxidation to maleic anhydride $C_6H_6 + O_2 \rightarrow C_4H_2O_3$	350°C 1 atm	$V_2O_5/MoO_2/ /Al_2O_3$	1-2	formation of inactive vanadium phase

fically based solution can be reached (ref. 147). Also, the operational strategy is influenced by the parameter used for optimization: maximum product output, minimum operational cost, maximum profit *etc*. Various strategies applied in practice have been tabulated in Table 3.10 after Kovarik and Butt (ref. 147); these authors also discuss in detail the mathemathics of these strategies. The practical solutions are essentially circumventions of the prob-

TABLE 3.10

Summary of operational strategies for a reactor subject to catalyst
deactivation. Reproduced with permission from (ref. 146), p. 499,
by courtesy of Marcel Dekker, Inc.

1. Vary reactor temperature with time to maintain a constant con-
   version with a constant reactor feed flow rate. A typical pol-
   icy for large throughput (10^6 tonne per year) and slow deacti-
   vation rates (months to years of catalyst life).
2. Vary throughput of the reactor feed while holding the reactor
   temperature and conversion constant. A possible policy for me-
   dium deactivation rates (weeks to months catalyst life) and
   small to medium throughput (about 10^5 tonne per year) systems.
3. Allow the conversion to fall while holding the reactor feed
   flow rate and reactor temperature constant. Similar applicati-
   ons as in Item 2.
4. Maintain the fresh feed rate and reactor temperature constant
   and let the recycle flow increase. Similar application as in
   Item 2.
5. Use a combination of reactors in parallel and the plicies of
   Items 1 or 3. Usually, with two reactors in parallel, one will
   be off-line for catalyst regeneration while the other is opera-
   ting. A typical policy for large throughput and medium to fast
   deactivation rates (days to months of catalyst life).
6. Continuous catalyst regeneration while maintaining constant
   conversion, throughput, and reactor temperature. A typical po-
   licy for large throughput, rapid deactivation systems (hours
   to days of catalyst life).

lems arising from deactivation. It was along these lines of cir-
cumventing the underlying problems of catalyst deactivation that
an ingenious feedback control policy was developed (ref. 148). Here
the inlet temperature is varied according to deactivation while
disregarding the mechanism of deactivation. The examples shown are
certainly impressive from a practical point of view: with stepwise
(rather than continuous) feedback, when conversion of a model reac-
tion drops from 87 to 82%, a temperature jump is applied and this
procedure is repeated until the maximum permissible inlet tempera-
ture is reached. Then the conversion decreases continuously to a
level when regeneration becomes necessary.

3.4.3 Dynamic models of deactivating reactive systems

When mathematically modeling the dynamics of homogeneous gaseous phase reactions the following form

$$r = f(T,c_i) = k(T) \cdot f(c_i) \qquad (3.201)$$

is usually used, assuming that the dependence of the rate on temperature and concentration can be separated into a temperature-dependent term,

$$k(T) = k_0 \cdot \exp(-A_E/RT) \qquad (3.202)$$

and a concentration-dependent term, which is formulated as

$$f(c_i) = \prod_{i=1}^{1} c_i^{n_i} \ . \qquad (3.203)$$

Based on this approach Szépe and Levenspiel (ref. 149) divided deactivating catalytic reaction systems into systems where the complete rate equation is separable and systems where the rate equations are not. The complete rate equation in the general form is given (ref. 148) by:

$$r = r \text{ (present conditions, past history).} \qquad (3.204)$$

In the case of hyperbolic rate equations where a term B, called the fouling factor, has been introduced to account for decreasing catalyst activity, for example

$$r = \frac{k \cdot a_A \cdot a_B}{(1 + K_A \cdot a_A + K_B \cdot a_B + B)^2} \ , \qquad (3.205)$$

the general form of the complete rate equation can be written as

$$r = \frac{r_1 \text{ (present conditions)}}{r_2[r_3 \text{ (present conditions)} + r_4 \text{ (past history)}]} . \qquad (3.206)$$

The complete rate equation is termed separable if the following eq. holds

$$r = r_0 \text{ (present conditions)} \cdot \tilde{a} \text{ (past history)} \qquad (3.207)$$

where $\tilde{a}$ is the activity of the catalyst which is defined as the ratio of the actual rate at time t and the initial rate at time $t = 0$

$$\tilde{a}(T_1,a_1,t_1) = \frac{r(T_1,a_1,t_1)}{r(T_1,a_1,0)} \ . \qquad (3.208)$$

This definition of catalyst activity holds for all deactivating catalytic systems irrespective of the form of the corresponding rate equation. A drawback of this definition is that the experimental determination of the initial activity, especially in rapidly deactivating systems, is rather difficult. In this case, a "deactivation disguised kinetics" is observed. Two examples are presented for this situation by Krishnaswamy and Kittrell (ref. 150): catalytic cracking of gas oil and hydrogen peroxide decomposition by supported catalyse enzyme. Gas oil cracking can either be described by second-order conversion model and concentration-independent deactivation kinetics or by a first-order conversion model and concentration-dependent deactivation kinetics. The two models only differ at very high (impracticable) overall conversions. The example for catalysis is worth mentioning because it demonstrates that enzyme catalysis can be described by the same mathematical model. Here high peroxide concentrations deactivate the enzyme. With fixed-bed reactors, the same models can be applied, as in the case of gas oil cracking.

Hence, in dealing with dynamic modeling of deactivating systems, a test for the separability of the different dependencies in the complete rate equation has to be performed first. According to Szépe and Levenspiel (ref. 144) and Löwe (ref. 151), this can be achieved by determining the initial activity and the activity under at least two reference conditions in at least one further activity state of the catalyst. In the case of separability, the activity obtained must be independent of the reference conditions. The required exact adjustment of the reference conditions in the initial activity state and the corresponding state, after a certain time on stream, can be attained with a differential external recycle reactor where, in the external recycle, the flow of individual components of the reaction mixture is regulated in such a way that the concentrations in the reactor are kept time-invariant (ref. 152).

Rate equations of deactivating catalytic systems are formulated in the following way by considering the rate of the occuring chemical reactions, without deactivation reactions, and the rate of deactivation of the catalyst (ref. 153)

$$r = f_1(T) \cdot f_2(c_i) \cdot f_3 \quad \text{(present activity of the catalyst pellet)} \quad (3.209)$$

$$r_d = f_4(T) \cdot f_5(c_i) \cdot f_6 \quad \text{(present state of the catalyst pellet)} \quad (3.210)$$

or

$$r = k(T) \cdot f_2(c_i) \cdot \tilde{a} \qquad (3.211)$$

$$r_d = k_d(T) \cdot f_5(c_i) \cdot \tilde{a}^d \qquad (3.212)$$

where r_d is the deactivation rate, k_d the deactivation rate constant and d the order of deactivation. Using eq. 3.211 and 3.212 for the four deactivation mechanisms represented by equations 3.197-3.200 the following kinetic equations are obtained

Impurity deactivation $r_{A_1} = k \cdot a_{A_1}^n \cdot \tilde{a}$

(3.213)

$(A_1 \rightarrow A_2, \; P \rightarrow W)$ $\dfrac{d\tilde{a}}{dt} \; r_d = k_d \cdot a_P^m \cdot \tilde{a}^d.$

Parallel self-poisoning $r_{A_1} = k \cdot a_{A_1}^n \cdot \tilde{a}$

(3.214)

$(A_1 \rightarrow A_2, \; A_1 \rightarrow p)$ $r_d = k_d \cdot a_{A_1}^m \cdot \tilde{a}^d$

Series self-poisoning $r_{A_1} = k \cdot a_{A_1}^n \cdot \tilde{a}$

(3.215)

$(A_1 \rightarrow A_2 \rightarrow W)$ $r_d = k_d \cdot a_{A_2}^m \cdot \tilde{a}^d$

Triangular self poisoning $r_{A_1} = (k_1 + k_2) a_{A_1}^n \tilde{a}$

(3.216)

$(A_1 \rightarrow A_2, \; A_1 \rightarrow P, \; A_2 \rightarrow P)$ $r_d = k_d (a_{A_1} + a_{A_2})^m \tilde{a}^d.$

In mathematically modeling deactivating catalytic systems it is frequently assumed that the function $f_5(c_i)$, eq. 3.212 is 1 and the deactivation rate of the catalyst is no longer concentration- and time-dependent, but only time-dependent. Szépe and Levenspiel (ref. 149) demonstrated that the four main types of activity decay equations reported in the literature, where the activity decreases linearly, exponentially, hyperbolically or according to a recip- rocal power function with time-on-stream, can be reduced to the simplest structure of deactivation models which are characterized by a separable complete rate equation and a concentration-indepen- dent activity decay of the order d, between 0 and 3: $d\tilde{a}/dt =$ $= k_d \cdot \tilde{a}^d$ (Table 3.11). Separable deactivation models may be extre- mely useful, but their applicability is limited. In nonseparable cases, a "deactivation function" Ψ is defined which is a function of various reaction parameters. Particular cases for nonseparable deactivation equations have been listed for linear, exponential, hyperbolic, and reciprocal power cases of deactivation

TABLE 3.11

Deactivation equations in terms of a concentration-independent d-th order activity decay. Reproduced with permission from (ref. 149). Copyright 1971 Pergamon.

Type of activity decay	Equation	Differential form	Exponent in the power law $-d\tilde{a}/dt = k_d\tilde{a}^d$
Linear	$\tilde{a} = \tilde{a}_0 - \beta_1 t$	$-d\tilde{a}/dt = \beta_1$	0
Exponential	$\tilde{a} = \tilde{a}_0 \exp(-\beta_2 t)$	$-d\tilde{a}/dt = \beta_2\tilde{a}$	1
Hyperbolic	$1/\tilde{a} = 1/\tilde{a}_0 + \beta_3 t$	$-d\tilde{a}/dt = \beta_3\tilde{a}^2$	2
Reciprocal power function	$\tilde{a} = k \cdot t^{-\beta_4}$	$-d\tilde{a}/dt = \beta_4 k^{1/\beta_4}\tilde{a}^{(\beta_4+1)/\beta_4}$	$(\beta_4+1)/\beta_4$

(analogous to the case of Table 3.11); in addition, deactivation according to the equations of Elovich and Wojciechowski were also considered (ref. 154).

The definition of Ψ depends on the model used as the basis of derivation. Of necessity, this model contains simplifications since a consideration of all the possible factors would make the equations too complicated. Three approaches have been selected from the literature and will be presented here. Besides the reaction schemes 3.197-3.200, more detailed reaction schemes are employed in which the formation of poison precursors and frequently observed phenomena of simultaneous reversible and irreversible deactivation reaction steps are considered. These are used to derive dynamic model equations. For example, deactivation of a Pt/γ-alumina reforming catalyst during methylcyclohexane dehydrogenation has been assumed to proceed *via* the following reaction scheme, which has been demonstrated by plotting relative reaction rates in the fluid phase *vs* normalized concentrations in the center of a catalyst pellet and comparing this plot with theoretical solutions on the basis of different poisoning mechanisms

$$MCH + 1 \underset{k_{-1}}{\overset{k_1}{\rightleftharpoons}} [MCH{-}1] \xrightarrow{k_2} [Tol{-}1] + 3H_2 \underset{k_{-3}}{\overset{k_3}{\rightleftharpoons}} Tol + 1$$

$$k_{-4} \updownarrow k_4$$

$$[P_1{-}1] + H_2 \qquad\qquad (3.217)$$

$$k_{-5} \updownarrow k_5$$

$$[P_2{-}1] + H_2$$

$$\downarrow k_6$$

$$[P_3]$$

where the species in brackets are surface complexes, $P_1{-}1$ is a precursor of a reversibly formed $P_2{-}1$-species and P_3 an irreversibly-formed poison deposited on the catalyst surface. Deactivating complex reaction systems can also be modeled by adding a coke-formation reaction to the set in the reaction network. Coupling of the coke-formation reaction and the main reactions is accomplished by introducing deactivation functions into each of the dynamic model equations for the rate of transformation of the single components (refs. 55,155).

The initial assumptions made by Beeckman and Froment (refs. 156, 157) to derive their deactivation function were:
    (i) both the main and coking reactions occur on one catalyst
        site which is the same for both processes;
   (ii) coverage of sites by coke occurs randomly;
  (iii) there are no concentration gradients of reactants or pro-
        ducts inside the catalyst pellet.
Froment and associates (ref. 158) claim that their deactivation function contain parameters directly related to the cause of deactivation, as opposed to other, empirical formulas. In addition to reactor deactivating experiments, the amount of coke accumulated was checked using a microbalance; these two methods, combined with theory, gave a surprisingly good agreement between the deactivation function and the experimental results in the case of butene dehydrogenation over a chromia-alumina catalyst. This reaction has already been mentioned in Section 3.1.4. Combining deactivation with kinetic data, treated in (ref. 55), the equation found to give the best fit - Eq. (3.9) in Section 3.1.4 - gave a good statistical

correlation, but another equation

$$r^0_B = \frac{A^0 \exp(-E/RT)(p_B - \frac{p_D p_H}{K})}{1 + K_B p_B + K_D p_D + K_H p_H} \qquad (3.218)$$

gave an even better fit. Here A^0 is the preexponential factor, K_B, K_D, K_H are the adsorption coefficients for butene, butadiene and hydrogen, respectively, the p-values are the partial pressures of the same components, see also under Eq. (3.9).

In addition to the above single-site treatment, the following approaches also consider deactivation reactions which involve more than one active site. Scheme 3.18 depicts the proposed mechanism of
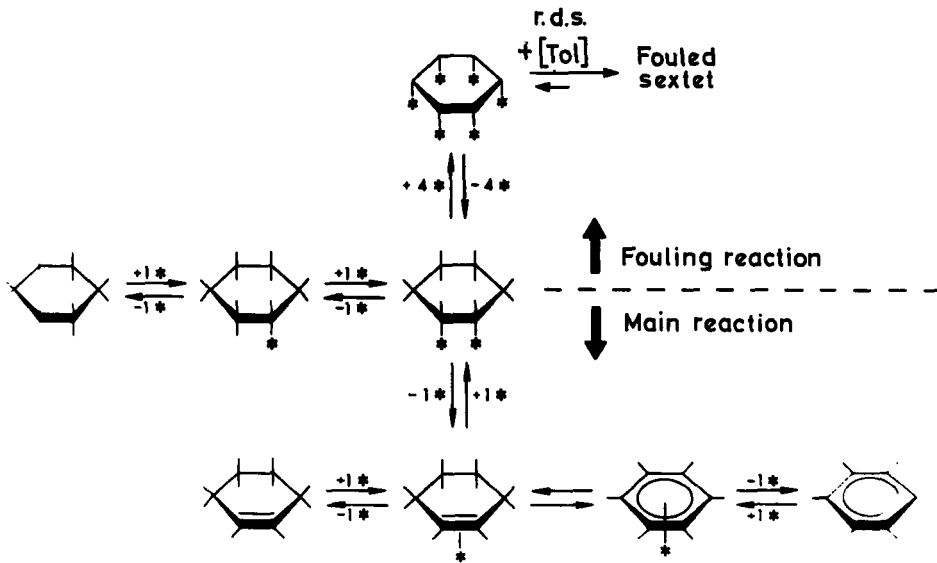
Scheme 3.18

methylcyclohexane (MCH) dehydrogenation and concomitant catalyst deactivation on Pt/Al_2O_3 (ref. 159). A fouling reaction would represent an interaction of the multiply bound C_6-skeleton with a gas--phase toluene (TOL) molecule according to a Rideal-Eley mechanism that initiates a site-consuming polymerization process. This is the rate-determining step in Scheme 3.18. The multiply bound species would lose all 11 hydrogen atoms in the ring. Thus, the fouling process would involve the following steps:

$$MCH(g) + 6(1) \xrightarrow{K_6} MCH(1)_6 + 11/2\ H_2(g) \qquad (3.219)$$

$$MCH(1)_6 + TOL(g) \xrightarrow{k_f} Fouled\ Sextet \qquad (3.220)$$
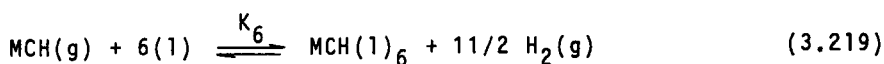
$$[MCH(1)_6]_s = K_6 \frac{[MCH]\ S_v^6}{[H_2]^{11/2}} \qquad (3.221)$$

$$\frac{dS_t}{dt} = -6k_f[MCH(1)_6]_s[TOL] = -6k_f K_6 S_v^6 \frac{[MCH][TOL]}{[H_2]^{11/2}} . \qquad (3.222)$$

(Compare the model with that shown in Fig. 3.217!) Here S_v represents the number of vacant sites, S_t the number of unfouled sites, K_6 the adsorption equilibrium constant for the fouling precursor and k_f the rate coefficient for the r.d.s. of fouling. Subscript s denotes surface concentration. Integrating (3.222), and also incorporating the empirical observation (ref. 134) that inhibition is proportional to toluene to the power -1/3:

$$S_t = K_3 S_v[TOL]^{1/3} \qquad (3.223)$$

we obtain:

$$a = (1 + kt)^{-1/5} \qquad (3.224)$$

where

$$k = \frac{30k_f K_6[MCH]}{K_3^6[TOL][H_2]^{11/2}} . \qquad (3.225)$$

Here K_3 is the adsorption equilibrium constant for toluene, k the fouling parameter in the hyperbolic decay function and "a" is the activity function for the dehydrogenation reaction. Plotting the value of "a" as a function of logarithmic fouling time, a good agreement is obtained between the model and experimental results from various sources at least until the catalyst activity decreases to about 25-30% of its initial value. The deviation of the data from the model led the authors to propose a "variable reaction order model" (ref. 160): this means that as fouling proceeds, fewer and fewer randomly located vacant sextets will be available. The multiplicity of continuous vacant multiplets, therefore, will become less and less. Thus, first sextets, then quadruplets, doublets, etc. participate in the reaction. On sulfided Pt-Re/Al$_2$O$_3$ catalysts, e.g., (ref. 140) the negative hydrogen exponent of -1.5 indicates that smaller ensembles, possibly doublets, are involved in the

r.d.s. of deactivation.

It is worth comparing the experimentally found deactivation data on Pt/Al_2O_3 and $Pt-Re/Al_2O_3$ with empirical results plotted on the basis of 10 different preceding publications (ref. 159). Figure 3.22 (ref. 160) shows the higher initial activity of Pt/Al_2O_3 al-
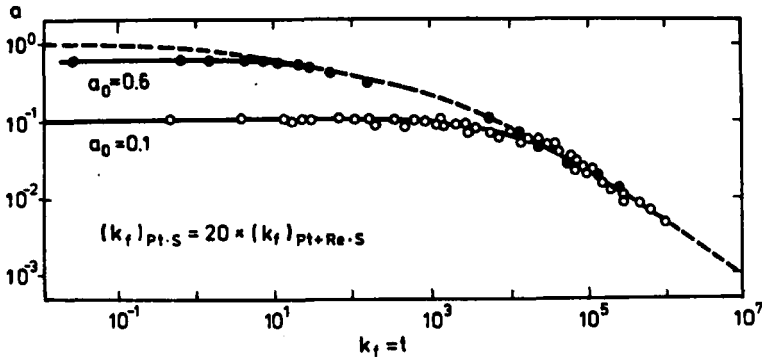
Fig. 3.22. Typical fouling data for sulfided reforming catalysts: the catalyst activity, "a" as a function of dimensionless fouling time, k_f = t. Shaded symbols mean Pt/Al_2O_3, open symbols, $Pt-Re/Al_2O_3$. Dashed line represents the empirical correlation drawn by plotting experimental data from 10 different publications as reported in (ref. 159). Reproduced with permission from (ref. 160).

ready mentioned in Section 3.4.1. The r.d.s. for the deactivation of $Pt-Re/SiO_2$ is 20 times smaller. Its curve joins the empirical curve at a much later point on the latter, where the multiplets involved in the fouling mechanism are much smaller than sextets (refs. 140,160).

Based on the multiplet deactivation model, an interpretation of temperature *versus* time curves was recently proposed for deactivating catalyst systems. The multiplet model gave much better agreement with selected experimental data than any single-power law (ref. 161).

Froment and associates (ref. 162) developed rigorous models for deactivation for single site and dual site "main" and deactivation reactions, assuming various number of active sites (1 to 5) per cluster of reaction sites. The cluster is defined "as a set of sites on the catalyst which are sufficiently close to one another to form the multi-site arrangement for the given reactions" (ref. 162). Their treatment allows - at least theoretically - the optimization of cluster size provided the site requirement of the main and co-

king reactions are known.

Corella and Asua (ref. 163) derived a generalized equation for the drop of activity "a" in time t as follows:

$$- \frac{da}{dt} = \frac{(\text{kinetic term}) (\text{pressure gradient})^{m+h}}{(\text{chemisorption strength term})^{h}} (\text{activity term})^{d}$$

(3.226)

where m and h are the number of active sites involved in the r.d.s. of the main reaction and of the deactivation reaction, respectively; $d = \frac{m+h-1}{m}$. The initial conditions they assumed were that: three consecutive steps lead to coking. The first step is adsorption of the species causing deactivation, the second step is the formation of coke precursor and the third step is coking. They assumed that either step 2 or step 3 can be rate-determining and that the adsorption in the first step may or may not be identical with that leading to the main reaction. Also, different coking mechanisms (degradation, polymerization, condensation) are considered. By combining these initial conditions, six basic mechanisms were derived, for which the actual forms of deactivation functions have been found and tabulated.

These data also allowed experimental verification. The cumene disproportionation reaction has the form:

2 cumene (C) $\rightleftharpoons$ p-diisopropylbenzene (D) + benzene (B). (3.227)

The results obtained on a commercial hydrocracking catalyst (Co-Mo zeolite embedded in an amorphous silica-alumina matrix (ref. 164)) were analysed in terms of these mechanisms. Four mechanisms were considered (ref. 165). The case that the adsorption of the reactant during the main reaction and during coking was different could be excluded, together with the case when the r.d.s. was a coke precursor, formation and deactivation occurred in series with the main reaction involving a gaseous product E from adsorbed D:

$$D + 1 \rightleftharpoons D 1 + H_2 \qquad (3.228)$$
$$D 1 \rightleftharpoons E + 1 \qquad (3.229)$$
$$E (g) + D 1 \rightarrow \text{coke precursor.} \qquad (3.230)$$

Two mechanisms were selected as being consistent with kinetic/deactivation data. In one of them, (3.228) is followed by the r.d.s. (3.231):

$$2 \ D \ 1 \longrightarrow \text{coke precursor} \qquad (2.231)$$

in the other, dimerization of the reactant C and product D occurs in a series-parallel type reaction. These two mechanisms cannot be separated.

3.4.4 Deactivation in the presence of diffusion

So far kinetic equations have been derived from simplified reaction schemes to account for the decay of catalytic activity in heterogeneous catalytic reactions. These are the entries into the conservation equations for single catalyst pellets or for fixed-bed reactors. The case of coupling diffusion and deactivating reactive systems was first considered by Wheeler (ref. 166) and later, in more detail, by Petersen and co-workers (ref. 78). Hence, by solving the continuity equations for the different deactivation mechanisms in a porous catalyst pellet, where the mass transport is only caused by diffusion processes and plotting the ratio of the actual rate and the initial rate with an unpoisoned pellet against the concentration in the center of the catalyst pellet, different regions can be realized which correspond to the different poisoning mechanisms. From a comparison with experimental data, conclusions regarding the working poisoning mechanism can be drawn.

The analytical solution of a first-order concentration-independent catalyst deactivation in a plug-flow reactor was derived by Krishnaswamy and Kittrell for the case of internal diffusion limitation (ref. 167). The solution obtained is an analogy of the Levenspiel plots (ref. 153) suggested for the kinetically controlled regime:

$$\ln \ln \frac{1}{1 - x} = \ln(A_0 \tau) - \frac{E}{RT} \qquad (3.232)$$

where x is the conversion of the reactant, A_0 is the pre-exponential factor, τ the space time. The slope of this "Arrhenius plot" gives the activation energy. With diffusion control, the second term of the equation will be $E/2RT$. Similarly, in the case of deactivating catalyst,

$$\ln \ln \frac{1}{1 - x} = \ln(k_p \tau) - k_{dp} t \qquad (3.233)$$

where k_p is the apparent reaction rate coefficient, k_{dp} the pseudo-deactivation rate constant, and t is the process time. Table 3.12 reveals that the behavior of k_{dp} is - according to formal

TABLE 3.12

Analogous characteristics of diffusion for deactivating and nondeactivating systems. After (refs. 167,168). Reproduced by permission of American Institute of Chemical Engineering.

Condition	Kinetic analysis	Deactivation analysis
Slope without diffusion	E	k_d
Slope with severe internal diffusion[a]	E/2	$k_d/2$
Slope with severe external diffusion[b]	$\rightarrow 0$	$\rightarrow 0$
Dependence on particle size	Reciprocal	Reciprocal

[a] In the case: $h \exp(-k_d t/2) \geq 5.0$, where h is the Thiele-modulus, k_d the deactivation rate constant, t the process time.

[b] In the case: Da $y >> 1.0$, where Da is the Damköhler number, $k/K_m a_s$, k being the reaction rate constant, K_m the mass transfer coefficient and a_s the external specific surface area of the particle; y is the fractional catalyst activity.

mathemathics - analogous to that of the energy of activation E_a in kinetic analysis in the case of internal diffusion limitation. Similarly, both values approach zero with severe external diffusion limitation (ref. 168). The limiting cases for kinetic and internal diffusion Levenspiel plots are also analogous, as shown in Table 3.13, in terms of pseudo-rate constants and effectiveness factors

TABLE 3.13
Catalyst deactivation in a plug flow reactor. After (refs. 167,169). Reproduced by permission of American Institute of Chemical Engineering.

Modulus	Effectiveness factor, η	
	Kinetic	Deactivation
h = 0	$\eta = 1$	$\eta_d = 1$
$h \exp(-k_d t/2) > 5$	$\eta = 1/h$	$\eta_d = 1/2$
$h \exp(-k_d t/2) > 1$	$\eta = \frac{1}{h} - \frac{1}{3h^2}$	$\eta_d = \frac{1}{2} + \frac{1}{6h \exp(-k_d t/2}$

$\ln \ln \frac{1}{1-x} = \ln k_p \tau - k_{dp} t$ (Eq. 3.233) where k is the pseudo-reaction rate constant = $k\eta$; k_{dp} the pseudo-deactivation rate constant, $k_d \eta_d$; η and η_d being the effectiveness factors, k and k_d the true rate constants for the reaction and deactivation, respectively. For denotions, see also Table 3.12.

(refs. 167,169). The internal diffusion limitation case was also theoretically extended for the n-th order of reaction and to other types of reactors, too (ref. 167). It was experimentally verified for the concentration-independent derivation of the catalyst deactivation of hydrogen peroxide decomposition on a fixed-bed catalysis column, already discussed in Section 3.4.2.

Wheeler (ref. 166) discussed different modes of deposition of poisons on the internal catalyst surface. If a parallel self-poisoning mechanism applies, with an effectiveness factor of 1, the poison is uniformly distributed throughout the pellet: whereas with an effectiveness factor <1 the poison is mainly deposited in the superficial regions of the catalyst pellets and this phenomenon is termed pore-mouth or shell poisoning. If a series of self-poisoning mechanisms applies with an effectiveness factor <1, initially the poison is mainly deposited in the interior of the catalyst which is termed core-poisoning and, if an impurity self-poisoning mechanism applies according to the rate of the poison deposition, uniform or pore mouth poisoning is expected. The deactivation curves of MCH dehydrogenation over Pt/Al_2O_3 presented in (ref. 134) correspond well to the uniform poisoning case (Figure 3.23). The time scale of the figure is very nonlinear. The value of <a> = 0.77 is achieved within 20 minutes while some 30 hours are required to obtain the rest of the curve.

Pore-mouth poisoning means that the poison is deposited predominantly at the outer ends of pores. The outer parts of the pores will be deactivated and a thin band of deactivation reaction zone moves forward separating the outer deactivated zone from the still active inner zone (ref. 170). This can eventually lead to pore plugging, *i.e.* to the complete blocking of the pore by the deactivating layer.

In a porous catalyst where the pores can be represented by a bundle of parallel cylinders, foulant deposition and penetration of the foulant precursor deep into the pore compete. A dimensionless fouling time t/τ_F can be defined, the value of which is unity when the thickness of the deposit at the pore mouth is equal to the pore diameter. According to the variation of the x_0 penetration depth as a function of this fouling time, five basic cases can be distinguished, as shown in Fig. 3.24 (ref. 171). The predominant poisoning mechanism will enormously affect the overall kinetics observed. For example, in a simple consecutive reaction $A \longrightarrow B \longrightarrow C$ the
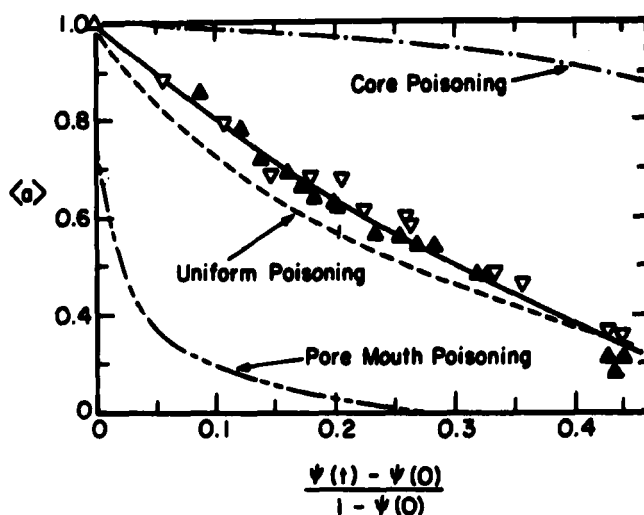
Fig. 3.23. Diagnostic deactivation curves for MCH dehydrogenation over a Pt/Al$_2$O$_3$ catalyst at 352°C, p(MCH) = 23 Torr, p(H$_2$) = 405 Torr. Data for two different pellets are shown, each having a nominal thickness of 0.1 cm and a catalyst effectiveness factor of 0.21. <a> = R/R$_0$ where R is the actual reaction rate, R$_0$ the initial reaction rate; Ψ(0) and Ψ(t) is the ratio of the center-plane reactant concentration to the bulk reactant concentration at time zero and t, respectively. Reproduced with permission from (ref. 134).

"pore yield" of intermediate B (the ratio of its production from the pore to the rate of consumption of A in the pore) increases monotonically with advancing deactivation in the poisoning case but it may decrease initially due to a yield loss caused by pore mouth restriction. When the pore mouth plugs, the yields of B increase abruptly and thereafter the whole reaction stops. With extreme mouth plugging, a subsequent increase in the yield of B cannot be observed. The theory was tested using the example of cumene cracking on a commercial FCC catalyst; here benzene represents the useful intermediate B. As Figure 3.25 illustrates, both cumene consumption and benzene yield *vs*. fouling time confirm the validity of Model IV, of Figure 3.24.

Various models have been presented to account for deactivation in porous systems. Following the initial treatments of Beeckman and Froment (refs. 156,157), where deactivation by coking with no diffusion limitation has been discussed, these same authors provided theoretical equations where the restriction of no diffusional limitation has been dropped (ref. 172). Single pores, when deacti-
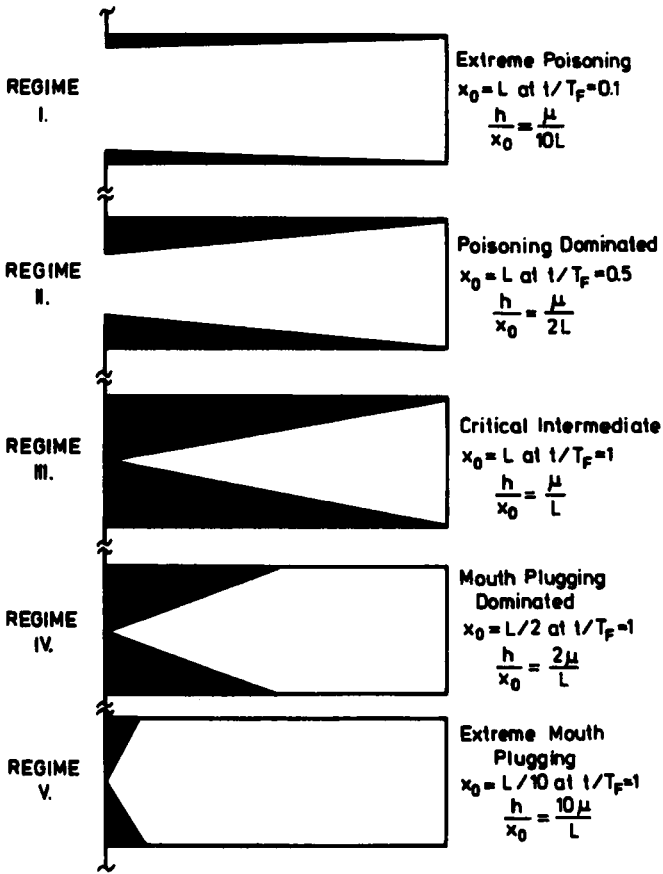
Fig. 3.24. Deposition of foulant by wedge-layering; five illustrative archetypes. Symbols: x_0 - penetration depths of foulant deposit in a pore; L = pore length; t = time-on-stream; τ_F - time-on-stream required to plug a pore of mean radius μ; h - mouth thickness of foulant deposit. Reproduced by permission from (ref. 171). Copyright 1985, Pergamon Journals Ltd.

vation occurs by site coverage and/or pore blockage, have been covered; also a pore network system was considered where deactivation was caused by site coverage only. A more recent study by the same group (ref. 158) also covered pore blockage for a network of pores. Here small pores blocked immediately after coverage, pores too large to be blocked and intermediate ones, which can be blocked given sufficient time, have been distinguished and separate deactivation functions derived for each class. An interesting feature of the derivation in (ref. 172) is a theoretical tortuosity factor equal to 4 (as opposed to previous values between 2 and 3.3). This is
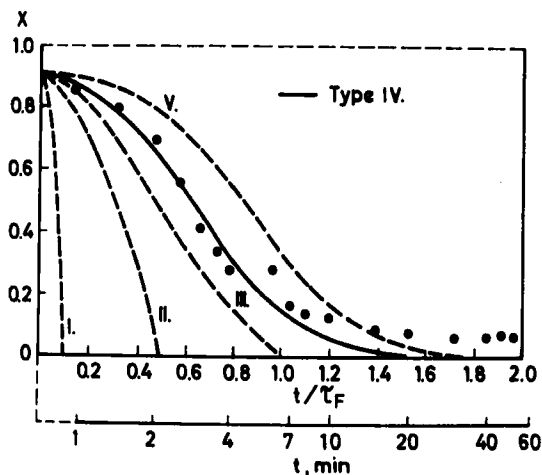
Fig. 3.25. Conversion of cumene cracking (X) as a function of dimensionless fouling time, t/τ_F over a commercial cracking catalyst (supported zeolite, L = 0.75 mm, μ = 7 $\pm$ 3 nm, specific surface: 70 m^2 g^{-1}). Comparison of theory and experiment: Roman numbers denote the various models shown in Figure 3.24. Reproduced by permission from (ref. 171). Copyright 1985 Pergamon Journals Ltd.

closer to the experimental values reported by several other authors being between 3 and 7.

Lee (ref. 173) proposed an approximate approach to the design of fixed-bed reactors, applicable in the case of diffusion limitation. This uses a factor called point effectiveness which is the ratio of the observed reaction rate to the intrinsic reaction rate under bulk conditions for fresh catalyst. A subsequent analysis of Lee and Butt (refs. 170,174) couples this factor with catalyst pellet effectiveness, ε_p, being

$$\varepsilon_p = \frac{\text{observed rate}}{\text{intrinsic rate at pellet surface conditions}} . \qquad (3.234)$$

The activity factor, F is

$$F = \frac{\text{rate of reaction for deactivated pellet}}{\text{rate of reaction for fresh pellet}} . \qquad (3.235)$$

These two quantities are coupled by the n_f effectiveness factor for the fresh pellet in terms of surface conditions:

$$\varepsilon_p = n_f \, F. \qquad (3.236)$$

The expressions for the fraction of catalyst deactivated (under pseudo-steady-state conditions, *i.e.* when the rate of poisoning is

much slower than the rate at which the concentration reaches the steady-state within the pellet) have been derived for uniform and pore-mouth poisoning, considering parallel (eq. (3.198)) and series (eq. (3.199)) poisoning mechanisms. The pellet effectiveness factors can then be calculated. Their comparison with two selected results of thiophene poisoning of benzene hydrogenation gave rather good agreement between theory and experiment. The combination of pellet effectiveness and reactor point effectiveness results in equations which can be used in practical reactor design, in terms of the principles of commercial reactor operation (ref. 147). The equations proposed offer exact quantification of intuitively expected facts (*e.g.*, that increasing reactor volume increases tolerance to the effect of deactivation, since the same amount of poison is distributed in a larger volume) and also of some facts which cannot be so easily grasped intuitively. For example, in the case of uniform deactivation and fixed residence time, the gas temperature - observed in an exothermic reaction - decreases monotonically with time, the catalyst temperature, however, shows a small minimum followed by a very marked maximum. The authors warn about incorrect conclusions based solely on the behavior at time zero and/or for fresh catalyst. This is due to the fact that the deactivating species can be consumed before reaching the reactor outlet and to the increasing reaction rate, as a consequence.

Another "trick" of diffusion may be the separation of individual reaction partners due to their diverse relative diffusivities. Hydrogen depletion inside a catalyst pellet may cause enhanced coking (ref. 175). Also, in steam reforming of methane, coking due to CO disproportionation, methane decomposition or reverse water gas reaction can occur within the pellet due to the diffusional separation of reaction partners under conditions when compositions at the pellet surface would not allow such reactions thermodynamically (ref. 172). Modeling fixed-bed reactors, equations considering deactivation [like eq. (3.213) - (3.216) or similar ones proposed in the literature] can be used as entries into the different mathematical reactor models discussed in Section 3.2.2. Care should be taken that the initial conditions on which the derivation of these equations have been based should correspond to those of the system to be modeled. We are far from being able to give exact or close--to-exact solutions for the general cases and have to be satisfied with gradually improving the approximations both from the theoretical and the reactor design point of view.

REFERENCES

1 M.W. Roberts and C.S. McKee, Chemistry of Metal-Gas Interface, Clarendon Press, Oxford, 1978.
2 W.N. Delgass, G.L. Haller, R. Kellermann and J.J. Lunsford, Spectroscopy in Heterogeneous Catalysis, Academic Press, New York, 1979.
3 R.L. Park, in R.B. Anderson and P.T. Dawson (Editors), "Introduction to surface spectroscopies" Experimental Methods in Catalytic Research, Vol. 3, Academic Press, New York, 1976, p. 1.
4 H.D. Hagstrum, J.E. Rowe and J.C. Tracy, in R.B. Anderson and P.T. Dawson (Editors), "Electron spectroscopy of solid surfaces" Experimental Methods in Catalytic Research, Vol. 3, Academic Press, New York, 1976, p. 42.
5 F.C. Tompkins, Chemisorption of Gases on Metals, Academic Press, New York, 1978.
6 G. Ertl, in J.R. Anderson and M. Boudart (Editors), "Kinetics of chemical processes on well-defined surfaces" Catalysis Science and Technology, Vol. 4, Springer, Berlin, 1983, p. 209.
7 H.-P. Boehm and H. Knözinger, in J.R. Anderson and M. Boudart (Editors), Catalysis Science and Technology, Vol. 4, Springer, Berlin, 1983, p. 39.
8 J.B. Peri, in J.R. Anderson and M. Boudart (Editors), Catalysis Science and Technology, Vol. 5, Springer, Berlin, 1984, p. 171.
9 S.H. Moon, H. Windawi and J.R. Katzer, Ind. Eng. Chem. Fundam., 20 (1981) 396.
10 T. Bánsági, J. Raskó and F. Solymosi, in G.M. Pajonk et al. (Editors), Spillover of Adsorbed Species, Stud. Surf. Sci. Catal. Vol. 17, Elsevier, Amsterdam, 1983, p. 109.
11 W.R. Moser, J.E. Cnossen, A.W. Wang and S.A. Krouse, J. Catal., 95 (1985) 21.
12 M. Nagai, L.L. Lucietto, Yao-En Li and R.D. Gonzalez, J. Catal., 101 (1986) 522.
13 F. Solymosi, A. Erdőhelyi and T. Bánsági, J. Catal., 68 (1981) 371.
14 F. Solymosi, A. Erdőhelyi and M. Kocsis, J. Chem. Soc. Faraday Trans. I, 77 (1981) 1003.
15 A. Erdőhelyi, M. Pásztor and F. Solymosi, J. Catal., 98 (1986) 166.
16 J. Raskó, L. Völgyesi, M. Lancz and F. Solymosi, Proc. 8th Internat. Congr. Catal. Berlin (West), 1984, Vol. 3, p. 671.
17 J.T. Kiss and R.D. Gonzalez, Proc. 8th Internat. Congr. Catal. Berlin (West), 1984, Vol. 2, p. 635.
18 J.L. Falconer and J.A. Schwarz, Catal. Rev.-Sci. Eng., 25 (1983) 141.
19 S. Tsuchiya, Y. Amenomiya and R.J. Cvetanovic, J. Catal., 19 (1970) 245.
20 V.V. Rozanov, J. Gland and A.V. Sklyarov, Kinet. Katal., 20 (1979) 1249.
21 H. Zimmer, V.V. Rozanov, A.V. Sklyarov and Z. Paál, Appl. Catal., 2 (1982) 51.
22 V.V. Rozanov and A.V. Sklyarov, Kinet. Katal., 19 (1978) 1533.
23 M.U. Kislyuk, A.V. Sklyarov and T.M. Dangyan, Izv. Akad. Nauk, SSSR, Ser. Khim., (1975) 2161; A.V. Sklyarov, V.V. Rozanov and M.U. Kislyuk, Kinet. Katal., 19 (1978) 416.
24 S.M. Gates, J.N. Russell, Jr. and J.T. Yates, Jr., Surface Sci., 159 (1985) 233.
25 G.A. Olah, Angew. Chem., 85 (1973) 183.
26 K.H. Röbschläger and E.G. Christoffel, Ind. Eng. Chem., Prod. Res. Dev., 18 (1979) 347.
27 J.R. Anderson, Adv. Catal., 23 (1973) 1.

180

28 R.L. Smith, P.A. Naro and J.A. Silvestri, J. Catal., 20 (1971) 359.
29 F.G. Gault, Adv. Catal., 30 (1981) 1.
30 S.G. Brandenberger, W.C. Callender and W.K. Meerbott, J. Catal., 42 (1976) 282.
31 B.B. Donnis, Ind. Eng. Chem. Prod. Res. Dev., 15 (1976) 254.
32 E.G. Christoffel and K.H. Röbschläger, Ind. Eng. Chem. Prod. Res. Dev., 17 (1978) 331.
33 M.C. Poutsma, ACS Monogr., No. 171 (1976) 496.
34 É. Miklósy, J. Papp and D. Kalló, Zeolites, 3 (1983) 139.
35 D.S. Santilli, J. Catal., 99 (1986) 327.
36 P.M. Pitts, J.E. Connor and L.N. Leun, Ind. Eng. Chem., 47 (1955) 770.
37 H. Pines, The Chemistry of Catalytic Hydrocarbon Conversions, Academic Press, New York, 1981.
38 N.S. Gnep and M. Guisnet, Bull. Soc. Chim. Fr. 5-6 (1977) 429.
39 G.A. Mills, H. Heinemann, T.H. Milliken and A.G. Oblad, Ind. Eng. Chem., 45 (1953) 134.
40 P.B. Weisz and E.W. Swegler, Science, 126 (1957) 31.
41 J.M. Parera, J.N. Beltramini, C.A. Querini, E.E. Martinelli, E.J. Churin, P.E. Aloe and N.S. Figoli, J. Catal., 99 (1986) 39.
42 E.G. Christoffel, Cat. Rev.-Sci. Eng., 24 (1982) 159.
43 I. Surjo and E.G. Christoffel, Chem. Ing. Tech., 50 (1978) 882.
44 E.G. Christoffel and Z. Paál, J. Catal., 73 (1982) 30.
45 A. Sárkány, H. Lieske, T. Szilágyi and L. Tóth, Proc. 8th Internat. Congr. Catal., Berlin (West), 1984, Vol. 2, p. 613.
46 S. Siegel, J. Catal., 30 (1973) 139.
47 S. Siegel, J. Outlaw and N. Garti, J. Catal., 52 (1978) 102.
48 A. Frennet, G. Lienard, A. Crucq and L. Degols, J. Catal., 53 (1978) 150.
49 Z. Paál, Adv. Catal., 29 (1980) 273.
50 V. Ponec and W.M.H. Sachtler, Proc. 5th Internat. Congr. Catal. Palm Beach, 1972, Vol. 1, Elsevier, Amsterdam, 1973, p. 645.
51 W.M.H. Sachtler and R.A. Van Santen, Adv. Catal., 26 (1977) 69.
52 V. Ponec, Adv. Catal., 32 (1983) 149.
53 H.C. de Jongste and V. Ponec, Bull. Soc. Chim. Belg., 88 (1979) 453.
54 K.H. Yang and O.A. Hougen, Chem. Eng. Progr., 46 (1950) 146.
55 F.J. Dumez and G.F. Froment, Ind. Eng. Chem. Fundam., 15 (1976) 291.
56 G.F. Froment and K.B. Bischoff, Chemical Reactor Analysis and Design, Wiley, New York, 1979.
57 F.J. Dumez, L.H. Hosten and G.F. Froment, Ind. Eng. Chem. Fundam., 16 (1977) 298.
58 M. Boudart, AIChE J., 18 (1972) 465.
59 M. Boudart, AIChE J., 2 (1956) 62.
60 F. Horn and R. Jackson, Arch. Rat. Mech. Anal., 47 (1972) 81.
61 J. Happel and P.H. Sellers, Adv. Catal., 32 (1983) 273.
62 A. Ozaki, Isotopic Studies of Heterogeneous Catalysis. Kodansha -Acad. Press, Tokyo - New York, 1977.
63 M. Feinberg and F.J.M. Horn, Chem. Eng. Sci., 29 (1974) 775; M. Feinberg, in C. Casley, W.H. Ray and W. Stewart (Editors), Dynamics and Modelling of Reacting Systems, Academic Press, 1980.
64 M. Feinberg, in L. Lapidus and N. Amundson (Editors), "Mathematical aspects of mass action kinetics" Chemical Reactor Theory: A Review, Prentice Hall, Englewood Cliffs, 1970, pp. 1-74.
65 J.J. Carberry, Chemical and Catalytic Reaction Engineering, McGraw Hill, New York, 1976.
66 J. Horiuti, Adv. Catal., 9 (1957) 339.

67 K. Tamaru, Dynamic Heterogeneous Catalysis, Academic Press, London 1978.

68 J. Wei and J.C.W. Kuo, Ind. Eng. Chem. Fundam., 8 (1969) 114.

69 J. Wei and J.C.W. Kuo, Ind. Eng. Chem. Fundam., 8 (1969) 124.

70 W.R. Paterson and J.J. Carberry, Chem. Eng. Sci., 38 (1983) 175.

71 S. Sundaresan, N.R. Amundson and R. Aris, AIChE J., 26 (1980) 529.

72 A.M. Kugelmann and J.C. Bonacci, J. Catal., 39 (1975) 10.

73 M.P. Ramage, K.R. Graziani and F.J. Krambeck, Chem. Eng. Sci., 35 (1980) 41.

74 R. Zurmühl, Matrizen, Springer, Berlin, 1964, p. 170.

75 J. Wei and C.D. Prater, Adv. Catal., 13 (1962) 137.

76 G.R. Gavalas, AIChE J., 19 (1973) 214.

77 R.K. Herz and L.L. Hegedus, Chem. Eng. Sci., 33 (1978) 1561.

78 L.L. Hegedus and E.E. Petersen, Catal. Rev.-Sci. Eng., 9 (1974) 245.

79 A.N. Namjoahi, B.D. Kulkarni and L.K. Doraiswamy, AIChE J., 30 (1984) 915.

80 R. Zurmühl, Matrizen, Springer, Berlin, 1964, p. 137.

81 D.J. Collins, R.J. Medina and B.H. Davis, Can. J. Chem. Eng., 61 (1983) 29.

82 D.J. Collins, K.J. Mulrooney, R.J. Medina and B.H. Davis, J. Catal., 75 (1982) 291.

83 A.J. Silvestri and C.D. Prater, J. Phys. Chem., 68 (1964) 3268.

84 D. Seddon, J. Catal., 98 (1986) 1.

85 M.S. Spencer, J. Catal., 67 (1981) 259.

86 I. Surjo and D.G. Christoffel, J. Catal., 60 (1979) 133.

87 C.A. Prater, A.J. Silvestri and J. Wei, Chem. Eng. Sci., 22 (1967) 1587.

88 A.J. Silvestri, C.D. Prater and J. Wei, Chem. Eng. Sci., 25 (1970) 407.

89 E.G. Christoffel, Ind. Eng. Chem. Prod. Res. Dev., 18 (1979) 143.

90 E.G. Christoffel, Ind. Eng. Chem. Prod. Res. Dev., 19 (1980) 430.

91 G. Li, Chem. Eng. Sci., 40 (1985) 939.

92 J.R. Kittrell, Adv. Chem. Engineering, 8 (1970) 97.

93 Y. Bard, Nonlinear Parameter Estimation, Academic Press, New York, 1974.

94 D.M. Himmelblau, Process Analysis by Statistical Methods, Wiley, New York, 1970.

95 G.F. Froment and C.H. Hosten, in J.R. Anderson and M. Boudart (Editors) Catalysis Science and Technology, Vol. 2, Springer, Berlin, 1981, p. 97.

96 D.A. Ratkowsky, Chem. Eng. Sci., 40 (1985) 1623.

97 D.D. Do and H.D. Do, Chem. Eng. Sci., 40 (1985) 977.

98 J. Cronin, Differential Equations, Marcel Dekker, New York, 1980, p. 128.

99 C.R. Wylie, Differential Equations, McGraw-Hill, New York, 1979, p. 518.

100 A. Lotka, J. Am. Chem. Soc., 42 (1920) 1595.

101 R.J. Field and R.M. Noyes, J. Chem. Phys., 60 (1974) 188.

102 I. Prigogine, Angew. Chem., 90 (1978) 704.

103 R.E. Cunningham and F.J.J. Williams, Diffusion in Gases and Porous Media, Plenum Press, New York, 1980.

104 J.O. Hirschfelder, C.F. Curtiss and R.B. Bird, Molecular Theory of Gases and Liquids, Wiley, New York, 1954.

105 E.L. Cussler, Multicomponent Diffusion, Elsevier, Amsterdam, 1976.

106 A. Wheeler, Adv. Catal., 3 (1951) 250.
107 M.F.C. Johnson and W.E. Stewart, J. Catal., 4 (1965) 248.
108 N. Wakao and J.M. Smith, Chem. Eng. Sci., 17 (1962) 825.
109 N. Wakao and J.M. Smith, Ind. Eng. Chem. Fundam., 3 (1964) 123.
110 M.R. Rao, N. Wakao and J.M. Smith, Ind. Eng. Chem. Fundam.,
     3 (1964) 127.
111 J.M. Smith, Chemical Engineering Kinetics, McGraw-Hill, Lon-
     don, 1981, p. 334.
112 F. Delannay (Editor), Characterization of Heterogeneous Cata-
     lysts, Marcel Dekker, New York, 1984.
113 M. Kotter, P. Lovera and L. Riekert, Ber. Bunsenges. physik.
     Chem., 80 (1976) 61.
114 E.G. Christoffel, L. Tran-Vinh and M. Baerns, Chem.-Ztg.,
     107 (1983) 349.
115 R. Aris, Ind. Eng. Chem. Fundam., 22 (1983) 150.
116 E.A. Mason and A.P. Malinauskas, Gas Transport in Porous Media:
     the Dusty-Gas Model, Elsevier, Amsterdam, 1983.
117 R. Jackson, Transport in Porous Catalysts, Elsevier, Amsterdam,
     1977.
118 J. Skrzypek, M. Grzesik and R. Szopa, Chem. Eng. Sci., 39
     (1984) 515.
119 J. Skrzypek, M. Grzesik and R. Szopa, Chem. Eng. Sci., 40
     (1985) 671.
120 P.G. Menon, G.B. Marin and G.F. Froment, Ind. Eng. Chem. Prod.
     Res. Dev., 21 (1982) 52.
121 G. Lietz, J. Völter, M. Dobrovolszky and Z. Paál, Appl. Catal.,
     13 (1984) 77.
122 J.B. Butt, Adv. Chem. Ser., 108 (1972) 259.
123 J.B. Butt and R.M. Bilimoria, ACS Symp. Ser., 72 (1978) 288.
124 M.J. Oudar, Cat. Rev.-Sci. Eng., 22 (1980) 171.
125 L.L. Hegedus and R.W. McCabe, Catal. Rev.-Sci. Eng., 23 (1981)
     377.
126 J.B. Butt, in J.R. Anderson and M. Boudart (Editors), Cata-
     lysis Science and Technology, Vol. 6, Springer, Berlin, 1984,
     p. 1.
127 J. Oudar and H. Wise (Editors), Deactivation and Poisoning of
     Catalysts, Marcel Dekker, New York, 1985; E.E. Petersen and
     A.T. Bell (Editors), Catalyst Deactivation, Marcel Dekker,
     New York, 1987.
128 B. Delmon and G.F. Froment (Editors), Catalyst Deactivation,
     Stud. Surf. Sci. Catal., Vol. 6, Elsevier, Amsterdam, 1980;
     B. Delmon and G.F. Froment (Editors), Catalyst Deactivation,
     Stud. Surf. Sci. Catal., Vol. 34, Elsevier, Amsterdam, 1987.
129 G.F. Froment, in B. Delmon and G.F. Froment (Editors),
     Catalyst Deactivation, Stud. Surf. Sci. Catal., Vol. 6,
     Elsevier, Amsterdam, 1980, p. 1.
130 L.D. Schmidt and D. Luss, J. Catal., 22 (1971) 269.
131 A.K. Galwey, P. Gray, J.F. Griffiths and S.M. Hasko, Nature,
     313 (1985) 668.
132 G.A. Somorjai, J. Catal., 27 (1972) 453.
133 I. Manninger, J. Catal., 89 (1984) 164.
134 L.W. Jossens and E.E. Petersen, J. Catal., 73 (1982) 377.
135 R.J. Koestner, M.A. Van Hove and G.A. Somorjai, J. Phys. Chem.,
     87 (1983) 203.
136 S.M. Davis and G.A. Somorjai, J. Catal., 65 (1980) 78.
137 Z. Paál, M. Dobrovolszky and P. Tétényi, J. Catal., 46 (1977)
     65.
138 P. Biloen, J.N. Helle, H. Verbeek, F.M. Dautzenberg and W.M.H.
     Sachtler, J. Catal., 63 (1980) 112.
139 P.G. Menon and G.F. Froment, J. Catal., 59 (1979) 138.
140 M.A. Pacheco and E.E. Petersen, J. Catal., 96 (1985) 499; 96
     (1985) 507.

141　V.K. Shum, J.B. Butt and W.M.H. Sachtler, J. Catal., 96 (1985) 371; 99 (1986) 126.

142　T.E. Fischer and S.R. Kelemen, J. Catal., 53 (1978) 24.

143　S.T. Sie, in B. Delmon and G.F. Froment (Editors), Catalyst Deactivation, Stud. Surf. Sci. Catal., Vol. 6, Elsevier, Amsterdam, 1980, p. 545.

144　B.-J. Ahn and J.M. Smith, AIChE J., 30 (1984) 739.

145　A. Brito-Alayon, R. Hughes and E.K.T. Kann, Chem. Eng. Sci., 36 (1981) 445.

146　P. J. Denny and M.V. Twigg, in B. Delmon and G.F. Froment (Editors), Catalyst Deactivation, Stud. Surf. Sci. Catal., Vol. 6, Elsevier, Amsterdam, 1980, p. 577.

147　F.S. Kovarik and J.B. Butt, Catal. Rev.-Sci. Eng., 24 (1982) 441.

148　H.H. Lee and J.B. Butt, AIChE J., 31 (1985) 302.

149　S. Szépe and O. Levenspiel, Proc. IV. Europ. Symp. Chem. React. Eng., Brussels, 1968, Pergamon Press, Oxford, 1971, p. 265.

150　S. Krishnaswamy and J.R. Kittrell, Ind. Eng. Chem. Proc. Des. Dev., 17 (1978) 200.

151　A. Löwe, Chem. Ing. Tech., 52 (1980) 777.

152　A. Löwe, Ind. Eng. Chem. Fundam., 19 (1980) 160.

153　O. Levenspiel, Chemical Reaction Engineering, Wiley, New York, 1972, p. 541.

154　J. Corella, J.M. Asúa and J. Bilbao, Can. J. Chem. Eng., 59 (1981) 647.

155　G.B. Marin and G.F. Froment, Chem. Eng. Sci., 37 (1982) 759.

156　J.W. Beeckman and G.F. Froment, Ind. Eng. Chem. Fundam., 18 (1979) 245.

157　J.W. Beeckman and G.F. Froment, Chem. Eng. Sci., 35 (1980) 805.

158　G.B. Marin, J.W. Beeckman and G.F. Froment, J. Catal., 97 (1986) 416.

159　M.A. Pacheco and E.E. Petersen, J. Catal., 86 (1984) 75.

160　M.A. Pacheco and E.E. Petersen, J. Catal., 88 (1984) 400.

161　M.A. Pacheco and E.E. Petersen, J. Catal., 98 (1986) 380.

162　J.W. Beeckman, In-Sik Nam and G.F. Froment, in B. Delmon and G.F. Froment (Editors), Catalyst Deactivation, Elsevier, Amsterdam, 1987, p. 365.

163　J. Corella and J.M. Asúa, Ind. Eng. Chem. Proc. Des. Dev., 21 (1982) 55.

164　R.P.L. Absil, J.B. Butt and J.B. Dranoff, J. Catal., 85 (1984) 415.

165　J. Corella, A. Monzón, J.B. Butt and R.P.L. Absil, J. Catal., 100 (1986) 149.

166　A. Wheeler, Adv. Catal., 3 (1951) 249; A. Wheeler, in P.H. Emmett (Editor), Catalysis, Vol. 2, Reinhold, New York, 1955, p. 105.

167　S. Krishnaswamy and J.R. Kittrell, AIChE J., 27 (1981) 120.

168　S. Krishnaswamy and J.R. Kittrell, AIChE J., 27 (1981) 125.

169　S. Krishnaswamy and J.R. Kittrell, AIChE J., 28 (1982) 273.

170　H.H. Lee and J.B. Butt, AIChE J., 28 (1982) 405.

171　R.F. Mann, F.Y.A. El-Kady and R. Marzin, Chem. Eng. Sci., 40 (1985) 249.

172　J.W. Beeckman and G.F. Froment, Ind. Eng. Chem. Fundam., 21 (1982) 243.

173　H.H. Lee, AIChE J., 27 (1981) 558.

174　H.H. Lee and J.B. Butt, AIChE J., 28 (1982) 410.

175　A. Ovenston and J.R. Walls, Chem. Eng. Sci., 37 (1982) 1.

This Page Intentionally Left Blank

Chapter 4

LABORATORY REACTORS

   For the improvement of existing or the introduction of new
heterogeneous catalytic processes, studies are usually carried out
on different scales, with laboratory reactors, pilot plants and
industrial plants. The tasks of laboratory investigations include
catalyst preparation, catalyst screening, scale-up from laboratory
equipment to pilot and industrial plants and process simulation
and optimization, as delineated previously in Scheme 2.1, for which
reliable kinetic data must be provided. These are usually obtained
with laboratory reactors which mostly represent small-scale models
of large-scale industrial reactors. Frequently applied laboratory
reactors are micropulse, fixed-bed, recycle and single-pellet
diffusion reactors. All of these reactors belong to the class
of flow reactors in which mass and energy are exchanged with the
environment of the reaction system.
   For performing the individual steps of kinetic analysis (Scheme
2.2) within the frame set up so far, however, the reactor types
mentioned show different suitabilities. The microcatalytic pulse
method has special advantages for the investigation of reaction
mechanisms and can be used for the kinetic analysis of complex
networks of first-order reactions. Gas chromatographic pulse reac-
tors, single-pellet diffusion reactors and differentially operated
fixed-bed reactors are well suited for supplying data that are
needed for deriving dynamic models. Depending on the problems
connected with the activity and selectivity behaviour of catalysts
in different reactor configurations under different operating con-
ditions and different running-in conditions, the parameters in the
model equations should be determined on the basis of data from
laboratory reactors that are scaled-down constructions of large-
-scale reactors.
   Laboratory reactors may be classified on the basis of different
aspects such as exchange or no exchange of mass and energy with the
environment of the reaction system, mode of residence time distri-
bution of volume elements of the fluid in the reaction system or
stationary or non-stationary operation.
   In the following sections, the operating principles of and measu-
rement procedures with the different laboratory reactors are pre-

sented. Finally, a brief discussion is given of transient operation, which is becoming a powerful method for clearing up kinetic problems in laboratory reactors.

4.1 MICROPULSE REACTORS

Pulse methods have found wide applications in qualitative and quantitative investigations of heterogeneous catalytic reactions (refs. 1-6). The underlying principle of micropulse reactors is the injection of a reactant pulse into a continuous flow of a carrier gas, which is then passed through a catalytic column. Two basic types of micropulse reactors may be distinguished, the microcatalytic pulse reactor and the gas chromatographic reactor, although all the literature data on micropulse reactors does not necessarily assigned to these two types. A microcatalytic pulse reactor system /Fig. 4.1 (ref. 7)/ consists of two columns, a catalytic column and a separation column. The pulse is usually large compared with the length of the catalytic column, which means that variation of the flow-rate of the carrier gas has a minor influence on the conversion in the catalytic column, and chromatographic effects during the passage of the reactant pulse are small. The quantity measured with microcatalytic pulse reactors is the conversion of reactants. In the gas chromatographic reaction system /Fig. 4.2 (ref. 7)/, the catalytic and separation columns are combined into one column, and the pulse is small compared with the length of the column, and therefore pronounced chromatographic effects occur. Information about individual rates of physical and chemical processes within the column is obtained from the shape of the elution peak which leaves the catalytic gas chromatographic column.
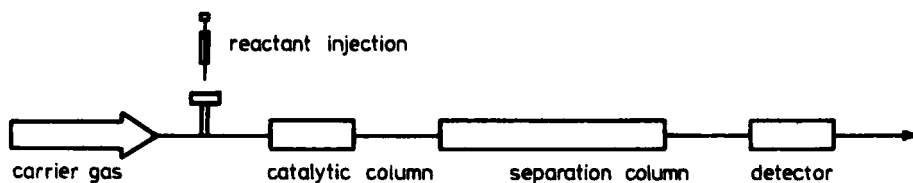
Fig. 4.1. Microcatalytic pulse method. Reproduced with permission from (ref. 7), p. 175, by courtesy of Marcel Dekker, Inc.
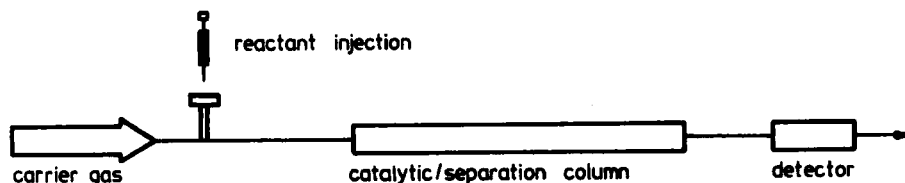
Fig. 4.2. Gas chromatographic pulse method. Reproduced with permission from (ref. 7), p. 176, by courtesy of Marcel Dekker, Inc.

4.1.1 Microcatalytic pulse method

Microcatalytic pulse techniques were introduced by Emmett and co-workers (refs. 8-10). The main applications of this technique are rapid screening of catalyst activity and selectivity and the investigation of underlying reaction mechanisms, *i.e.*, within the framework set up for the kinetic analysis of complex reaction networks, the microcatalytic pulse method is well suited for the first step. Reaction mechanisms are usually investigated with microcatalytic pulse reactors by a non-kinetic method as described in Section 3.1.3, involving the comparison of product distributions obtained from the conversion of model compounds with product distributions expected from theoretically postulated mechanisms. If the model compounds do not deliver specific product distributions that permit a discrimination between rival theoretical mechanisms, labelling of the reactants with radioactive (ref. 11) or stable (ref. 12) isotopes is a useful method that is especially advantageous with the microcatalytic pulse technique because only small amounts of reactants are needed.

Another major benefit of the pulse technique is the interaction of reactants in the initial state of the catalyst surface, from which extensive information on initial selectivities and catalyst deactivation is available. The disadvantage of the microcatalytic pulse technique arises from the difficulty in deriving quantitative kinetic results. This is caused by the continuously changing partial pressures over the length of the catalytic column and by adsorption on the catalyst, as a result of which calculations of partial pressures and contact times of the reactants within the column become uncertain. In monomolecular reactions, however, the conversion is independent of the pulse shape and identical kinetic results are obtained with the pulse method and the stationary flow

method, as was first stressed by Bassett and Habgood (ref. 13).

Like catalytic flow reactors, microcatalytic pulse reactors can be mathematically modelled by making use of a number of simplifying assumptions or arrangements. Thus the reactant pulse which enters the catalytic column can be broadened in a dispersion column to such an extent that, during passage through the catalytic column, no further broadening of the entrance pulse occurs. The resulting set of differential equations may be solved analytically or numerically for different entrance pulse shapes by assuming power law or hyperbolic rate equations, and calculated conversions may be compared with measured conversions.

Until recently, only simply reversible or irreversible reactions had been quantitatively investigated, see, for example (refs. 14-17). The microcatalytic pulse technique may, however, be applied for the investigation of at least the selectivity behaviour of a catalyst for complex pseudomonomolecular reaction systems. This is demonstrated with two examples. In each instance the kinetics of simultaneous isomerization and cracking of the five hexane isomers on different Pt/Al_2O_3 catalysts is investigated, but different parameter determination procedures are used.

Example 4.1: Kinetic analysis of simultaneous isomerization and cracking of the five hexane isomers by use of the Wei-Prater method (ref. 18).

In Fig. 4.3. a flow diagram of the microcatalytic reaction system is presented. To achieve isothermal conditions, the microcatalytic reactor (I.D. 0.24 cm) is heated with a fluidized sand bed. In order to vary the contact time of the pulse in the catalytic bed by variation of the carrier gas velocity, the pulse width must be small compared with the length of the catalytic column. The length of the catalytic column cannot be chosen arbitrarily long, however, owing to chromatographic effects and pressure drops. A major difficulty in operating microcatalytic reactors is the restriction of the reaction conditions to the operating conditions of the gas chromatograph. Usually the two columns are decoupled through a cooling trap, which produces difficulties with quantitative sampling of the frozen products to the gas chromatograph. With the present reaction system this problem is circumvented by means of two regulating valves. The carrier gas velocity and the total pressure of the reaction system are adapted with the pressure drop over the first valve downstream of the microcatalytic pulse reactor. A constant carrier gas velocity through the gas
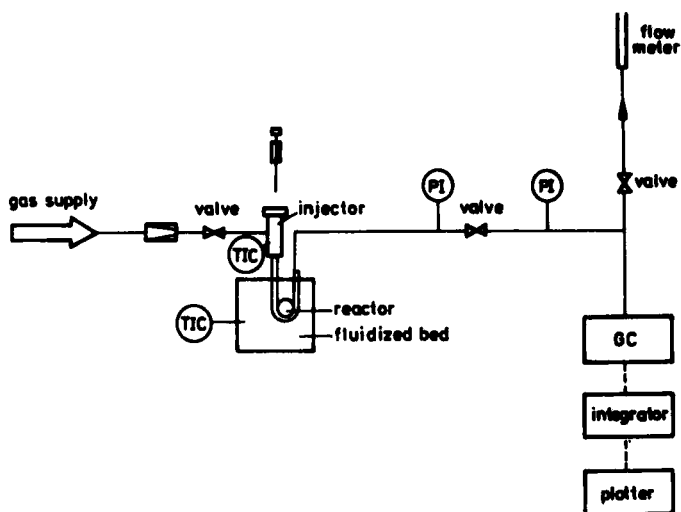
Fig. 4.3. Microcatalytic pulse reactor system for kinetic investigations of complex pseudo-mass action systems. Reproduced with permission from (ref. 18).

chromatograph is adjusted with the second valve, connected with a capillary splitter.

The reaction conditions were as follows: particle diameter, 0.1 - 0.3 mm; carrier gas, hydrogen; carrier gas velocity, 50 - 500 ml/min (STP); input pulses, 0.3 μl of reactant, 480 mg of catalyst (0.35 wt% Pt/Al$_2$O$_3$); total pressure, 1.05 MPa; and temperature, 400°C. The products were analyzed by gas chromatography with a squalane capillary column.

The effect of pulse size on 2,2-dimethylbutane conversion is shown in Fig. 4.4, which indicates that the reactions follow pseudomonomolecular kinetics within the range of applied reaction conditions. The Wei-Prater method can, therefore, be employed for kinetic analysis.

The determination of the selectivity behaviour of the catalyst can be accomplished without explicit consideration of the reaction time by means of the relative rate constants, which follow from a parametric representation of the curved reaction paths in terms of b_j. The diagonal matrix of the rate constants of the hypothetical system takes the following form:
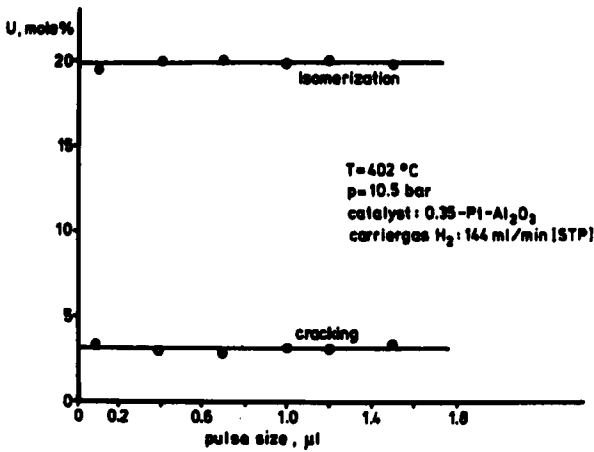
Fig. 4.4. Influence of pulse size on 2,2-dimethylbutane isomeriza-
tion and cracking conversion. Reproduced with permission from
(ref. 18).

$$
\Lambda' = \begin{bmatrix} 1 & \ldots & 0 \\ 0 & \dfrac{\lambda_2}{\lambda_1} & \\ \cdot & & \\ \cdot & & \\ \cdot & & \\ 0 & \ldots & \dfrac{\lambda_5}{\lambda_1} \end{bmatrix} \tag{4.1}
$$

The equilibrium composition vector a, which is needed for the
transformation of the rate constant matrix into an orthogonally
similar matrix, was calculated from free energy data to be

$$
a_{400^{\circ}C} = \begin{bmatrix} 0.211 \\ 0.3371 \\ 0.2639 \\ 0.0655 \\ 0.1226 \end{bmatrix} \begin{bmatrix} \text{n-hexane} \\ \text{2-methylpentane} \\ \text{3-methylpentane} \\ \text{2,3-dimethylbutane} \\ \text{2,2-dimethylbutane} \end{bmatrix} . \tag{4.2}
$$

According to the procedure given in the previous section, the ray
vector x_r,

$$
x_r = \begin{bmatrix} 0.1425 \\ 0.3196 \\ 0.606 \\ 0.1087 \\ 0.2234 \end{bmatrix} \tag{4.3}
$$

and the initial compositions α_{x_i} of the artificial straight-line
reaction paths,

$$a_{x_1}(0) = \begin{bmatrix} 0 \\ 0.2718 \\ 0.1256 \\ 0.1856 \\ 0.4169 \end{bmatrix} \quad a_{x_2}(0) = \begin{bmatrix} 0 \\ 0.4107 \\ 0.2954 \\ 0.1031 \\ 0.1908 \end{bmatrix} \quad a_{x_3}(0) = \begin{bmatrix} 0.1474 \\ 0 \\ 0.5023 \\ 0.0777 \\ 0.2725 \end{bmatrix} \quad (4.4)$$

are determined. A linear combination of these compositions and the ray vector using orthogonality relationships (and calculating the fifth eigenvector from orthogonality relationships also) yields the following eigenvector matrix X:

$$X = \begin{bmatrix} 0.1425 & 0.7337 & -18.7398 & 0.3289 & 1.9635 \\ 0.3195 & 0.5175 & 12.414 & -11.9176 & 22.8484 \\ 0.206 & 0.5399 & 12.0566 & 11.5603 & -8.828 \\ 0.1087 & -0.2108 & -0.6308 & -1.0778 & -41.2515 \\ 0.2234 & -0.5804 & -4.0999 & 2.1063 & 30.1946 \end{bmatrix} \quad (4.5)$$

The relative rate constant matrix Λ' for the characteristic system is obtained from a parametric depiction of the two curved reaction paths with initial compositions

$$\alpha^1(0) = \begin{bmatrix} 0 \\ 0.79 \\ 0.002 \\ 0.032 \\ 0.175 \end{bmatrix} \quad \text{and} \quad \alpha^2(0) = \begin{bmatrix} 0 \\ 0 \\ 0 \\ 0 \\ 1 \end{bmatrix} \quad (4.6)$$

on the reaction hyperplane of the reversible reaction system in terms of the characteristic directions:

$$\Lambda' = \begin{bmatrix} 1 & . & . & . & 0 \\ 0 & 2.1 & & & . \\ . & & 3.4 & & . \\ . & & & 6.4 & . \\ 0 & . & . & . & 10.8 \end{bmatrix} \quad (4.7)$$

The individual values of the rate constant matrix for simultaneous isomerization and cracking of the hexane isomers are given in Fig. 4.5. A plot of relative reaction paths (Fig. 4.6) reveals good agreement between the experimental and calculated (solid lines) reaction paths. Further, the rate constants can be discussed with respect to the underlying reaction mechanism. Assuming that the hexanes are interconverted mainly *via* a bifunctional mechanism where the species are (de)hydrogenated on the platinum function and skeletal rearrangements on the acidic function are the rate-determining steps, the rate constants (Fig. 4.5) satisfactorily reflect the different rates at which tertiary carbenium ions are rearranged

into tertiary or secondary carbenium ions, secondary into secondary or tertiary, and primary *via* protonated cyclopropane ring intermediates into primary ions.
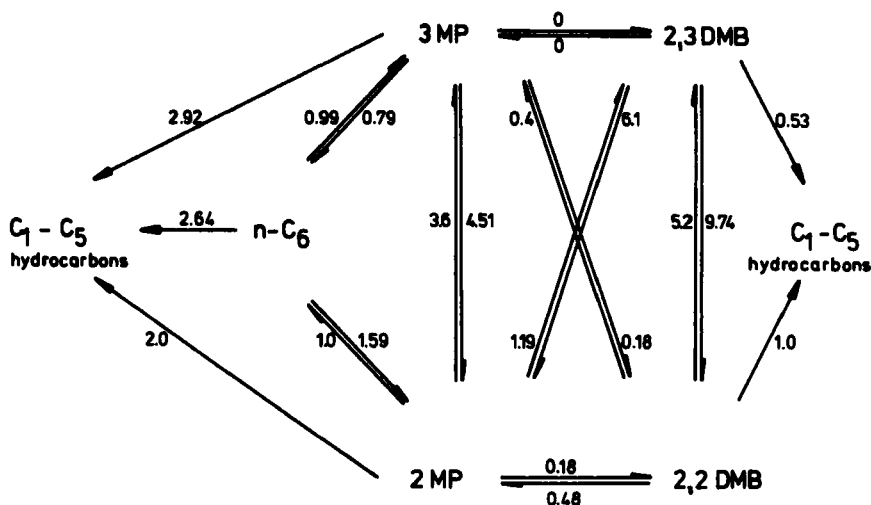
Fig. 4.5. Relative rate constants for simultaneous isomerization and cracking of the five hexane isomers. Reproduced with permission from (ref. 18).

Example 4.2: Kinetic analysis of interconversion and cracking of n-hexane and the methylpentanes by use of the "two-point" method (refs. 19,20). In the "two-point" method, just two compositions, $\alpha_i(0)$ and $\alpha_i(t)$, on individual reaction trajectories are considered for determination of the rate constants, where $\alpha_i(0)$ denote initial composition vectors and $\alpha_i(t)$ composition vectors which must all be obtained at the same reaction time t. This suggests using the pulse technique under conditions of constant carrier gas flow-rates, large pulse sizes compared with the length of the catalyst bed and the absence of chromatographic effects, which means under conditions where no broadening of the entrance peak occurs on passing through the microcatalytic reactor.

The pulse microreactor used had an inner diameter of 4 mm. The reaction conditions were as follows: catalyst, commercial 0.5 wt% $Pt/\eta-Al_2O_3$-platforming catalyst; amount of catalyst, 300 mg; particle diameter, 0.4 - 0.9 mm; carrier gas, H_2; carrier gas velocity, 180 ml/min; input pulses, 0.1 - 0.2 µl of reactant; reaction
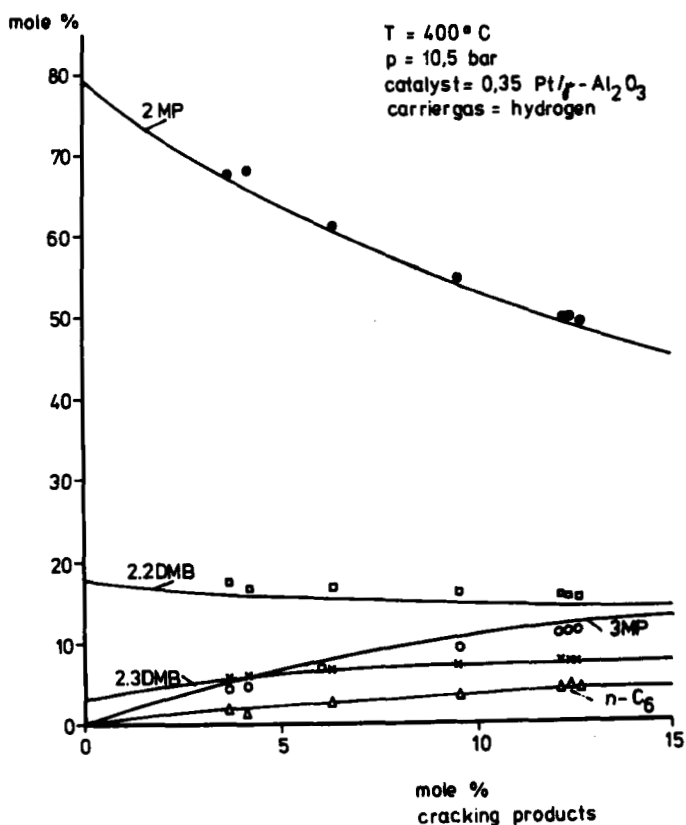
Fig. 4.6. Comparison of experimental and calculated (solid line) reaction paths. Reproduced with permission from (ref. 18).

temperature, 380°C; and total pressure, 2.8 bar. Catalyst samples were pre-treated in a flow of hydrogen for 12 h at 500°C and before starting each set of experiments the catalyst was treated with ten 5-µl pulses of reactant at the reaction temperature. After this treatment the peak areas of the inlet and outlet pulses of the microcatalytic reactor no longer varied. At the reaction temperature applied only small amounts of dimethylbutanes could be detected among the products and these were included into amount of hydro-cracking products.

Scheme 4.1 was used for relating the rate of change of composi-tion with concentrations of the individual species, showing that there are reversible reactions among the three hexane isomers and irreversible reactions for the formation of C_1-C_5 hydrocarbons.

cracking + cyclization products

Scheme 4.1

The rate of change of composition is given by

$$\alpha(t) = K \cdot (0) \tag{4.8}$$

where

$$\alpha(t) = \begin{bmatrix} \text{n-hexane} \\ \text{2-methylpentane} \\ \text{3-methylpentane} \end{bmatrix} \tag{4.9}$$

is the composition vector and

$$K = \begin{bmatrix} -\sum\limits_{j=1}^{3} k_{ji} & k_{12} & k_{13} \\ k_{21} & -\sum\limits_{j=1}^{3} k_{ji} & k_{23} \\ k_{31} & k_{32} & -\sum\limits_{j=1}^{3} k_{ji} \end{bmatrix} \tag{4.10}$$

is the rate constant matrix. The solution to eq. 4.8 is

$$\alpha(t) = X \, e^{-\Lambda t} \, X^{-1} \alpha(0) \tag{4.11}$$

where X is the matrix of eigenvectors and Λ the diagonal matrix of the eigenvalues of K. Replacing the composition vectors $\alpha(t)$ and $\alpha(0)$ by concentration matrices $A(t)$ and $A(0)$, which are formed from all composition vectors used for the determination of the coefficient matrix, and multiplying from the right by $A(0)^{-1}$ and X, we obtain

$$[A(t) \, A(0)^{-1}] \, X = X \, e^{-\Lambda t}. \tag{4.12}$$

The initial concentration matrix and the corresponding product concentration matrix used for the evaluation of the rate constants of the reactive system under consideration are given in eq. 4.13.

$$A(0) = \begin{bmatrix} \alpha_1(0) & \alpha_2(0) & \alpha_3(0) & \alpha_4(0) & \alpha_5(0) & \alpha_6(0) \\ 99.22 & 0.08 & 0.19 & 26.78 & 71.63 & 26.98 \\ 0.00 & 99.52 & 0.54 & 72.57 & 27.59 & 0.66 \\ 0.00 & 0.30 & 99.27 & 0.33 & 0.17 & 71.48 \end{bmatrix}$$

$$\begin{matrix} \alpha_7(0) & \alpha_8(0) & \alpha_9(0) & \alpha_{10}(0) & \alpha_{11}(0) & \alpha_{12}(0) \\ 67.93 & 0.58 & 0.0 & 51.11 & 50.07 & 0.55 \\ 0.40 & 25.90 & 72.05 & 47.71 & 0.00 & 47.5 \\ 31.12 & 73.52 & 27.95 & 0.00 & 49.29 & 51.23 \end{matrix}$$

$$\begin{bmatrix} \alpha_{13}(0) & \alpha_{14}(0) & \alpha_{15}(0) & \alpha_{16}(0) & \alpha_{17}(0) & \alpha_{18}(0) \\ 74.36 & 16.78 & 14.11 & 12.33 & 64.23 & 24.86 \\ 11.93 & 66.69 & 16.98 & 19.87 & 11.95 & 61.77 \\ 13.10 & 16.28 & 68.58 & 66.35 & 23.01 & 13.51 \end{bmatrix}$$

$$(4.13)$$

$$A(t) = \begin{bmatrix} \alpha_1(t) & \alpha_2(t) & \alpha_3(t) & \alpha_4(t) & \alpha_5(t) & \alpha_6(t) \\ 57.78 & 11.12 & 9.07 & 17.15 & 36.3 & 19.43 \\ 13.78 & 47.77 & 20.64 & 29.50 & 23.38 & 20.03 \\ 7.87 & 15.0 & 49.76 & 13.37 & 10.9 & 36.04 \end{bmatrix}$$

$$\begin{matrix} \alpha_7(t) & \alpha_8(t) & \alpha_9(t) & \alpha_{10}(t) & \alpha_{11}(t) & \alpha_{12}(t) \\ 41.13 & 9.24 & 10.38 & 26.48 & 35.87 & 8.86 \\ 16.77 & 28.85 & 40.37 & 35.78 & 15.86 & 35.42 \\ 21.73 & 40.48 & 24.61 & 8.88 & 31.82 & 34.13 \end{matrix}$$

$$\begin{bmatrix} \alpha(t) & \alpha_{14}(t) & \alpha_{15}(t) & \alpha_{16}(t) & \alpha_{17}(t) & \alpha_{18}(t) \\ 33.24 & 15.88 & 15.46 & 14.28 & 40.91 & 19.37 \\ 19.7 & 34.41 & 24.8 & 26.09 & 19.87 & 41.72 \\ 14.41 & 18.83 & 38.57 & 40.63 & 18.92 & 18.2 \end{bmatrix}$$

The concentrations in eq. 4.6 are given in mol%. For calculating the rate constant matrix, at least three initial composition vectors and the corresponding product compositions are needed, which form 3 x 3 square matrices with the individual concentrations as the entries. The concentration matrices in eq. 4.13 are formed from 18 initial composition vectors and the corresponding product concentration vectors, which means that a total of 54 experimental points can be considered for calculating the nine rate constants which are connected with the reaction Scheme 4.1. The rate coefficients, in contrast to curve-fitting procedures, are directly obtained from

the closed solution of the system of differential equations, eq. 4.8.

The calculation was performed in the following way. First, composition vectors on three reaction trajectories on the reaction hyperplane in the composition space were used for determining the rate coefficient matrix, then, in subsequent calculations, composition vectors on three further reaction trajectories were always added. Hence, six calculations were performed, each based on a large amount of experimental data. In all instances where the number of composition vectors in the composition matrix exceeded the number of components in the composition vector, both concentration matrices $A(0)$ and $A(t)$ were multiplied by the transpose of $A(0)$. The eigenvectors and eigenvalues of the matrix $A(t) A(0)^{-1}$ were calculated with a programmable pocket computer. The results of the calculations are given in Table 4.1.

TABLE 4.1

Relative rate constants of simultaneous isomerization and hydrogenolysis of n-hexane and the two methylpentanes

number of trajectories considered reaction	Relative rate constants					
	3	6	9	12	15	18
n-hexane → 2-methylpentane	0.25	0.26	0.29	0.26	0.27	0.27
n-hexane → 3-methylpentane	0.11	0.12	0.13	0.12	0.13	0.12
n-hexane → $\Sigma C_1 - C_5$	0.21	0.26	0.25	0.24	0.27	0.26
2-methylpentane → n-hexane	0.2	0.14	0.15	0.16	0.17	0.16
2-methylpentane → 3-methylpentane	0.31	0.33	0.33	0.31	0.31	0.30
2-methylpentane → $\Sigma C_1 - C_5$	0.32	0.45	0.42	0.38	0.4	0.42
3-methylpentane → n-hexane	0.13	0.13	0.14	0.13	0.14	0.14
3-methylpentane → 2-methylpentane	0.42	0.47	0.48	0.45	0.45	0.44
3-methylpentane → $\Sigma C_1 - C_5$	0.21	0.20	0.17	0.18	0.17	0.16

For some individual reactions such as hydrogenolysis of n-hexane and 2-methylpentane and isomerization of 3-methylpentane, rate constants calculated on the basis of composition vectors on three or nine reaction trajectories differ by up to 30%. Further increases

in the number of composition vectors considered only causes a small
variation in the calculated rate coefficients, which just reflect
the errors in concentration measurements of the experimental
equipment used.

A question to be considered is the transferrability of kinetic
data from pulse experiments to steady-state flow conditions. In
contrast to steady-state flow conditions, with the pulse method
concentrations in the gaseous flow change in time and space. For
linear reactive systems where the measured conversions are inde-
pendent of reactant concentrations, this means no restriction.
Problems arise when the catalyst sample itself operates under non-
-steady-state conditions during passage of the pulse through the
catalyst bed. Non-steady-state operation of the catalyst can be
caused by different phenomena. The restriction to transferring
results in reactive systems like the present one will be mainly
caused by adsorption sites with different strengths. Active sites
on the catalyst on which the adsorption times are long will contri-
bute to only a small extent to the measured product distributions
under steady-state operation. With the pulse method, however, where
the reactants usually contact a "fresh" catalyst surface, a frac-
tion of reactant molecules will be adsorbed on strong adsorption
centers and subsequently desorb very slowly, thus causing a decre-
ase in the peak area of the reactant pulse during passage through
the catalyst bed and a non-steady-state operation of the catalyst.
This difficulty may be circumvented with the present reaction
system, where the reactants and products display a similar adsorp-
tion behaviour, by pre-treating the catalyst sample with a large
number of reactant pulses. The strong adsorption sites will be
blocked by this procedure and steady-state operation of the catalyst
can be achieved. Hence with the reaction system under consideration
the kinetic data from the microcatalytic pulse experiments can be
used to predict catalyst activity and selectivity in steady-state
flow reactors.

4.1.2 Gas chromatographic pulse method

Several unusual phenomena may arise from the fact that the cata-
lytic column is also used for the separation of the reactant and
reaction product(s). In this way, different chemical entities
become chemically separated in the column and also the shape of the
elution peaks may give substantial information on the rate parame-
ters of physical and chemical rate processes. Earlier results have

been critically reviewed by Langer and Patton (ref. 3).

The gas chromatographic pulse method was first proposed by Bassett and Habgood (ref. 13), Magee (ref. 21) and Roginskii, Yanovskii and co-workers (refs. 22,23). They gave a mathemathical description of elementary processes for a few simple limiting cases and also presented experimental examples using dehydrogenation of cyclohexane as a simple model reaction occurring essentially without by-products. The procedure using the gas chromatographic method is as follows. A mathematical model is set up which accounts for the processes occurring during the passage of the reactant pulse through the chromatographic column. If axial convection and axial dispersion in the fluid phase, diffusion in the solid phase and adsorption and desorption on and from the solid surface are considered, the model is defined in the following way:
Fluid phase:

$$\frac{\partial a}{\partial t} + u \frac{\partial a}{\partial z} - D_{ax} \frac{\partial^2 a}{\partial z^2} - \frac{3(1 - \varepsilon)}{\varepsilon R} Q = 0 \qquad (4.14)$$

Solid phase:

$$\frac{\partial \bar{a}}{\partial t} - D_{eff}/\beta \left(\frac{\partial^2 \bar{a}}{\partial r^2} + \frac{2}{r}\frac{\partial \bar{a}}{\partial r}\right) - N = 0. \qquad (4.15)$$

The two differential equations are coupled through a mass transfer term

$$Q = D_{eff} \frac{\partial \bar{a}}{\partial r}\bigg|_{r=R} \qquad (4.16)$$

which indicates that the amount of reactant diffusion into the pellet is proportional to the concentration gradient in the external surface of the pellet. The symbols in eqs. 4.14 - 4.16 are a = concentration in the fluid phase, $\bar{a}$ = concentration in the pellet, u = flow velocity, t = time variable, z = axial coordinate in the column, r = radial coordinate in the pellet, R = pellet radius, D_{ax} = axial dispersion coefficient, D_{eff} = effective pore diffusion coefficient, based on the total cross-section normal to the direction of diffusion, β = pellet porosity and ε = fixed-bed porosity, N is related to the adsorption rate through

$$N = k_a \left(\bar{a} - \frac{a_s}{K_a}\right) \qquad (4.17)$$

where k_a = adsorption rate constant, K_a = adsorption equilibrium constant and a_s = surface concentration. The initial and boundary

conditions are

$\partial \bar{a}/\partial r = 0$ at $r = 0$ for $t > 0$

$a = \bar{a} = a_s \equiv 0$ for $t = 0$ and $0 \leq z \leq L$ (4.18)

$a = a_0(t)$ for $z = 0$ and $t \geq 0$.

The mathematical model, eqs. (4.14) and (4.15), can be extended to account for chemical reaction, film diffusion, surface diffusion, etc. (refs. 2,24). Roginskii and co-workers derived a method for calculating the conversion, rate coefficient and activation energy for rectangular and triangular input pulses for zero-, first- and second-order reactions. Here a linear (Henry-type) adsorption isotherm was assumed (ref. 23). A theoretical derivation was also put forward for a more general case where the surface (serving both as an adsorbent and as a catalyst) is inhomogeneous, but the resulting equations remained largely formal (ref. 25).

The model parameters can be fitted either in the time, the Laplace or the Fourier domain, or by the method of moments (ref. 26). Fitting in the Laplace or Fourier domain and the method of moments are only applicable for linear systems. If the mathematical models include several parameters to be determined, then fitting in the time, the Laplace or the Fourier domain is connected with the usual difficulties. With linear models the method of moments, however, permits an independent determination of the individual parameters by fitting to straight lines. As Kubin (ref. 27) and Kucera (ref. 28) first demonstrated, the experimentally measurable moments m_n of elution curves are related to the solution of the partial differential equations, eqs. (4.14 - 4.16), in the Laplace domain:

$$m_n = (-1)^n \lim_{s \to 0} \frac{d\tilde{a}(s)}{ds} \qquad (4.19)$$

where $\tilde{a}(s)$ is the transformed concentration. The first absolute moment μ_1 and the second central moment are given by

$$\mu_1 = \frac{m_1}{m_0} = \frac{\int_0^\infty ta\, dt}{\int_0^\infty a\, dt}$$

and   (4.20)

$$\mu_2' = \frac{\int_0^\infty (t - \tau)^2 a\, dt}{m_0} \;.$$

Making use of the Dirac function for the shape of the entrance pulse, the moments will be

$$\mu_1 = [1 + \frac{1-\epsilon}{\epsilon} \beta(1 + K_a)]L/u$$

$$\frac{\mu_2'}{L/u} = \frac{2D_{ax}}{u^2}[1 + \frac{1-\epsilon}{\epsilon}\beta(1 + K_a)]^2 + \frac{2(1-\epsilon)}{\epsilon} \quad (4.21)$$

$$\times[\beta \frac{K_a^2}{k_a} + \frac{1}{D_{eff}} \frac{R^2\beta^2}{15}(1 + K_a)^2].$$

The experimental procedure for determining the parameters K_a, k_a, D_{ax} and D_{eff} involves measuring the retention time and the variance of elution curves at different flow-rates of the carrier gas and at different pellet diameters. The retention times are then plotted against the residence time L/u and the adsorption equilibrium constant is obtained from the slope of the straight line. Plotting $\mu_2'/(L/u)$ against $1/u^2$ also gives a straight line. From the slope of this line, D_{ax} can be calculated, whereas the intercept on the ordinate includes the quantities k_a and D_{eff}. These two parameters can be determined by plotting the intercepts on the ordinate at different pellet diameters against the squares of the pellet radii. Again, a straight line is obtained which gives k_a from the intercept on the ordinate and D_{eff} from the slope. Thus, for the determination of individual parameters of the mathematical model, only linear regression procedures are needed.

Boniface and Ruthven (ref. 29) developed a method involving the use of third and fourth moments for describing systems in which three distinct resistances to mass transfer can be distinguished: diffusion through the external fluid film, through pellett macropores and through the crystal micropores. With the increasing importance of zeolite catalysts, such methods certainly are of interest. The authors reported satisfactory results in the chromatography of argon on zeolites, i.e., with a system still far from those used in real catalysis.

The physical separation of the reactant and product(s) along the catalytic/chromatographic column gives rise to the possibility of reaching conversion values far higher than those corresponding to thermodynamic equilibrium, as illustrated by the example of cyclohexane dehydrogenation (ref. 22). Dehydrogenation of n-butenes to butadiene over chromia-alumina could also be realized with yields exceeding the equilibrium values by 1.5-2-fold (ref. 30). Whereas the above effects are due to physical separation of the components (which are, therefore, also thermodynamically separated),

an unexpected and yet unexplained exceeding of equilibrium yields
was reported when cyclohexane pulses were introduced periodically
at high frequency on to a Pt/Al_2O_3 chromatographic column (ref. 31).
Comparison of calculation and experiments led the same authors to
the conclusion that several crucial points arise when a chromatog-
raphic reactor is simulated by a computer. Apart from the "transi-
ent promoting effect" mentioned (giving rise to unexpectedly high
yields), competitive adsorption of each species, correction of the
volumetric flow-rate as a consequence of chemical expansion and the
number of assumed mixing cells have been pointed out (ref. 32).
Within the framework of laboratory tests of catalyst activity and
selectivity, the gas chromatographic method supplies information
on the rates of physical and/or chemical rate processes which are
needed when constructing suitable dynamic reactor models. The
effective diffusion coefficient, the adsorption rate constant and
the adsorption equilibrium constant depend on the system properties
and therefore can be used for model predictions.

In addition to the restriction to linear systems, further limi-
tations exist. Some of the parameters, such as the axial dispersion
coefficient, depend on the reactor configuration and cannot be used
for modelling other reactor configurations. If the model is
incorrect, the uniqueness of the parameters is affected and even
parameters such as the adsorption rate constants, which are inde-
pendent of the reactor configuration, cannot be transferred. A
properly designed system, on the other hand, can supply very
reliable data. It was found that using either the moment method or
fitting in the Fourier domain could result in accurate values of,
for example, adsorption equilibrium constants K and dispersion
coefficients D; also, the effective diffusivities are good, within
the range of engineering requirements. Gangwal *et al.* (ref. 33)
expressed an optimistic view of the possible use of chromatographic
methods for evaluation of the properties of flow systems, even if
rate coefficient for physisorption and mass transfer coefficient
could not be measured by chromatographic techniques.

As far as the axial dispersion is concerned, an interesting new
experimental setup was proposed (ref. 34). A "pseudo-infinite
cylinder" was constructed by placing cylindrical pellets one above
another instead of packing a column in a random way. The gas flows
in the annulus between the adsorbent pellets and the tube wall,
and high gas speeds can be achieved. The authors claimed that this
system permits one to express axial dispersion in the annular space

between pellet and wall theoretically by using the first two
moments according to Kubin (ref. 27) and Kučera (ref. 28) for
evaluation.

Example 4.3: Determination of the adsorption equilibrium constant,
the axial dispersion coefficient and the effective diffusivity in
the system methylcyclopentane - Pt/Al$_2$O$_3$ using the gas chromatog-
raphic pulse method (ref. 35). The experiments were performed with
a gas chromatographic pulse reactor under the following operating
conditions: column, 140 mm x 2.5 mm I.D.; mean diameters of cata-
lyst particles, 0.13, 0.21 and 0.3 mm; temperature, 100-200°C;
carrier gas, N$_2$; carrier gas velocity, 30-120 ml/min; catalyst,
commercial 0.3 wt% Pt/γ-Al$_2$O$_3$ platforming catalyst; total pressure,
1 bar; pulse size, <1 μl; peak width of inlet pulse, <1 s; and
peak width of elution peaks, 20-1000 s. The shapes of the inlet
and elution pulses were monitored with either flame ionization or
thermal conductivity detectors. The integrals needed for the
determination of the moments of the elution curves were calculated
by use of the Simpson rule.
   With the experimentally proved assumptions of an isothermal
column, plug flow at all carrier gas velocities and only small con-
centration gradients in the phase boundary between the fluid and
solid phase, the following processes are considered in the mathema-
tical model describing the flow of reactant pulses through the
catalyst bed: axial convection and dispersion in the fluid phase,
diffusion within the porous structure of the solid phase and ad-
sorption on and desorption from the solid surface, which
results in the model equations eq. 4.14 - 4.18. The application of
the method of moments for the determination of the different model
parameters requires that the assumptions of linear rate equations
for all processes that contribute to broadening of the reactant
pulse during passage of the column are fulfilled. The moments of
the elution curves are independent of the concentration of reactant
pulses with linear processes and depend on concentration with non-
-linear processes. The moments μ_1 [s] and μ_2' [s^2] as defined by
eq. (4.20) are plotted in Fig. 4.7 and indicate that the moments
are independent of reactant pulse concentration. Eq. 4.21 relates
the adsorption equilibrium constant K$_a$ to the first absolute moment.
For different particle diameters the first absolute moment is
plotted against the residence time L/u for 4 temperatures. With
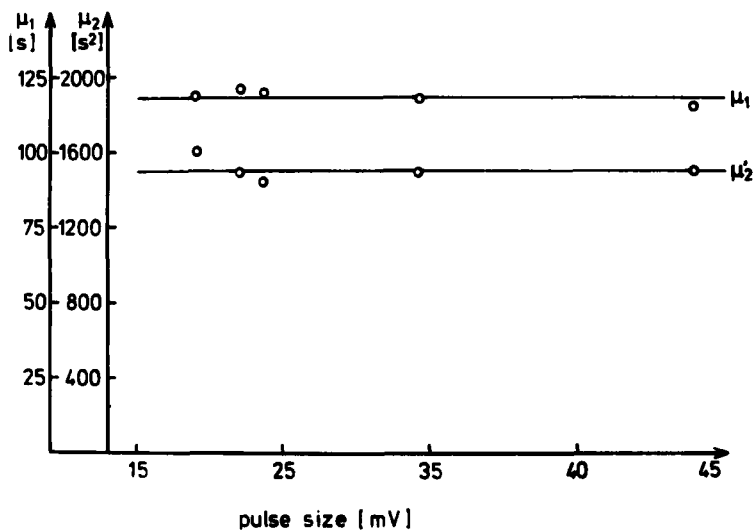
Fig. 4.7. Dependence of the first absolute and the second central moment of elution peaks on methylcyclopentane concentration (expressed as instrument reading in mV). Reproduced with permission from (ref. 35).
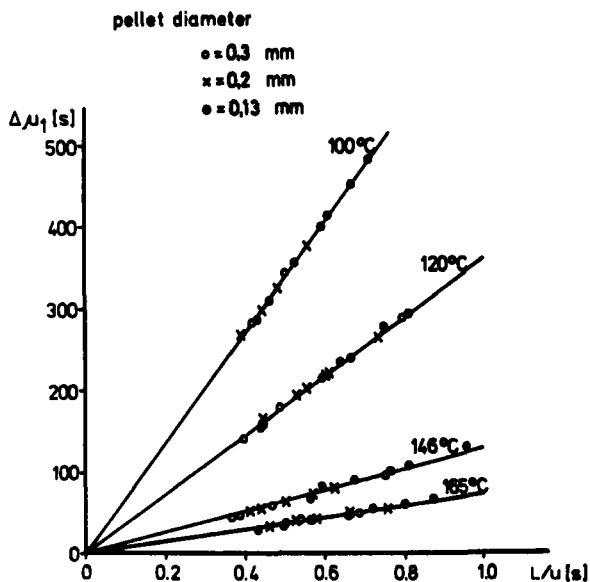
Fig. 4.8. Dependence of the first absolute moment of methylcyclopentane elution peaks on residence time L/u. Reproduced with permission from (ref. 35).

the porosity of the solid material β = 0.65 and the porosity of the fixed bed ε = 0.48 the following values for the adsorption equilibrium constant are obtained (Fig. 4.8):

T [^{O}C]	100	120	146	6??
K_a	1123 $\pm$ 44	603 $\pm$ 22	215 $\pm$ 7	125 $\pm$ 3

from which a temperature coefficient of the adsorption equilibrium constant of 47.5 $\pm$ 2.1 kJ/mol is determined.
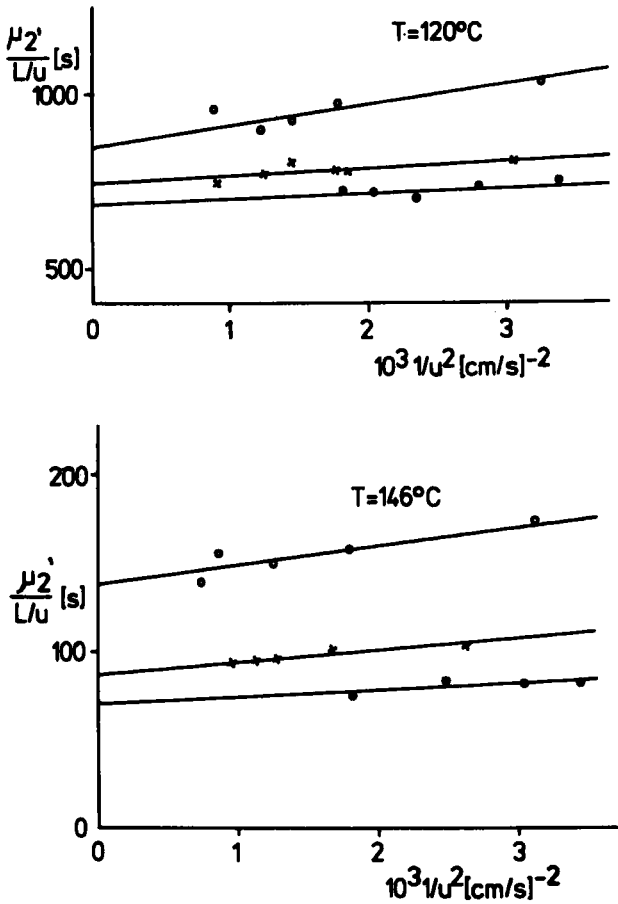
Fig. 4.9. Dependence of the second central moment of methylcyclopentane elution peaks on flow-rate at two temperatures. Reproduced with permission from (ref. 35).

According to eq. 4.21, the second central moment is related to the axial dispersion coefficient, the effective diffusivity, the adsorption rate constant, the porosities of the pellets and the fixed bed and the flow-rate. In Fig. 4.9 a and b $\mu_2'/(L/u)$ is plotted against the reciprocal of the square of the flow-rate for different particle diameters at two temperatures. The intercepts on the ordinate of Fig. 4.9. are plotted against the pellet cross--sections in Fig. 4.10 a and b. For the axial dispersion coefficients the following values are obtained:

Pellet diameter [mm]	0.13	0.21	0.3
D_{ax} [cm^2/s]	0.11 $\pm$ 0.04	0.26 $\pm$ 0.1	0.38 $\pm$ 0.06

and for the effective diffusion coefficient in the porous pellet D_{eff} = 0.013 $\pm$ 0.006 cm^2/s. From the intercepts on the ordinate of Fig. 4.10 the following desorption rate constants are determined:

k_{des} [s^{-1}]	0.5	1.05	4.9	8.4
T [^{o}C]	100	120	146	165

which result in an activation energy for desorption of E_A = = 64.1 $\pm$ 0.33 kJ/mol.

The advantage of evaluating data from chromatographic pulse reactor experiments with the method of moments is that the model parameters can be individually determined by fitting to straight lines. There are some restrictions on the applicability of the method. At low temperatures the reactant pulses are broadened to a large extent when passing through the chromatographic column and strong tailing of the elution peaks occurs, introducing large errors into the computed moments. With increasing temperature only slight broadening of the elution peaks is observed, so the reliable experimental determination of the model parameters involves substantial difficulties. For example, as the results plotted in Fig. 4.8 indicate, the first absolute moment is 410 s at a residence time of 0.6 and a temperature of 100°C whereas the value decreases to 45 s at a temperature of 165°C. At 200°C the first absolute moment is only 1-2 s, which means that the elution peak coincides with the entrance peak and no broadening is observed.
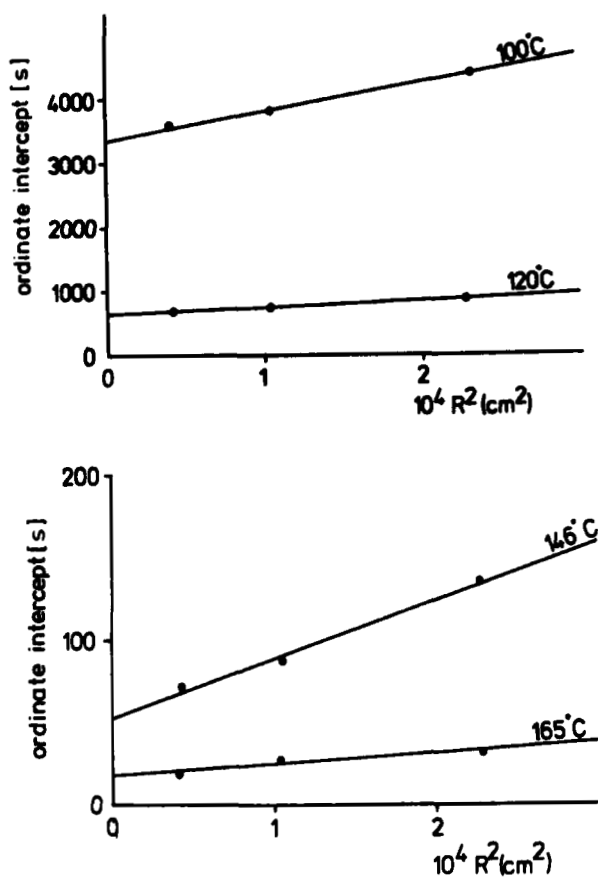
Fig. 4.10. Determination of effective diffusivities and desorption rate constants at various temperatures. Reproduced with permission from (ref. 35).

Semenenko *et al.* (ref. 30) reported a maximum value of the peak width of butenes and butadiene at the outlet of the chromia-alumina column as a function of temperature. At reactor temperatures between 25 and 150°C the maximum width was reported to be at 65°C. The authors claimed that this would mean that strongest chemisorption takes place at this temperature. The yield of butadiene starts to become significant above this temperature.

4.2 SINGLE-PELLET DIFFUSION REACTORS

Up to now the single-pellet diffusion reactor has been used to
only a limited extent for the kinetic analysis of heterogeneous
catalytic reactions. Single-pellet diffusion reactors permit con-
centration and temperature measurements in the flowing phase and
in the centre of the catalyst pellet. This is realized by passing
the fluid along one front of a cylindrical pellet and attaching a
closed chamber to the other front of the pellet, as shown in Fig.
4.11 (ref. 36). Laboratory configurations like these are based on
the theoretical work of Zeldovich (ref. 37) and have been verified
experimentally by Roiter *et al.* (ref. 38) in such a way that the
temperature of the catalyst pellet was increased until the flow of
reactant equalled zero in the centre of the pellet. Under these
conditions, reaction orders can easily be derived from the measured
concentrations under simultaneous diffusion effects.

Smith and co-workers developed three experimental setups and
discussed the governing equations for all three versions. They
differ from each other with respect to the place and mode of
sampling. The reactor depicted in Fig. 4.11 - which will be used
for detailed illustration of the method - corresponds to the design
reported by Suzuki and Smith (ref. 39) with a closed static chamber
below the pellet. Another design involves a constant carrier gas
flow in the sampling chamber (ref. 40). The pulse is introduced to
the upper face and the response is measured with a detector placed
in the stream leaving the lower face. This more rapid method pro-
vided diffusivity data from the first moment only. It was not
possible, however, to determine both diffusivity and adsorption
rate constants from the same set of experiments. In the third
method (ref. 41), the cylindrical catalyst pellet is exposed on one
end face to a stream flowing through a chamber and the response is
measured from the effluent of the same chamber, *i.e.*, only one
face of the pellet is used. The equations are solved in the Laplace
domain and the first two moments are used for evaluation. The first
moment is simply the residence time in the chamber and in the
porous pellet; the second moment includes the diffusion time. To
increase the accuracy of the determination of the latter, a small
chamber volume and a long ("deep") particle should be used.

Petersen and co-workers (refs. 42,43) extended the applications
of single-pellet diffusion reactors and demonstrated their advan-
tages in determining physical diffusion coefficients, reactive
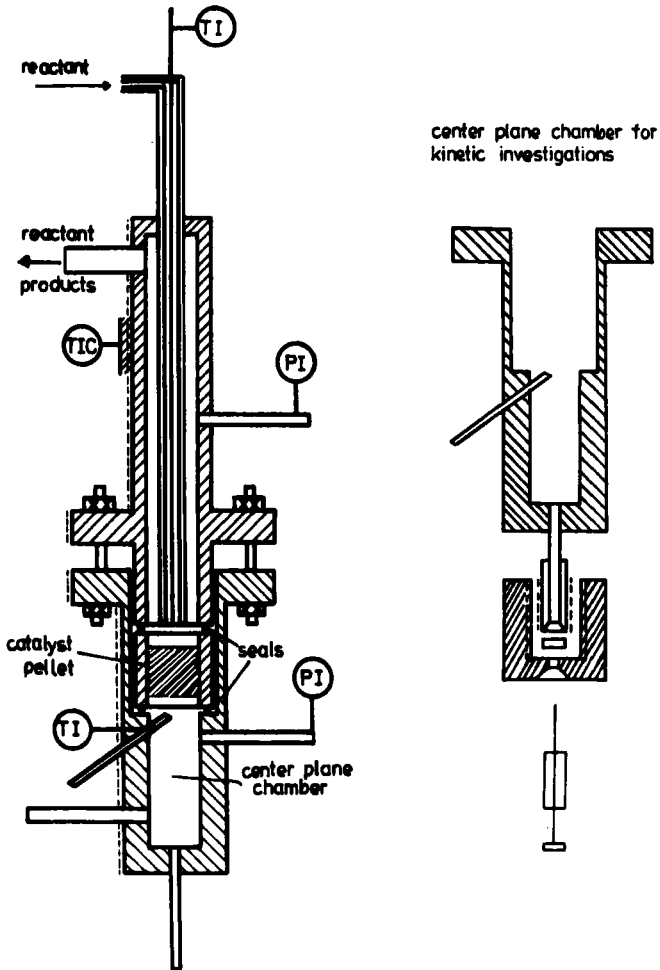
Fig. 4.11. Single-pellet diffusion reactor. Reproduced with per-
mission from (ref. 36).

effective diffusivities and kinetic reaction orders and in distin-
quishing between different deactivation mechanisms once the
kinetics of the chemical reaction are known. According to Hegedus
and Petersen (ref. 42), physical mass transport parameters within
the pellet can be obtained with a measuring instruction based on
the dusty gas model (refs. 44,45), which accounts for mass trans-
port in porous media by three transport mechanisms, Knudsen diffu-
sion, bulk diffusion and viscous flow which results in the model
equation eq. 3.191.

In permeability measurements (Fig. 4.12), where the molar flow
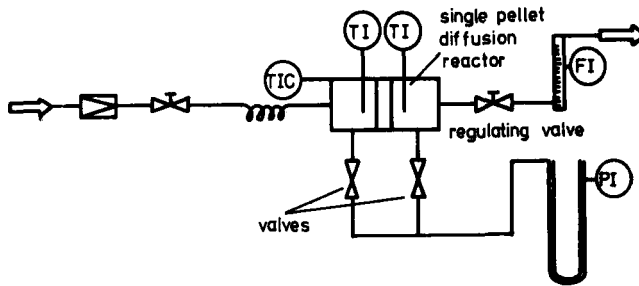
Fig. 4.12. Flow diagram of permeability measurements with a single-
-pellet diffusion reactor. Reproduced with permission from (ref.
36).

of a gaseous species through the catalyst pellet is monitored at
different total pressures in the pellet and different pressure
drops over the pellet, eq. 3.191 is reduced to eq. 3.192, which on
integration yields

$$J \ R \ T \ L \ / \ \Delta \ P = D_{K,eff} + (B_0/\mu) \ P \qquad (4.22)$$

$i.e.$, $D_{K,eff}$ and C_0/μ are determined from the slope and the inter-
cept on the ordinate of the straight line that is obtained from
plotting $J \ R \ T \ L \ / \ P$ against the average total pressure in the
pellet.

In counter-diffusion measurements (Fig. 4.13), eq. 3.191 is
reduced to eq. 3.194. From the integrated form of eq. 3.194, eq.
3.195, the effective diffusivity $D_{12,eff}$ can be calculated by means
of an trial and error procedure.

In addition to the determination of effective diffusivities
which are based on physical concepts of the underlying transport
mechanisms, effective diffusivities under reaction conditions can
be determined with the single-pellet diffusion reactor (Fig. 4.14).
For a first-order reaction the experimental procedure follows from
the material balance over an isothermal catalyst pellet:

$$d^2 \ \Psi_A/d\eta^2 = h^2 \ \Psi_A. \qquad (4.23)$$

With the boundary conditions $\Psi_A = 1$ at $\eta = 0$ and $d\Psi_A/d\eta = 0$ at
$\eta = 1$, the solution to this equation is
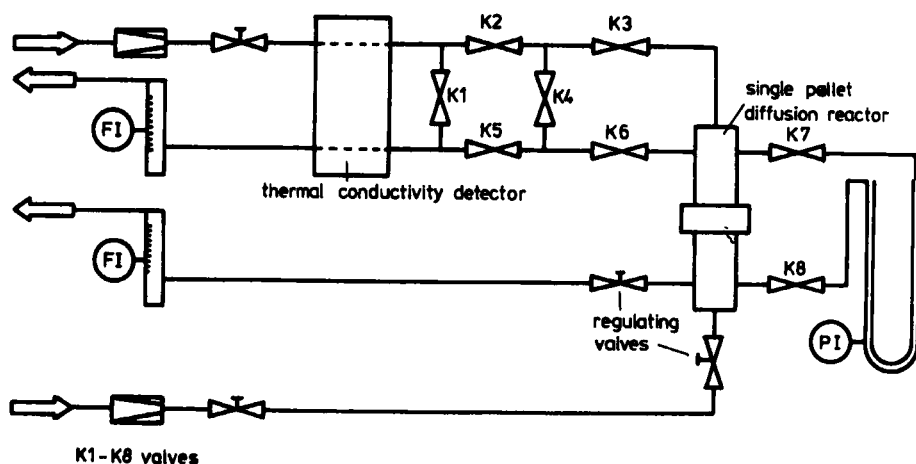
Fig. 4.13. Flow diagram of isobaric counter diffusion measurements with the single-pellet diffusion reactor. Reproduced with permission from (ref. 36).
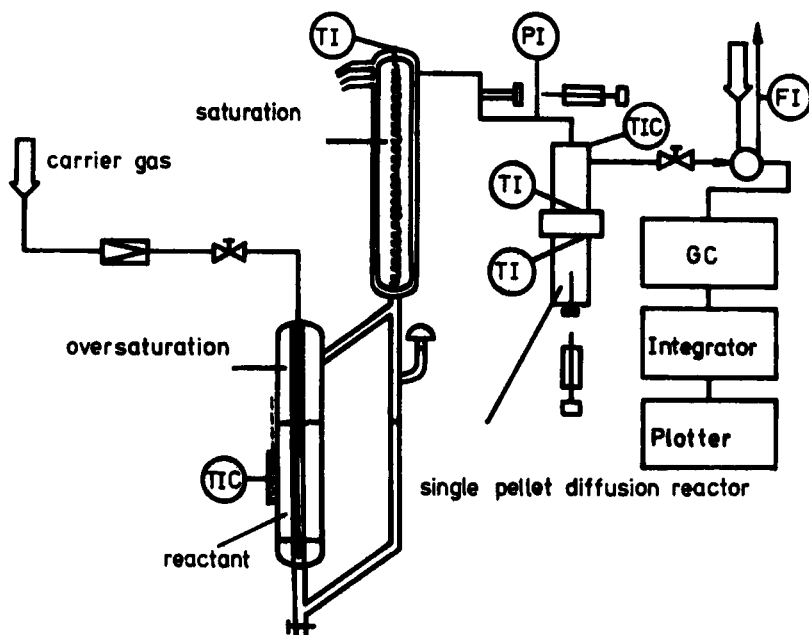
Fig. 4.14. Flow diagram of measurements with the single-pellet diffusion reactor under reaction conditions. Reproduced with permission from (ref. 36).

$$r = \frac{\tan h(h)}{h} \, ka_A(0)\pi R^2 L$$

or

$$\Psi_A(1) = \frac{a_A(1)}{a_A(0)} = \frac{1}{\cos h(h)} \qquad (4.24)$$

where Ψ_A is a dimensionless concentration, R = pellet radius, L =
= length of pellet, a_A = concentration of component A, $a_A(1)$ =
= centre plane concentration, r = overall reaction rate, h =
= Thiele modulus = Lk_1/D_{eff} and η = y/L. From a measurement of the
concentration in the bulk phase and the corresponding centre plane
concentration, the Thiele modulus is obtained. With the knowledge
of the overall reaction rate in the bulk phase, the effective
diffusion coefficient $D_{eff} = L^2 k_1/h^2$ is calculated.

D_{eff}, however, cannot be compared directly with the effective
diffusion coefficients determined by use of the dusty gas model.
D_{eff} is based on the total cross-section normal to the diffusion
direction and is defined as the ratio of the flux through this
cross-section to the concentration gradient, and hence corresponds
to D_{eff} obtained from the gas chromatographic method and to the
diffusivity, which is usually used in the concept of effectiveness
factors. By use of the Bosanquet or related equations (ref. 46),
effective diffusivities obtained with the procedure considered so
far under reaction conditions can be compared with effective mole-
cular and Knudsen diffusivities.

A further application of single-pellet diffusion reactors is
the investigation of deactivation mechanisms. For this, according
to Hegedus and Petersen (ref. 42), material balances are solved
analytically or numerically for different deactivation mechanisms
such as core poisoning, pore mouth poisoning, uniform poisoning
and series, parallel or triangle self-poisoning and different
Thiele moduli. The solutions are plotted in a diagram with the
relative reaction rate in the bulk phase and the dimensionless
centre plane concentration as ordinates. From a comparison of expe-
rimental values with these solutions, information on the underlying
deactivation mechanism is obtained.

Jossens and Petersen (ref. 47) described a reactor setup that
permits the direct determination of deactivation kinetics. This
consists of a differential recycle reactor and a single-pellet

reactor. The use of this dual system permits the investigator to maintain constant product and reactant concentrations in space and time. One of the main advantages of the system is to present deactivation data at early times of a catalyst life. Most data reported by this research group, which were discussed in Section 3.4, were obtained with this setup.

The main potential for single-pellet diffusion reactor applications arises from proving theoretical concepts such as the interaction of external and internal mass transfer rates with isothermal and non-isothermal catalyst pellets, the uniqueness and stability of steady states of catalyst pellets, inhomogeneous catalyst pellets, and so on. At least two advantages of single-pellet reactors have been claimed over batch and flow reactors in analyzing first-order reaction networks (ref. 48). One is that the matrix of the intrinsic rate constants can be obtained non-iteratively from concentration measurements, although conditions of non-iterative solution for the other reactor types also exist. Another advantage is that both the rate constants and the diffusion constants can be determined under conditions where gradientless operation is not possible in the other two reactor types.

For practical testing of commercial catalysts, drawbacks for the application of single-pellet diffusion reactors stem from the preparation of the single pellets. Single pellets are prepared by pressing catalyst powder into a titanium or stainless-steel support ring. The structure of the secondary pore system depends strongly on the compression time and the pressure used in the press device. Usually the secondary pore structure causes limitations of measured conversions by internal mass transfer rates even with bimodal pore structures, because the diffusion distances in the primary pore system are normally small. A prediction of effective diffusitivies therefore presupposes a mode of preparation of the single pellet that ensures similar pellet porosities and secondary pore structures to those of commercial catalysts.

Example 4.4: Kinetic analysis of diffusion-disguised first-order reaction networks with a single-pellet diffusion reactor. Before investigating the kinetics of interconversion and cracking of n-hexane and the methylpentanes, the question was considered of whether diffusion rates through the porous pellet and the rates of surface reactions within the pellet can be obtained independently with the single-pellet diffusion reactor, by measuring effective

diffusivities and rates of n-hexane conversions on Pt/Al_2O_3 pellets with different porosities. First the overall reaction order of n-hexane conversion was determined by solving the continuity equation for simultaneous diffusion and reaction in the catalyst pellet, assuming that the mass transport through the pellet is caused only by diffusion:

$$d^2 \Psi_A/d\eta^2 = h^2 \cdot \Psi_A^n \qquad (4.25)$$

for different reaction orders n and plotting calculated centre plane concentrations against concentrations in the bulk phase. For first-order reactions centre plane concentrations are independent of bulk phase concentrations. The results obtained for n-hexane conversion yielding isohexanes and hydrogenolysis products are given in Fig. 4.15, indicating that the hydrocarbon partial pressure dependence of n-hexane isomerization and cracking rates is +1. The reaction conditions were as follows: reaction temperature, 436°C; total pressure, 1050 Torr; n-hexane partial pressure, 10-80 Torr; carrier gas, hydrogen; carrier gas velocity, 100 ml/min (STP) (the flow velocities were high enough to ensure that film diffusion effects did not influence the measured effective diffusitivies); catalyst pellet, 1 g of catalyst powder (particle diameter 0.2 mm) was pressed at 1000 bar into the cylindric pellet holder; pellet diameter, 12.9 mm; length of pellet, 7.2 mm; temperature gradients along the pellet did not exceed 1°C.

In Table 4.2 rate constants for n-hexane conversion, which are calculated from conversion measurements in the bulk phase at different n-hexane partial pressures and effective diffusivities, are presented for three pellets pressed at 500, 1000 and 2000 bar. As the results reveal, with increasing press pressure during preparation of the pellet the effective diffusivity decreases from 0.029 to 0.014 cm^2/s, whereas within experimental error the same rate constant for n-hexane conversion is obtained. The porosity of the pellet decreases only slightly with increasing press pressure. Hence, the decrease in the effective diffusivity is mainly caused by an increase in the tortuosity factor.

The flow diagram for investigating the kinetics of simultaneous interconversion and hydrogenolysis of n-hexane and methylpentanes is depicted in Fig. 4.16. A hydrogen carrier gas flow loaded with reactants by oversaturator/saturator systems is passed on one side of the catalyst pellet. To the opposite side of the cylindrical pellet, a closed chamber is attached from which small samples for
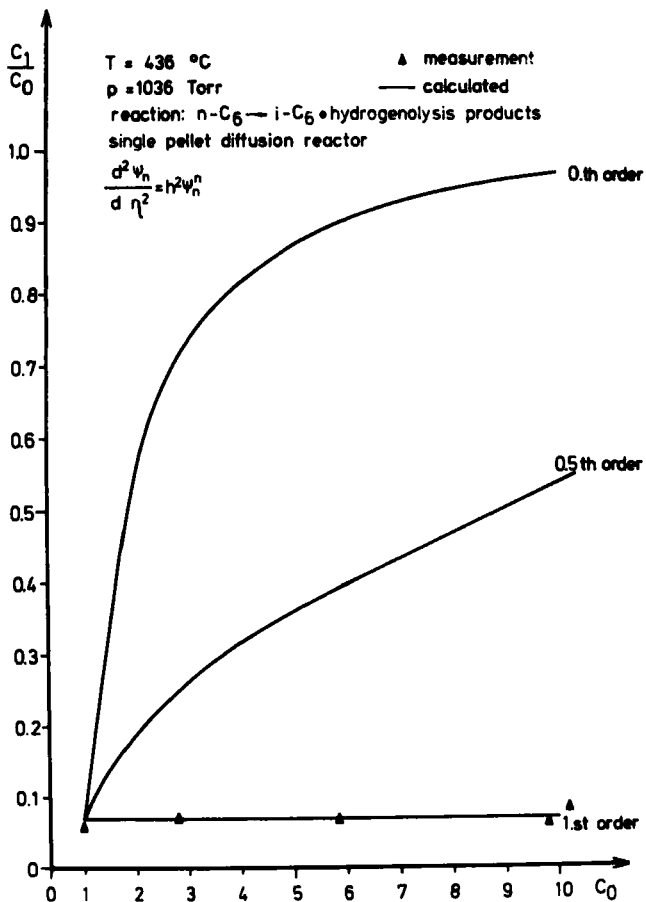
Fig. 4.15. n-Hexane partial pressure dependence of isomerization and cracking rates of n-hexane. Reproduced with permission from (ref. 36).

gas chromatographic analysis can be withdrawn with a syringe (Fig. 4.11). Special attention was paid when drawing these samples that always the same amount of gaseous phase from the centre plane chamber was sampled. The three saturators contained n-hexane and 2- and 3-methylpentane and could be cooled independently of each other, so the same partial pressures of individual reactants and reactant mixtures could be achieved. By means of a valve system, the feed flows or the product flow could be passed through the sample loop of a gas chromatograph (100-m squalane capillary column, flame ionization detector). Temperatures were monitored on both sides of the catalyst pellet. The temperature gradients through the

TABLE 4.2

Influence of pressure in the press device during pellet preparation on effective pellet diffusivities and rate constants. Reproduced with permission from (ref. 49).

	press pressure [bar]	weight [g]	length [mm]	porosity	BET area [m^2/g]	rate constant[a] [s^{-1}]	D_{eff} [cm^2/s]
pellet 1	500	1	7.2	0.72	349	0.49	0.029
pellet 2	1.000	1	6.78	0.7	369	0.47	0.019
pellet 3	2.000	1	6.29	0.67	367	0.44	0.014

[a]reaction conditions: reaction, n-hexane → isohexanes + cracking products; temperature, 436°C; total pressure, 1050 Torr; n-hexane partial pressure, 10-80 Torr; carrier gas, hydrogen; carrier gas velocity, 100 ml/min [STP].
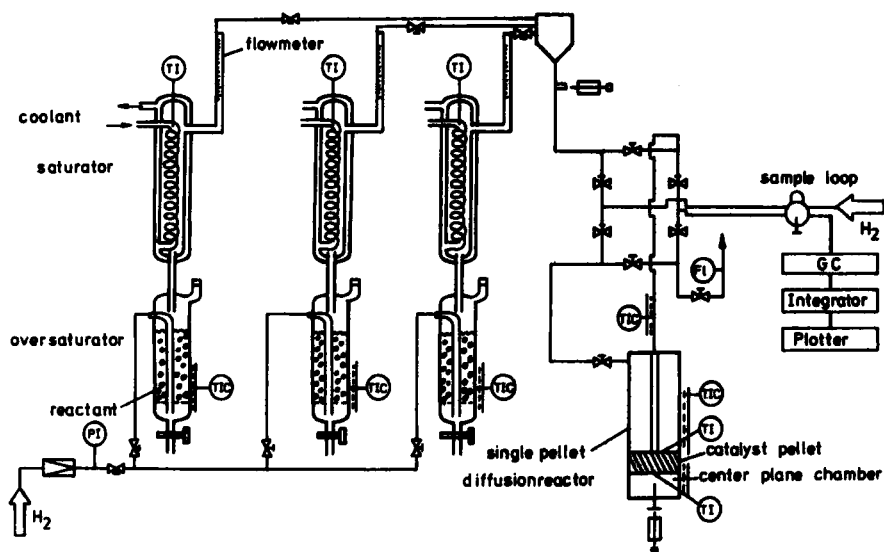
Fig. 4.16. Flow diagram of experimental set-up for kinetic investigation of the interconversion and hydrogenolysis of n-hexane and the methylpentanes.

pellet did not exceed 1°C. Interconversion and hydrogenolysis of hexane/methylpentanes were carried out at an alkane partial pressure of 22 Torr, a total pressure of 1050 Torr at 335°C on a

catalyst pellet pressed at 500 bar (pellet diameter 12.9 mm, length 7.2 mm). The change in composition of n-hexane/methylpentanes on interconversion with time in a single-pellet diffusion reactor can be represented by the set of differential equations eq. 3.109, which on integration yield

$$\alpha(0) = X[1/\cosh(h_\Lambda)] \ X^{-1} \ \alpha(1). \qquad (4.26)$$

Introducing concentration matrices A(1) and A(0) formed from corresponding bulk and centre plane concentration column vectors, the following equation is obtained after some rearrangements:

$$[A(0) \ A(1)^{-1}] \ X = X[1/\cosh(h_\Lambda)]. \qquad (4.27)$$

From the experimentally determined matrix $[A(0) \ A(1)^{-1}]$ the eigenvectors and eigenvalues are calculated. The matrix consisting of the single bulk phase composition vectors at the reactor exit is given by

$$A(1) = \begin{vmatrix} .0125 & .0092 & .5349 & .9553 & .3187 & .0091 \\ .0202 & .9574 & .4301 & .0103 & .0145 & .4395 \\ .9425 & .0098 & .0076 & .0067 & .6431 & .5277 \end{vmatrix}. \ (4.28)$$

The corresponding matrix of centre plane compositions is given by

$$A(0) = \begin{vmatrix} .0887 & .1064 & .3109 & .5671 & .2044 & .0832 \\ .1567 & .5794 & .3617 & .1373 & .1311 & .3358 \\ .5067 & .0927 & .0801 & .0647 & .4367 & .3595 \end{vmatrix}. \ (4.29)$$

Multiplying both matrices by the transpose of the matrix [A(1)] and calculating the eigenvectors and eigenvalues of the matrix $[A(0) \ A(1)^{-1}]$ with a library program, the following eigenvalues and eigenvectors are obtained: $\lambda_1 = 0.788$, $\lambda_2 = 0.506$, $\lambda_3 = 0.467$.

$$X = \begin{vmatrix} .45690 & -.65039 & -.45709 \\ .74591 & -.09398 & .80729 \\ .48462 & .75376 & -.37331 \end{vmatrix}. \qquad (4.30)$$

Relative rate constants calculated from these eigenvalues and eigenvectors are given in Scheme 4.2.

Calculated and experimental reaction paths are shown in Fig. 4.17, where the reaction paths have been projected on to the reaction plane of the reversible three-component system n-hexane - - 2-methylpentane - 3-methylpentane in the coordinate system of the
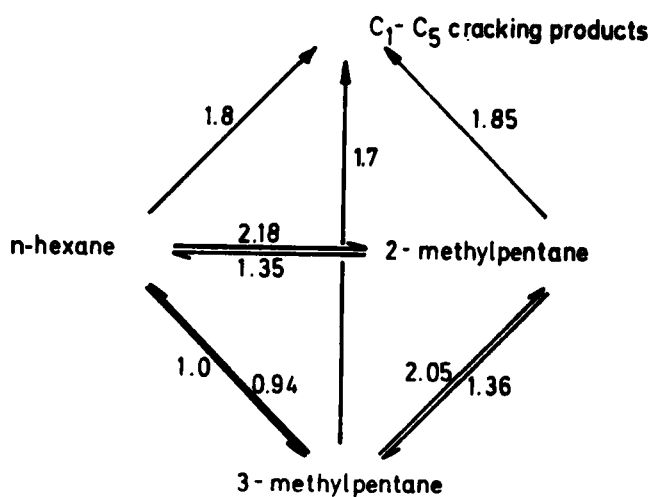
Scheme 4.2
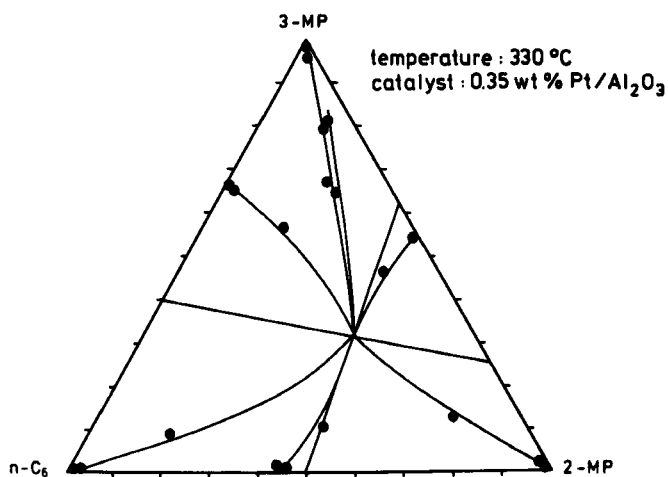
Fig. 4.17. Experimental and calculated (solid lines) reaction paths projected on the (1, 1, 1) reaction hyperplane of the reversible subsystem. Reproduced with permission from (ref. 49).

pure components. There is good agreement between calculated and measured reaction paths, which signifies the applicability of the parameter determination procedure described so far at least with respect to the aims set out in previous sections.

Owing to the low reaction temperature at which the reactions were performed, only platinum reactions contribute to the measured product distributions. The alumina carrier of the catalyst used displays no activity for skeletal rearrangements of hydrocarbons at this temperature. Hydrogenolysis reactions of n-hexane and the two methylpentanes proceed at nearly the same rate (Scheme 4.2).

A limitation to the applicability of the diffusion reactor is that in the closed centre plane chamber thermodynamic equilibrium concentrations may be obtained although starting from different initial compositions at a certain reaction temperature. This situation will always be found with small diffusivities compared with corresponding reaction rate constants. In these instances a kinetic analysis of reaction systems is not possible. Mathematically the matrix $[A(0)]$ then has the rank one and therefore the matrix $[A(0) \, A(1)^{-1}]$ also and all eigenvalues are zero except for one. These difficulties can be circumvented by lowering the reaction temperature or by reducing the thickness of the pellet.

A decrease in the reaction temperature, however, may not be suitable, especially with complex reaction systems, because the reaction mechanism by which the reactants are transformed into products may change. This is the case with the present reaction system. Above $ca.$ 430°C products are mainly formed via a bifunctional mechanism, where platinum only displays (de)hydrogenation activity and skeletal rearrangements of the hydrocarbons occur on the acidic sites and large amounts of dimethylbutanes are observed among the products. Below $ca.$ 400°C mainly platinum reactions contribute to the measured product distributions. In this instance only small amounts of dimethylbutanes are observed among the products, because dimethylbutane formation from methylpentanes involves slow reactions on platinum. Variation of the thickness of the catalyst pellet over a wide range is also restricted.

4.3 FIXED-BED REACTORS

Continuously operated fixed-bed reactors are laboratory devices that are most frequently used for testing commercial catalysts with the objectives set forth in previous sections (refs. 50-52). There are essentially two modes of running catalytic fixed-bed reactors: the differential method and the integral method. With the differential method, conversions are kept below 5-10%, where the kinetic analysis can be based directly on rates, whereas with the integral

method, kinetic analysis is based on conversions versus W/F_{A0} data (W = weight of the catalyst, F_{A0} = mol/h) because the chemical rates are changing continuously over the length of the reactor. By differentiation of conversion vs. W/F_{A0} data, rates can also be obtained.

Laboratory reactors for both operating modes are presented in Figs. 4.18 and 4.19. The fixed-bed reactor depicted in Fig. 4.18 is well suited for operation as a differential reactor. A 2-10 g amount of catalyst is packed between two layers of inert material. To maintain isothermal conditions, the catalyst can be diluted with inert material. Plug flow is achieved by sufficiently high flow velocities and a tube to particle diameter ratio of at least 10 to prevent too much channelling at the tube wall. Temperature is measured and controlled by means of thermocouples of 0.5 mm diameter which are introduced into radially brazed steel capillaries of 1 mm O.D. A small part of the reactant can be withdrawn directly after the catalyst section for analysis.

The reactor configuration can also be used as an integral reactor. In this instance a reaction path in the composition space is obtained by starting with a certain initial composition and varying the contact time for each composition point on the reaction path either by different flow-rates or different masses of catalyst, or both.

Fig. 4.19 shows a typical integral reactor. Owing to the large conversions, the reaction rate changes over the length of the reactor and frequently temperature profiles arise. It is therefore useful to equip it with devices that allow one to measure concentration and temperature profiles. In the given reactor configuration this is achieved by introducing a steel capillary radially into the tube wall. A jacketed thermocouple (0.5 mm diameter) is inserted into the capillary up to the reactor axis. In addition, a small gaseous flow is withdrawn through the steel capillary, which is controlled by means of a regulating valve, and is then passed through a sample loop which can be closed with two other valves. At a certain moment all sample loop valves are closed and the individual sample loops are attached one by one to the sampling valve of the gas chromatograph. The advantages of these sampling devices are applicability to high reactor pressures, simple installation, no dead volumes and determination of concentrations over the total length of the reactor at a certain reaction time. With such an integral reactor, a total reaction path in the
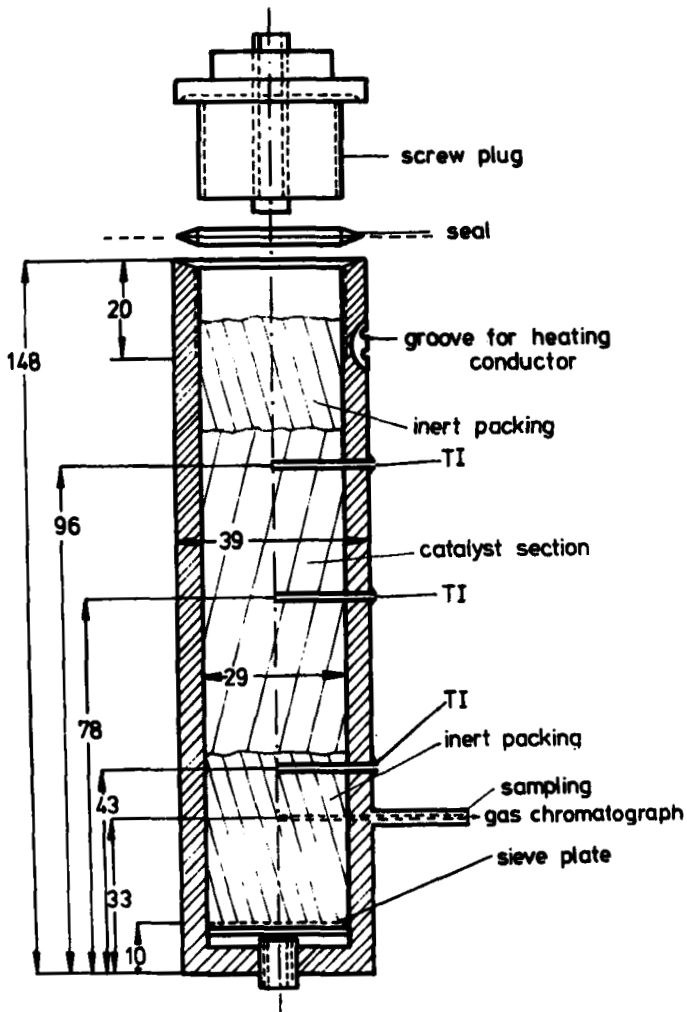
Fig. 4.18. Catalytic fixed-bed reactor for differential and integral operation. Reproduced with permission from (ref. 7), p. 191, by courtesy of Marcel Dekker, Inc.

composition space is obtained with one run.

Kinetic analysis on the basis of differential or integral fixed--bed reactor data is complicated by the interaction of hydrodynamics, mass and heat transfer, see, *e.g.*, (ref. 53) and chemical reaction. Two approaches are possible. Either, all possible effects in the mathematical reactor model are considered or the various heat and mass transfer resistances are eliminated by suitable reaction conditions by which the reactor model decomposes into a
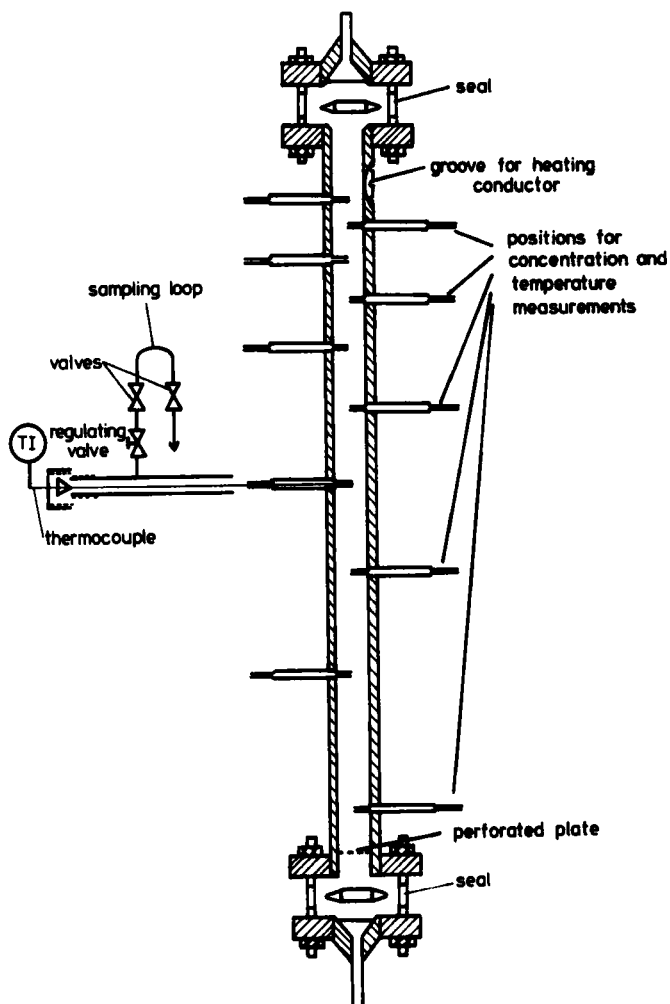
Fig. 4.19. Catalytic fixed-bed reactor with devices for concentra-
tion and temperature measurements along the length of the fixed
bed. Reproduced with permission from (ref. 7), p. 192, by courtesy
of Marcel Dekker, Inc.

kinetic model. The first procedure yields unwieldy partial diffe-
rential equations with problems in determining the model parameters,
as already discussed. With the second procedure, suitable reaction
conditions have to be adapted to eliminate dispersion effects in
the bulk flow and mass and heat transfer effects between catalyst
pellets and the bulk phase and within the catalyst pellet.

Example 4.5: Investigation of total pressure dependence of
n-hexane isomerization and cracking rates (ref. 54). For the
interpretation of experimental results for the total pressure
dependences of isomerization and cracking rates of n-hexane, the
mode of adjusting the flow-rate within the open fixed-bed reactor
is important, because increasing the system pressure results in an
increased reactant residence time under otherwise constant reaction
conditions. This can be analyzed in the following way. Assume that
the reaction rate of the heterogeneous catalytic reaction can be
described by an equation according to the law of mass action, $r_A =$
$= k \cdot a_A^n$, and that the fixed-bed reactor can be modelled like an
ideal plug-flow reactor,

$$F \cdot dU = r_A \cdot dW \qquad (4.31)$$

where F = molar flow of component A, U = conversion and W = weight
of catalyst. For a first-order reaction, $r_A = k \cdot a_A$; on integration
of eq. 4.31 the following equation is obtained:

$$W/F = - \frac{\ln(1 - U)}{k_1 \cdot a_{A0}} \qquad (4.32)$$

and for a zero-order reaction

$$W/F = U/k_0 \qquad (4.33)$$

where k_1 and k_0 are the rate constants for first- and zero-order
reactions, respectively. Rearranging eqs. 4.32 and 4.33 results in

$$U = 1 - \exp(-k_1 \cdot a_{A_0} \cdot W/F) = 1 - \exp(-k_1 W/\dot{u}) = 1 - \exp(-k_1 \rho_b \cdot t_r)$$
$$(4.34)$$

and

$$U = k_0 \cdot W/F = k_0 \cdot W/(\dot{u} \cdot a_{A_0}) = k_0 \cdot \rho_b \cdot t_r/a_{A_0} \qquad (4.35)$$

where $\dot{u}$ = volumetric flow-rate under the reaction conditions in a
fixed-bed reactor, a_{A_0} = initial concentration [mol/volume], $\rho_b =$
= density of fixed bed [g/volume] and t_r = reaction time of reac-
tants in reactor.

Hence, on keeping the reaction time of the reactants in the
reactor constant during system pressure variation, for a first-
-order reaction the conversion is independent of the total system
pressure whereas for a zero-order reaction the conversion decreases
hyperbolically with increasing total system pressure.
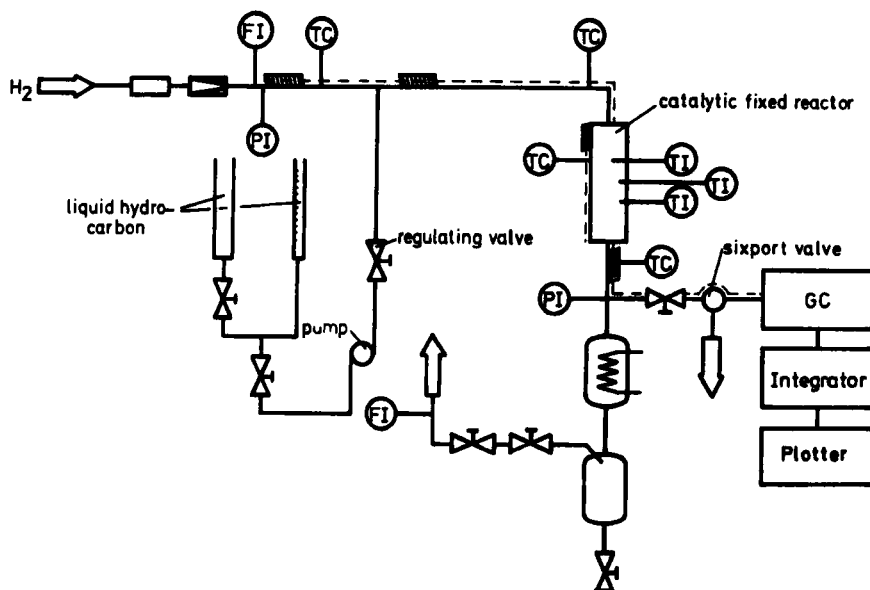
Fig. 4.20. Flow diagram of the catalytic fixed-bed reactor depicted in Fig. 4.18.

If, on the other hand, the liquid hourly space velocity, defined as the ratio of the volumetric flow-rate of liquid hydrocarbons at standard temperature and pressure and the reactor volume, is kept constant during variation of the system pressure, for a first--order reaction the conversion increases with increasing total system pressure whereas for a zero-order reaction the conversion is independent of the system pressure. Keeping the space velocity constant, a decrease in conversion with increasing system pressure signifies a negative reaction order in the formal kinetic rate equation. The liquid hourly space velocity, which is directly pro-portional to W/F, is frequently used as a measure of hydrocarbon flow-rates in open fixed-bed reactors.

Isomerization and cracking of n-hexane was investigated in the fixed-bed reactor shown in Fig. 4.18. The flow diagram is given in Fig. 4.20. The reaction conditions were as follows: particle diameter, 0.4-0.5 mm; catalyst, 2-10 g of commercial platforming 0.36 wt% Pt/Al_2O_3; temperature, 420-450°C; pressure, 4-54 bar; hydrogen:hydrocarbon molar ratio, 10-40; and space velocity, 2-70 h^{-1}. The products were analyzed by gas chromatography with a 100-m squalane capillary column. The reactions were performed over

U(mol %)

80

60

40

20

0

T = 450 °C

H_2/hydrocarbon = 20

t_r = constant

● total conversion
○ isomerization
× cracking

0   10   20   30   40   50   P(bar)
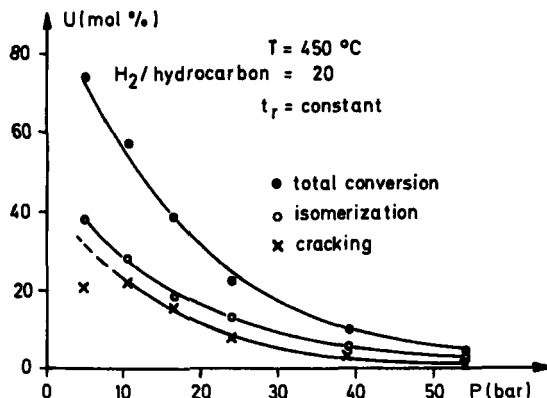
Fig. 4.21. Dependence of total, isomerization and cracking conver-
sions on total pressure at constant hydrogen:hydrocarbon molar
ratio and constant reaction time t_r (the total conversion includes
dehydrocyclization products). Reproduced with permission from
(ref. 54).

catalysts heated only up to the reaction temperature chosen and on
catalyst pre-treated in such a way that the platinum function lost
its isomerization, cyclization and hydrogenolysis activity (refs.
55,56). In the following figures the partial and total pressure
dependences of isomerization and cracking rates of n-hexane on
fresh and partially deactivated catalysts are plotted. Figs. 4.21
and 4.22 reveal that the total conversion and isomerization and
cracking conversions decrease with increasing total pressure, which
varies from 5 to 54 bar when the hydrogen:hydrocarbon molar ratio
and the reaction time or the space velocity [volume of reactant
(STP)/reaction volume·time], respectively, are kept constant.
According to the considerations discussed so far, this indicates
that under the reaction conditions used the isomerization and
cracking rates of n-hexane on fresh Pt/Al_2O_3 have a negative
overall reaction order with respect to the partial pressures of
hydrogen and hydrocarbon when modelling these rates by a simple
power law expression:

$$r = k \cdot P_{HC}^a \; P_{H_2}^b . \qquad (4.36)$$

In Figs. 4.23 and 4.24 the isomerization and cracking rates of
n-hexane are plotted against n-hexane and hydrogen partial pressu-
res [the rates were obtained at conversions <15% by $r = \Delta U/(W/F)$].
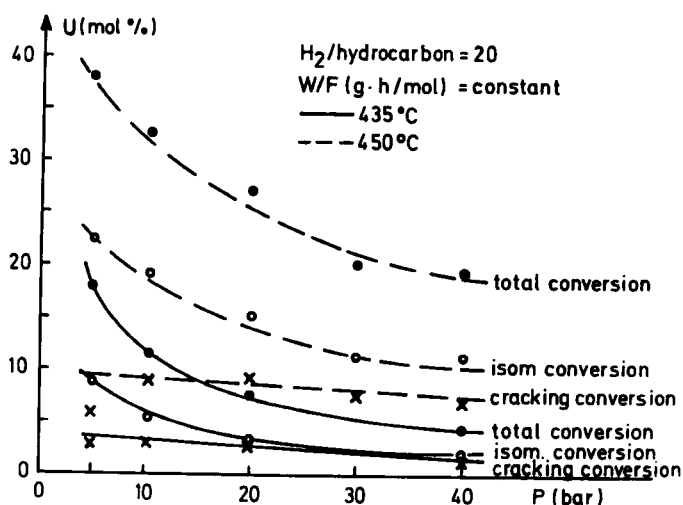
Fig. 4.22. Dependence of total, isomerization and cracking conversions on total pressure at constant hydrogen:hydrocarbon molar ratio and constant space velocity W/F [g·h/mol] (the total conversion includes dehydrocyclization products). Reproduced with permission from (ref. 56).

The results indicate that the hydrocarbon partial pressure dependences of n-hexane isomerization and cracking rates are +1, whereas the hydrogen partial pressure dependences are -1.5. The hydrogen partial pressure dependences change on the pre-treated Pt/Al_2O_3 catalysts to $ca.$ -1 (Fig. 4.25), whereas the hydrocarbon pressure dependences remain +1, which signifies that on pre-treated Pt/Al_2O_3 catalysts the products are mainly formed via a bifunctional mechanism and on fresh catalysts mainly platinum reactions contribute to the measured product distributions.

Example 4.6: Kinetics of interconversion and cracking of the five hexane isomers on a bifunctional 0.35 wt% Pt/Al_2O_3 catalyst. The experiments were performed at $435°C$, a total pressure of 10.5 bar, a hydrogen:hydrocarbon molar ratio of 20 and space velocities of 6-60 h^{-1} with an isothermally operated fixed-bed reactor (Fig. 4.18; I.D. 30 mm, length 150 mm, 2-16 g of catalyst packed between two layers of inert material, particle diameter 0.4-0.5 mm). The catalyst was heated to $450°C$ in the presence of dried hydrogen, followed by pre-conversion of n-hexane at this temperature for 1 h at a total pressure of 10.5 bar, a hydrogen:hydrocarbon partial

reactant: n-hexane

catalyst: fresh 0.35 Pt/γ-Al$_2$O$_3$

T = 450 °C

P$_{H_2}$ = 15.8 bar

$r = k \cdot P_{HC}^a \cdot P_{H_2}^b$

differential reactor

10^2 r[mole/g·h]

cracking

1.2

0.8

0.4

0

a = 1

10^2 r[mole/g·h]

isomerization

2

1

0

a = 1

0   0.4   0.8   P$_{HC}$[bar]
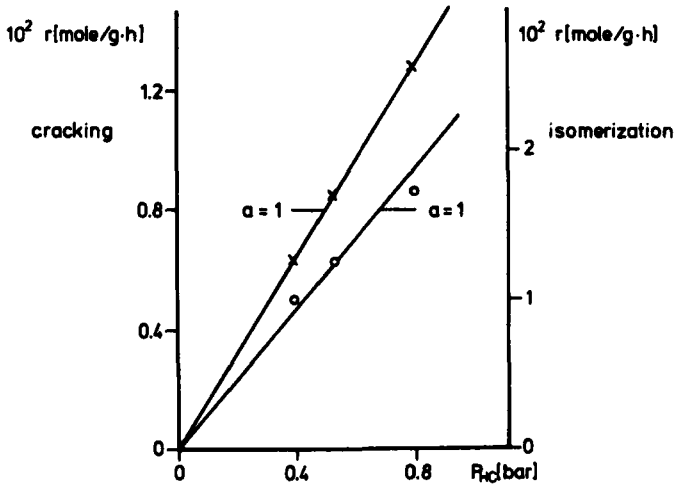
Fig. 4.23. Dependence of isomerization and cracking rates
[mol/(g·h)] of n-hexane on n-hexane partial pressure. Reproduced
with permission from (ref. 56).

pressure ratio of 20 and space velocities of 6-24 h^{-1} to achieve
an activity and selectivity level of the catalyst that were
constant during a set of experiments and could be reproduced with
different catalyst samples. For evaluation of the rate constants
connected with the reaction scheme given earlier in Fig. 4.6, the
Wei-Prater method (ref. 57) and the method proposed by Gavalas
(ref. 58), which were described in detail in Section 3.2.4, (ii)
and (iii), respectively, were used because the dynamics of the
reaction system can be modelled with a set of first-order differen-
tial equations (see example 4.5). The operating conditions of the
catalytic fixed-bed reactor were chosen in such a way that the
reactor model is quasi-identical with the kinetic model, the time
variable being replaced by a space variable. Hence, the continuity
equations for the ideal open isothermal fixed-bed reaction are
given by

reactant: n-hexane
catalyst: fresh 0.35 Pt/Al$_2$O$_3$
T = 450 °C
P$_{HC}$ = 0.35 bar
r = k · P$_{HC}^a$ · P$_{H_2}^b$
differential reactor

10^2 r/P$_{HC}$
[mole/gh·bar]

isomerization b = -1.5

cracking b = -1.56

P$_{H_2}$ [bar]
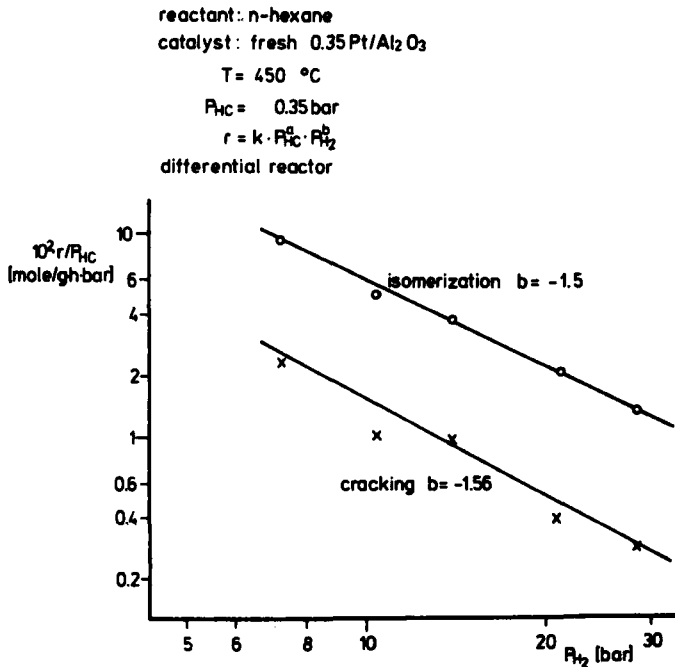
Fig. 4.24. Dependence of isomerization and cracking rates r
[mol/(g·h)] of n-hexane on hydrogen partial pressure. Reproduced
with permission from (ref. 56).

$$r_i = -\frac{dU_i}{d(W/F)} = -\sum_{j=1}^{5} k_{ji} P_i + \sum_{\substack{j=1 \\ j \neq i}}^{5} k_{ij} P_j \qquad i = 1,\ldots,5 \qquad (4.37)$$

which are rewritten with a constant reaction volume and constant
molar hydrogen:hydrocarbon ratio as

$$\frac{1}{P_{HC}^0} r_i = -\sum_{j=1}^{5} k_{ji} U_i + \sum_{\substack{j=1 \\ j \neq i}}^{5} k_{ij} U_j \qquad i = 1,\ldots,5 \qquad (4.38)$$

where P_{HC}^0 is the initial hydrocarbon partial pressure and U_i the
conversion of component i.

Determining the coefficient matrix in the model equations by
use of the Wei-Prater method, the procedure given in Section 3.2.4
(ii) is applied. For the transformation of the rate constant matrix
into an orthogonally similar matrix, the equilibrium composition
vector for the five-component system n-hexane--2-methylpentane--
--3-methylpentane--2,3-dimethylbutane--2,2-dimethylbutane is needed,
which was calculated from free energy data (API Project 44):

reactant: n-hexane

catalyst: partially deactivated 0.35 Pt/Al$_2$O$_3$

T = 450 °C

P$_{HC}$ = 0.35 bar

r = k P$_{HC}$ P$_{H_2}^b$

differential reactor
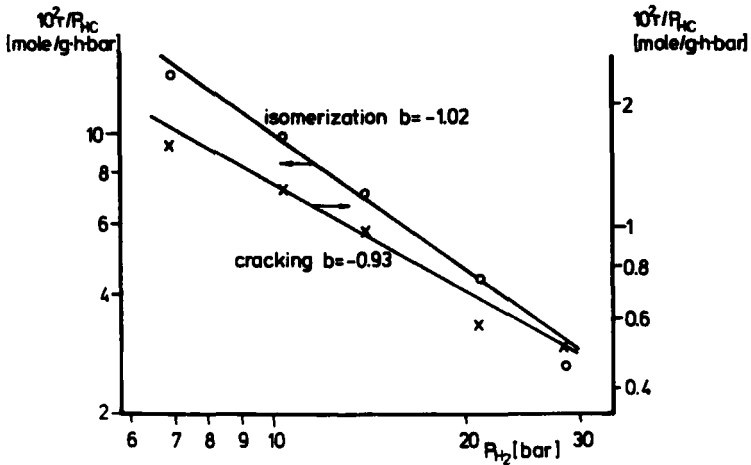
Fig. 4.25. Dependence of isomerization and cracking rates of n-hexane on hydrogen partial pressure. The 0.35 wt% Pt/Al$_2$O$_3$ catalyst was thermally pre-treated at 530°C for 12 h followed by conversion of n-hexane at this temperature for 1 h at a total pressure of 10.5 bar, a hydrogen:hydrocarbon molar ratio of 20 and a space velocity of 15 h^{-1}. Reproduced with permission from (ref. 56).

$$ ^a\text{calcd} = \begin{bmatrix} 0.2201 \\ 0.3352 \\ 0.2693 \\ 0.0639 \\ 0.1115 \end{bmatrix} \begin{bmatrix} \text{n-hexane} \\ \text{2-methylpentane} \\ \text{3-methylpentane} \\ \text{2,3-dimethylbutane} \\ \text{2,2-dimethylbutane} \end{bmatrix} \quad \text{at } 435°C. \qquad (4.39) $$

The ray vector was determined starting from three initial compositions near the equilibrium vector, and measuring reaction paths up to 70% cracking conversion:

$$ x_r = \begin{bmatrix} 0.2213 \\ 0.3358 \\ 0.2468 \\ 0.0715 \\ 0.1247 \end{bmatrix} . \qquad (4.40) $$

With the procedure presented in Section 3.2.4 (ii), three artifi-
cial straight-line reaction paths were obtained. The results are
given in Fig. 4.26 a-c, where, on the basis of (ref. 57), the
concentrations of four components are plotted against the corres-
ponding concentrations of the fifth component (ref. 59). For
determination of the initial compositions $\alpha_{x_1}(0)$, $\alpha_{x_2}(0)$ and $\alpha_{x_3}(0)$,
the actual initial compositions and measured composition points on
the reaction paths were purged of x_r, x_r and x_1, and x_r, x_1 and x_2,
respectively. From Fig. 4.26 a-c the following initial composition
vectors were obtained by a least-squares fit (linear regression
coefficients 0.999):

$$
\alpha_{x_1}(0) = \begin{bmatrix} 0.3264 \\ 0.3602 \\ 0.302 \\ 0.011 \\ 0 \end{bmatrix} \qquad
\alpha'_{x_1}(0) = \begin{bmatrix} 0 \\ 0.2844 \\ 0.1305 \\ 0.198 \\ 0.387 \end{bmatrix}
$$

$$
\alpha_{x_2}(0) = \begin{bmatrix} 0.6024 \\ 0.0948 \\ 0 \\ 0.0958 \\ 0.107 \end{bmatrix} \qquad
\alpha'_{x_2}(0) = \begin{bmatrix} 0 \\ 0.4757 \\ 0.39 \\ 0.0574 \\ 0.0769 \end{bmatrix} \qquad (4.41)
$$

$$
\alpha_{x_3}(0) = \begin{bmatrix} 0.2186 \\ 0.612 \\ 0 \\ 0.0785 \\ 0.0908 \end{bmatrix} \qquad
\alpha'_{x_3}(0) = \begin{bmatrix} 0.2244 \\ 0 \\ 0.5467 \\ 0.063 \\ 0.1659 \end{bmatrix} \quad .
$$

By use of the relationship $x_i = \alpha_{x_i}(0) + \gamma x_r$ and the orthogonality
relationship $x_r^T D^{-1} x_i = 0$ among the eigenvectors, from the initial
composition vectors of the artificial straight lines $a_{x_i}(0)$ the
following eigenvectors are calculated:

$$
x_1 = \begin{bmatrix} 4.29787 \\ 1.282466 \\ 2.38847 \\ -2.26128 \\ -4.7075 \end{bmatrix} \quad
x_2 = \begin{bmatrix} -10.76502 \\ 7.281 \\ 7.359 \\ -0.627848 \\ -2.247552 \end{bmatrix} \quad
x_3 = \begin{bmatrix} 0.368 \\ -15.1107 \\ 14.0434 \\ -0.32017 \\ 2.0196 \end{bmatrix} \quad . \qquad (4.42)
$$

The last eigenvector x_4 is also calculated from orthogonality
relationships. For this the eigenvectors already determined are
transformed into the orthogonal system by multiplication by $D^{-1/2}$
and normalized:

determination of α $_{x_1}$

X$_r$

mole fraction

mole fraction

0.4

0.3

2.2 DMB

2 MP

0.3

0.3

0.2

2.3 DMB

0.2

0.1

3 MP

0.1

0.2   0.15   0.1   0.05   0

mole fraction   n-C$_6$

determination of α $_{x_2}$

X$_r$

mole fraction

mole fraction

0.3

0.2

2.2 DMB

0.2

0.2

2 MP

0.15

0.1

2.3 DMB

0.1

0

3 MP

n-C$_6$

0.2   0.3   0.4   0.5   0.6   mole fraction
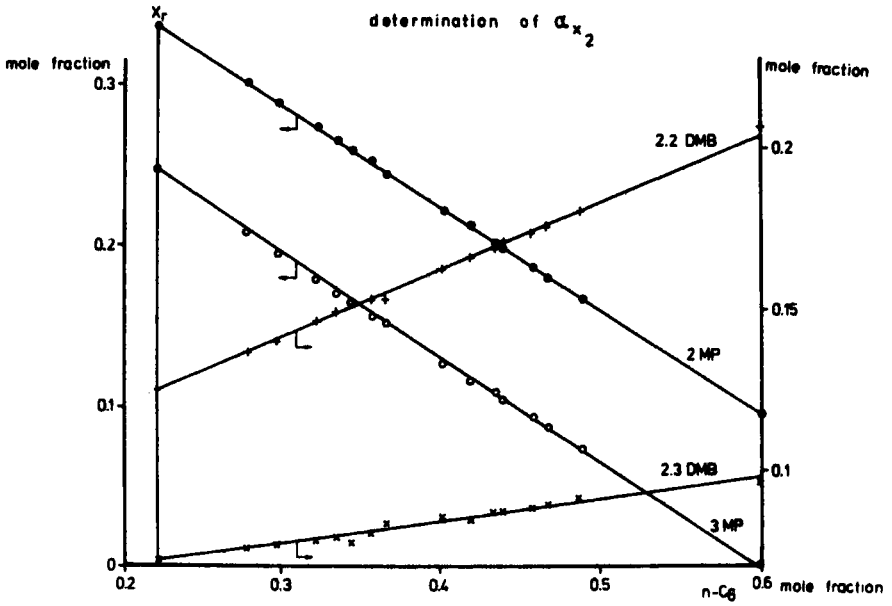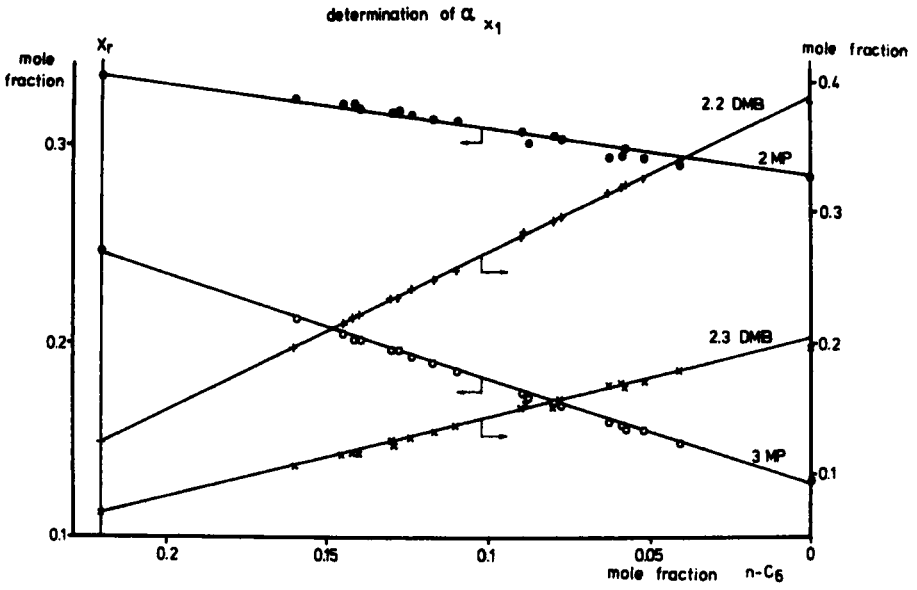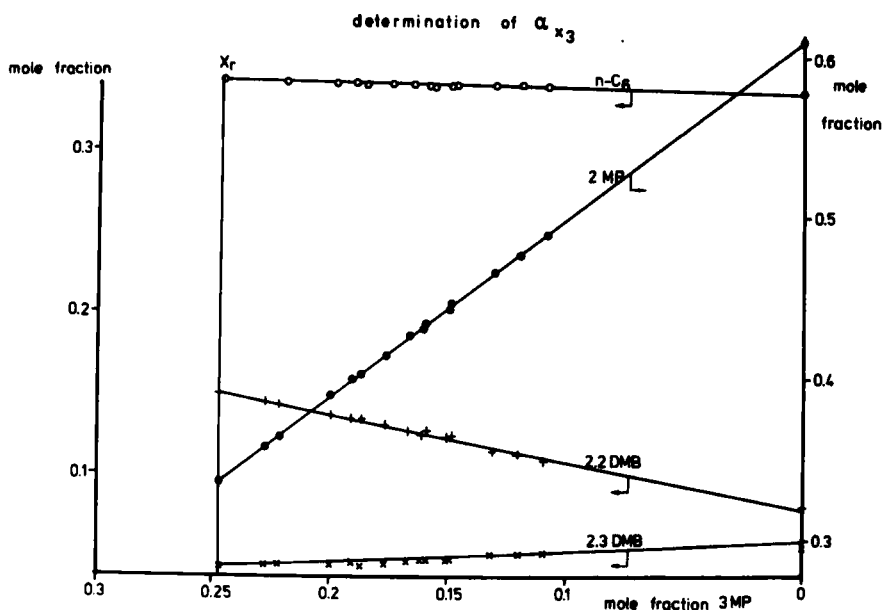
Fig. 4.26. Artificial straight-line reaction paths projected on to the [1, 1, 1, 1, 1] hyperplane parallel to the ray vector. Composition points in (b) are purged of x_1 and in (c) of x_1 and x_2. The solid lines were obtained by least-squares fits. Reproduced with permission from (ref. 59). Copyright 1979 American Chemical Society.

$$\bar{x}_i = D^{-1/2} x_i \qquad (4.43)$$

$$\bar{X}_i = \frac{\bar{x}_r}{\bar{x}_i^T \, \bar{x}_i} \qquad (4.44)$$

where $\bar{x}_i$ is a characteristic vector in the orthogonal system, $\bar{X}_i$ is a normalized vector and $\bar{x}_r^T$ is the transposed vector. The normalized vectors in the orthogonal system are then

$$\bar{X}_r = \begin{bmatrix} 0.470614 \\ 0.578729 \\ 0.474473 \\ 0.282303 \\ 0.372525 \end{bmatrix} \qquad \bar{X}_1 = \begin{bmatrix} 0.46461 \\ 0.11234 \\ 0.23342 \\ -0.45368 \\ -0.715 \end{bmatrix}$$

$$\bar{X}_2 = \begin{bmatrix} 0.74951 \\ -0.41078 \\ -0.46323 \\ 0.08113 \\ 0.21986 \end{bmatrix} \qquad \bar{X}_3 = \begin{bmatrix} 0.02057 \\ -0.68486 \\ 0.71011 \\ -0.03324 \\ 0.15871 \end{bmatrix}$$

$$(4.45)$$

x_4 is calculated from an arbitrary vector which is successively
purged of eigenvectors $x_r, \ldots, x_3$:

$$\bar{x}_4 = \begin{bmatrix} 0.02122 \\ -0.12111 \\ 0.03943 \\ 0.84073 \\ -0.52583 \end{bmatrix} \quad x_4 = \begin{bmatrix} -3.6002 \\ 25.3622 \\ 7.40064 \\ 76.8696 \\ 63.5082 \end{bmatrix} . \qquad (4.46)$$

From x_4 the initial compositions of the fifth artificial straight-
-line reaction path are

$$\alpha_{x_4}(0) = \begin{bmatrix} 0.2288 \\ 0.2866 \\ 0.2618 \\ 0.2228 \\ 0 \end{bmatrix} \quad \alpha'_{x_4}(0) = \begin{bmatrix} 0.2177 \\ 0.3591 \\ 0.2396 \\ 0 \\ 0.1836 \end{bmatrix} . \qquad (4.47)$$

The matrix of the eigenvectors is given in the following equation:

$$X = \begin{bmatrix} 0.2213 & 4.298 & -10.765 & 0.368 & -3.600 \\ 0.3358 & 1.282 & 7.281 & -15.111 & 25.362 \\ 0.2468 & 2.388 & 7.359 & 14.043 & -7.401 \\ 0.0715 & -2.261 & -0.629 & -0.320 & -76.869 \\ 0.1247 & -4.708 & -2.248 & 2.019 & 63.508 \end{bmatrix} . \qquad (4.48)$$

Ratios of the eigenvalues of the rate constant matrix are obtained
from a parametric representation of an arbitrary reaction path, for
which the following initial composition was chosen:

$$\alpha(0) = \begin{bmatrix} 0.0 \\ 0.7832 \\ 0.0047 \\ 0.0318 \\ 0.1793 \end{bmatrix} . \qquad (4.49)$$

With this reaction path, λ_1/λ_r could only be obtained with a large
error, as this reaction path did not contain sufficient b_1. A
second curved reaction path with the initial composition

$$\alpha(0) = \begin{bmatrix} 0 \\ 0 \\ 0 \\ 1.0 \\ 0 \end{bmatrix} \qquad (4.50)$$

was therefore used for determining the eigenvalues. From the slopes
of the plots in Fig. 4.27 a and b, the eigenvalues obtained are
$\lambda_r = 1$, $\lambda_1 = 2.7$, $\lambda_2 = 4.88$, $\lambda_3 = 8.3$ and $\lambda_4 = 12.7$. With the
ratios of the eigenvalues the relative rate constant matrix is
calculated using $K = X\Lambda'X^{-1}$, where Λ' is the diagonal matrix of the
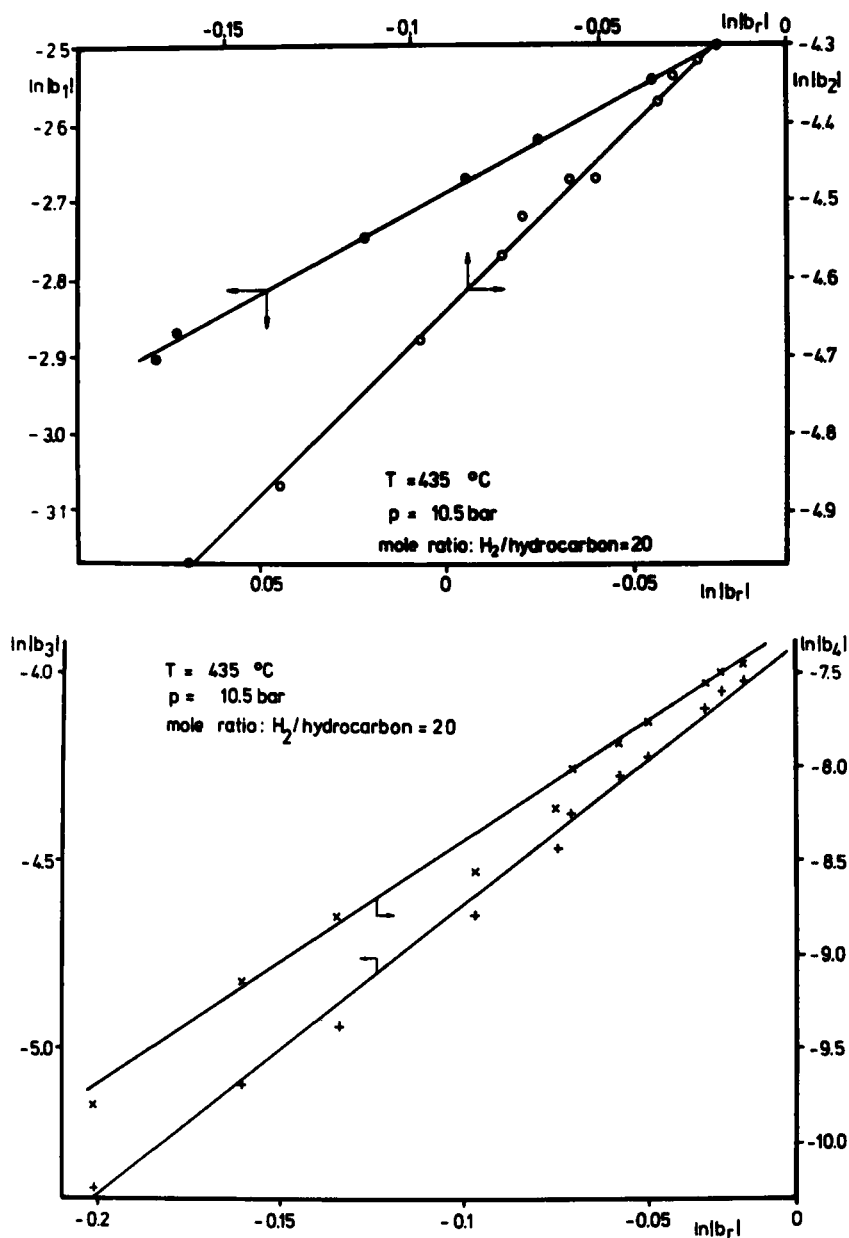
Fig. 4.27. Parametric representation of curved reaction paths in terms of the characteristic directions. From the slopes of the plots of ln b_i *vs.* ln b_r relative characteristic roots of the coefficient matrix are obtained. Reproduced with permission from (ref. 59). Copyright 1979 by American Chemical Society.
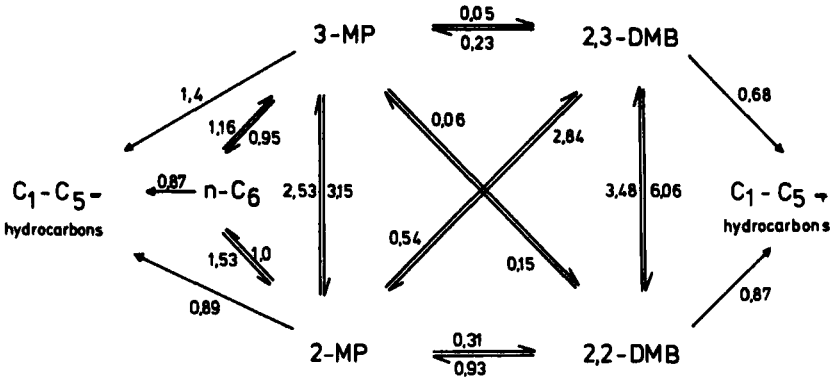
Fig. 4.28. Relative rate constants for interconversion and cracking of the hexane isomers. Reproduced with permission from (ref. 59). Copyright 1979 by American Chemical Society.

eigenvalues. The results are given in Fig. 4.28.

For a comparison of experimental and calculated reaction paths, absolute rate constants of the hypothetical system are needed; these are obtained from a plot of $\ln b_i$ vs. W/F: $\lambda_r = 0.0065\ s^{-1}$, $\lambda_1 = 0.0185\ s^{-1}$, $\lambda_2 = 0.032\ s^{-1}$, $\lambda_3 = 0.054\ s^{-1}$, $\lambda_4 = 0.083\ s^{-1}$. The results are given in Fig. 4.29, showing that the agreement between the measured and calculated reaction paths with the initial composition $\alpha(0) = [0.4/0/0.3/0/0.3]$ is rather good, indicating that the basic assumptions incorporated in the simplified dynamic model and in the parameter determination procedure are justified.

Using the method proposed by Gavalas (ref. 58) for parameter determination - *cf*. Section 3.4.2 (iii) - the experimental requirements compared with the Wei-Prater method are largely reduced. Reaction paths starting with the following initial composition vectors which span the space were determined:

$$\alpha_1(0) = \begin{bmatrix} 0 \\ 0.785 \\ 0.005 \\ 0.032 \\ 0.179 \end{bmatrix} \quad \alpha_2(0) = \begin{bmatrix} 0 \\ 0 \\ 0 \\ 1 \\ 0 \end{bmatrix} \quad \alpha_3(0) = \begin{bmatrix} 0.4 \\ 0 \\ 0.3 \\ 0 \\ 0.3 \end{bmatrix}$$

$$\alpha_4(0) = \begin{bmatrix} 0.1 \\ 0.1 \\ 0.7 \\ 0 \\ 0.1 \end{bmatrix} \quad \alpha_5(0) = \begin{bmatrix} 1 \\ 0 \\ 0 \\ 0 \\ 0 \end{bmatrix} .$$

$$(4.51)$$
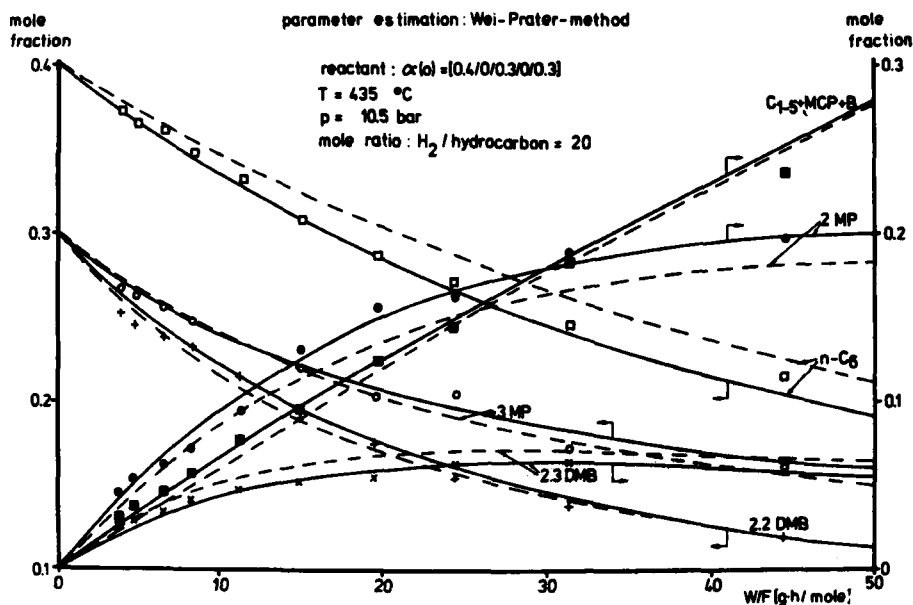
Fig. 4.29. Comparison of experimental reaction paths and reaction paths calculated (solid lines) with the coefficient matrix given in Fig.4.28. Dashed lines were determined by the use of initial reaction rates. Reproduced with permission from (ref. 59). Copyright 1979 by American Chemical Society.

From the experimental data the matrix $W(\lambda)$ was calculated. In Fig. 4.30 the smallest eigenvalue of $W(\lambda)$, which was calculated with a library program using the Householder-Givens method, is plotted against λ. In the absence of measurement errors the function $\mu(\lambda)$ would attain its minimum value, zero, at the points $\lambda_1,\ldots,\lambda_n$, because in this instance the matrix $W(\lambda)$ is positive definite for all λ, except for $\lambda_1,\ldots,\lambda_n$, for which the matrix is positive semi-definite. As the experimental data are subject to errors, $\mu(\lambda)$ attains minima at points which only approximate the true $\lambda_1,\ldots,\lambda_n$. The lambda values obtained from the calculation are $\lambda_1 = 0.0081$, $\lambda_2 = 0.0186$, $\lambda_3 = 0.0301$, $\lambda_4 = 0.0591$ and $\lambda_5 = 0.1185$. The corresponding eigenvectors are given in eq. 4.52:

$$ X^{-1} = \begin{bmatrix} 0.4192 & 0.4096 & 0.4341 & 0.4625 & 0.5041 \\ -0.249 & -0.0396 & -0.0271 & 0.5483 & 0.7969 \\ 0.4626 & -0.3208 & -0.4482 & 0.3711 & 0.591 \\ 0.0179 & -0.6305 & -0.7118 & -0.1855 & 0.2472 \\ -0.0081 & 0.0705 & -0.053 & -0.8965 & 0.4339 \end{bmatrix} . \quad (4.52) $$
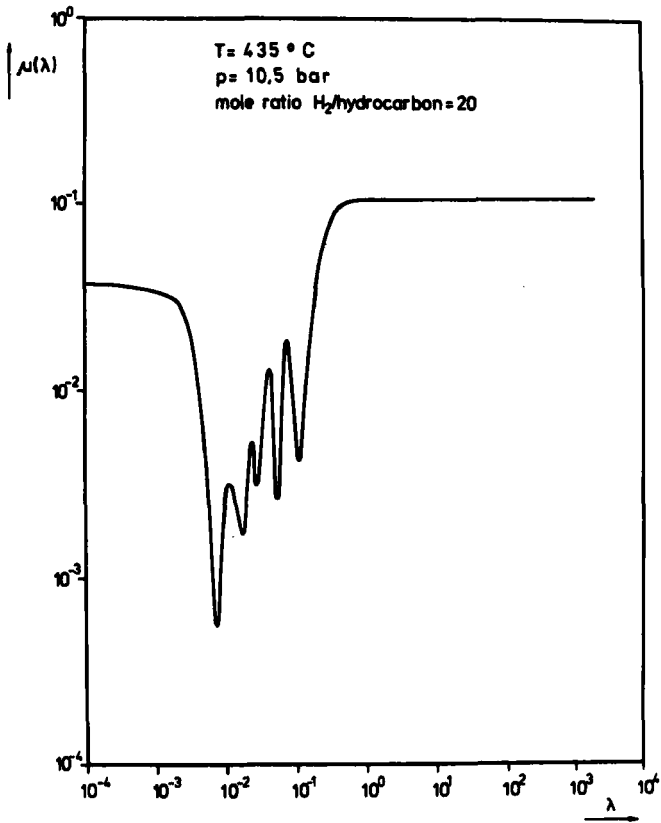
Fig. 4.30. Evaluation of the eigenvalues of the rate constant matrix for simultaneous isomerization and cracking of the five hexane isomers with the procedure proposed by Gavalas. Reproduced with permission from (ref. 60). Copyright 1980 American Chemical Society.
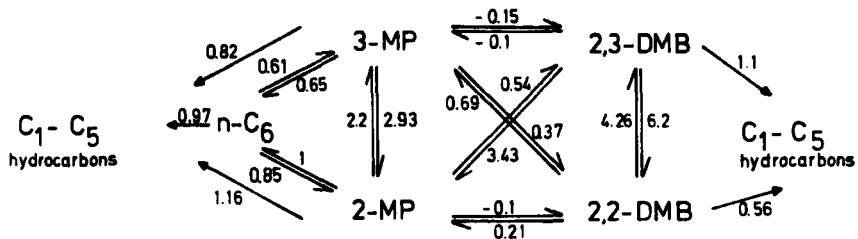
Fig. 4.31. Relative rate constants for interconversion and cracking of the hexane isomers obtained by use of the procedure proposed by Gavalas. Adapted from (ref. 60).

The rate constants which were calculated from the eigenvalues and eigenvectors by use of the equation $K = X\Lambda X^{-1}$ are given in Fig. 4.31 (ref. 44).

A comparison of experimental reaction paths and reaction paths calculated by use of the coefficient matrix determined according to the method proposed by Gavalas (ref. 58) is given in Fig. 4.32, showing reasonable agreement between the experimental and computed reaction paths (ref. 60).
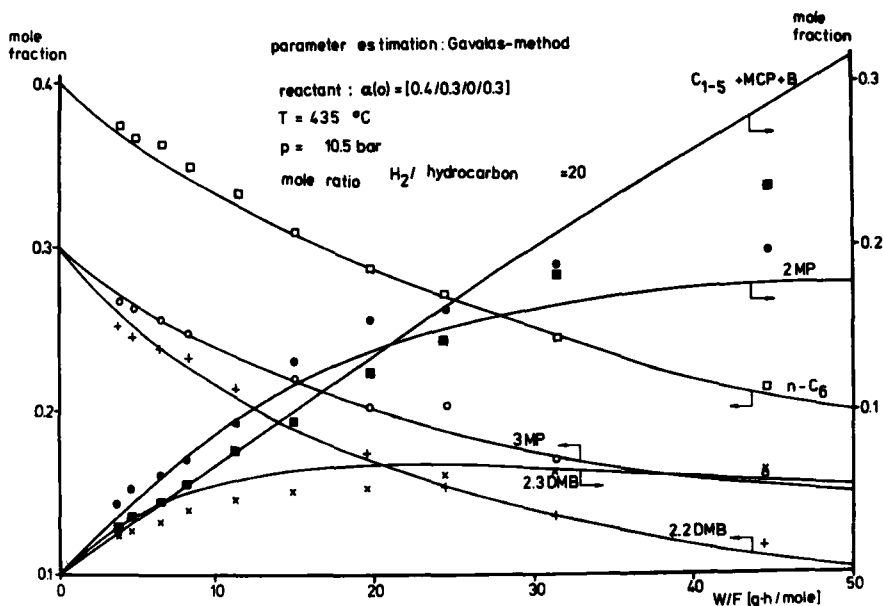
Fig. 4.32. Comparison of experimental and calculated (solid lines) reaction paths. The coefficient matrix was determined according to the method proposed by Gavalas. Reproduced with permission from (ref. 60). Copyright 1980 American Chemical Society.

4.4. RECYCLE REACTORS

Some shortcomings of integral flow reactors (possibility of concentration and temperature gradients between solid catalyst and fluid stream, dispersion effects in the fluid stream, the rates obtained are averaged over a range of concentrations) and differential flow reactors (chemical analysis at low concentrations) are overcome with recycle reactors, where perfect mixing is achieved

by external or internal recycling of the gas phase with recycle
ratios (ratio of recycle flow and feed flow) greater than 25.
External circulation is impeded by mechanical recycle pumps, which
usually require cooling and subsequent reheating of the recycle
flow. Internal recycle reactors are mainly of two types: either
the catalyst basket is rotated (ref. 61) or the gas phase is recir-
culated through the stationary catalyst by means of turbines incor-
porated in the reactor (refs. 62-64). The latter configuration has
some advantages because the temperature can be easily measured
within the stationary catalyst bed and the velocity profiles of the
gas flow through the catalyst bed are better defined than with a
rotating catalyst basket.

The vibrating piston reactor represents yet another configura-
tion. Here, a central vibrating piston keeps the fluid moving
through the catalyst, which is placed in several tubes around the
piston, with axes parallel to the piston axis. Such a system was
used, for example, for determining the likely mechanism of methanol
etherification on an acidic ion-exchange catalyst from both steady-
-state and transient data (ref. 65).

The benefits of recycle reactors result from the possibility of
adjusting exactly the physical and chemical conditions around the
catalyst in arbitrary regions of large-scale tubular reactors, $i.e.$,
of reproducing the surroundings of the catalyst over the length of
a large-scale tubular reactor by an adjustable set of conditions
in the recycle reactor. Hence the recycle reactor should be advan-
tageous in testing catalysts for use in existing large-scale
tubular reactors, which, however, presupposes a knowledge of
temperature and concentration profiles within the large-scale
fixed-bed reactor, which often is not available. A further benefit
of recycle reactors is that as a result of perfect mixing, the
material balances, such as those with CSTR, are merely algebraic
equations and are given by eq. 4.53:

$$\frac{\dot{v}c_i - \dot{v}_0 c_{i0}}{W} = r_i \left[\frac{\text{mole } i}{\text{h g}} \right] \tag{4.53}$$

$\dot{v}_0$ is the rate of inlet mass flow, $\dot{v}$ the rate of outlet mass flow
with concentrations of substance i, c_i and c_{i0}, respectively as
illustrated by Fig. 4.33.

With the computer facilities available nowadays, however, the
resulting parameter estimation with algebraic model equations is

$$\frac{\dot{v}c_i - \dot{v}_0 c_{i0}}{m_{cat}} = \eta \left[\frac{mole}{h \cdot g_{cat}}\right]$$
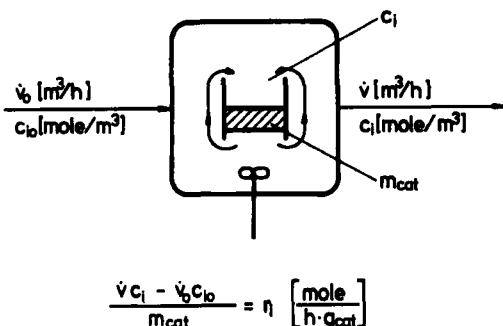
Fig. 4.33. Schematic diagram of an internal recycle reactor. Reproduced with permission from (ref. 7), p. 196, by courtesy of Marcel Dekker, Inc.

apparently of no decisive advantage of catalyst testing with gradientless recycle reactors as compared with catalyst testing with integral flow reactors.

For the investigation of underlying reaction networks, there are two potential applications of recycle reactors. One application has been demonstrated by Bennet (ref. 66), who operated recycle reactors with the transient method by superimposing reaction concentration pulses on the inlet stream of the recycle reactor, which allowed the determination of rates of individual elementary steps of single heterogeneous catalytic reactions. The advantage of operating recycle reactors in the transient mode stems from the fact that, in contrast to transient operation of fixed-bed reactors, only ordinary differential equations arise in the mathematical model, and they are more easily handled with respect to parameter estimation than the corresponding partial differential equations for fixed-bed reactors (see also Section 4.5).

A further useful application was developed by Levenspiel (ref. 67) and Löwe (ref. 68) for cases where deactivation of the catalyst proceeds on a similar time scale to that occurring with chemical reactions. Then the overall reaction rate is influenced by variations in the concentrations and changing activity of the catalyst, and the assignment of the proportions in which the individual effects contribute to the measured reaction rate is complicated. According to Levenspiel, the most useful reactor configuration for investigating rate equations with nth-order kinetics and decay is the recycle reactor, where the concentrations within the reactor are kept unchanged with time by changing the flow-rates.

The activity and concentration dependences of the rate are then decoupled and can be studied separately.

The advantages of recycle reactors for testing catalysts to control the activity and selectivity of a catalyst under operation for replacement, to select improved catalysts for existing processes and to select catalysts for new processes under development have been outlined by Berty (ref. 69). Some care in operating recycle reactors is necessary, however, especially if the kinetic data are to be used to predict the performance of catalysts in tubular reactors. Owing to different residence time distributions in both reactor configurations, reactions in the homogeneous phase of reactive intermediates formed on the catalyst surface or reactions occurring on the reactor material may contribute to the measured product distributions with the recycle reactor but can be neglected with fixed-bed reactors (for example, in the gas phase oxidation of butene, both reaction possibilities proved to be important with recycle reactors). With respect to the three steps of kinetic analysis (investigation of the underlying reaction network, mathematical modelling of chemical kinetics and of the reactor and parameter estimation in the model equations), recycle reactors offer no special advantages over fixed-bed reactors. Neither reactor configuration is well suited for investigating the underlying reaction networks, especially for complex reactions. On the other hand, reactor modelling is usually easier with recycle reactors. The use of kinetic data obtained from recycle reactions to predict the performance of catalysts in large-scale tubular reactors presupposes, however, that the activity and selectivity of the catalyst are the same in both operation modes. If the actual activity and selectivity of catalysts depend on the history of the catalyst, there are always severe restrictions on the validity of such predictions.

4.5 TRANSIENT RESPONSE METHOD

Steady-state methods often do not provide adequate information on the true kinetics and mechanism of complex catalytic processes. As a perturbation is imposed on the system, the way in which a new steady state is reached gives additional information on the character of the underlying sequence of reaction steps. This is called the transient response of the system and was reviewed by Kobayashi and Kobayashi (ref. 70). They claimed that the information obtained

this way serves as "a much more sound basis regarding the under-
lying sequence of events than do models discriminated merely
mathemathically among many postulated models" (ref. 70).

Following the earlier review (ref. 70), Kobayashi (ref. 71)
investigated the response of the concentration of component Y (the
product of a reaction X → Y) in the outlet gas mixture one can
obtain with a step-change of the concentration of component X in
the inlet gas stream. The basic types of response curves are shown
in Fig. 4.34 and the corresponding rate-controlling steps are given
in Table 4.3. Kobayashi derived these curves by computer modelling
of a few irreversible model processes with various assumptions. The
rate constant sets were chosen in a way such that the response time
would be within 20-200 min, *i.e.*, within practicable limits. On
increasing the rate coefficients by two orders of magnitude the
shape of the curves did not change, as demonstrated for type I, II
and III responses, respectively, although the new steady state was
reached within 1-2 min. Reversible reactions were dealt with only
tangentially in Kobayashi's paper; it was demonstrated that the
reversibility of the reaction is responsible for the delay of the
response curve in the initial stage of the response.

One of the model reactions studied by Kobayashi was the oxida-
tion of ethylene on a silver catalyst in a fixed-bed reactor (ref.
72). Here C_2H_4 and O_2 were components X and C_2H_4O, H_2O and CO_2
were components Y. Two types of step changes were studied:
increasing the concentration of one or both components X from zero
and decreasing them from a fixed value to zero. A detailed analysis
of his very thorough study would be beyond the scope of this book;
it is sufficient to summarize the results that the S-shape response
for CO_2 followed by an overshoot mode was taken as an indication
of a stable surface intermediate. This decomposed on decreasing the
ethylene feed to zero with a false start response and could be
desorbed as acetic acid when the surface was reduced with hydrogen.
The transient data suggested that the intermediate is formed in a
reaction between adsorbed monoatomic oxygen species and ethylene
and decomposed to give CO_2 and H_2O.

Recent advances in transient kinetics have been surveyed in a
symposium proceedings (ref. 73). Here also methods other than the
concentration changes described by Kobayashi were discussed, such
as forced feed cycling, *i.e.*, periodic change of flow direction in
a tube reactor (ref. 74), stepwise temperature and pressure
changes (ref. 75), *etc.*
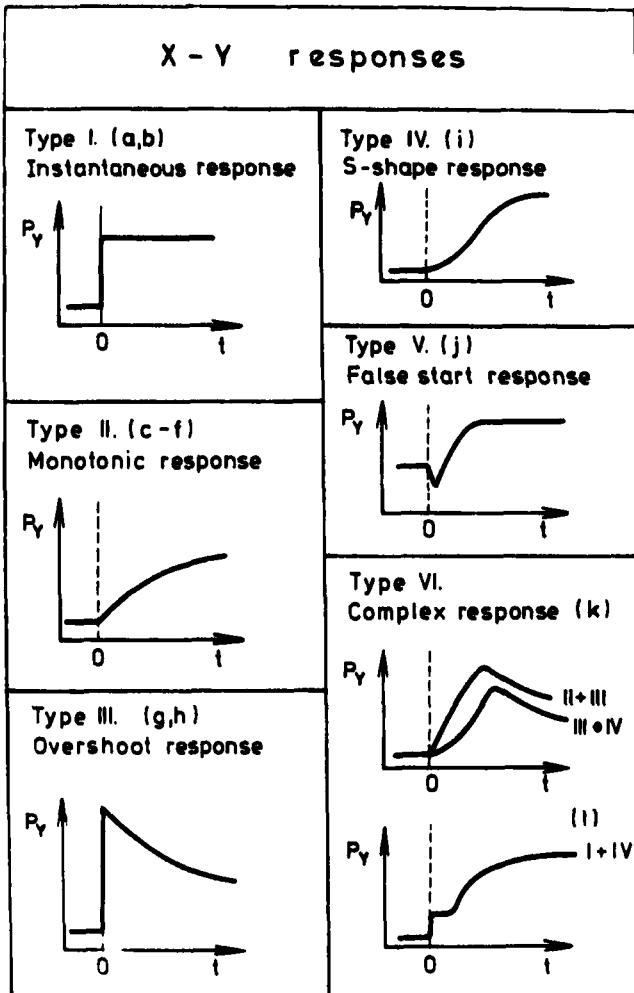
Fig. 4.34. Classification of the mode of transient response curves.
For explanation, see Table 4.3. Reproduced with permission from
(ref. 71). Copyright 1982 Pergamon Journals Ltd.

Let us consider first the concentration profile changes and the
information obtained from this method. It is obvious that a sharp
quasi-Dirac spike will suffer tremendous shape changes when it
passes through the catalyst column (ref. 76). If, however, one
applies a long pulse, these changes are negligible compared with
the total amount of feed introduced (Fig. 4.35).

Margitfalvi and co-workers (refs. 77,78) used such "slug pulses"

TABLE 4.3
Classification of the mode of transient response curves.
Reproduced with permission from (ref. 71). Copyright 1982 Pergamon
Journals Ltd.

Type of X-Y response (see Fig. 4.34)	Rate-controlling steps or characteristics of the reaction mechanism
Type I Instantaneous response	(a) Surface reactor (b) Adsorption of reactant
Type II Monotonic response	(c) Desorption of product (d) Combination of (a) and (c) (e) Combination of (b) and (c) (f) Combination of (a) or (b) and rapid readsorption of product
Type III Overshoot response	(g) Regeneration of active surface species or of active sites (h) Competitive adsorption of reaction components
Type IV S-shape response	(i) Presence of some stable surface intermediates
Type V False-start response	(j) Inhibition of adsorbed reactant to the reaction
Type VI Complex response	(k) Combination of two (or more) factors of types I-IV (l) Progress of two (or more) reaction paths in parallel with different reaction mechanisms

lasting for 60 s for studying the conversion of $\underline{n}$-hexane over
Pt/Al$_2$O$_3$ catalyst. The pulse shape was nearly rectangular; in this
way, the start and the end of the pulses corresponded to step
changes as defined by Kobayashi (refs. 70,71) in the increasing and
decreasing modes of operation, respectively. The responses of
various products should correspond to the curve shapes shown in
Fig. 4.34, and conclusions could be drawn on their possible
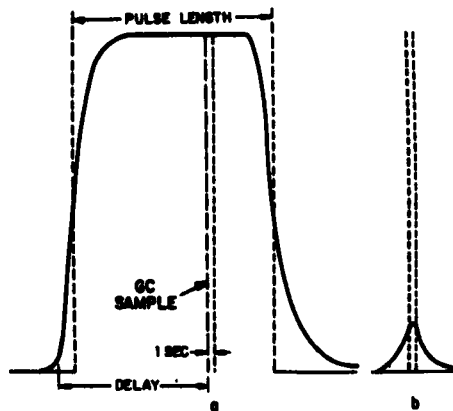
Fig. 4.35. Pulse shapes in the square ("slug") pulse method (a) and in the conventional ("spike") pulse method (b). Solid lines give the pulse shape after passage through the catalyst bed. Trigger level refers to the point at which the pulse detector is triggered by the leading edge of the pulse. Reproduced with permission from (ref. 76). Copyright 1982 American Chemical Society.

formation pathway. The results were not interpreted in terms of exact rate coefficients such as those shown in Fig. 4.6; instead, various product classes were selected, namely fragments, isohexanes, methylcyclopentane and benzene. The responses with respect to these products are shown in Fig. 4.36.
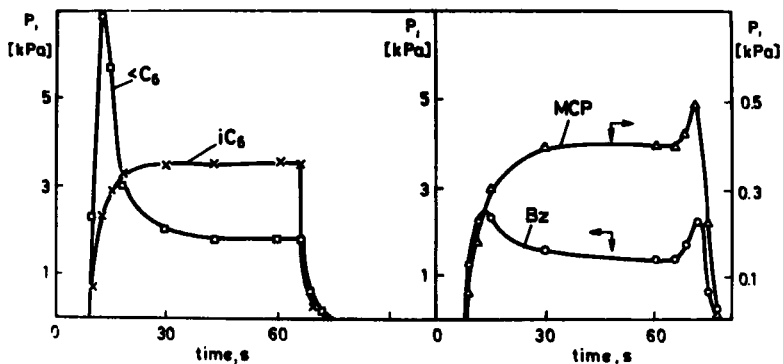
Fig. 4.36. Transient response mode of four product classes in n-hexane transformation over 0.5% Pt/Al$_2$O$_3$ at 480°C. Introduction of a rectangular "slug pulse" of n-hexane (hydrogen mixture), p(n-hexane) = 16.4 kPa, pulse length = 60 s. Reproduced with permission from (ref. 77).

Hydrogenolysis products show an overshoot type of response. This is true also when individual C_1-C_5 fragments are plotted, including isobutane and isopentane, which must have been products of complex reactions. This latter response differs from the monotonic response for C_6 isomers (2-methylpentane and 3-methylpentane). At the start of the pulse, the formation of methylcyclopentane showed a monotonic increase and that of benzene an overshoot character; both products showed a false start at the end of the slug pulse.

The authors (refs. 77,78) attributed the overshoot <u>starting</u> response for benzene and hydrogenolysis to competition of surface species for active sites (Table 4.3). Here product desorption cannot be rate controlling. One of the species competing for active sites can be hydrogen; as hydrocarbon displaces hydrogen, the probability of the formation of surface species with large site requirements is high. As a steady hydrocarbon coverage has been reached, the fraction of adjacent free sites and hence the probability of multi-site intermediates decrease, and an overshoot response is observed. Both types of products have deeply dehydrogenated surface species attached to several metal atoms (ref. 79), so this response is not surprising. For the <u>decreasing</u> branch, the false start response of benzene only was interpreted, namely that the rate-determining step is a combination of adsorbed hydrogen and deeply dehydrogenated surface precursors (as shown also by TPR studies discussed in Section 3.1.2). As the amount of available hydrogen increases at the end of the slug pulse, the appearance of benzene in the gas phase will be enhanced. The rate of desorption of hydrogenolysis products must be fast and unhindered. The deeply dehydrogenated character of these precursors is in accordance with their response to the change in the partial pressure of hydrogen and hydrocarbons, both product classes showing low selectivities at higher hydrocarbon (refs. 77,78) and hydrogen (refs. 79,80) partial pressures. The positive orders of methylcyclopentane and isohexane formation and their monotonic response indicate another, less dehydrogenated surface species for these reactions. It can be suggested that the false start response for methylcyclopentane at the end of the slug may be attributed to some dehydrogenated intermediates of C_5 cyclization (ref. 81) being hydrogenated off the surface.

It was demonstrated in Fig. 4.35 that one of the problems to be overcome is fast analysis, permitting one to follow the response functions with as little delay and distortion as possible. Fast-
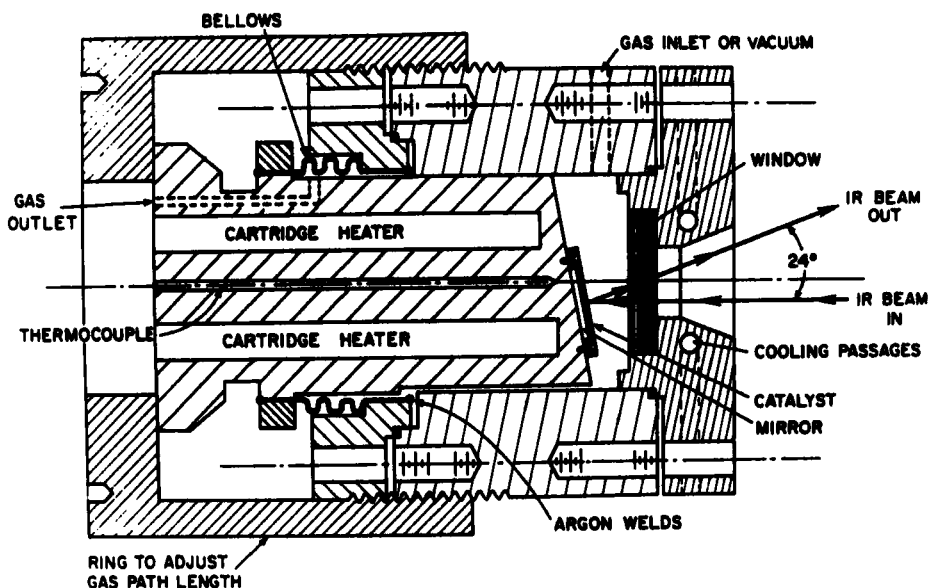
Fig. 4.37. IR cell reactor for transient experiments. Reproduced with permission from (ref. 74). Copyright 1982 American Chemical Society.

-response mass spectrometry (refs. 82,83) and various spectroscopic techniques (refs. 74,84,85) have been recommended and used. Wave-front-shape analysis is one of the methods suitable for obtaining information from non-instantaneous response curves (ref. 86). This method permits one to consider slow sorption and/or reaction steps.

The use of fast-response analytical techniques is essential when combining transient response studies with non-kinetic methods. Several infrared cells have been developed for this purpose. These studies usually involved CO or NO as reactant or product molecules (see Section 3.1.1). Bennett (ref. 74) described an IR reactor which he and co-workers used for study of the interaction of CO and CO_2 with various catalyst surfaces (refs. 87,88). The cell (Fig. 4.37) operates in the reflection mode; the use of one sample and one reference cell results in the cancellation of gas phase IR bands. The reactor cell has a very low volume (2 ml); the temperature of the catalyst disc can be controlled and the optical window can be protected by separate cooling. Operation at a flow-rate of 2 ml s^{-1} gives a residence time of 1 s; the use of 5 mg of catalyst ensures that the cell serves as a differential reactor.

Barshad and Gulari (ref. 85) placed a monolithic "honeycomb"-
-supported Pd catalyst in a see-through Fourier-transform infrared
(FTIR) spectrometer in order to follow the transient response in
CO oxidation. This fast-scan technique reveals details that are
not observable with external detectors. For example, CO desorbs on
introduction of oxygen into a CO-pre-treated reactor and cannot be
detected by outer detectors. Although the results were difficult
to interpret mathemathically, the authors concluded that oxidation
involves surface reaction between adsorbed CO and atomic oxygen,
the rate being a complex function of surface coverage by both
reactants.

Another example of combining non-kinetic methods used scanning
electron microscopy of active and fouled nickel catalysts together
with their transient response in acetylene hydrogenation to
ethylene and/or ethane (ref. 89). The rough "moonscape" picture of
the fresh catalyst turned into a nearly fluid appearance after
deactivation (seen by a magnification of 900x). Fouling profoundly
alters the catalyst response to a step increase or decrease in the
hydrogen concentration in the feed into a continuous stirred tank
reactor; the ethylene response was almost eliminated and the
acetylene response was slowed by fouling with an increase in
hydrogen concentration, whereas they accelerated when the hydrogen
concentration was decreased. There is a single overshoot response
character of acetylene concentration. The authors regarded their
results as a warning to apply steady-state conditions and scaling
factors when the underlying chemical phenomena are apparently of
more complex character.

In the 1980s, numerous studies have been published dealing with
the application of transient response methods for <u>continuous</u>
<u>stirred tank reactors (CSTR)</u>. Several reactions have been studied
in this way, *e.g.*, cyclohexane dehydrogenation on Pt/Al_2O_3 (ref.
90); CO oxidation on Cu (ref. 91) and Pd/Al_2O_3 (ref. 85) as well as
ammonia synthesis (refs. 92-94). Some other reactions have been
reviewed in (ref. 93).

For example, an overshoot of benzene concentration was found in
cyclohexane dehydrogenation in a Berty reactor at 1.2 bar between
280 and $400^{\circ}C$ (no diluent added). The cyclohexane chemisorption
rate was regarded as rate determining. Rapid benzene desorption
was claimed. The hydrogen produced would, according to the authors,
compete with cyclohexane for surface sites; at the same time, it
helps to regenerate them, which is the reason for an increasing

rate after the minimum.

The transient response curves for NH_3 showed an overshoot behaviour following a step change in feed composition (Berty reactor, $400^{\circ}C$, 2.4 MPa) when the molar fraction of hydrogen was between 0.1 and 0.5. With higher hydrogen concentrations, a monotonic response was reported (refs. 92,93). The authors challenged Kobayashi's hypothesis that the rate-controlling step would determine the mode of response; instead, they suggested a series of steady states through which adsorbed hydrogen and nitrogen would pass (ref. 92). A maximum was observed in the reaction rate at a hydrogen molar fraction of 0.70; an overshoot response was reported when the initial and final hydrogen concentrations lay on different branches of the maximum curve. A detailed mechanism has been suggested by the same group (ref. 93).

The transient response of a recycle reactor has been used for modelling its kinetic parameters by the method of moments (ref. 95). Following Suzuki and Smith (ref. 24), expressions were derived to determine intraparticle diffusion, first-order reversible adsorption and first-order chemical reaction.

Transient response studies become more and more widespread. For example, recent studies used this technique to investigate transport properties in a bimodal reforming catalyst in a diffusion cell (cf. Section 3.3.2). Bidisperse tortuosity factors could be determined experimentally (refs. 96,97). Also, interesting results were reported for determination of reversible and irreversible coke formation on a Pt/Al_2O_3 catalyst (cf. Section 3.4) and their role in the initial period of catalyst operation (ref. 98).

Transient response studies revealed that "forced feed composition cycling" gave a better time-average yield than steady-state operation (ref. 94). This means a periodic change of feed composition between synthesis gas and pure hydrogen with cycle times of a few minutes. The best hydrogen molar fraction in the synthesis gas was 0.375 at $400^{\circ}C$ and 2.4 MPa. Using forced feed composition cycling, yields up to 30% higher than those obtained under steady-state conditions could be achieved. This indicates the possible industrial importance of non-steady-state methods. The present state-of-art has been reviewed by Matros (refs. 99,100). He listed twelve industrially important processes, in which transient methods may improve performance, including SO_2 oxidation, olefin polymerization, ethanol dehydration, hydrocarbon oxidation and chlorination. Concentration, space velocity and temperature changes in addition to

the periodic reversal of the feed direction on the catalyst bed have been proposed as means for the generation of transient phenomena. The results expected are higher conversions and selectivities at lower cost or a better distribution of the molecular mass of polymers.

These examples illustrate how transient response data can supply information with respect to likely surface species, which can be combined with other data to support one or another reaction scheme. The reactions selected are close to those hydrocarbon conversions treated in several "Examples" in this book; the present results may be less quantitative but more instructive as far as the possible elementary steps are concerned. We believe that the combination of as many methods as possible and their mathemathical evaluation must be, after all, the best way to obtain a deeper insight at more and more sophisticated levels into Nature's phenomena and, at the same time, this would be a good approach to develop better and better man-made processes.

REFERENCES

1   H.B. Singh, G.E. Klinzing and J. Coull, 66th Annual Meeting, American Institute of Chemical Engineers, Philadelphia, 1973.
2   T. Furusawa, M. Suzuki and J.M. Smith, Catal. Rev.-Sci. Eng. 13 (1976) 43.
3   S.H. Langer and J.E. Patton, Adv. Anal. Chem. Instrum. 11 (1973) 293.
4   W.R. Chaudhary and L.K. Doraiswamy, Ind. Eng. Chem. Prod. Res. Develop. 10 (1971) 218.
5   M.I. Yanovskii and A.D. Berman, J. Chromatogr. 69 (1972) 3.
6   J.B. Galeski and J.W. Hightower, Can. J. Chem. Eng. 48 (1970) 151.
7   E.G. Christoffel, Cat. Rev.-Sci. Eng. 24 (1982) 159.
8   R.J. Kokes, H.H. Tobin and P.H. Emmet, J. Am. Chem. Soc. 77 (1955) 5860.
9   W.K. Hall and P.H. Emmett, J. Am. Chem. Soc. 79 (1957) 2091.
10 W.K. Hall, D.S. McIver and H.P. Weber, Ind. Eng. Chem. 52 (1960) 421.
11 E.I. Semenenko, S.Z. Roginskii and M.I. Yanovskii, Kinet. Katal. 6 (1965) 320.
12 C. Corolleur, S. Corolleur and F.G. Gault, J. Catal. 24 (1972) 385.
13 D.W. Bassett and H.W. Habgood, J. Phys. Chem. 64 (1960) 769.
14 T. Hattori and Y. Murakami, J. Catal. 10 (1968) 114.
15 T. Hattori and Y. Murakami, J. Catal. 31 (1973) 127.
16 T. Hattori and Y. Murakami, J. Catal. 33 (1974) 365.
17 T. Hishida, T. Uchijima and Y. Yoneda, J. Catal. 17 (1970) 287.
18 E.G. Christoffel, T. Surjo and K.H. Röbschläger, Can. J. Chem. Eng. 58 (1980) 513.
19 E.G. Christoffel and B. Kind, J. East China Inst. of Chem. Techn. 11 (1985) 9.
20 E.G. Christoffel and C.-L. Li, J. East China Inst. of Chem. Techn. 11 (1985) 17.

21 E.M. Magee, Ind. Eng. Chem. Fundam. 2 (1963) 32.
22 S.Z. Roginskii, M.J. Yanovskii and G.A. Gaziev, Kinet. Katal.
    3 (1962) 529.
23 G.A. Gaziev, V.Y. Filinovskii and M.J. Yanovskii, Kinet. Katal.
    4 (1963) 688.
24 M. Suzuki and J.M. Smith, Chem. Eng. Sci. 26 (1971) 22.
25 S.Z. Roginskii and A.L. Rozental, Kinet. Katal. 5 (1964) 104.
26 P.A. Ramachandran and J.M. Smith, Ind. Eng. Chem. Fundam.
    17 (1978) 146.
27 M. Kubin, Collect. Czech. Chem. Commun. 30 (1965) 1104.
28 E. Kucera, J. Chromatogr. 19 (1965) 237.
29 H.A. Boniface and D.M. Ruthven, Chem. Eng. Sci. 40 (1985) 1401.
30 E.I. Semenenko, S.Z. Roginskii and M.I. Yanovskii, Kinet. Katal.
    5 (1964) 490.
31 D. Schweich and J. Villermaux, Ind. Eng. Chem. Fundam. 21 (1982)
    52.
32 D. Schweich and J. Villermaux, Ind. Eng. Chem. Fundam. 21 (1982)
    47.
33 S.K. Gangwal, R.R. Hudgins and P.L. Silveston, Can. J. Chem.
    Eng. 57 (1979) 609.
34 J. Valuš and P. Schneider, Chem. Eng. Sci. 40 (1985) 1457.
35 E.G. Christoffel and K.H. Röbschläger, Chem. Ing. Tech. 50
    (1978) 796.
36 E.G. Christoffel and J.C. Schuler, Chem.-Ing.-Tech. 52 (1980)
    844.
37 Ya.B. Zeldovich, Zh. Fiz. Khim. 13 (1939) 163.
38 V.A. Roiter, G.P. Korneichuk, M.G. Leperson, N.A. Stukanovskaya
    and B.I. Tolchina, Zh. Fiz. Khim. 24 (1950) 459.
39 M. Suzuki and M.J. Smith, AIChE J. 18 (1972) 326.
40 G. Dogu and J.M. Smith, Chem. Eng. Sci. 31 (1976) 123.
41 B.-J. Ahn and J.M. Smith, Chem. Eng. Sci. 40 (1985) 1313.
42 L.L. Hegedus and E.E. Petersen, Catal. Rev.-Sci. Eng. 9 (1974)
    245.
43 J.R. Balder and E.E. Petersen, Chem. Eng. Sci. 23 (1968) 1287.
44 E.A. Mason and A.P. Malinauskas, Gas transport in porous
    media: the dusty-gas model, Elsevier, Amsterdam, 1983.
45 R.B. Evans, G.M. Watson and E.A. Mason, J. Chem. Phys.
    35 (1961) 2067.
46 D.S. Scott and F.A.L. Dullien, AIChE J. 8 (1962) 113.
47 L.W. Jossens and E.E. Petersen, J. Catal. 73 (1982) 366.
48 R.K. Herz and L.L. Hegedus, Chem. Eng. Sci. 33 (1978) 1561.
49 E.G. Christoffel, J. Catal. 81 (1983) 273.
50 R. Aris, Elementary reactor analysis, Prentice-Hall, Englewood
    Cliffs, 1969.
51 J.M. Smith, Chemical engineering kinetics, McGraw-Hill, New
    York, 1970.
52 J.J. Carberry, Chemical and catalytic reaction engineering,
    McGraw-Hill, New York, 1976.
53 W.R. Paterson and J.J. Carberry, Chem. Eng. Sci. 38 (1983) 175.
54 T.I. Surjo and E.G. Christoffel, Chem.-Ing.-Tech. 50 (1978) 882.
55 E.G. Christoffel, Chem. Ztg. 102 (1978) 391.
56 E.G. Christoffel and Z. Paál, J. Catal. 73 (1982) 30.
57 J. Wei and C.D. Prater, Adv. Catal. 13 (1962) 137.
58 G.R. Gavalas, AIChE J. 19 (1973) 214.
59 E.G. Christoffel, Ind. Eng. Chem. Prod. Res. Develop. 18 (1979)
    143.
60 E.G. Christoffel, Ind. Eng. Chem. Prod. Res. Develop. 19 (1980)
    430.
61 J.J. Carberry, Ind. Eng. Chem. 56 (1964) 39.
62 J.A. Makoney, J. Catal. 32 (1974) 247.

63 C.O. Bennett, M.B. Cutlib and C.C. Yang, Chem. Eng. Sci.
    27 (1972) 2255.
64 J.M. Berty, J.O. Hambrich, T.R. Malone and D.S. Ullock, AIChE
    Meeting, New Orleans, 1969.
65 K. Klusáček and P. Schneider, Chem. Eng. Sci. 37 (1982) 1523.
66 C.O. Bennett, Catal. Rev.-Sci. Eng. 13 (1976) 121.
67 O. Levenspiel, J. Catal. 25 (1972) 265.
68 A. Löwe, Ind. Eng. Chem. Fundam. 19 (1980) 160.
69 J.M. Berty, Catal. Rev.-Sci. Eng. 20 (1979) 97.
70 M. Kobayashi and H. Kobayashi, Catal. Rev.-Sci. Eng. 10 (1974)
    139.
71 M. Kobayashi, Chem. Eng. Sci. 37 (1982) 393.
72 M. Kobayashi, Chem. Eng. Sci. 37 (1982) 403.
73 A.T. Bell and L.L. Hegedus (Editors) ACS Catalysis under
    Transient Conditions, Symposium Series, No. 178, American
    Chemical Society, Washington, D.C., 1982.
74 C.O. Bennett, in (ref. 73) p. 1.
75 J.R. Creighton and J.M. White, in (ref. 73), p. 33.
76 R.J.H. Voorhoeve, L.E. Trimble, S. Nakajima and E. Bands, in
    (ref. 73), p. 253.
77 J. Margitfalvi, P. Szedlacsek, M. Hegedus and F. Nagy, Appl.
    Catal. 15 (1985) 69.
78 J. Margitfalvi, M. Hegedus, P. Szedlacsek and F. Nagy, Acta
    Chim. Hung. 119 (1985) 213.
79 Z. Paál and P.G. Menon, Catal. Rev.-Sci. Eng. 25 (1983) 229.
80 Z. Paál, H. Zimmer and P. Tétényi, J. Mol. Catal. 25 (1984) 99.
81 C.O. O'Donohoe, J.K.A. Clarke and J.J. Rooney, J. Chem. Soc.
    Faraday Trans. I, 76 (1980) 345.
82 C.J. Machiels, in (ref. 73), p. 239.
83 B.J. Savatsky and A.T. Bell, in (ref. 73), p. 105.
84 S.H. Oh and L.L. Hegedus, in (ref. 73), p. 79.
85 Y. Barshad and E. Gulari, J. Catal. 94 (1985) 468.
86 E. Fiolitakis and H. Hofmann, in (ref. 73), p. 277;
    E. Fiolitakis, U. Hoffmann and H. Hoffmann, Chem. Eng. Sci.
    34 (1979) 677; 685; 35 (1980) 1030.
87 A. Ueno, J.K. Hochmuth and C.O. Bennett, J. Catal. 49 (1977)
    225.
88 A. Ueno and C.O. Bennett, J. Catal. 54 (1978) 31.
89 M.R. Bilimoria, D.D. Bruns and J.E. Bailey, AIChE J. 26 (1980)
    319.
90 P. Ledoux, Y.S. Hsia and S. Kovenklioglu, J. Catal. 98 (1986)
    367.
91 E.E. Miró, D.R. Ardiles, E.A. Lombardo and J.O. Petunchi,
    J. Catal. 97 (1986) 43.
92 A.K. Jain, Li Chengyue, P.L. Silveston and R.R. Hudgins, Chem.
    Eng. Sci. 40 (1985) 1029.
93 Li Chengyue, R.R. Hudgins and P.L. Silveston, Can. J. Chem.
    Eng. 63 (1985) 795.
94 Li Chengyue, R.R. Hudgins and P.L. Silveston, Can. J. Chem.
    Eng. 63 (1985) 803.
95 G. Garza-Tobias, J. Jimenez-Ocana and M.A. Rosales, Can. J.
    Chem. Eng. 60 (1982) 123.
96 J. Biswas, D.D. Do, P.F. Greenfield and J.M. Smith, Appl. Catal.
    32 (1987) 217.
97 J. Biswas, D.D. Do, P.F. Greenfield and J.M. Smith, Appl. Catal.
    32 (1987) 235.
98 J. Biswas, P.G. Gray and D.D. Do, Appl. Catal. 32 (1987) 249.
99 Yu.Sh. Matros, Unsteady Processes in Catalytic Reactors, Stud.
    Surf. Sci. Catal., Vol. 22, Elsevier, Amsterdam, 1984.
100 G.K. Boreskov and Yu.Sh. Matros, Catal. Rev.-Sci. Eng.
    25 (1983) 551.

252

SYMBOLS

A_E	activation energy, kJ/kmol
A_i	reacting species in a reaction system
a_i	concentration in the gas phase, mol/cm^3
$\bar{a}_i$	concentration in the porous medium, mol/cm^3
a_1	concentration of vacant active centres
a_{1t}	total molar concentration of active centres
b_i	concentration of hypothetical species, mol/cm^3
C_i	constant
c_0/μ	d'Arcy flow parameter, cm^2/(s·mbar)
c_s	surface concentration
D_{12eff}	effective molecular diffusion coefficient, cm^2/s; $D_{12eff} = D_{12}\beta/\tau$
D_{12}	molecular diffusion coefficient, cm^2/s
D_{eff}	effective diffusion coefficient, cm^2/s
D_K	Knudsen diffusion coefficient, cm^2/s
D_{Keff}	effective Knudsen diffusion coefficient, cm^2/s
D_{ax}	axial dispersion coefficient, cm^2/s
D	diagonal matrix of equilibrium concentrations
D^{-1}	inverse of D
F	total molar flow of feed hydrocarbons, mol/h
F_{A_0}	molar feed rate of reactants, kmol/h
ΔG	free reaction enthalpy
h	Thiele modulus; Planck's constant
ΔH	reaction enthalpy
I	unit matrix
J_i	molar flow of species i, mol/(cm^2·s)
J	sum of least squares, minimization criterion
K	rate constant matrix
k	reaction rate constant; Boltzmann constant
K_a	adsorption equilibrium constant
k_a	adsorption rate constant
k_{des}	desorption rate constant
K_i	equilibrium constant
k_s	rate constant of surface reaction
L	thickness of single pellet; length of fixed bed, cm
1	active centre on catalyst surface
l	linkage class (see p. 84)
m	number of initial states
n	number of components in state vector

N	adsorption term, defined by eq. 4.17
P	total pressure, bar; empirical steric factor, defined by eq. 2.3
P_i	partial pressure, bar
Q	mass transfer term, defined by eq. 4.16
r	reaction rate, mol/(g·h)
r_0	initial rate
r_{ad}	adsorption rate
r_{des}	desorption rate
R	radius of catalyst pellet, cm; gas constant
S	stoichiometric subspace
s	stoichiometric number
s_r	stoichiometric number of rate-determining step
ΔS	reaction entropy
t	time, s
T	temperature, K
U	overall heat transfer coefficient
u	flow velocity, cm/s
W	weight of catalyst, g
$W(\lambda)$	symmetric matrix
X	matrix of eigenvectors; conversion
x_i	molar fraction; characteristic vector
x	distance
y	distance
z	distance
Z_{AB}	number of collisions between reactant molecules
Z	impact rate, number of molecules/(s·cm^2)

GREEK SYMBOLS

$\alpha(t)$	composition vector
α^*	equilibrium composition vector
β	composition vector in the hypothetical component system
β	porosity of catalyst
γ	scalar, defined by eq. 3.123
$\gamma(j)$	jth row of X
ϵ	porosity of fixed bed
η	effectiveness factor
λ_i	eigenvalue of rate constant matrix
Λ	diagonal matrix of eigenvalues
μ	dynamic viscosity

$\mu(\lambda)$	smallest eigenvalue of $W(\lambda)$
μ_1	first absolute moment
μ_2'	second central moment
ρ	density, g/cm^3
θ	surface coverage
τ	tortuosity factor
Ψ_i	normalized concentration

Other symbols are defined in the text.

SUBJECT INDEX

AUTHOR INDEX

STUDIES IN SURFACE SCIENCE AND CATALYSIS

Advisory Editors: B. Delmon, Université Catholique de Louvain, Louvain-la-Neuve, Belgium
J.T. Yates, University of Pittsburgh, Pittsburgh, PA, U.S.A.

This Page Intentionally Left Blank